Examination of Tumour Tissues by Direct MALDI-Mass Spectrometry Imaging and Profiling

Marie Claude DJIDJA

A thesis submitted in partial fulfilment of the requirements of
Sheffield Hallam University for the degree of Doctor of Philosophy

Faculty of Health and Wellbeing

September 2009

ACKNOWLEDGMENTS

First, I would like to thank my supervisor Professor Malcolm Clench for his constant support and invaluable trust all along the PhD, the opportunity to work with him and present my work at several international and national meetings and conferences. It has been a great three years full of fun and knowledge. I would like to extend special thanks to Dr Vikki Carolan for her helpful and critical advices in writing this thesis.

I would like also to thank Dr Simona Francese, Emmanuelle Claude and Dr Marten Snel for being there and providing me valuable help, support as well as their expertise and friendship.

I also gratefully acknowledge Dr Paul Loadmann and Dr Chris Sutton at the Institute of Cancer Therapeutics in Bradford, Mr Peter Scriven at the Academic Surgical Oncology Unit, Sheffield University and Professor Michel Salzet at the Laboratoire de Neurobiologie des Annelides in France, for their assistance and great advices all along this project.

I would like to thank friends and colleagues who put up with me during hard and joyful times and provided me laughs, coffee, hot chocolate and chocolate bars. I would like to thank especially Robert Widdowson, Dr Louise Hurst-Prince, Hugui, Paul Trim, Dr Caroline Earnshaw, Dr Tasneem Muharib, Dr David Anderson, Philippa Hart, Laura Cole and Claire Bradford.

My special thanks go to my family and parents, Elisa and Benoit, who support me throughout my studies and help me to achieve what I have accomplished so far, which would not have been possible without their help.

I especially thank Matou for being here for all this time and even trying to understand Mass Spec in order to make it easier for me.

At last and from far the least, I would like to send a special thank to Xaviou for being always there for me. You cheered me up with your contagious positive mind, made it enjoyable for me even when living in another country and I will be eternally grateful.

Abstract

The purpose of the work described in this thesis was to develop and apply efficient methodologies based on MALDI-MSI for the direct analysis and targeting of protein tumour biomarkers within both frozen and formalin fixed paraffin embedded (FFPE) cancerous tissue sections.

Method development for protein analysis directly in tumour tissue sections were performed using tumour xenograft models. This involved improvements in sample preparation, such as tissue washing protocols, and the development of data pre-processing methods prior to statistical analysis using a freely available software package, which referred to as *SpecAlign*.

The use of MALDI-MSI for studying proteome patterns directly from tumour tissue sections with no requirement for known targets is demonstrated. In addition, *in situ* identification of proteins within tumour tissue sections was achieved and correlated with their localisation. The method demonstrated here involved the use of octyl glucoside, a non-ionic detergent, which aims to improve the solubilisation and detection of low abundance and membrane-associated proteins within tumour tissue section after on-tissue digestion. The coupling of MALDI-MSI with ion mobility separation (IMS) has been found to improve the specificity and selectivity of the method.

Combining these two methodological approaches allowed the targeting and identification of known tumour biomarkers and potential protein markers in various tumour tissue samples including frozen AQ4N dosed colon tumour xenografts and FFPE human adenocarcinoma tissue sections. The localisation and identification of proteins correlated to tumour growth and aggressiveness were studied using IMS-Tag MALDI-MSI, a novel concept developed in this work.

In order to demonstrate its use as a potential biomarker discovery tool, MALDI-MSI was used for high throughput analysis of proteins within tissue micro arrays. Combining MALDI-MSI with statistical analysis allowed the design of a novel tumour classification model based on proteomic imaging information after on-tissue digestion.

Another challenge for the MALDI-MSI technology is to achieve more targeted quantitative approaches for *in situ* analysis of proteins. A proof-of-concept based on multiple reaction monitoring (MRM) analysis with MALDI-MSI is described using a high repetition rate solid state laser. This aimed to improve the sensitivity and specificity of the methodology for the investigation of peptides/proteins directly within tumour tissue sections.

Table of Contents

List of Figures

List of Tables

Abbreviations

ACN: acetonitrile

α-CHCA: α-cyano-4-hydroxycinnamic acid

ANI: aniline

AR: antigen retrieval

ATF6: UPR-specific transcription factor activating transcription factor 6

CAIX: carbonic anhydrase IX

$CHCl_3$: chloroform

CID: collision-induced dissociation

CMC: carboxymethylcellulose

dH_20: deionised water

2-D: two-dimensional

DA: discriminant analysis

DMPK: drug metabolism and pharmacokinetic

eIF-2α: α subunit of the regulating initiator of the mRNA translation machinery

ER: endoplasmic reticulum

ES: early stage

ESI: electrospray ionisation

EtOH: ethanol

FFPE: formalin fixed and paraffin embedded

FT-ICR: Fourier-transform ion cyclotron resonance

GLUT-1: glucose transporter 1

GLUT-3: glucose transporter 3

Grp78: glucose-regulated protein 78

HE: haematoxylin and eosin

Her2: human epidermal growth factor receptor 2

HIF-1: hypoxia-inducible factor 1

HPLC: high performance liquid chromatography

Hsp: heat shock protein

IHC: immunohistochemistry

IMS: ion mobility separation

ip: intraperitoneally

Ire1: inositol-requiring enzyme 1

ITO: indium-tin-oxide

LC: liquid chromatography

MALDI: matrix assisted laser desorption ionisation

MALDI-MS: matrix assisted laser desorption ionisation mass spectrometry

MALDI-MSI: matrix assisted laser desorption ionisation Mass spectrometry Imaging

MS: mass spectrometry

MS/MS: tandem mass spectrometry

m/z: mass-to-charge ratio

MeOH: methanol

MLN: metastatic lymph node

mRNA: messenger ribonucleic acid

MRI: magnetic resonance imaging

MRM multiple reaction monitoring

N_2 laser: nitrogen laser

Nd:YAG: neodymium-doped yttrium aluminium garnet

Nd:YVO_4: yttrium vanadate

OcGlc: Octyl-α/β-glucoside

OCT: optimum cutting temperature

ODD: oxygen-dependent degradation domain

o-MALDI-TOF MS: orthogonal MALDI-TOF MS

oa-TOF MS: orthogonal axial-TOF MS

OPN: osteopontin

OPLS: orthogonal partial least-squares

OPLS-DA: orthogonal partial least-squares-discriminant analysis

PAI-1: plasminogen activator inhibitor 1

PANTHER: Protein ANalysis THrough Evolutionary Relationships

PCA: principal component analysis

PCA-DA: principal component analysis-discriminant analysis

PERK: pancreatic kinase like ER

PHDs: prolyl hydroxylases

PLS: Partial least-squares

PMF: peptide mass fingeprint

PTM: post-translational modification

Q: quadrupole

QqTOF: quadrupole time-of-flight

RF: radio frequency

ROI: region of interest

SA: sinapinic acid

SIMS: secondary ion mass spectrometry

S/N: signal-to-noise ratio

TAP: tumour-activated prodrug

TIC: total ion count

TFA: trifluoroacetic acid

TLC: thin layer chromatography

TWIMS: traveling wave IMS

TNM: tumour node metastasis

TOF: time-of-flight

TOF MS: time-of-flight mass spectrometry

2-DE, 2D-PAGE: two-dimensional gel electrophoresis

u-PAR: urokinase-type plasminogen activator receptor

UPR: unfolded protein response

VEGF: vascular endothelial growth factor

VHL: von Hippel Lindau protein

XBP1: X-box binding protein 1

CHAPTER 1

Introduction

1.1 Molecular Insights into Cancer

1.1.1 Molecular origins of cancer

Cancer remains a major public health issue despite progression in detection and therapy. It refers to a group of more than 100 different diseases and caused about 13 % of death worldwide in 2004 [1]. It occurs when cells in a part of the body begin to grow out of control which leads to a tumour. Most cancers form a tumour which can be benign or malignant. Benign tumours are not cancerous, they can usually be treated or removed. Malignant tumours yield cancer cells.

Cancer diseases have different causes as well as molecular and biological origins. This has been reviewed by Croce [2] where it is described that normal cells transform into cancer cells following alterations of genes that regulate and control cell growth and differentiation. Genetic changes, usually somatic events including alteration of oncogenes, tumour-suppressor genes and microRNA genes, can lead to cancer [3, 4].

Oncogenes encode proteins that regulate cell proliferation and/or programmed cell death such as apoptosis and can be grouped in six categories including transcription factors, chromatin remodelers, growth factors, growth factor receptors, signal transducers and apoptosis regulators. Oncogene activation and alteration have been shown to be closely associated with cancer initiation and progression [5]. It has been reported that most hematopoietic cancers, such as leukemia, and also soft tissue sarcoma are initiated by the activation of an oncogene followed by the alteration of tumour-suppressor genes and additional oncogenes [6]. The inhibition of a tumour-suppressor gene followed by alteration of oncogenes and other tumour-suppressor genes have been shown to initiate most carcinoma [7].

MicroRNAs consist of a single RNA strand comprising between 21 and 23 nucleotides and act as gene expression regulators. MicroRNAs have been found to be involved in cancer initiation and progression [8]. They can be highly expressed or down-regulated in cancer cells depending on their targets in the specific tissue. When up-regulated, microRNAs act as oncogenes by down-regulating tumour-suppressor genes [9].

As originate from changes in cells, there are several types of cancers which are primarily defined according to the microscopic characteristics of the tumour, i.e. based on type of cells from which the disease originates and histological patterns. Among them are the following examples, including epithelial tumours or **carcinoma** which are tumours derived from epithelial cells. Adenocarcinoma types refer to cancers that originate in glandular tissues. **Sarcoma** are types of tumours composed of mesenchymal cells while **Lymphoma** and **leukemia** are haemopoietica and Lymphoid tumours.

Tumour classifications are based on the grading, which describes the abnormality of the cells, and the staging which defines the extent of the disease are also used to determine and help clinical prognosis as well as appropriate treatments [10, 11]. Edmondson and Steiner have reported a grading system of classification for primary carcinoma of the liver and identified up to 4 grades including grade I, II, III and IV. However, if cell differentiation has been of significance for prognosis for some tumour types, research is still undergoing to improve such way of tumour classification [10, 11].

The stage of the tumour is also used for tumour classification in combination with the grading and is based on both clinical and pathological examinations [10, 12]. The tumour node metastasis (TNM) classification is the staging classification system used where **T** provides information about the presence or absence of a primary tumour as well as its size. **N** is used for assessing the presence of regional nodes and **M** provides information on existing distant metastases.

The identification of oncogenes involved in tumour initiation and progression has led to the development of new therapeutic drugs that target oncogenic proteins [13–15]. Several molecular pathways, including those which involve oncogenic products as well as proteins that are known to participate in oncogenic pathways and processes, cellular stress and metastasis, are usually observed in solid tumours. Additional protein targets are required for the improvement and development of anticancer drugs. Furthermore tumour classifications may most likely be based on molecular information, i.e. genomic and proteomic data that provide insights into tumour progression, aggressiveness and resistance to therapy.

1.1.2 The tumour micro-environment

The tumour micro-environment remains complex and is not yet fully understood. However, it is known to be a host of physiological stresses and where several molecular pathways occur, yielding abnormal cellular metabolism and cell proliferations. Here, some key molecular responses, including the unfolded protein response (UPR), hypoxia and tumour metastases, which are correlated with the tumour micro-environment are described.

1.1.2.1 The unfolded protein response (UPR) in cancer

Proteins are fundamental to cell functioning and cell processes via metabolism, cell signaling and immune responses. After synthesis by the ribosomes, secretory and membrane proteins, which account for about one third of the cell's proteins, undergo a folding process within the endoplasmic reticulum (ER) [16]. Protein folding is a process which takes place in a calcium-rich, oxidised and energetic milieu and is assisted by molecular chaperones. Molecular chaperones are proteins which play a critical role in stabilising and facilitating nascent protein folding processes as well as ensuring that the desired conformation is obtained [17]. The ER resident, glucose-regulated protein 78 (Grp78) is a key molecular chaperone within the ER [18, 19] and provides the trigger for activation of the signal cascade known as the unfolded protein response (UPR) [20, 21].

In mammalian cells, the UPR is activated when misfolded or unfolded proteins are accumulated in the lumen of the ER [22]. The three key receptors are:

- the transmembrane kinases: inositol-requiring enzyme 1 (Ire1) and pancreatic kinase like ER (PERK)
- the UPR-specific transcription factor activating transcription factor 6 (ATF6).

In the absence of cellular stress, Grp78 binds to the ER transmembrane sensor proteins *i.e.* Ire1, PERK and ATF6 and maintains them in an inactive form. When unfolded proteins are accumulated in the ER lumen, Grp78 is recruited to ensure protein folding. The initial steps in the activation of the UPR consist of two main functions. Firstly, PERK is dimerised and activated leading to the phosphorylation of eIF-2α, the α subunit of the regulating initiator of the mRNA translation machinery. This results in a period of translation attenuation producing cell cycle arrest in the G1 phase [20, 21].

UPR activation also yields an increased production of proteins involved in the functions of the UPR, *i.e.* an up-regulation of molecular chaperones of malfolding proteins including Grp78, in order to export misfolded proteins to the proteasome for degradation. This response is promoted by the migration of ATF6 and XBP1 (X-box binding protein 1) to the nucleus. The aim of these two preliminary responses is to remove the accumulated misfolded proteins from the ER lumen so that normal function of the ER can be restored. If the disruption is prolonged, apoptosis is initiated. Figure 1.1 displays the currently understood mechanism of the UPR [20].

The UPR is poorly characterised in cancer, however it has been shown that the UPR could be seen as a key mechanism in permitting tumour cell survival in an acidotic, hypoxic and glucose deprived environment and in altering chemosensitivity to a variety of established anticancer agents [23–26]. Targeting proteins that are involved in the UPR cascade directly within tumour tissue sections may result in an improved understanding of tumour behaviour and treatment response.

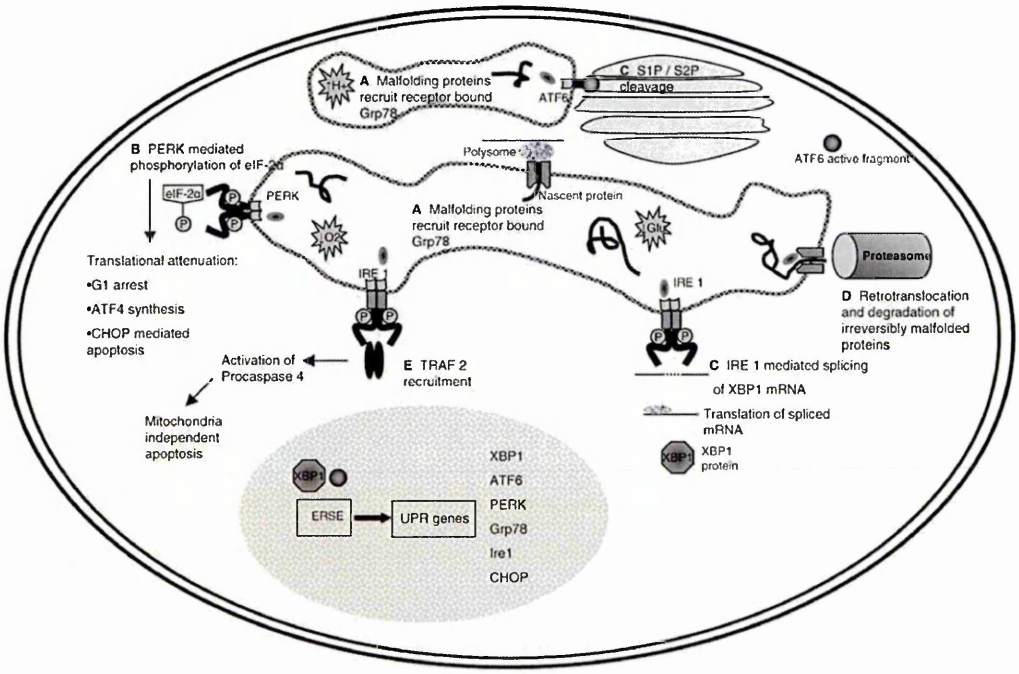

Figure 1.1: **Diagram of the unfolded protein response in human cells** [20].
A Recruitment of Grp78 to chaperone or assist malfolded proteins which leads to dissociation from its conformational binding state to the transmembrane receptors PERK, Ire1 and ATF6. **B** Activation of PERK leads to the phosphorylation of eIF-2α, the inhibition of translation and results in cell cycle arrest. **C** and **D** Migration of ATF6 and XBP1 to the nucleus, which promotes upregulation of molecular chaperones including Grp78 in order to ensure misfolded protein degradation. **E** If disruption is prolonged, apoptosis is initiated.

1.1.2.2 Hypoxia in solid tumours

To permit growth and expansion, solid tumours must develop their own vasculature system (called angiogenesis) which is also critical in enabling tumour cells to metastasise to distant organs [27, 28]. Due to their inadequate structure and function, these new tumour vessels have been found to create micro environmental stressors including hypoxia, acidosis, glucose deprivation and disturbance of calcium homeostasis [23, 29, 30].

Hypoxia is a characteristic feature in most rapidly growing solid tumours and their metastases. Tissue hypoxia results from an inadequate supply of oxygen (O_2) that disturbs the biological functions of the cells [31, 32]. Studies have shown that up to 60% of solid tumours may contain hypoxic regions that are heterogeneously localised within the tumour [33]. Tumour hypoxia is strongly related to tumour propagation, malignant progression and resistance to chemotherapy as well as radiotherapy [34–37].

The hypoxia micro-environment induces adaptive changes to tumour cell metabolism and influences tumour cell biology [31, 38–40]. Cells exposed to hypoxia are usually stopped at the G_1/S-phase boundary, thus resulting in several changes in the cellular proteome [41]. These hypoxia-induced proteome changes may promote tumour propagation as tumour cells may adapt to nutrient deprivation or escape this environment [37]. Figure 1.2 [42] displays a schematic representation of tumour hypoxia. Several studies have reported that tumour hypoxia alters the molecular mechanisms of intracellular signal transduction, gene regulation angiogenesis and apoptosis [42, 43].

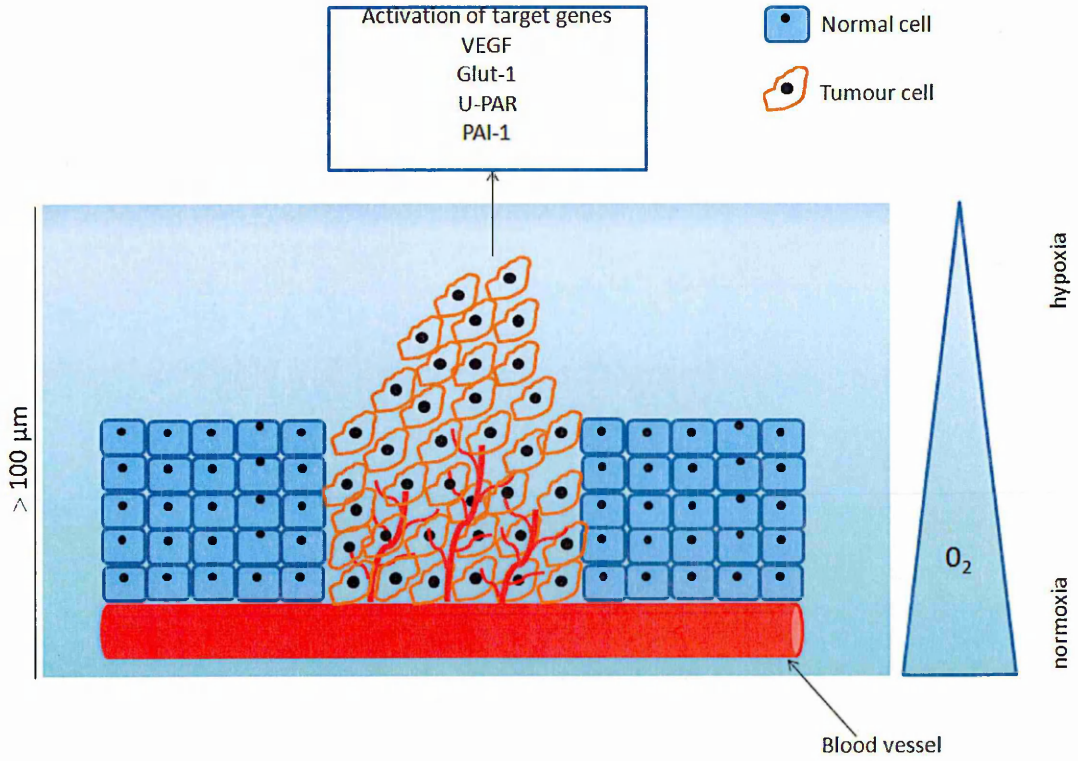

Figure 1.2: **Tumour hypoxia in human cells** (adapted from [42]).
When tumour cells develop their own vascular supply, tumour hypoxia arises in regions with a lack of oxygen. As a consequence, hypoxic cells activate genes involved in angiogenesis (vascular endothelial growth factor (VEGF)), glucose transport (glucose transporter 1 (GLUT-1)) and cell migration (urokinase-type plasminogen activator receptor (u-PAR) and plasminogen activator inhibitor 1 (PAI-1)). Increased angiogenesis encourages tumour growth as well as tumour metastasis.

The hypoxia-inducible factor 1α (HIF-1α) has been shown to be over-expressed in several malignant tumours including breast, head and neck, ovarian, gastric and prostate cancers [44–47]. Hypoxic cells encourage tumour growth as they activate target genes involved in angiogenesis (vascular endothelial growth factor (VEGF)), glucose transport (glucose transporter 1 (GLUT-1)) and cell migration (urokinase-type plasminogen activator receptor (u-PAR) and plasminogen activator inhibitor 1 (PAI-1)) [37, 42]. Understanding these pathways and molecular mechanisms may improve chemotherapy development.

Several strategies are currently under investigation to target hypoxic cells within the tumour micro-environment. This involves the development of therapies that aim to increase the oxygen availability in the tumour micro-environment [48, 49]. Other therapies consist of the use of bioreductive drugs that are selectively activated in hypoxic regions of the tumour [50–52]. Besides these therapies, research based on the development of drugs that target proteins involved in hypoxic responses and angiogenesis have been reported [53, 54].

1.1.2.3 Tumour metastasis

Metastasis is a complex process which is often observed in cancer. It involves a series of linked sequential steps favoring the spreading of a subpopulation of cells from the primary neoplasm to distant organs to initiate tumour growth [55–58]. A failure or limitation at any stage of these steps can arrest the entire metastasis process. The formation of angiogenesis is essential for rapid primary tumour growth but also for metastasis formation [57, 59–62]. Synthesised and secreted angiogenic factors have been found to establish a capillary network from the surrounding normal tissues [63]. Metastasis begins with the invasion of the host stroma by tumour cells [64]. These tumour cells are then released into the circulation through vasculature and lymph channels that offer less resistance to tumour cell penetration [58]. Tumour cells which survive during the circulation process can be trapped in the capillary beds of distant organs via capillary endothelial cells and further proliferate within these organs after extravasation from capillary beds [57, 60]. In order to survive and continue growing, these micro tumours must develop new angiogenesis and hence can continue to spread to other organs, there-

fore creating additional metastasis. Figure 1.3 displays the main steps involved in the metastatic cascade [55].

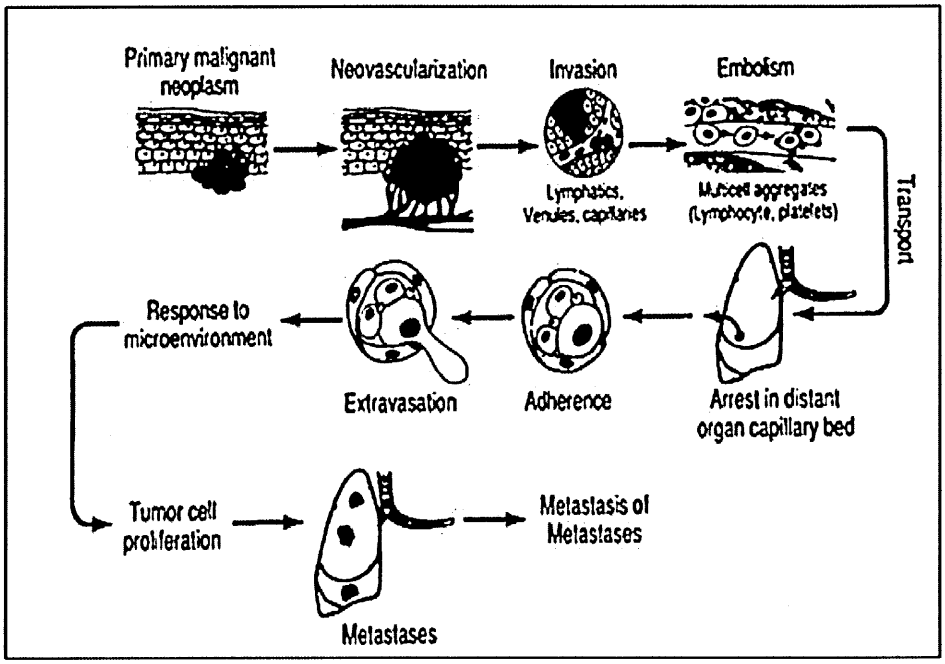

Figure 1.3: **The main steps involved in the metastatic cascade** [55].
Angiogenesis is a critical step for primary tumour growth as well as metastasis formation. Angiogenesis facilitates the invasion of the surrounding host stroma by tumour cells which are released into the circulation to further develop metastases in distant organs.

Understanding the neovasculature system at the molecular level is of great interest as it can allow the development of target agents that inhibit the function of ligands and/or receptors involved in the angiogenic process and therefore improve cancer metastasis targeting.

1.2 Proteomic Analysis by Mass Spectrometry

Research is currently being performed in many areas including biotechology, chemistry, bioinformatics and proteomics in order to improve the prevention and early detection of cancer as well as to reduce mortality [65–67]. Proteomics refers to the study of the complete protein composition of a cell or a tissue sample [68–70]. Understanding cancer requires the identification of diagnostic biomarkers, i.e. proteins and other biomolecules which are correlated to disease states or represent potential therapeutic targets. Mass spectrometry is one technique of choice for proteomics studies and has allowed the identification of several cancer biomarkers [67].

1.2.1 Principles of mass spectrometry

Mass spectrometry (MS) is a powerful analytical technique that allows the separation and structural characterisation of compounds based on their molecular weights. The technique consists of the analysis of ions contained in a gas phase based on their mass-to-charge ratio (m/z). The data generated are processed with a computer and appropriate software tools in order to produce a mass spectrum of the analysed sample where all the m/z values are displayed against their intensities.

A mass spectrometer consists of three fundamental parts (Figure 1.4):

- the **ionization source**
- the **analyser**
- and the **detector.**

With the rapid advances and improvements in mass spectrometry, each of these elements are selected specifically depending on the desired experiment and compound being analysed. However, the principle of MS remains the same in all applications. Briefly, the sample is introduced into the ionization source of the instrument where gas-phase ions are generated. These ions are then extracted into the analyser and separated according to their mass (m) -to-charge (z) ratios (m/z). The separated ions are detected and the signals are sent to a data system where m/z ratios are stored together with their relative abundance, yielding a mass spectrum.

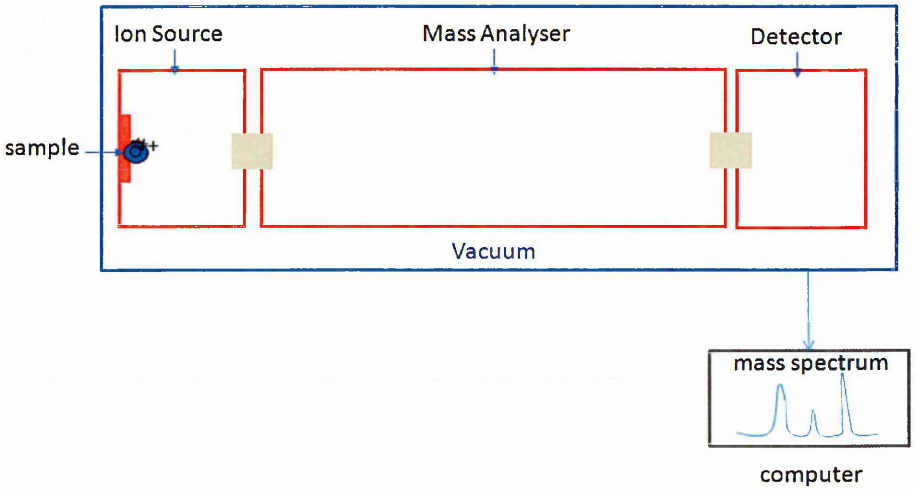

Figure 1.4: **Principles of a mass spectrometer instrument.**
Ions are generated in the ionisation source prior to being separated according to their mass-to-charge ratio (m/z). The detector registers the number of ions emerging from the analyser in order to provide an ion count. A mass spectrum is then generated, plotting the m/z values against their respective ion counts or intensities.

1.2.1.1 Ion sources

Several ionisation techniques are used with MS depending on the physicochemical properties of the samples to be analysed and the desired fragmentation. Electrospray ionization (ESI) and matrix-assisted laser desorption ionisation (MALDI) are commonly used for the majority of biochemical analyses, including protein analysis, as they are soft ionisation techniques which produce ions from non-volatile large and complex species contained in solution into a vacuum.

1.2.1.1.1 *Electrospray ionisation (ESI)*

Electrospray ionisation (ESI) occurs at atmospheric pressure and the resulting ions are transferred to the mass spectrometer. Under atmospheric pressure, an electrospray can be generated by applying a high electric field to a liquid going through a capillary tube [71]. Figure 1.5 displays a diagram of ESI process. Several applications have reported the use of ESI coupled to LC, HPLC and capillary electrophoresis (CE) for the analysis of proteins, polymers and also small polar molecules [71–73].

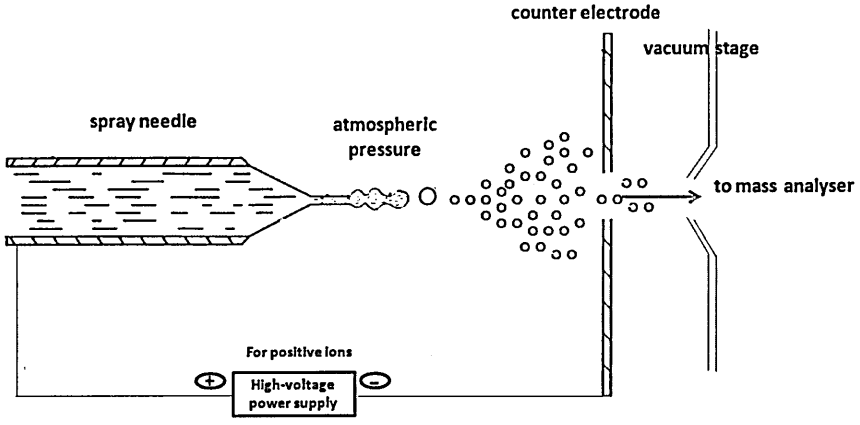

Figure 1.5: **Diagram of the principle of electrospray ionisation** [71].
During electrospray ionisation, a flow of liquid-phase analytes is nebulised under atmospheric pressure by applying a high voltage to the capillary. The ESI process generates vapor phase ions that can be analyzed for mass-to-charge ratio within the mass spectrometer.

1.2.1.1.2 *Matrix-assisted laser desorption/ionisation (MALDI)*

Matrix-assisted laser desorption/ionisation (MALDI) involves solid-state ionisation of compounds. The sample is first mixed with a matrix, which is usually a small organic molecule with a high absorption at the laser wavelength. The matrix aims to crystalise with the analyte of interest in order to produce analyte ions once irradiated with the laser. Briefly, the ablation of the crystal (matrix-analyte) by the laser pulses induces the sublimation of the matrix which leads to a transfer of internal energy to the analyte, thus resulting in ionisation [74, 75]. However the full ionisation mechanism is not fully understood yet. The most accepted mechanism involves a proton-cation transfer along with photo-ionised matrix [76, 77]. Briefly, it consists of a two-step mechanism where, first, ion formation occurs after the matrix absorbs the laser energy in order to facilitate initial charge separation. Then, the excited states of the matrix act as buffers and transfer the energy to the ion plume through proton, photon or electron transfer. Figure 1.6 shows a diagram of the principle of MALDI. MALDI is a soft ionisation technique; the sample destruction is minimised as the laser energy is absorbed by the matrix, hence increasing sensitivity.

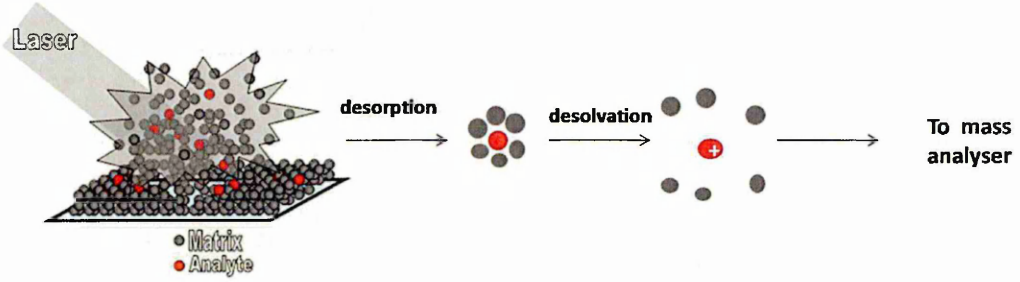

Figure 1.6: **Diagram of the matrix-assisted laser desorption ionisation** MALDI involves the co-crystallisation of the matrix and the analyte. The matrix absorbs the laser energy, thus leading to a transfer of internal energy to the analyte and inducing the formation of ions.

Several applications have reported the use of MALDI-MS for the analysis of intact proteins as well as microorganisms [78, 79]. The choice and optimisation of the matrix is critical for the analysis and is closely associated with the laser wavelength as well as the compound to be analysed. Important general properties of appropriate matrices for a given analysis include: their ability to strongly absorb the laser energy, their stability

in a condensed phase under high-vacuum conditions and their ability to induce efficient ionisation of the analysed compounds [80]. A variety of matrices have been developed therefore and are used in many applications [81, 82].

Figure 1.7 displays the chemical structures and molecular weights of the commonly used UV-MALDI matrices, which are derivatives of benzoic acid.

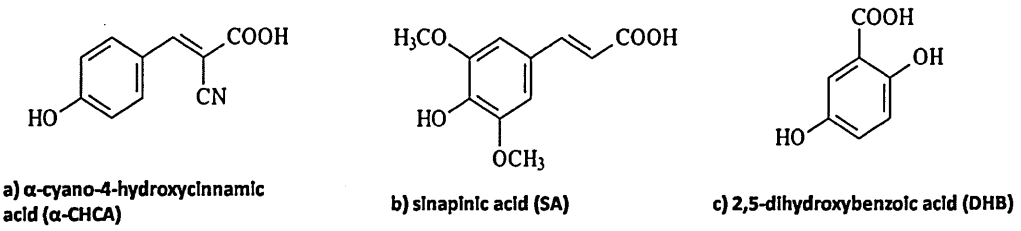

a) α-cyano-4-hydroxycinnamic acid (α-CHCA) b) sinapinic acid (SA) c) 2,5-dihydroxybenzoic acid (DHB)

Figure 1.7: **Molecular structures of commonly used UV-MALDI matrices.** These matrices are derivatives of benzoic acid.

1.2.1.2 Mass analysers

Ions produced in the ion source are then separated in the mass analyser. There are several types of mass analyser, including quadrupole, quadrupole ion traps, time-of-flight (TOF), magnetic sectors and Fourier transform. These mass analysers present different features including the upper mass limit, the ion transmission and the resolution. Hence, the compatibility of the analyser with the ionisation method may vary.

1.2.1.2.1 *Quadrupole mass analysers*

Quadrupole mass analysers consist of four hyperbolic rods. In a quadrupole (Q) mass analyser, the separation of the ions according to their m/z is based on the stability of their trajectories in an oscillating electric field applied to the rods [80]. Figure 1.8 displays a schematic description of a quadrupole mass analyser. The rod pairs are electrically connected together: a radio frequency (RF) voltage is applied to a rod pair while a direct current field is applied to the other rod pair. The stability of the ion trajectories within the rods is used for their separation. Quadrupole analysers usually show excellent selectivity, however they present a mass range limitation as well as low resolution.

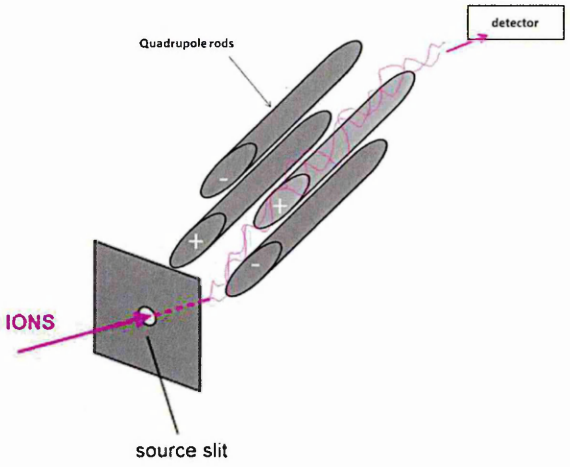

Figure 1.8: **Schematic of a quadrupole mass analyser** (adapted from [80]). Quadrupole analysers are made up of four hyperbolic rods. Ions oscillate in the electric field created by the rods. The stability of the ion trajectories within the rods is used for their separation.

1.2.1.2.2 *Time-of-flight mass analyser*

Time-of-flight (TOF) mass analysers are commonly used with MALDI because of the pulsed nature of the laser desorption ionisation and provide excellent m/z resolution, accurate mass capabilities and can operate at high repetition rates [80]. In TOF analysers, ions are separated in time, based on their velocity after being accelerated in a field-free tube between the source and the detector. TOF instruments can be used in a linear or reflector mode.

In linear mode, desorbed ions are accelerated into the TOF tube at a specific electric field and are allowed to fly a distance (d) which is fixed by the TOF tube length. Figure 1.9 displays a schematic diagram of the principle of a linear TOF instrument.

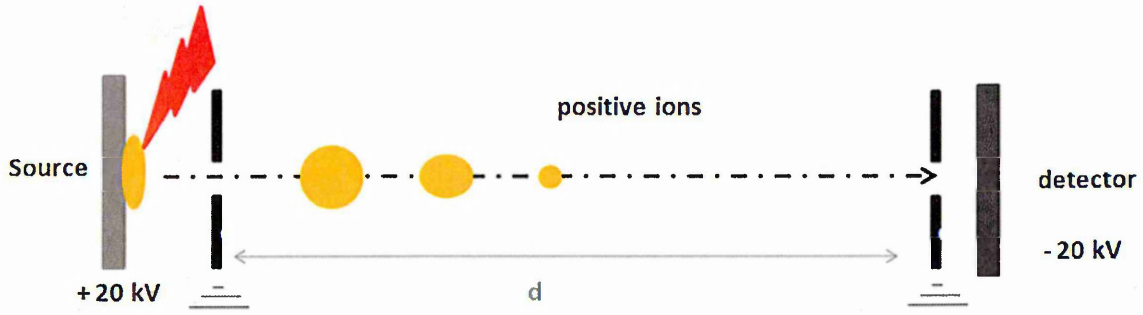

Figure 1.9: **Schematic of a time-of-flight mass analyser operating in linear mode** (adapted from [80]).
Ions are separated in time, based on their velocities in a field free time-of-flight tube and are finally detected by an ion detector. The time each ion takes to travel through the mass spectrometer is measured precisely.

The kinetic energy of a given ion (E) is defined by the equation 1.1, where V is the accelerating potential and q the total charge of the ion.

$$E = \frac{1}{2}mv^2 = qV = zeV \tag{1.1}$$

It is possible to correlate the m/z of a given ion to the time (t) needed to drift through a fixed distance (d) before reaching the detector, by the following equation:

$$t^2 = \frac{m}{z}\left(\frac{d^2}{2Ve}\right) \tag{1.2}$$

The advantages of TOF analysers include the fast, sequential detection of all the ions with differing flight time and mass. Therefore, they provide high transmission of the generated ions and hence an improved sensitivity. High molecular weight compounds including proteins, monoclonal antibodies and polymers with a m/z above 300 kDa and present at low concentration have been detected using TOF mass analysers operating in linear mode [79, 83]. However, low mass resolution can usually be observed in linear mode. Low mass resolution can result from a variety of factors including the spread in the initial average velocity of ions produced in the ion source. It is common to improve the resolution by introducing a delayed pulse extraction. The delayed time extraction consists of introducing a short time delay between the ionisation and the ion extraction in order to compensate the spread in the distribution of the initial kinetic energy of the

ions leaving the source. In the case of MALDI ion sources, this allows the ion plume to further expand before the extraction. Therefore, by adjusting the delay time and pulsed voltage, ions with the same m/z and different kinetic energy leaving the source will eventually reach the detector at the same time.

TOF analysers can also be used in reflector mode in order to improve the mass resolution. It involves the use of grids which are in a constant electric field and act as mirrors to compensate the kinetic energy spread between ions leaving the source by reflecting them back along the flight tube prior to detection. More energetic ions will penetrate deeper into the grid, while ions with the same m/z and less kinetic energy will have a shorter path back along the tube. As a result, both ions will eventually reach the detector at the same time. Figure 1.10 displays a schematic diagram of the principle of a reflector TOF mass analyser. Using a TOF analyser in reflector mode has been found to increase the mass resolution, however a loss of sensitivity as well as a mass limitation are observed [80, 84]. Peptides, lipids and small molecules are usually analysed in reflector mode.

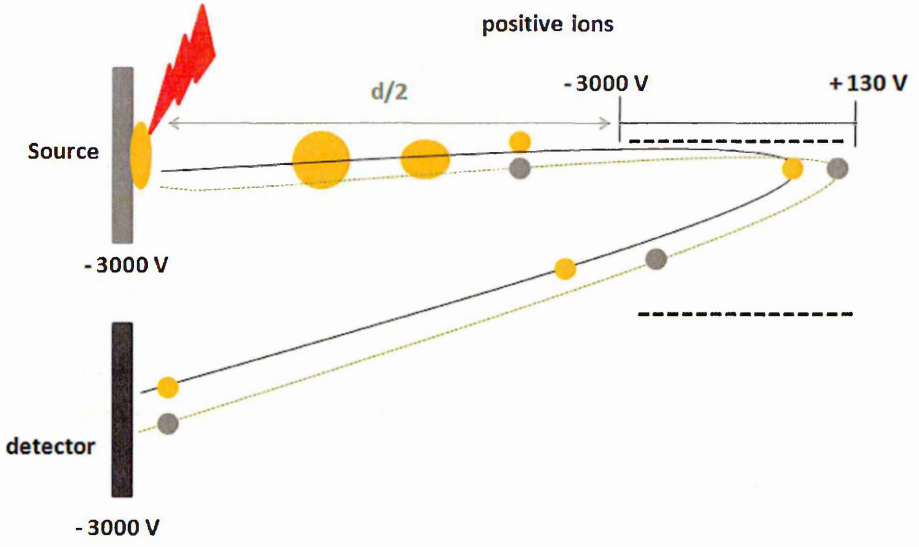

Figure 1.10: **Schematic of a time-of-flight mass analyser operating in reflector mode** (adapted from [80]).
The energy dispersion of two isobaric ions leaving the source is corrected in the reflector. The ion with a higher kinetic energy will spend more time in the reflector compared to the one with a lower kinetic energy, so that both ions will reach the detector at the same time.

1.2.1.2.3 *Tandem mass spectrometry (MS/MS)*

Tandem mass spectrometry (MS/MS) consists of selecting a particular ion of a compound present in the sample to be analysed for fragmentation purposes in order to determine its structure or other properties. MS/MS can be achieved within field-free regions of the analyser with respect that the selected ion has sufficient energy to dissociate [80, 84, 85]. Another way to perform MS/MS consists of applying collisions with neutral gas; this is often called collision-induced dissociation (CID). Two mass analysers can therefore be coupled together. The two analysers are separated with a collision cell, where an inert gas is used to collide with the selected ions and produce fragmentation.

Quadrupole and TOF mass analysers are often coupled together, hence resulting in a QqTOF hybrid instrument, where q represents a radio frequency (RF)-only quadrupole and is used as a collision cell. Figure 1.11 displays a schematic diagram of a QqTOF hybrid instrument. In a QqTOF instrument, the m/z of a precursor ion may be specifically selected in the quadrupole analyser followed by collision-induced dissociation (CID) in the collision cell. The product ions are further analysed in the TOF which enhances the sensitivity and improves the S/N. QqTOF instruments have been reported to improve the resolution and the mass accuracy [85]. However a mass range limitation is often observed.

Peptides produced after enzymatic protein digestion are usually fragmented by MS/MS. The peptide sequence obtained by MS/MS can be used for protein identification using database search [80].

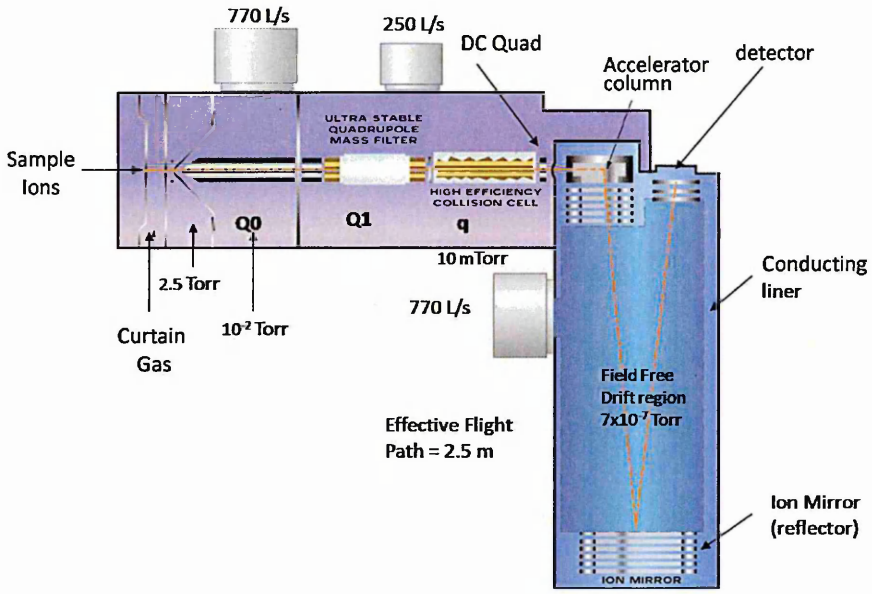

Figure 1.11: **Schematic diagram of an Applied Biosystems Q-Star® Pulsar *i* QqTOF instrument.**

1.2.2 Ion mobility separation and mass spectrometry

1.2.2.1 Ion mobility separation/MALDI-TOF MS

Ion mobility separation (IMS) is a technique which permits gas-phase separations of ion packets based on their structural and conformational properties. In IMS, ions are separated according to their velocity based on their collision cross-section (Ω), as they drift through an inert gas following application of a weak electric field [86, 87]. Gas-phase collision cross-section values can be obtained with the following equation [86]:

$$\Omega = \frac{3ze}{16N}\left[\frac{2\pi}{\mu k_b T}\right]^{0.5}\frac{1}{K_0} \tag{1.3}$$

where variables are as followed: N represents the background gas number density, ze the ionic charge, μ is the reduced mass of the ion-neutral pair, k_b is the Boltzmann's constant, T the gas temperature and K_0 is the mobility corrected to 273.2 K and 760 Torr.

Several improvements made in IMS technologies have been reported, including changes in geometries and devices, such as the use of an ion trap for ion accumulation and ejec-

tion into the drift tube as well as reducing the radial ion diffusion, in order to achieve a better combination of IMS with mass spectrometry [88]. This has been shown to allow fast detection and characterisation of structural and conformational properties of compounds contained in a complex mixture.

The use of MALDI-TOF MS, especially orthogonal MALDI-TOF MS (o-TOF MS) geometry, combined with IMS has been demonstrated for fast separation of compounds, including proteins, peptides, lipids and small molecules present in complex matrices, while maintaining good mass spectral data quality as well as improved sensitivity [88–90]. This is very beneficial as sample purification by means of LC/MS and 2-DE separation techniques are not required. Small deviations observed in compound collision cross-sections generate differences in mobility drift time, hence specific separation and characterisation of the given analytes.

Recent improvements in IMS/o-TOF MS instrument designs have been shown to improve the signal transmission and separation power of IMS-MS [91]. This is discussed in detail below.

1.2.2.2 Travelling wave IMS/oa-TOF MS technology: MALDI SYNAPT^{TM} HDMS system

The use of a travelling wave system incorporated into IMS combined with an orthogonal axial-TOF MS (oa-TOF MS) geometry has been described [91]. Here, the ion transmission and ion mobility separation power is increased using travelling wave technologies in the radio frequency (RF) ion guide chambers and the IMS cell. Figure 1.12 displays a schematic diagram of the MALDI SYNAPT^{TM} HDMS system, which has been used in the work described in this thesis (chapters 3, 4, 5 and 6).

In the travelling wave ion guide compartment (T-wave ion guide, see figure 1.12), ions are driven to the IMS cell by applying continuous sequence waves throughout the RF electrodes at regular time intervals. This aims to reduce the travel time of the ions to the IMS cell [92]. The travelling wave IMS (TWIMS) compartment consists of 61 electrode pairs and is composed of 3 components, including a trap, an IMS and a transfer cell [91]. The IMS cell is placed between the trap and transfer compartments,

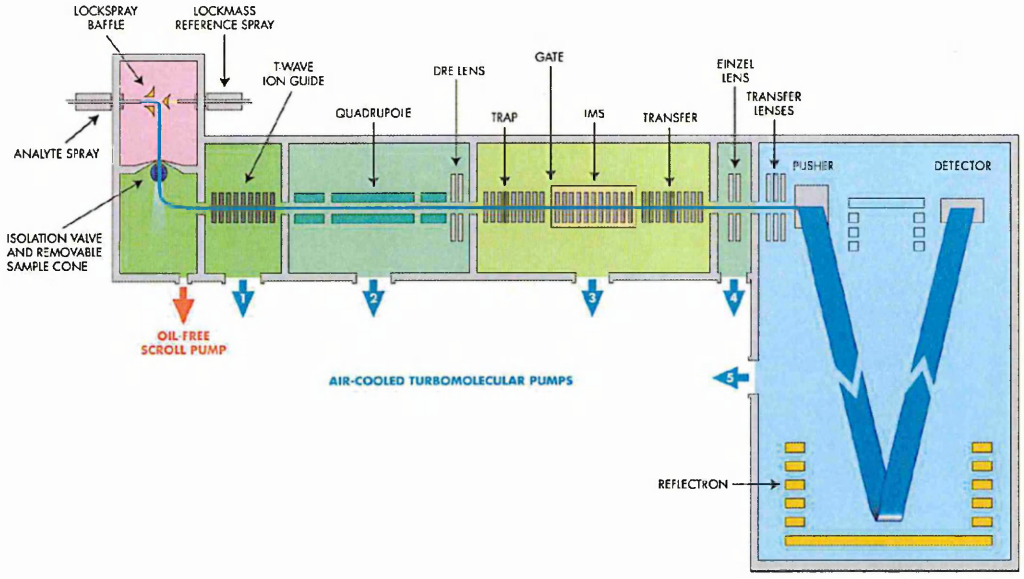

Figure 1.12: **Schematic diagram of the MALDI SYNAPT^{TM}HDMS system** [91] (reproduced with permission from Elsevier publisher).

which are composed of 33 electrode pairs with RF applied and are 100 mm long. The last RF electrode of the trap cell acts as an ion gate operating at a modulated voltage, hence creating continuous ejection of ions into the IMS cell. Once in the IMS cell, ions are subjected to travelling waves at moderate pressures which allow mobility-based separation. That is, high mobility ions are transported at a faster speed than low mobility ions throughout the waves. Travelling waves are still applied in the transfer cell in order to maintain the mobility separation of the ions.

The use of an oa-TOF MS geometry has been found to provide fast data acquisition since the MS is synchronised with the ejection of ions from the T-wave ion guide cell to the IMS cell [93]. Such an approach offers promise for the IMS-MS analyses of complex mixtures [94] and also the possibility of identifying proteins directly from such matrices with no requirement for sample purification. Different types of MS/MS experiments can be performed using such a technology. Ions can be collisionally dissociated in either or both the trap and transfer chambers, while maintaining the mobility information of the parent and product ions [91].

1.2.3 Protein analysis by mass spectrometry

Mass spectrometry is a technology of choice for proteomics studies [95, 96]. It allows the accurate determination of protein molecular weights as well as protein identifications via tandem mass spectrometry (MS/MS) [97–99]. Even more desirable is the detection and identification of low abundance proteins present in a given sample. Mass spectrometry has been shown to allow the characterisation of proteins at concentrations in the low subpicomole range [100, 101]. Several separation techniques may be coupled with MS in order to perform purification steps prior to protein characterisation with MS. Among them, two-dimensional gel electrophoresis (2D-gel or 2D-PAGE) and liquid chromatography (LC) are the most commonly used.

1.2.3.1 Two-dimensional gel electrophoresis

Two-dimensional gel electrophoresis (2-DE) is a technique widely used for protein separation and purification prior to MS. It allows protein separation in a two-dimensional gel. This is based on the isoelectric point of the proteins in one dimension and on their molecular weight in the other dimension. Studies have described the use of 2-DE for the evaluation of protein extracts from complex mixtures such as cells and tissue samples [102, 103]. Differences between samples can be evaluated and relative quantification of protein ratios between independent gels can be performed [103, 104].

Combining 2-DE with MALDI-TOF mass spectrometry has become popular as it allows the analysis and identification of small amounts of proteins isolated from the gel spots [101, 105, 106]. The strategy commonly used is described in figure 1.13 [80]. The method is based on the comparison of data obtained by mass spectrometry analysis with those stored in a database. The sensitivity and mass accuracy of mass spectrometry allow a rapid identification of numerous protein candidates contained in a given sample. Several studies have reported the identification of protein cancer biomarkers using 2-DE separation coupled to MALDI-TOFMS [107]. However, 2-DE methods have limited sensitivity and reproducibility compared to liquid chromatography-tandem mass spectrometry (LC-MS/MS) approaches [108].

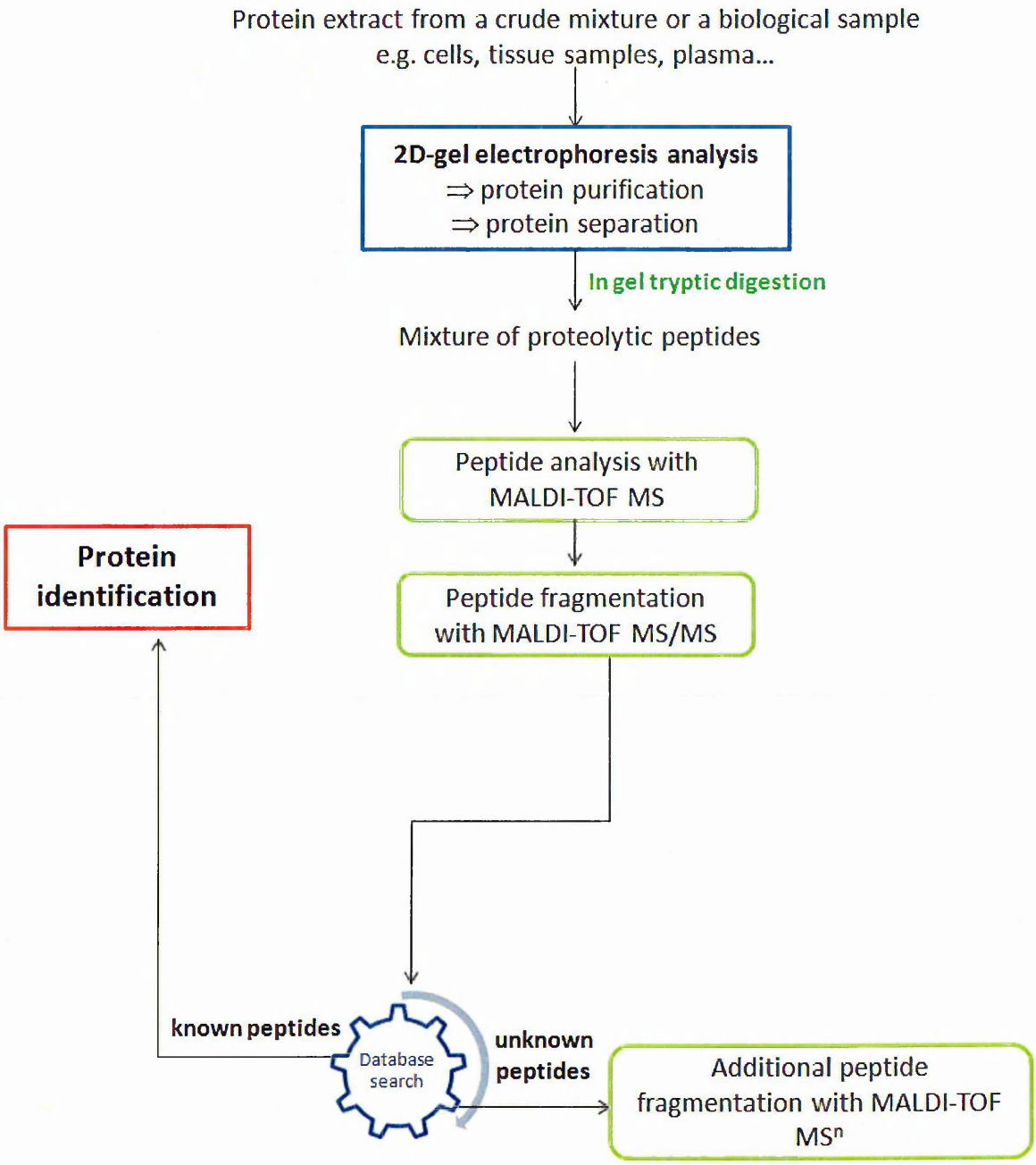

Figure 1.13: **Schematic workflow commonly used for the identification of protein using 2-DE combined with mass spectrometry**. (adapted from [80])
This method allows the purification and separation of protein extracts from crude mixtures using 2-DE. Protein identification can be performed using the intact protein masses determined by mass spectrometry. However in most cases, in-gel tryptic digestion is performed followed by peptide analysis with mass spectrometry. A peptide mass fingerprint database search is either achieved for protein identification or sequencing MS analyses are carried out in order to fully identify the protein of interest.

1.2.3.2 Liquid chromatography-tandem mass spectrometry

Reversed phase liquid chromatography coupled to tandem mass spectrometry is another technique widely used to purify, concentrate, separate and identify peptides obtained after enzymatic digestion of proteins extracted from complex mixtures [109–112]. LC-MS/MS systems comprise conventional high performance liquid chromatography (HPLC) columns and pumps coupled to a tandem mass spectrometer. Briefly, peptide mixtures are separated by liquid chromatography prior to electrospray ionisation and MS/MS analysis. Rapid screening and identification of peptides present in a given sample can be achieved. Several studies have described the use of LC-MS/MS to enhance the separation and identification of proteins present in various types of samples, including cells, tissues and plasma [113, 114]. It can also be used to discriminate between healthy and cancerous tissue samples [115]. The use of LC-MS/MS has also been shown to improve the detection and identification of protein present at low abundance in crude mixtures [101].

Both 2-DE and LC-MS/MS techniques are powerful methods to study the proteome of a given sample as they not only allow the separation and identification of proteins but also discrimination between diseased and healthy samples. However information regarding the spatial localisation of protein biomarkers within tissue samples is lost. The ability to detect, identify and study the distribution of protein biomarkers within tumour tissue sections in a single experiment is of significant interest to improve the understanding of tumour biology and to help enhance clinical diagnostics and prognostics.

1.3 Mass Spectrometry Imaging

Direct molecular analysis of biological tissues is a method of choice for better understanding of tumour processes but it is extremely challenging. *In vivo* molecular imaging techniques, such as magnetic resonance imaging (MRI) and near-infra red or fluorescence imaging, are typically used to detect high level targeted analytes within the tissue, however these techniques are often time consuming and are limited when investigating unknown compounds. Immunohistochemistry (IHC) staining is a method commonly used to study the spatial distribution and expression of proteins within tissue sections, however this technique is limited as it requires a specific known target, as well as a specific antibody.

Mass spectrometry imaging techniques are useful tools that can be used to map the distribution of several compound classes including proteins, lipids, drugs and small molecules directly in tissue sections with no requirement of pre-defined targets. This provides molecular information in many areas of biological research and creates new fundamental research opportunities in several fields. In this section, insights into mass spectrometry imaging techniques, with an emphasis on MALDI-mass spectrometry imaging (MALDI-MSI) for the investigation of proteins within tumour tissue sections, will be given.

1.3.1 Secondary ion mass spectrometry imaging

Secondary ion mass spectrometry (SIMS) was one of the first techniques used for imaging mass spectrometry, yielding two-dimensional ion density images from thin biological tissue sections [116]. In SIMS, a pulsed ion beam up to 30 keV, usually Cs^+ or Ga^+, is used to bombard a sample, thus initiating the desorption process. The primary ion beam can be focused on a tissue sample surface to spot sizes as small as 10 nm in diameter, although they are usually operated with a spot size of 0.130 μm diameter, and ion images at specific m/z ratios are generated. Using the SIMS imaging technique, high resolution images of compound distribution at the cellular level within tissue samples can be generated [117].

SIMS has been found to be suitable for the analysis of inorganic low molecular weight compounds such as metals and cations, but the technique has been found to be limited in terms of sensitivity for the investigation of organic molecules such as proteins [118]. However, biological tissue sections, including kidney tissue sections, have been analysed and imaged using SIMS technology [119].

Improvements in SIMS methodologies, including matrix enhanced SIMS, have been found to increase the ionisation and sensitivity for the detection of low molecular weight peptides and proteins (typically $m/z < 20000$) [117, 120]. A further improvement consisted of coating the tissue section surface with a thin layer of metal prior to analysis. This aims to enhance the signal intensity of several biomolecules such as lipids and fatty acids [121]. The resulting ion peaks are often observed as metal adducts and may be difficult to interpret in some cases, however improved image sensitivity was achieved.

1.3.2 MALDI-mass spectrometry imaging

MALDI-mass spectrometry imaging (MALDI-MSI) is a technique which combines the high efficiency of MALDI-MS in providing structural information of compounds present in a biological tissue section while giving information related to their spatial localisation within the tissue section [122, 123]. Briefly, tissue sections obtained from frozen or archived samples are first uniformly coated with a MALDI matrix which aims to crystallise with the surface compounds to be analysed. Then, multiple single mass spectra are acquired across the tissue section at a spatial resolution predefined by the operator and the instrument capacity by irradiating the coated tissue sections with very short laser pulses. These mass spectra are then processed together using imaging software in order to generate ion density maps which represent the spatial distribution of a given analyte within the tissue section with its relative abundance or intensity. This provides a visualisation of the localisation of each specific analyte within the tissue section in a two-dimensional (2-D) molecular intensity or heat map. The acquisition of series of 2-D molecular images using consecutive serial tissue sections can also be used to reconstruct 3-D volumetric localisation of the compounds of interest within the tissue sample being analysed [124–126].

MALDI-MSI is rapidly becoming a powerful technology for studying the distribution and for the *in situ* identification of several classes of compounds including proteins, peptides, lipids, drugs and other small molecules directly within biological tissue sections [127]. It may hence provide and create new fundamental and translational research opportunities in various fields including cancer biomarker discovery as well as tumour classification systems.

1.3.2.1 Tissue sample preparation prior to matrix application

MALDI-MS imaging of frozen and formalin fixed paraffin embedded (FFPE) tissue sections has been reported for the *in situ* investigation of proteins and peptides [128]. Depending on the type of tissue sample being analysed, appropriate tissue sample preparation is required. Various work has been performed in order to develop standard protocols and methodologies for tissue preparation, including tissue sample collection, tissue sectioning, washing protocols and chemical pre-treatments, such as on-tissue digestion, prior to matrix deposition [129, 130].

1.3.2.1.1 *Tissue sample collection and handling*

Tissue collection is an important step for MALDI-MSI experiments. Since protein and peptide profile patterns and localisation within the tissue sample reflect changes occurring during disease progression, degradation of tissue samples during collection may affect considerably the expression and distribution of proteins/peptides within the tissue section. Tissue samples must be carefully surgically removed in order to maintain the native shape of the tissue as well as the integrity of the spatial arrangement of compounds present in the tissue sample and also avoid compound degradation [129].

Immediately after removal, fresh tissue samples may be snap-frozen in liquid nitrogen or fixed in formalin. Most studies report the use of frozen tissue sections for MALDI-MSI analysis. Tissue samples are frozen by first loosely wrapping the sample in aluminium foil (this may be optional, however the foil acts to stabilize more malleable tissues as well as to inhibit tissue adhesion to the sides of the liquid nitrogen dewar) and by then gently freezing in liquid nitrogen [129, 131]. Another method, which has been applied in the work reported in this thesis, consists of gently immersing the tissue in a beaker containing isopentane, which has been previously immersed in liquid nitrogen. The

snap-frozen tissues may remain stored at -80°C for at least a year with no significant degradation [131].

Formalin fixation paraffin embedding is the most convenient method commonly used to conserve tissue samples for study by pathologists in clinical practice. The formalin fixative creates protein cross-linking via methylene bridges, hence formalin fixed paraffin embedded (FFPE) tissue samples can be stored over many years. This creates a huge sample bank for clinical use. The analysis of FFPE tissue sections by MALDI-MSI is achieved after performing on-tissue enzymatic digestion, which will be discussed in another section (section 1.3.2.1.4).

1.3.2.1.2 *Tissue sectioning*

Thin tissue sections are cut at about -15 to -20°C using a cryostat (the optimum cutting temperature depends on the tissue type being analysed) followed by mounting onto either a conductive MALDI target plate or histological glass slides. The tissue section thickness has been shown to affect the observed MS signal sensitivity [129]. For MALDI MS analysis of mammalian tissues, an optimum tissue section thickness is between 5 and 20 μm, depending on the tissue sample type as well as the analysis to be performed.

The tissue sample is maintained on the cryostat cutting block using a medium such as an optimum cutting temperature polymer(OCT). However, one should avoid contact between the OCT and the surface of the tissue to be sectioned. The presence of OCT inhibits ion formation in MALDI MS analysis. The use of carboxymethylcellulose (CMC) has also been reported for embedding tissue samples prior to sectioning [132]. Here, no signal inhibition was observed in the MALDI-MSI analysis.

1.3.2.1.3 *Tissue washing methods*

Following tissue sectioning, washing steps are usually performed in order to remove residual salts, small molecules and lipids present in the tissue sections, which can either interfere with proteins/peptides by forming adducts or inhibit or suppress protein signals in the obtained mass spectra. Several protocols have described the use of a series of ethanol solutions, typically from 70 to 95 %, for washing tissue sections [129, 133, 134]. This process aims to enhance the matrix co-crystallisation process onto the tissue section, hence resulting in improved direct MALDI-MS profiling and imaging data quality

[130].

The use of organic solvents such as chloroform and xylene has also been successfully reported as an efficient washing method for tissue sections [135]. Rinsing tissue sections with such solvents aims to decrease the lipid content present in the tissue sections and improve protein detection.

1.3.2.1.4 *On-tissue enzymatic digestion and specific MALDI imaging*

MALDI-MSI allows the detection and localisation of proteins from tissue sections, however the sensitivity for protein signal detection is usually limited to 30-40 kDa. On-tissue (*in situ*) enzymatic digestion is a sample pre-treatment which has been found to considerably increase the amount of protein information obtained by direct MALDI-MSI analysis [136–138]. It can be used to improve the detection of some proteins which are not detected by direct MALDI-MSI analysis due to either their molecular weight or their low abundance in tissue samples. Using on-tissue digestion as a sample pre-treatment has been reported for the study of protein distribution and identification within FFPE tissue sections with MALDI-MSI [137, 139], and hence provides new methodologies for retrieving proteomic information directly from archived tissue sections. Another advantage of such a methodology is that protein identification can be correlated with observed protein distribution within the tissue section. This is achieved by performing peptide MS/MS fragmentation directly within tissue sections, thus allowing the identification of proteins [140].

Specific MALDI-MS imaging has also been reported for more targeted approaches for biomarker identification within tissue sections [141, 142]. This sample pre-treatment methodology is referred to as *Tag-Mass Specific MALDI-MSI*. Briefly, it is based on indirect detection of a probe (such as oligonucleotide and antibody) via an indicator called Tag-Mass added to the probe. The Tag-Mass consists of a photocleavable linker, that has a specific absorption band close to that of MALDI lasers (i.e. 337-355 nm), and which is attached to a tag of known mass which can be detected by MALDI-MSI. Figure 1.14 displays a description of the Tag-Mass concept. This forms photocleavable linker tagged oligonucleotide or secondary antibody probes which are deposited onto the tissue section and followed by *in situ* hybridisation of the tag-Mass probe for specific MALDI-MSI of mRNA and proteins within the tissue sections. MALDI-MSI analysis is

then performed, leading to the detection of the tags, which provides a localisation and relative abundance of mRNAs or proteins, thus yielding a specific unique signature for the probed molecules.

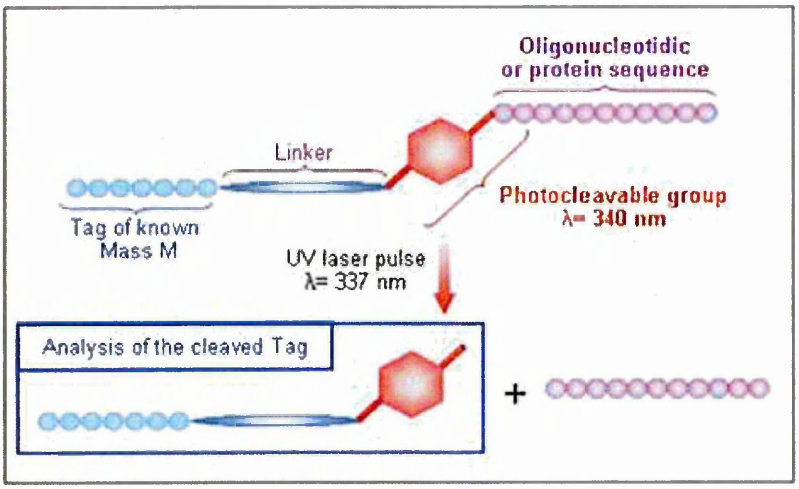

Figure 1.14: **Schematic of the photocleavable linker/tag system or Tag-Mass for used indirect detection of mRNA and proteins after photo-dissociation under the MALDI UV laser wavelength** [141].
The Tag-Mass is a photocleavable linker tagged oligonucleotide or secondary antibody probe and can hybridises to its complementary mRNA sequences or attaches to the target proteins. Then, the linker is photocleaved after MALDI laser irradiation, thus inducing tag release and leading to the characteristic signal of the tag in the resulting mass spectrum.

1.3.2.2 Matrices and matrix deposition

Sample pre-treatment methodologies, such as on-tissue digestion or Tag-Mass Specific MALDI-MSI, may enhance the signal detected as well as the observed sensitivity and specificity of the technique. However, the choice of the matrix and the matrix deposition method are of great importance in obtaining high-quality spectra directly from thin tissue sections as well as keeping intact the spatial integrity of compound distribution within the tissue surface.

1.3.2.2.1 *Matrices used for MALDI-MSI*

Several MALDI matrices are available, depending on the target analyte. Derivatives of benzoic acid, cinnamic acid and related aromatic compounds, have all been found to be good MALDI matrices for proteins and peptides. Sinapinic acid, 3,5-dimethoxy-

4-hydroxycinnamic acid (SA), is routinely used for higher molecular weight proteins, whereas α-cyano-4-hydroxycinnamic acid (α-CHCA) is commonly used for low molecular weight peptides species [129]. The matrix solution concentration used is also a factor to take into account for direct tissue analysis with MALDI-MSI, since it allows an optimal crystal coverage as well as an improved mass spectral signal quality. In addition, many matrix/solvent combinations can be used, thus allowing improved spectral signals in terms of protein profiling and imaging. 50:50 acetonitrile/water and ethanol/water have been found to be good solvent combinations, providing good results for a variety of tissues analysed by MALDI-MSI [131].

The use of solid ionic matrices has also been reported for direct analysis of tissue sections with MALDI-MSI [135]. Ionic MALDI matrices are formed following an acid/base reaction, by coupling ionic liquids with UV-MALDI matrices, hence yielding improved matrix solutions as well as mass spectral quality and signal sensitivity [143]. Coupling common UV-MALDI matrices, such as α-CHCA and SA, with aniline or dimethylaniline derivatives has significantly improved signal intensities and enhanced the sensitivity for MALDI-MS profiling and imaging of proteins and peptides directly within tissue sections [135, 137].

1.3.2.2.2 *Matrix deposition methods*

Matrix deposition onto the tissue section also represents an important step of the sample preparation carried out prior to MALDI-MSI analysis as it affects the reproducibility of the methodology as well as the spectral quality and spatial resolution that can be achieved. Several methods for matrix deposition, including manual and robotic methods, have been described [136, 137, 144].

Matrix solutions can be spotted onto the tissue section using an automatic pipette. This methodology is commonly used for direct MALDI-MS profiling experiments [131, 145]. Robotic devices allow the deposition of microdroplets onto the tissue section, yielding accurate spot arrays of matrix solutions and other reagents, such as enzyme, onto the tissue section. This has been found to improve the reproducibility as well as data quality obtained with MALDI-MS imaging analyses [144, 146]. However the inter spot distance can be a limiting factor for MALDI-MS imaging spatial resolution.

Spraying methods are also commonly used to achieve good matrix coverage onto tissue sections using airbrush devices [147]. This allows an even matrix coating onto tissue sections, however, compound delocalisation can be observed in some cases. Automatic spraying instruments are also commercially available, hence producing a homogenous thin layer of matrix and/or proteases on the tissue sections [148].

1.3.2.3 Data acquisition

Two modes of data acquisition are used in MALDI-MSI: **profiling** and **imaging**. Figure 1.15 displays a schematic description of data acquisition modes.

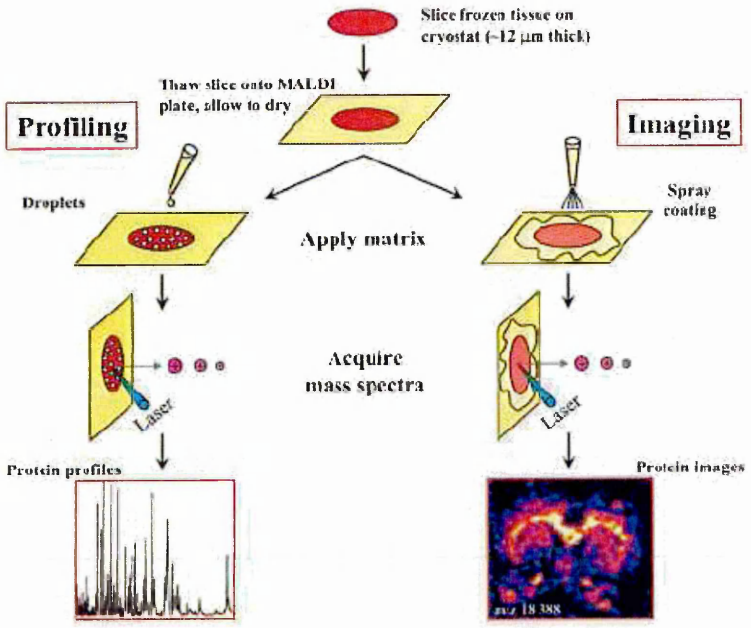

Figure 1.15: **Schematic description of MALDI-MS profiling and imaging analysis** [149].

The aim of the profiling experiment is to obtain a relatively quick characterisation of the biological compound content within a tissue section as well as comparing their patterns from a discrete number of spots. Matrix is applied as droplets (spots) on the tissue, by using either an automatic pipette (200 nL to 500 nL droplets) or an automated spotter. MS analysis is then performed on each individual matrix droplet by summing 200 or more consecutive laser shots taken across the droplet surface, thus generating a mass spectrum. However, because of the MALDI TOF mass spectrometer limitations in detecting higher molecular weight compounds, most of the detected signals are below m/z 40000 Da. Furthermore, most intense signals result from soluble and abundant compound species.

In an imaging experiment, the laser can probe the tissue in a raster and thousands of spots can produce an array, with each spot corresponding to a full mass spectrum. An image is then constructed from a selected m/z value by integrating the corresponding signal intensity. Mass spectrometry images can be acquired either in microprobe or microscope mode. Each of these modes has its advantages and limitations.

1.3.2.3.1 *Microprobe mode*

The microprobe mode is the most commonly used for MALDI-MS imaging data acquisition [150, 151]. It involves a correlation between mass spectra and the position on the sample where they are acquired. A focused laser spot allows acquisition of several mass spectra corresponding to the spatial coordinates of the region of the sample being analysed. Molecular ion images are generated by collecting mass spectra using a spot-to-spot laser raster across the tissue section and reconstructed from the obtained mass spectra once the imaging experiment is completed. Therefore, the spatial resolution achievable in microprobe mode is strongly related to the laser irradiation spot size, typically 25-150 μm depending on the instrument.

1.3.2.3.2 *Microscope mode*

Another way to acquire mass spectrometric images is by operating in microscope mode [152]. The microscope imaging mode involves the use of an ion-optical microscope. In this case, all information gained within the ionised sample region is projected onto a position-sensitive detector. The spatial resolution of the molecular images depends on the microscope magnification, the ion-optics and the resolution of the detector.

1.3.2.4 Instrumentation

MALDI-MSI allows the examination of several molecules, especially proteins and peptides, directly from tissue sections. This makes the technique a valuable and promising tool in biomedical and clinical research fields. Several improvements in MALDI-MSI instrumentation are currently being made in order to improve spatial resolution, mass resolution as well as data acquisition time. This includes development of new laser technologies and mass analysers.

1.3.2.4.1 *Lasers*

The laser is a key factor in MALDI-MSI experiments [153], since it affects the amount of ions generated in the source, the spatial resolution as well as the data acquisition time. The laser beam commonly used in MALDI-MSI analysis is between 100 and 150 μm in diameter. Since MALDI-MS imaging analyses are usually acquired in microprobe mode, the spatial resolution in the observed images is limited by the laser beam spot size. However, methods aiming to improve MALDI-MS image spatial resolution have been developed and consist of either reducing the laser spot size [118, 154] or oversampling methodologies [155], the latest consists of obtaining data in such a way that the distance between points on the sample is smaller than the size of the focused spot. Unfortunately, limitations associated with signal sensitivity and analysed mass range were also observed. The microscope imaging mode has also been used to improve the image spatial resolution, however less molecules are desorbed when the resolution is less than about 10 nm [152].

High resolution MALDI-MS images are also associated with long data acquisition times. Common standard nitrogen (N_2) lasers are being replaced by solid-state lasers, which present a high repetition rate, for MALDI-MS profiling and imaging experiments. High-repetition rate solid-state lasers have been found to enhance mass spectral quality and signal sensitivity [156]. The use of 1 kHz repetition rate Nd:YAG (neodymium-doped yttrium aluminium garnet; Nd:$Y_3Al_5O_{12}$) lasers for MALDI-MS imaging produced improved signal intensity and sensitivity as well as decreased data acquisition time [156–158].

1.3.2.4.2 *Mass analysers*

A variety of mass analysers have been used for MALDI-MSI. Among them TOF, TOF/TOF and QqTOF are the most used [159]. MALDI-TOFMSI has been found to provide both acceptable mass accuracy and spectral resolution power [160].

The use of Fourier-transform ion cyclotron resonance (FT-ICR) for MS imaging has produced high spectral quality in terms of achieved spectral resolution and MS^n analyses [160]. However, long data acquisition times may be associated with such methodologies.

1.3.2.5 MALDI-MSI applications

Several studies have reported the successful use of MALDI-MSI to map protein and peptide distribution within biological tissue sections and tumour biopsies [145, 161]. This provided the localisation of tumour regions within tissue sections and the study of protein expressions associated with tumour grade and stage. Therefore this demonstrates the possibility of using the technique for high-throughput protein analysis [140] and generating tumour subclassification as well as predicting clinical outcome.

The potential of the technique has also been demonstrated for the analysis of drug distribution within tissue and whole body rat tissue sections with no requirement for labeled analytes [162]. This presents huge benefits for drug metabolism and pharmacokinetic (DMPK) studies in terms of cost and time of analysis.

The use of IMS combined with MALDI-MSI is a very promising approach as it brings another dimension of separation and may generate less complex mass spectral data than conventional MALDI-MSI. Ion mobility separation between proteins, peptides, lipids and small molecules can be achieved prior to direct MALDI-MS characterisation, hence resulting in more specific and sensitive data imaging information [117, 132, 163].

The use of on-tissue enzymatic digestion has been found to produce complex mass spectral data where numerous signals are observed in the mass range m/z 800-3000 [163]. Another benefit of such a technology is the use of IMS-MS/MS analysis for specific and sensitive *in situ* identification of peptides/proteins resulting from on-tissue digestion.

More detailed reviews of the applications of MALDI-MSI are given in the introduction sections of chapters 2, 3, 4, 5, 6 and 7.

1.4 Aims of the Study

The need for protein biomarkers to improve early detection, diagnosis and prognosis of cancer diseases is of importance, since this can help in tumour classification and the development of targeted approaches for therapeutic treatments. Such aims require powerful, reproducible and robust tools and technologies that can provide insights into the molecular organisation of the tumour micro environment, localise and identify proteins and protein interactions as well as allow high-throughput analysis. MALDI-MSI is a technology which has a huge potential as a translational research technology for cancer biomarker discovery [164].

The aims of the study reported in this thesis are firstly to develop and improve efficient methodologies for the study of protein distribution and identification directly within both frozen and FFPE tumour tissue sections.

These methodologies were further applied to examine a range of tumour samples but in particular to identify and study the distribution of proteins significantly associated with the UPR within FFPE adenocarcinoma tissue sections.

The methodologies developed in this study aimed also to explore other complex molecular processes occurring within the tumour micro-environment, including hypoxia, and to achieve high-throughput protein analysis within tumour tissue sections in order to design tumour classification models.

References

[1] World Health Organisation. Cancer. *Cancer Facts and Figures*, 2009.

[2] Croce C.M. Oncogenes and cancer. *New England Journal of Medicine*, 358:502–411, 2008.

[3] Capon D.J., Chen E.Y., Levinson A.D., Seeburg P.H., and Goeddel D.V. Complete nucleotide sequences of the T24 human bladder carcinoma oncogene and its normal homologue. *Nature*, 302:33–37, 1983.

[4] McCoy M.S., Toole J.J., Cunningham J.M., Chang E.H., Lowy D.R., and Weinberg R.A. Characterization of a human colon/lung carcinoma oncogene. *Nature*, 302: 79–81, 1983.

[5] Shaulian E. and Karin M. AP-1 in cell proliferation and survival. *Oncogene*, 20: 2390–2400, 2001.

[6] Ohta M., Inoue H., Cotticelli M.G., Kastury K., Baffa R., Palazzo J., Siprashvili Z., Mori M., McCue P., Druck T., Croce C.M., and Huebner K. The FHIT gene, spanning the chromosome 3p14.2 fragile site and renal carcinoma-associated t(3;8) breakpoint, is abnormal in digestive tract cancers. *Cell*, 84:587–597, 1996.

[7] Milsom C.C., Yu J.L., Mackman N., Micallef J., Anderson G.M., Guha A., and Rak J.W. Tissue factor regulation by epidermal growth factor receptor and epithelial-to-mesenchymal transitions: effect on tumor initiation and angiogenesis. *Cancer Research*, 68:10068–10076, 2008.

[8] Calin G.A., Dumitru C.D., Shimizu M., Bichi R., Zupo S., Noch E., Aldler H., Rattan S., Keating M., Rai K., Rassenti L., Kipps T., Negrini M., Bullrich F., and Croce C.M. Frequent deletions and down-regulation of micro-RNA genes miR15 and miR16 at 13q14 in chronic lymphocytic leukemia. *Proceedings of the National Academy of Sciences*, 99:15524–15529, 2002.

[9] Volinia S., Calin G.A., Liu C.G., Ambs S., Cimmino A., Petrocca F., Visone R., and Iorio M. A microRNA expression signature of human solid tumors defines cancer gene targets. *Proceedings of the National Academy of Sciences*, 103:2257–2261, 2006.

[10] Ishak K.G., Anthony P.P., and Sobin L.H. *Histologica Typing of Tumours of the Liver.* Springer-Verlag Berlin Heidelber, 1994.

[11] Golub T.R., Slonim D.K., Tamayo P., Huard C., Gaasenbeek M., Mesirov J.P., Coller H., and Loh M.L. Molecular classification of cancer: class discovery and class prediction by gene expression monitoring. *Science*, 286:531–437, 1999.

[12] Hermanek P. and Sobin L.H. *TNM classification of Malignant Tumour, fourth edition.* Springer-Verlag Berlin Heidelber, 1992.

[13] Workman P. Combinatorial attack on multistep oncogenesis by inhibiting the Hsp90 molecular chaperone. *Cancer Letters*, 206:149–157, 2004.

[14] Kauraniemi P., Hautaniemi S., Autio R., Astola J., Monni O., Elkahloun A., and Kallioniemi A. Effects of Herceptin treatment on global gene expression patterns in HER2-amplified and nonamplified breast cancer cell lines. *Oncogene*, 23:1010–1013, 2004.

[15] Hopkins T.G., Marples M., and Stark D. Sunitinib in the management of gastrointestinal stromal tumours (GISTs). *European Journal of Surgical Oncology*, 34: 844–845, 2008.

[16] Stryer L. *Biochemistry Fourth Edition.* W.H. Freeman and Company, New York, 1995.

[17] Kiang J.G. and Tsokos G.C. Heat shock protein 70 kDa: molecular biology, biochemistry, and physiology. *Pharmacology and Therapeutics*, 80:183–201, 1998.

[18] Lee A.S. GRP78 induction in cancer: therapeutic and prognostic implications. *Cancer Research*, 67:3496–3499, 2007.

[19] Shnyder S.D., Mangum J.E., and Hubbard M.J. Triplex profiling of functionally distinct chaperones (ERp29/PDI/BiP) reveals marked heterogeneity of the endoplasmic reticulum proteome in cancer. *Journal of Proteome Research*, 7:3364–3372, 2008.

[20] Scriven P., Brown N.J., Pockley A.G., and Wyld L. The unfolded protein response and cancer: a brighter future unfolding? *Journal of Molecular Medicine*, 85:331–341, 2007.

[21] Lee A.S. Mammalian stress response: induction of the glucose-regulated protein family. *Current Opinion in Cell Biology*, 4:267–273, 1992.

[22] Watowich S.S. and Morimoto R.I. Complex regulation of heat shock- and glucose-responsive genes in human cells. *Molecular and Cellular Biology*, 8:393–405, 1988.

[23] Feldman D.E., Chauhan V., and Koong A.C. The unfolded protein response: a novel component of the hypoxic stress response in tumors. *Molecular Cancer Research*, 3:597–605, 2005.

[24] Lee E., Nichols P., Spicer D., Groshen S., Yu M.C., and Lee A.S. GRP78 as a novel predictor of responsiveness to chemotherapy in breast cancer. *Cancer Research*, 66: 7849–7853, 2006.

[25] Dong D., Ko B., Baumeister P., Swenson S., Costa F., Markland F., Stiles C., Patterson J.B., Bates S.E., and Lee A.S. Vascular targeting and antiangiogenesis agents induce drug resistance effector GRP78 within the tumor microenvironment. *Cancer Research*, 65:5785–5791, 2005.

[26] Langer R., Feith M., Siewert J.R., Wester H.J., and Hoefler H. Expression and clinical significance of glucose regulated proteins GRP78 (BiP) and GRP94 (GP96) in human adenocarcinomas of the esophagus. *BioMed Central*, 8:70, 2008.

[27] Folkman J. What is the evidence that tumors are angiogenesis dependent? *Journal of the National Cancer Institute*, 82:4–6, 1990.

[28] Folkman J. and Shing Y. Angiogenesis. *Journal of Biological Chemistry*, 267: 10931–10934, 1992.

[29] Vaupel P., Kallinowski F., and Okunieff P. Blood flow, oxygen and nutrient supply, and metabolic microenvironment of human tumors: a review. *Cancer Research*, 49: 6449–6465, 1989.

[30] Hu M. and Polyak K. Microenvironmental regulation of cancer development. *Current Opinion in Genetics and Development*, 18:27–34, 2008.

[31] Hockel M and Vaupel P. Tumor hypoxia: definitions and current clinical, biologic, and molecular aspects. *Journal of the National Cancer Institute*, 93:266–276, 2001.

[32] Kunz M. and Ibrahim S.M. Molecular responses to hypoxia in tumor cells. *Molecular Cancer*, 2:23, 2003.

[33] Vaupel P. and Mayer A. Hypoxia in cancer: significance and impact on clinical outcome. *Cancer and Metastasis Reviews*, 26:225–239, 2007.

[34] Hockel M., Schlenger K., Mitze M., Schaffer U., and Vaupel P. Hypoxia and radiation response in human tumors. *Seminars in Radiation Oncology*, 6:3–9, 1996.

[35] Harris A.L. Hypoxia-a key regulatory factor in tumour growth. *Nature Reviews Cancer*, 2:38–47, 2002.

[36] Nordsmark M., Bentzen S.M., Rudat V., Brizel D., Lartigau E., Stadler P., Becker A., and Adam M. *et al.* Prognostic value of tumor oxygenation in 397 head and neck tumors after primary radiation therapy. An international multi-center study. *Radiotherapy and Oncology*, 77:18–24, 2005.

[37] Rademakers S.E., Span P.N., Kaanders J.H.A.M., Sweep F.C.G.J., van der Kogel A.J., and Bussink J. Molecular aspects of tumour hypoxia. *Molecular Oncology*, 2:41–53, 2008.

[38] Sutherland R.M. Tumor hypoxia and gene expression: implications for malignant progression and therapy. *Acta Oncologica*, 37:567–574, 1998.

[39] Cuvier C., Jang A., and Hill R.P. Exposure to hypoxia, glucose starvation and acidosis: effect on invasive capacity of murine tumor cells and correlation with cathepsin (L + B) secretion. *Clinical and Experimental Metastasis*, 15:19–25, 1997.

[40] Kallinowski F., Schlenger K.H., Runkel S., Kloes M., Stohrer M., Okunieff P., and Vaupel P. Blood flow, metabolism, cellular microenvironment, and growth rate of human tumor xenografts. *Cancer Research*, 49:3759–3764, 1989.

[41] Giaccia A.J. Hypoxic Stress Proteins: Survival of the Fittest. *Seminars in Radiation Oncology*, 6:46–58, 1996.

[42] Carroll V.A. and Ashcroft M. Targeting the molecular basis for tumour hypoxia. *Expert Reviews in Molecular Medicine*, 7:1–16, 2005.

[43] Brizel D.M., Scully S.P., Harrelson J.M., Layfield L.J., Bean J.M., Prosnitz L.R., and Dewhirst M.W. Tumor oxygenation predicts for the likelihood of distant metastases in human soft tissue sarcoma. *Cancer Research*, 56:941–943, 1996.

[44] Zhong H., De Marzo A.M., Laughner E., Lim M., Hilton D.A., Zagzag D., Buechler P., and Isaacs W.B. *et al.* Overexpression of hypoxia-inducible factor 1alpha in common human cancers and their metastases. *Cancer Research*, 59:5830–5835, 1999.

[45] Vergis R., Corbishley C.M., Norman A.R., Bartlett J., Jhavar S., Borre M., Heeboll S., and Horwich A. *et al.* Intrinsic markers of tumour hypoxia and angiogenesis in localised prostate cancer and outcome of radical treatment: a retrospective analysis of two randomised radiotherapy trials and one surgical cohort study. *Lancet Oncology*, 9:342–351, 2008.

[46] Moon E.J., Brizel D.M., Chi J.T., and Dewhirst M.W. The potential role of intrinsic hypoxia markers as prognostic variables in cancer. *Antioxidants and Redox Signaling*, 9:1237–1294, 2007.

[47] Koukourakis M.I., Giatromanolaki A., Sivridis E., Simopoulos C., Turley H., Talks K., Gatter K.C., and Harris A.L. Hypoxia-inducible factor (HIF1A and HIF2A), angiogenesis, and chemoradiotherapy outcome of squamous cell head-and-neck cancer. *International Journal of Radiation Oncology, Biology, Physics*, 53:1192–1202, 2002.

[48] Kaanders J.H., Bussink J., and van der Kogel A.J. ARCON: a novel biology-based approach in radiotherapy. *Lancet Oncology*, 3:28–37, 2002.

[49] Kaanders J.H., Pop L.A., Marres H.A., Bruaset I., van den Hoogen F.J., Merkx M.A., and van der Kogel A.J. ARCON: experience in 215 patients with advanced head-and-neck cancer. *International Journal of Radiation Oncology, Biology, Physics*, 52:769–778, 2002.

[50] von Pawel J., von Roemeling R., Gatzemeier U., Boyer M., Elisson L.O., Clark P., Talbot D., and Rey A. *et al.* Tirapazamine plus cisplatin versus cisplatin in advanced non-small-cell lung cancer: A report of the international CATAPULT I study group. Cisplatin and tirapazamine in subjects with advanced previously untreated non-small-cell lung tumors. *Journal of Clinical Oncology*, 18:1351–1359, 2000.

[51] Cairns R.A., Papandreou I., Sutphin P.D., and Denko N.C. Metabolic targeting of hypoxia and HIF1 in solid tumors can enhance cytotoxic chemotherapy. *Proceedings of the National Academy of Sciences*, 104:9445–9450, 2007.

[52] Albertella M.R., Loadman P.M., Jones P.H., Phillips R.M., Rampling R., Burnet N., Alcock C., Anthoney A., and Vjaters E. *et al.* Hypoxia-selective targeting by the bioreductive prodrug AQ4N in patients with solid tumors: results of a phase I study. *Clinical Cancer Research*, 14:1096–1104, 2008.

[53] Horsman M.R. and Siemann D.W. Pathophysiologic effects of vascular-targeting agents and the implications for combination with conventional therapies. *Cancer Research*, 66:11520–11539, 2006.

[54] Patterson D.M. and Rustin G.J. Vascular damaging agents. *Clinical Oncology*, 19: 443–456, 2007.

[55] Fidler I.J. Critical factors in the biology of human cancer metastasis: twenty-eighth G.H.A. clowes memorial award lecture. *Cancer Research*, 50:6130–6138, 1990.

[56] Liotta L.A and Kohn E.C. The microenvironment of the tumour-host interface. *Nature*, 411:375–379, 2001.

[57] Fidler I.J. The pathogenesis of cancer metastasis: the 'seed and soil' hypothesis revisited. *Nature Reviews Cancer*, 3:453–458, 2003.

[58] Pantel K. and Brakenhoff R.H. Dissecting the metastatic cascade. *Nature Reviews Cancer*, 4:448–456, 2004.

[59] Fidler I.J. and Ellis L.M. The implications of angiogenesis for the biology and therapy of cancer metastasis. *Cell*, 79:185–188, 1994.

[60] Takeda A., Stoeltzing O., Ahmad S.A., Reinmuth N., Liu W., Parikh A., Fan F., Akagi M., and Ellis L.M. Role of angiogenesis in the development and growth of liver metastasis. *Annals of Surgical Oncology*, 9:610–6, 2002.

[61] Rudmik L.R. and Magliocco A.M. Molecular mechanisms of hepatic metastasis in colorectal cancer. *Journal of Surgical Oncology*, 92:347–359, 2005.

[62] Folkman J. The role of angiogenesis in tumor growth. *Seminars in Cancer Biology*, 3:65–71, 1992.

[63] Folkman J. How is blood vessel growth regulated in normal and neoplastic tissue? G.H.A. Clowes memorial Award lecture. *Cancer Research*, 46:467–473, 1986.

[64] Liotta L.A. Tumor invasion and metastases–role of the extracellular matrix: Rhoads Memorial Award lecture. *Cancer Research*, 46:1–7, 1986.

[65] Srinivas P. R., Kramer B. S., and Srivastava S. Trends in biomarker research for cancer detection. *Lancet Oncology*, 2:698–704, 2001.

[66] Srinivas P. R., Verma M., Zhao Y., and Srivastava S. Proteomics for cancer biomarker discovery. *Clinical Chemistry*, 48:1160–1169, 2002.

[67] Rifai N., Gillette M.A., and Carr S.A. Protein biomarker discovery validation: the long uncertain path to clinical utility. *Nature Biotechnology*, 24:971–983, 2006.

[68] Anderson N. L. and Anderson N.G. The human plasma proteome: history, character, and diognostic prospects. *Molecular and Cellular Proteomics*, 1:845–867, 2002.

[69] Anderson N.L. The roles of a multiple proteomics platforms in a pipeline for new diagnostics. *Molecular and Cellular Proteomics*, 4:1441–1444, 2005.

[70] Gutman S. and Kessler L.G. The US Food and Drug Administration perspective on cancer biomarker development. *Nature Reviews Cancer*, 6:565–571, 2006.

[71] Fenn J.B., Mann M., Meng C.K., Wong S.F., and Whitehouse C.M. Electrospray ionization for mass spectrometry of large biomolecules. *Science*, 246:64–71, 1989.

[72] Cech N.B. and Enke C.G. Practical implications of some recent studies in electrospray ionization fundamentals. *Mass Spectrometry Reviews*, 20:362–387, 2001.

[73] Venter H., Ashcroft A.E., Keen J.N., Henderson P.J., and Herbert R.B. Molecular dissection of membrane-transport proteins: mass spectrometry and sequence determination of the galactose-H+ symport protein, GalP, of Escherichia coli and quantitative assay of the incorporation of [ring-2-13C]histidine and (15)NH(3). *Biochemical Journal*, 363:243–252, 2002.

[74] Tanaka K., Waki H., Ido Y., Akita S., Yoshida Y., Yoshida T., and Matsuo T. Protein and polymer analyses up to m/z 100 000 by laser ionization time-of-flight mass spectrometry. *Rapid Communication in Mass Spectrometry*, 2:151–153, 1988.

[75] Karas M. and Hillenkamp F. Laser desorption ionization of proteins with molecular masses exceeding 10,000 daltons. *Analytical Chemistry*, 60:2299–2301, 1988.

[76] Karas M. and Kruger R. Ion formation in MALDI: the cluster ionization mechanism. *Chemical Reviews*, 103:427–439, 2003.

[77] Knochenmuss R. Ion formation in UV-MALDI. *Analyst*, 131:966–986, 2006.

[78] Hillenkamp F., Karas M., Beavis R.C., and Chait B.T. Matrix-assisted laser desorption/ionization mass spectrometry of biopolymers. *Analytical Chemistry*, 63: 1193A–1203A, 1991.

[79] Fenselau C. and Demirev P.A. Characterization of intact microorganisms by MALDI mass spectrometry. *Mass Spectrometry Reviews*, 20:157–171, 2001.

[80] de Hoffmann E. and Stroobant V. *Mass Spectrometry: Principles and Applications, second edition.* John Wiley and Sons, Inc., 2001.

[81] Harvey D.J. Matrix-assisted laser desorption/ionization mass spectrometry of carbohydrates. *Mass Spectrometry Reviews*, 18:349–450, 1999.

[82] Pan C., Xu S., Zhou H., Fu Y., Ye M., and Zou H. Recent developments in methods and technology for analysis of biological samples by MALDI-TOF-MS. *Analytical and Bioanalytical Chemistry*, 387:193–204, 2007.

[83] Chaurand P., Schwartz S.A., and Caprioli R.M. Imaging mass spectrometry: a new tool to investigate the spatial organization of peptides and proteins in mammalian tissue sections. *Current Opinion in Chemical Biology*, 6:676–681, 2002.

[84] Cotter R.J, Griffith W., and Jelinek C. Tandem time-of-flight (TOF/TOF) mass spectrometry and the curved-field reflectron. *Journal of Chromatography B*, 855: 2–13, 2007.

[85] Futrell J.H. Development of tandem mass spectrometry: one perspective. *International Journal of Mass Spectrometry*, 200:495–508, 2000.

[86] Clemmer D.E. and Jarrold M.F. Ion Mobility measurements and their applications to clusters and biomolecules. *Journal of Mass Spectrometry*, 32:577–592, 1997.

[87] Valentine S.J., Counterman A.E., and Clemmer D.E. Conformer-dependent proton-transfer reactions of ubiquitin ions. *Journal of the American Society for Mass Spectrometry*, 8:954–961, 1997.

[88] Woods A.S., Ugarov M., Egan T., Koomen J., Gillig K.J., Fuhrer K., Gonin M., and Schultz J.A. Lipid/peptide/nucleotide separation with MALDI-ion mobility-TOF MS. *Analytical Chemistry*, 15:2187–2195, 2004.

[89] Kurulugama R.T., Nachtigall F.M., Lee S., Valentine S.J., and Clemmer D.E. Overtone mobility spectrometry: part 1. Experimental observations. *Journal of the American Society for Mass Spectrometry*, 20:729–737, 2009.

[90] Valentine S.J., Stokes S.T., Kurulugama R.T., Nachtigall F.M., and Clemmer D.E. Overtone mobility spectrometry: part 2. Theoretical considerations of resolving power. *Journal of the American Society for Mass Spectrometry*, 20:738–750, 2009.

[91] Pringle S.D., Giles K., Wildgoose J.L., Williams J.P., Slade S.E., Thalassinos K., Bateman R.H., Bowers M.T., and Scrivens J.H. An investigation of the mobility separation of some peptide and protein ions using a new hybrid quadrupole/travelling wave IMS/oa-ToF instrument. *International Journal of Mass Spectrometry*, 261: 1–12, 2007.

[92] Giles K., Pringle S.D., Worthington K.R., Little D., Wildgoose J.L., and Bateman R.H. Applications of a travelling wave-based radio-frequency-only stacked ring ion guide. *Rapid Commununication in Mass Spectrometry*, 18:2401–2414, 2004.

[93] Hoaglund C.S., Valentine S.J., Sporleder C.R., Reilly J.P., and Clemmer D.E. Three-dimensional ion mobility/TOFMS analysis of electrosprayed biomolecules. *Analytical Chemistry*, 70:2236–2242, 1998.

[94] Scarff C.A., Patel V.J., Thalassinos K., and Scrivens J.H. Probing hemoglobin structure by means of traveling-wave ion mobility mass spectrometry. *Journal of the American Society for Mass Spectrometry*, 20:625–31, 2009.

[95] Roepstorff P. Mass spectrometry in protein studies from genome to function. *Current Opinion in Biotechnology*, 8:6–l 3, 1997.

[96] Yates J.R. Mass spectrometry and the age of the proteome. *Journal of Mass Spectrometry*, 33:1–19, 1998.

[97] Roepstorff P. Mass spectrometry of proteins. *Trends in Analytical Chemistry*, 12: 413–421, 1993.

[98] Siuzdak G. The emergence of mass spectrometry in biochemical research. *Proceedings of the National Academy of Sciences*, 91:11290–11297, 1994.

[99] Kuster B. and Mann M. Identifying proteins and post-translational modifications by mass spectrometry. *Current Opinion in Structural Biology*, 8:393–400, 1998.

[100] Valaskovic G.A., Kelleher N.L., and McLafferty F.W. Attomole protein characterization by capillary electrophoresis-mass spectrometry. *Science*, 273:1199–202, 1996.

[101] Gygi S.P., Han D.K., Gingras A.C., Sonenberg N., and Aebersold R. Protein analysis by mass spectrometry and sequence database searching: tools for cancer research in the post-genomic era. *Electrophoresis*, 20:310–319, 1999.

[102] Hanash S. Disease Proteomics. *Nature*, 422:226–232, 2003.

[103] Zhou G., Li H., DeCamp D., Chen S., Shu H., Gong Y., Flaig M., and Gillespie J.W. *et. al.* 2D differential in-gel electrophoresis for the identification of esophageal scans cell cancer-specific protein markers. *Molecular and Cellular Proteomics*, 1:117–24, 2002.

[104] Shin B.K., Wang H., Yim A.M., Le Naour F., Brichory F., Jang J.H., Zhao R., and Puravs E. *et. al.* Global profiling of the cell surface proteome of cancer cells uncovers an abundance of proteins with chaperone function. *Journal of Biological Chemistry*, 278:7607–7616, 2003.

[105] Henzel W.J., Billeci T.M., Stults J.T., Wong S.C., Grimley C., and Watanabe C. Identifying proteins from two-dimensional gels by molecular mass searching of peptide fragments in protein sequence databases. *Proceedings of the National Academy of Sciences*, 90:5011–5015, 1993.

[106] Jungblut P. and Thiede B. Protein identification from 2-DE gels by MALDI mass spectrometry. *Mass Spectrometry Reviews*, 16:145–162, 1997.

[107] Drake R.R., Cazare L.H., Semmes O.J., and Wadsworth J.T. Serum, salivary and tissue proteomics for discovery of biomarkers for head and neck cancers. *Expert Review of Molecular Diagnostics*, 5:93–100, 2005.

[108] Hancock W.S., Wu S.L., and Shieh P. The challenges of developing a sound proteomics strategy. *Proteomics*, 2:352–359, 2002.

[109] Yates J.R., Speicher S., Griffin P.R., and Hunkapiller T. Peptide mass maps: A highly informative approach to protein identification. *Analytical Biochemistry*, 214: 397–408, 1993.

[110] Mann M., Hendrickson R.C., and Pandey A. Analysis of proteins and proteomes by mass spectrometry. *Annual Review of Biochemistry*, 70:437–73, 2001.

[111] Adkins J.N., Varnum S.M., Auberry K.J., Moore R.J., Angell N.H., Smith R.D., Springer D.L., and Pounds J.G. Toward a human blood serum proteome: analysis by multidimensional separation coupled with mass spectrometry. *Molecular Cell Proteomics*, 1:947–955, 2002.

[112] Wang W., Zhou H., Lin H., Roy S., Shaler T.A., Hill L.R., Norton S., Kumar P., Anderle M., and Becker C.H. Quantification of proteins and metabolites by mass spectrometry without isotopic labeling or spiked standards. *Analytical Chemistry*, 75:4818–4826, 2003.

[113] Shen Y., Jacobs J.M., Camp D.G., Fang R., Moore R.J., Smith R.D., Xiao W., Davis R.W., and Tompkins R.G. Ultra-high-efficiency strong cation exchange LC/RPLC/MS/MS for high dynamic range characterization of the human plasma proteome. *Analytical Chemistry*, 76:1134–1144, 2004.

[114] Naldi M., Andrisano V., Fiori J., Calonghi N., Pagnotta E., Parolin C., Pieraccini G., and Masotti L. Histone proteins determined in a human colon cancer by high-performance liquid chromatography and mass spectrometry. *Journal of Chromatography A*, 1129:73–81, 2006.

[115] Marko-Varga G., Lindberg H., Lfdahl C.G., Jnsson P., Hansson L., Dahlbck M., Lindquist E., and Johansson L. *et. al.* Discovery of biomarker candidates within disease by protein profiling: principles and concepts. *Journal of Proteome Research*, 4:1200–1212, 2005.

[116] Pacholski M.L. and Winograd N. Imaging with mass spectrometry. *Chemical Reviews*, 99:2977–3005, 1999.

[117] Heeren R.M., McDonnell L.A., Amstalden E., Luxembourg S.L., Altelaar A.F.M., and Piersma S.R. Why dont biologists use SIMS?: A critical evaluation of imaging MS. *Applied Surface Science*, 252:6827–6835, 2005.

[118] Chaurand P., Schriver K.E., and Caprioli R.M. Instrument design and characterization for high resolution MALDI-MS imaging of tissue sections. *Journal of Mass Spectrometry*, 42:476–489, 2007.

[119] Touboul D., Roy S., Germain D.P., Chaminade P., Brunelle A., and Laprvote O. MALDI-TOF and cluster-TOF-SIMS imaging of fabry disease biomarkers. *International Journal of Mass Spectrometry*, 260:158–165, 2007.

[120] McDonnell L.A., Heeren R.M., de Lange R.P., and Fletcher I.W. Higher sensitivity secondary ion mass spectrometry of biological molecules for high resolution, chemically specific imaging. *Journal of the American Society for Mass Spectrometry*, 17:1195–1202, 2006.

[121] Delcorte A., Bour J., Aubriet F., Muller J.F., and Bertrand P. Sample metallization for performance improvement in desorption/ionization of kilodalton molecules: quantitative evaluation, imaging secondary ion MS, and laser ablation. *Analytical Chemistry*, 75:6875–6885, 2003.

[122] Caprioli R.M., Farmer T.B., and Gile J. Molecular imaging of biological samples: localization of peptides and proteins using MALDI-TOF MS. *Analytical Chemistry*, 69:4751–4760, 1997.

[123] Chaurand P., Stoeckli M., and Caprioli R.M. Direct profiling of proteins in biological tissue sections by MALDI mass spectrometry. *Analytical Chemistry*, 71: 5263–5270, 1999.

[124] Crecelius A.C., Cornett D.S., Caprioli R.M., Williams B., Dawant B.M., and Bodenheimer B. Three-dimensional visualization of protein expression in mouse brain structures using imaging mass spectrometry. *Journal of the American Society for Mass Spectrometry*, 16:1093–1099, 2005.

[125] Andersson M., Groseclose M.R., Deutch A.Y., and Caprioli R.M. Imaging mass spectrometry of proteins and peptides: 3D volume reconstruction. *Nature Methods*, 5:101–108, 2008.

[126] Sinha T.K., Khatib-Shahidi S., Yankeelov T.E., Mapara K., Ehtesham M., Cornett D.S., Dawant B.M., Caprioli R.M., and Gore J.C. Integrating spatially resolved three-dimensional MALDI IMS with *in vivo* magnetic resonance imaging. *Nature Methods*, 5:57–59, 2008.

[127] Rohner T.C., Staab D., and Stoeckli M. MALDI mass spectrometric imaging of biological tissue sections. *Mechanisms of Ageing and Development*, 126:177–185, 2005.

[128] Wisztorski M., Lemaire R., Stauber J., Menguelet S.A., Croix D., Math O.J., Day R., Salzet M., and Fournier I. New developments in MALDI imaging for pathology proteomic studies. *Current Pharmaceutical Design*, 13:3317–3324, 2007.

[129] Schwartz S.A., Reyzer M.L., and Caprioli R.M. Direct tissue analysis using matrix-assisted laser desorption/ionization mass spectrometry: practical aspects of sample preparation. *Journal of Mass Spectrometry*, 38:699–708, 2003.

[130] Seeley E.H., Oppenheimer S.R., Mi D., Chaurand P., and Caprioli R.M. Enhancement of protein sensitivity for MALDI imaging mass spectrometry after chemical treatment of tissue sections. *Journal of the American Society for Mass Spectrometry*, 19:1069–1077, 2008.

[131] Chaurand P., Schwartz S.A., Reyzer M.L., and Caprioli R.M. Imaging mass spectrometry: principles and potentials. *Toxicologic Pathology*, 33:92–101, 2005.

[132] Trim P.J., Henson C.M., Avery J.L., McEwen A., Snel M.F., Claude E., Marshall P.S., West A., Princivalle A.P., and Clench M.R. Matrix-assisted laser desorption/ionization-ion mobility separation-mass spectrometry imaging of vinblastine in whole body tissue sections. *Analytical Chemistry*, 80:8628–8634, 2008.

[133] Chaurand P., Schwartz S.A., Billheimer D., Xu B.J., Crecelius A., and Caprioli R.M. Integrating histology and imaging mass spectrometry. *Analytical Chemistry*, 76:1145–1155, 2004.

[134] Djidja M., Carolan V., Loadman P.M., and Clench M.R. Method development for protein profiling in biological tissues by matrix-assisted laser desorption/ionisation mass spectrometry imaging. *Rapid Communication in Mass Spectrometry*, 22:1615–1618, 2008.

[135] Lemaire R., Wisztorski M., Desmons A., Tabet J.C., Day R., Salzet M., and Fournier I. MALDI-MS direct tissue analysis of proteins: improving signal sensitivity using organic treatments. *Analytical Chemistry*, 78:7145–7153, 2006.

[136] Shimma S., Furuta M., Ichimura K., Yoshida Y., and Setou M. A novel approach to *in situ* proteome analysis using chemical inkjet printing technology and MALDI-QIT-TOF tandem mass spectrometer. *Journal of Mass Spectrometry Society Japan*, 54:130–140, 2006.

[137] Lemaire R., Desmons A., Tabet J.C., Day R., Salzet M., and Fournier I. Direct analysis and MALDI imaging of formalin-fixed, paraffin-embedded tissue sections. *Journal of Proteome Research*, 6:1295–1305, 2007.

[138] Groseclose M.R., Andersson M., Hardesty W.M., and Caprioli R.M. Identification of proteins directly from tissue: *in situ* tryptic digestions coupled with imaging mass spectrometry. *Journal of Mass Spectrometry*, 42:254–262, 2007.

[139] Stauber J., Lemaire R., Franck J., Bonnel D., Croix D., Day R., Wisztorski M., Fournier I., and Salzet M. MALDI imaging of formalin-fixed paraffin-embedded tissues: application to model animals of Parkinson disease for biomarker hunting. *Journal of Proteome Research*, 7:969–978, 2008.

[140] Groseclose M.R., Massion P.P., Chaurand P., and Caprioli R.M. High-throughput proteomic analysis of formalin-fixed paraffin-embedded tissue microarrays using MALDI imaging mass spectrometry. *Proteomics*, 8:3715–3724, 2008.

[141] Lemaire R., Stauber J., Wisztorski M., Van Camp C., Desmons A., Deschamps M., Proess G., Rudlof I., Woods A.S., Day R., Salzet M., and Fournier I. Tag-mass: specific molecular imaging of transcriptome and proteome by mass spectrometry based on photocleavable tag. *Journal of Proteome Research*, 6:2057–2067, 2007.

[142] Lemaire R., Menguellet S.A., Stauber J., Marchaudon V., Lucot J.P., Collinet P., Farine M.O., Vinatier D., Day R., Ducoroy P., Salzet M., and Fournier I. Specific MALDI imaging and profiling for biomarker hunting and validation: fragment of the 11s proteasome activator complex, Reg alpha fragment, is a new potential ovary cancer biomarker. *Journal of Proteome Research*, 6:4127–4134, 2007.

[143] Armstrong D.W., Zhang L.K., He L., and Gross M.L. Ionic liquids as matrixes for matrix-assisted laser desorption/ionization mass spectrometry. *Analytical Chemistry*, 73:3679–3686, 2001.

[144] Aerni H., Cornett D.S., and Caprioli R.M. Automated acoustic matrix deposition for MALDI sample preparation. *Analytical Chemistry*, 78:827–834, 2006.

[145] Stoeckli M., Chaurand P, Hallahan D.E., and Caprioli R.M. Imaging mass spectrometry: A new technology for the analysis of protein expression in mammalian tissues. *Nature Medicine*, 7:493–496, 2001.

[146] Franck J., Wisztorski M., Stauber J., Elayed M., Salzet M., and Fournier I. Shimadzu CHIP-1000 for clinical tissue application in MALDI imaging. Technical report, Shimadzu Biotechnology, 2007.

[147] Anderson D.M., Carolan V.A., Crosland S., Sharples K.R., and Clench M.R. Examination of the distribution of nicosulfuron in sunflower plants by matrix-assisted laser desorption/ionisation mass spectrometry imaging. *Rapid Communication in Mass Spectrometry*, 23:1321–1327, 2009.

[148] Schuerenberg M., Luebbert C., Deininger S.O., Mueller R., and Suckau D. A new matrix application device for MALDI tissue imaging. Technical report, Bruker Daltonics, 2007.

[149] Chaurand P., Schwartz S.A., and Caprioli R.M. Profiling and imaging proteins in tissue sections by MS. *Analytical Chemistry*, 76:87A–93A, 2004.

[150] Todd P.J., Schaaff T.G., Chaurand P., and Caprioli R.M. Organic ion imaging of biological tissue with secondary ion mass spectrometry and matrix-assisted laser desorption/ionization. *Journal of Mass Spectrometry*, 36:355–369, 2001.

[151] McDonnell L.A. and Heeren R.M. Imaging mass spectrometry. *Mass Spectrometry Reviews*, 26:606–643, 2007.

[152] Luxembourg S.L., Mize T.H., McDonnell L.A., and Heeren R.M. High-spatial resolution mass spectrometric imaging of peptide and protein distributions on a surface. *Analytical Chemistry*, 76:5339–5344, 2004.

[153] Goodwin R.J., Pennington S.R., and Pitt A.R. Protein and peptides in pictures: Imaging with MALDI mass spectrometry. *Proteomics*, 8:3785–3800, 2008.

[154] Spengler B. and Hubert M. Scanning microprobe matrix-assisted laser desorption ionization (SMALDI) mass spectrometry: instrumentation for sub-micrometer resolved LDI and MALDI surface analysis. *Journal of the American Society for Mass Spectrometry*, 13:735–748, 2002.

[155] Jurchen J.C., Rubakhin S.S., and Sweedler J.V. MALDI-MS imaging of features smaller than the size of the laser beam. *Journal of the American Society for Mass Spectrometry*, 16:1654–1659, 2005.

[156] Holle A., Haase A., Kayser M., and Hohndorf J. Optimizing UV laser focus profiles for improved MALDI performance. *Journal of Mass Spectrometry*, 41:705–716, 2006.

[157] Applied B. Multiplexing MALDI Mass Spectrometry Imaging using Dynamic Pixel Imaging. Technical report, Applied Biosystems/MDS Siex, 2007.

[158] Simmons D.A. Improved MALDI-MS imaging performance using continuous laser rastering. Technical report, MDS Analytical Technologies, 2008.

[159] Stoeckli M., Farmer T.B., and Caprioli R.M. Automated mass spectrometry imaging with a matrix-assisted laser desorption ionization time-of-flight instrument. *Journal of the American Society for Mass Spectrometry*, 10:67–71, 1999.

[160] Taban I.M., Altelaar A.F., van der Burgt Y.E., McDonnell L.A., Heeren R.M., Fuchser J., and Baykut G. Imaging of peptides in the rat brain using MALDI-FTICR mass spectrometry. *Journal of the American Society for Mass Spectrometry*, 18:145–151, 2007.

[161] Reyzer M.L., Caldwell R.L., Dugger T.C., Forbes J.T., Ritter C.A., Guix M., Arteaga C.L., and Caprioli R.M. Early Changes in Protein Expression Detected by Mass Spectrometry Predict Tumor Response to Molecular Therapeutics. *Cancer Research*, 64:9093–9100, 2004.

[162] Hopfgartner G., Varesio E., and Stoeckli M. Matrix-assisted laser desorption/ionization mass spectrometric imaging of complete rat sections using a triple quadrupole linear ion trap. *Rapid Communication in Mass Spectrometry*, 23:733–736, 2009.

[163] Djidja M.C., Francese S., Loadman P.M., Sutton C.W., Scriven P., Claude E., Snel M.F., Franck J., Salzet M., and Clench M.R. Detergent addition to tryptic digests and ion mobility separation prior to MS/MS improves peptide yield and protein identification for *in situ* proteomic investigation of frozen and formalin-fixed paraffin-embedded adenocarcinoma tissue sections. *Proteomics*, 9:2750–2763, 2009.

[164] Fournier I., Wisztorski M., and Salzet M. Tissue imaging using MALDI-MS: a new frontier of histopathology proteomics. *Expert Reviews Proteomics*, 5:413–424, 2008.

CHAPTER 2

Direct Proteomic Investigation in Tumour Tissue Sections using MALDI-MSI

2.1 Introduction

Growth and invasion of an organ or tissue by tumour cells require signalling between tumour cells and the tissue in order that the tumour grows without the inflammatory response that could inhibit such progression [1–3]. Biomarkers are biological molecules that are measurable indicators of a specific physiological state and changes occurring during a disease process [4]. Enhancing the understanding of cancer relies heavily upon the identification of diagnostic biomarkers *i.e.* proteins and other biomolecules which are correlated to disease states or represent potential therapeutic targets [5–7]. Proteins play a fundamental function in cell process either via metabolism or cell signalling and immune responses. The ability to use proteomic profiling to differentiate tissue section regions and to discriminate between relevant biomolecules can improve the selection and identification of those whose expression is closely associated with the tumour growth and/or progression, and thus improve the development of chemotherapeutic agents [8–10].

MALDI-MSI is a technique that enables the screening of proteomic information directly from a tissue section with no requirement for specific targets and could aid the identification of target proteins whose functionality can help biomarker discovery [11]. Several papers have already reported the successful use of the technique to investigate the distribution of proteins directly within tissue sections [12–16]. MALDI-MSI has also been used to investigate changes in protein profiles within tumour tissue sections [17–19] and changes occurring in response to therapeutic agents [20, 21]. These studies show that MALDI-MSI can be used to distinguish between cancerous and normal tissues, thus highlighting the benefit of the technique for rapid characterisation of a disease at the protein level.

Xenografts are human cells or human cell lines grown in immunodeficient mice. Tumour xenografts are mainly produced in two ways: human tumour cells are either injected subcutaneously into a nude mouse to generate an ectopic xenograft or to produce an orthotopic tumour model, which involves the implantation of the tumour into the animal organ from which it arose, so that tumour cells grow in their equivalent native environment. Tumour xenografts are extensively used in cancer research as they can

be used to produce a broad spectrum of major tumour types [22]. The possibility also exists of *ex vivo* genetic or therapeutic manipulation before xenotransplantation. The progression of a large number of easily observable synchronized tumours can be monitored, so that initiation of treatment can begin when the tumours reach an optimal size.

In the work reported here, xenograft tissue samples, grown from the MCF-7 breast cancer cell line, were used for method development for direct proteomic profiling and imaging within tumour tissue sections by MALDI-MS. Numerous protein signals were detected and their distribution studied directly within MCF-7 xenograft tumour tissue sections. This allowed discrimination of tumour regions from necrotic areas.

MALDI-MSI is a potential tool for aiding both biomarker discovery and clinical investigations as several studies have shown that the technique is complementary to other imaging techniques that require labelled analytes (i.e. autoradiography, fluorescence imaging) because of its molecular specificity. However as each MALDI-MSI experiment generates a large set of data, data pre-processing is required in order to facilitate result interpretation as well as statistical analysis. For this purpose, a workflow for MALDI-MSI data pre-processing was described by Norris *et al.* [23]. Several data pre-processing software packages are commercially available, but most of them are specific to an application or an instrument, thus making data pre-processing relatively difficult in some cases. In the work reported here the use of a freely available software tool *SpecAlign* [24] to aid data pre-processing prior to statistical analysis is described. A report of the results shown in this chapter can be found in Djidja *et al* [25].

2.2 Materials and Samples

2.2.1 Chemicals and materials

Sinapinic acid (SA), α-cyano-4-hydroxycinnamic acid (α-CHCA), ethanol (EtOH), methanol (MeOH), acetonitrile (ACN), chloroform ($CHCl_3$), xylene, trifuoroacetic acid (TFA), haematoxylin, eosin, trifluoroacetic acid (TFA) and human haemoglobin protein standard were obtained from Sigma-Aldrich (Dorset, UK).

2.2.2 Tissue samples

2.2.2.1 Rat liver tissues

Rat liver samples were obtained from the Sheffield Hallam University laboratory (Biomedical Research Centre, Sheffield Hallam University, Sheffield, UK) directly after animal sacrifice. Samples were immediately snap-frozen in a beaker containing cold isopentane, which was previously immersed in liquid nitrogen. Frozen tissue samples were stored at -80°C to minimize protein degradation through enzymatic proteolysis and to preserve the sample's morphology.

2.2.2.2 MCF-7 Breast tumour xenografts

All animal procedures including animal treatment and tumour system and transplantation were carried out at the Institute of Cancer Therapeutics (Bradford, UK).

2.2.2.2.1 *Animal treatment*

Investigations and all animal procedures were carried out under a project licence issued by the UK Home Office and the United Kingdom Co-ordinating Committee on Cancer Research (UKCCCR) [26]. Female Balb/C immunodeficient nude mice (Harlan UK, Blackthorn, UK) aged 6-8 weeks were used. Mice received CRM diet (SDS, Witham, UK) and water *ad libitum*. Animals were kept in cages in an air-conditioned room with regular alternating cycles of light and darkness.

2.2.2.2.2 *Tumour system*

MCF-7 breast tumour xenografts were obtained from the Institute of Cancer Therapeutics (Bradford, UK). The transplantation of tumour was performed as follows: briefly, 24 hours prior to tumour transplantation, in order to stimulate tumour growth, a slow-release oestrogen pellet (Innovative Research, Sarasota, FL, USA) was implanted subcutaneously in the upper dorsal area of the animal under brief general inhalation anaesthesia. MCF-7 human mammary adenocarcinoma tumours were excised from a donor animal, placed in sterile physiological saline containing antibiotics and cut into small fragments of approximately 2 mm^3. Under brief general inhalation anaesthesia, tumour fragments were implanted in the left and right flank of each mouse using a trocar. Once the tumours had reached a desired volume, usually between 200 and 400 mm^3, as measured by callipers, mice were sacrificed. Tumours were excised and immediately snap-frozen in liquid nitrogen and stored at -80°C to minimise protein degradation and keep the original sample's morphology until further analysis.

2.2.3 Tissue preparation

Rat liver and MCF-7 xenograft samples were sectioned using a cryostat (Leica Microsystems, Milton Keynes, UK) operating at -20°C. 10 μm sections were cut and thaw-mounted on either a TLC foil, from which the stationary phase had been previously removed, or on histological Polysine^{TM} glass slides (Menzel-Glaser, Germany).

Rinsing procedures were established to increase the MS data quality. These rinsing steps consisted of immersing sections for one minute through a series of ethanol solutions of decreasing water concentrations from 50 to 90%. Washing the tissue sections with EtOH aims to remove residual salts as well as fixing the tissue section. After the EtOH washes the section was immersed in $CHCl_3$ in order to decrease the lipids in the tissue section [27]. Indeed lipids present within the tissue section may interfere with the desirable analyte, here proteins, thus making potentially difficult the detection of proteins by direct MALDI-MSI analysis.

2.3 Methods and Instrumentation

2.3.1 Matrix deposition

For direct protein analysis, sinapinic acid (SA) was used as matrix. For direct protein profiling the matrix was prepared at 25 mg/mL in ACN:dH_20:TFA (1:1:0.2 in volume). Several spots (300 nL) of matrix were directly deposited onto specific regions of the section according to the histological study using an automatic pipette. Figure 2.1 shows a digital scan of a tumour xenograft section in which the darker region in the center represents necrotic tissues and the surrounding part is mainly tumour cells. The small circles on the image show where matrix spots were deposited in order to generate average mass spectra of the different regions. For imaging experiments, SA solution was prepared at 25 mg/mL in 100% EtOH: 0.2% TFA. The matrix solution was spray coated onto the tissue section using a gravity fed pneumatic air spray gun set to 40 psi. Approximately 15 to 20 spray cycles gave a homogeneous matrix coverage.

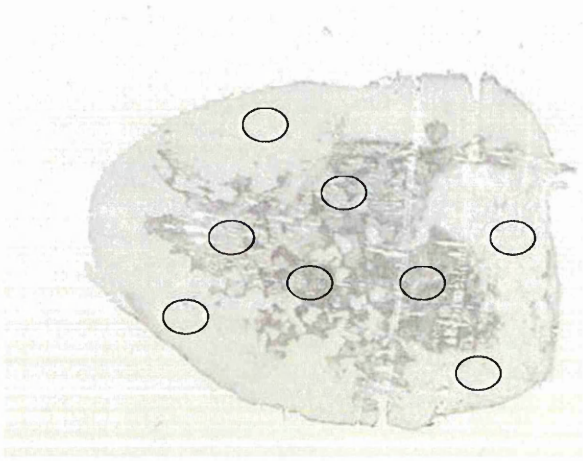

Figure 2.1: **Schematic showing the deposition of matrix spots onto a MCF-7 breast tumour xenograft tissue section.**
A digital scan of a breast tumour xenograft tissue section is shown. Depositions of matrix spots are represented by circles on the tissue section image.

2.3.2 Haematoxylin and eosin (HE) staining protocol

Frozen MCF-7 breast tumour xenograft tissue sections were allowed to dry at room temperature and then fixed by using a series of EtOH solutions of increasing water concentration (100, 95 and 70%) stored at -20°C for three minutes in each solution. The sections were then dipped in tap water for two minutes until clear. The nuclei were stained by immersing the tissue sections in haematoxylin for 30 seconds, followed by a wash under running tap water (a gentle stream of water running into a staining jar was used). The sections were then dehydrated in 70 and 95% EtOH solutions for three minutes and immersed for 20 seconds in eosin solution made at 5% in EtOH. Following eosin staining, the tissue sections were washed twice in 95% EtOH solutions for five minutes each time until clear, followed by two washes in 100% EtOH for five minutes. Tissue sections were then fully dehydrated in xylene for 15 minutes and coverslipped.

2.3.3 MALDI-MSI data acquisition

MALDI-MSI data were acquired in the linear and positive mode using both an Applied Biosystems (Ontario, Canada) Voyager DE^{TM} PRO and a Voyager DE^{TM} STR equipped with a 337 nm nitrogen (N_2) laser operating at a repetition rate of 20 Hz. Full scan mass spectra were recorded in the m/z between 2000 to 50000. 200 to 500 laser shots were averaged to create a spectrum from each droplet. Mass spectra were internally calibrated using signals from the α and β chains of haemoglobin peaks in the spectra.

2.3.4 MALDI-MS profiling and imaging data processing

Protein profiles were pre-processed using SpecAlign which has the ability to perform spectral alignment as an additional pre-processing step [24, 25]. Imaging data acquisition was performed at a spatial resolution of 250 μm. Protein images were generated with BioMap 3.7.5.5 software (Novartis, Basel, Switzerland) capable of monitoring the amplitude of selected mass signals and reconstructing 2-D ion density maps.

2.4 Results and Discussion

2.4.1 Evaluation and optimisation of the matrix concentration

The development and improvement of the MALDI-MSI method for the investigation of protein directly within tumour tissue sections was performed using frozen rat liver tissue sections. For most applications sinapinic acid has been found to be an excellent matrix for protein analysis resulting in a superior quality mass spectrum containing over 300 individual signals [28]. It also provides good signal-to-noise ratio (S/N) and a low baseline compared to α-CHCA for instance, which is more suitable for low molecular weight compounds. However some improvements were made to increase the crystallization process on the tumour tissue sections. This demonstrates that adjustments of the concentration of the matrix solution and the TFA can provide increased protein signal intensities.

Figure 2.2 shows that higher matrix concentrations result in improved quality spectra. MS analyses performed on each droplet clearly show that a 25 mg/mL matrix solution yields the highest number of ion signals with an improved resolution when compared with a 10 mg/mL solution.

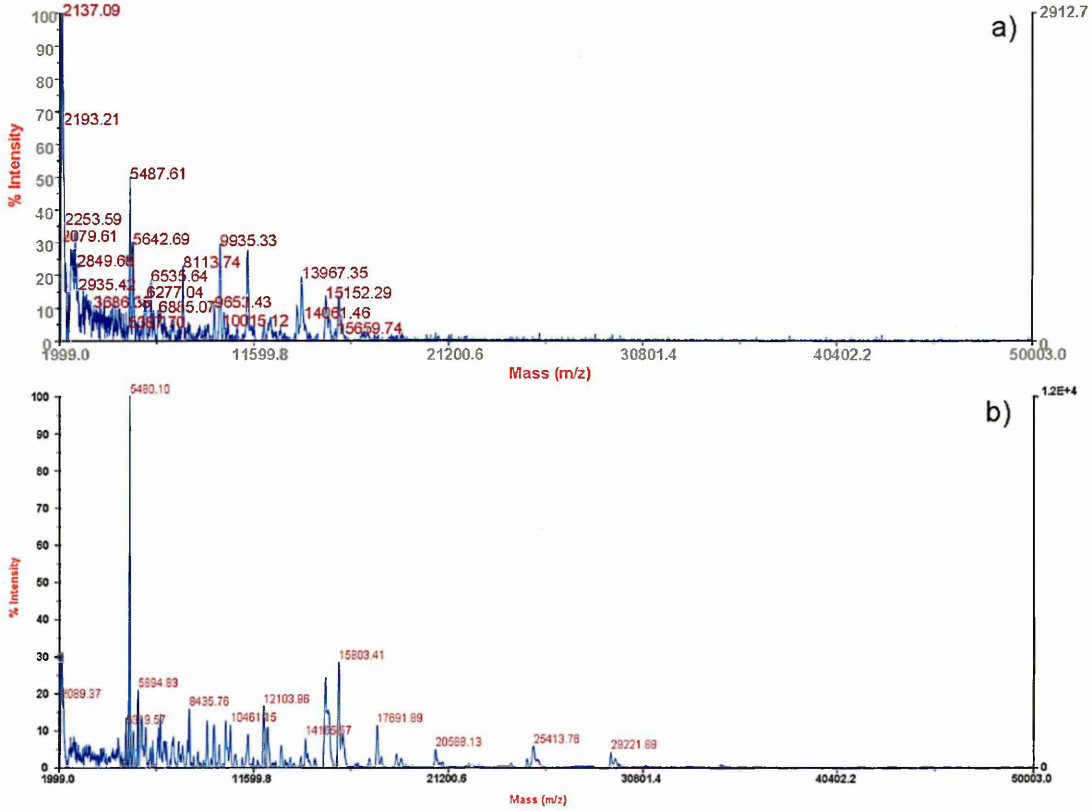

Figure 2.2: **Effect of matrix concentration on the resulting mass spectra from a rat liver section.**
Solutions of SA were made up in EtOH:dH_2O:TFA (1:1:0.1) at concentrations of (a) 10 mg/mL and (b) 25 mg/mL. 300 nL matrix spots were deposited on rat liver tissue sections and direct protein profiles were acquired. Protein signals are detected above m/z 20000 when using a matrix concentration of 25 mg/mL.

The TFA concentration was also found to affect the obtained protein profiles. Figures 2.3a, b and c show that an increased concentration of TFA improved the observed protein signal intensities. However a TFA concentration of 1% was found to inhibit some ion signals. Using 0.5% TFA was found to be an optimum concentration of TFA added to the matrix solution. The analysis of the rat liver samples allowed the improvement of the sample preparation as well as the optimisation of the MALDI-MSI method for direct protein analysis in tumour tissue sections.

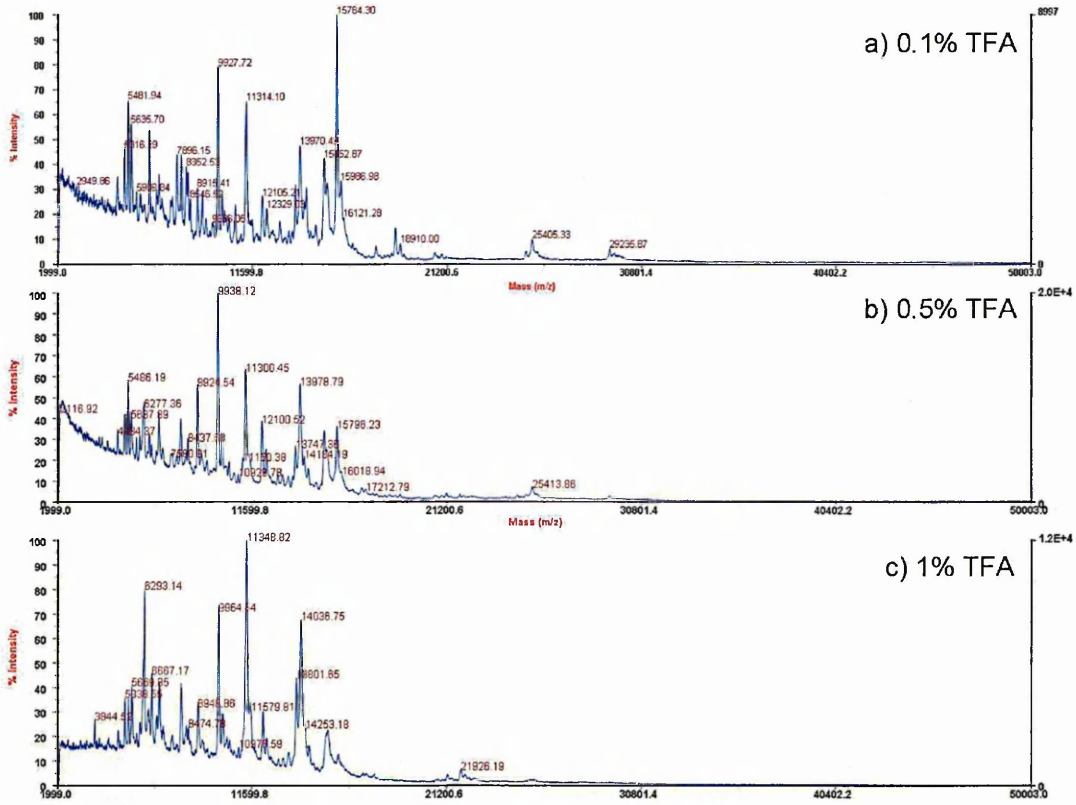

Figure 2.3: **Effect of TFA concentration on the protein profiles obtained from a rat liver section.**
Solutions of SA (25 mg/mL) were made up in 50% ethanol with various concentration of TFA set at 0.1% (a), 0.5% (b) and 1% (c) respectively. 300 nL matrix spots were deposited on rat liver tissue sections and direct protein profiles were acquired. 0.5% TFA yields improved protein profiles.

2.4.2 Direct protein profiling and imaging in MCF-7 xenograft tissue sections using MALDI-MS

The method previously described in section 2.4.1 was optimised and used to investigate protein expression in MCF-7 breast tumour xenograft samples. As breast tissues are primarily adipose tissues the detection of low molecular mass compounds only may result from the limited access to proteins due to the high lipid content. Therefore a tissue-washing procedure previously described by Lemaire *et al.* was applied and improved [27]. In this published work, a washing method using organic solvents such as chloroform ($CHCl_3$), hexane, toluene, acetone and xylene was studied. This allowed the extraction of lipids from the tissue before analysis by MALDI-MSI. This procedure improved detection of peptides/proteins (m/z 5000-30000) by enhancing signal sensitivity.

In the work reported here, tissue sections were first washed in increasing concentrations of ethanol (from 50% to 90%) for 1 minute followed by a wash with $CHCl_3$ for 30 seconds. This aimed to remove residual salts from the tissue sections as well as reduce lipid content. Figure 2.4 shows protein profiles obtained from a xenograft section. A good number of proteins were observed, after rinsing the section with $CHCl_3$.

Spectra were acquired from the necrotic and tumour regions of the section. Different profiles were obtained from each region in terms of protein intensities. Numerous protein signals were observed in the tumour area, some of which were detected only in the tumour cells. Protein signals at m/z 11298.8 and m/z 3999.9 were mostly detected in the tumour area compared to the necrotic region. This shows the specificity of the technique for a given sample.

In both necrotic and tumour region spectra, peaks at m/z 7654.4 and m/z 15328 may correspond to haemoglobin doubly and singly charge peaks respectively. Haemoglobin peaks were used to calibrate all spectra and so minimise the observed shifts in apparent mass values.

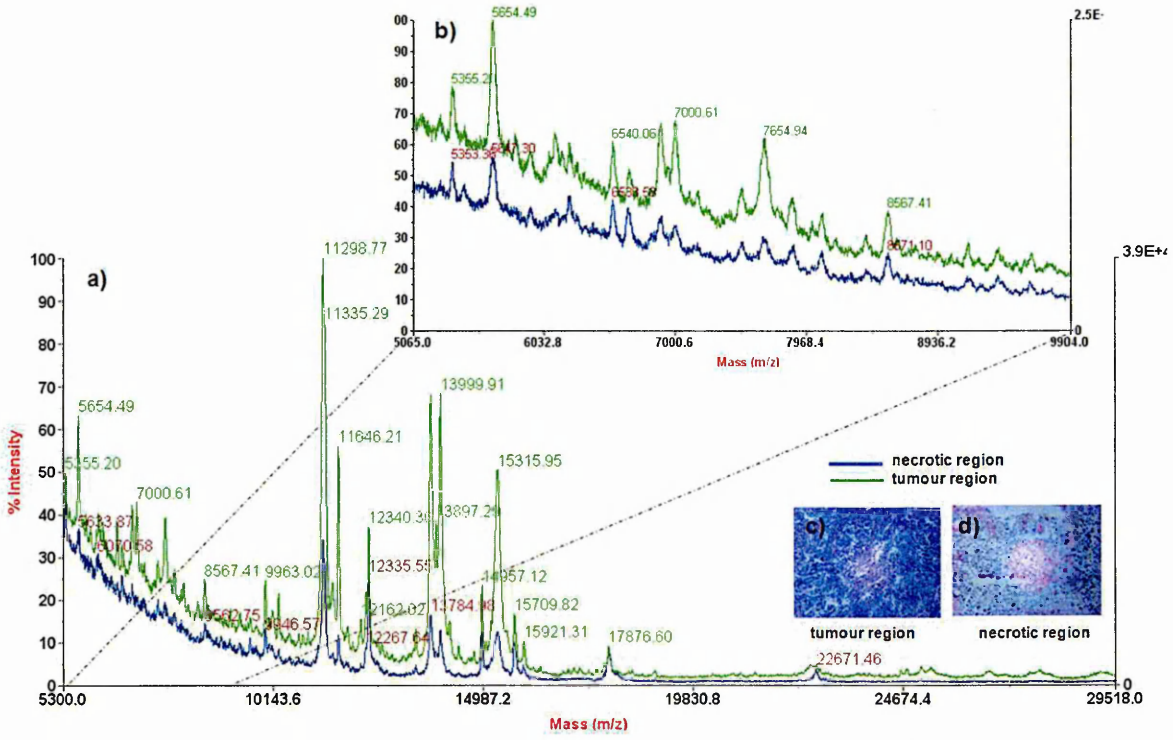

Figure 2.4: **MALDI-MS protein profiles and microscopic images obtained directly from a MCF-7 xenograft tissue section.**
Panel a displays the obtained protein profiles from both tumour and the necrotic regions. The green trace displays protein profile obtained from the tumour region and the blue trace shows the protein profile obtained from the necrotic region. Numerous protein signals were detected. Differences in protein signal intensities were noticed, this can be highlighted in both the entire mass spectrum and the zoomed in spectrum (panel b). Panels c and d display the microscopic images obtained after HE histological staining of the section: the microscopic images were obtained from tumour and necrotic regions respectively.

MALDI-MS imaging was also performed to investigate protein distribution within the section. Figures 2.5a, b and c show images obtained following HE staining of a MCF-7 xenograft section. Protein distributions within the tumour and necrotic area were generated. Figure 2.5d shows the section after matrix coverage. MALDI-MS images were acquired at a spatial resolution of 250 μm. The protein distributions shown in figures 2.5e, f, g and h were in good agreement with results from profiling analysis as well as the histological staining since protein localisation as well as difference observed in signal intensities allowed the discrimination between necrotic and tumour regions. Signals at m/z 14154 and m/z 24995 were abundant in the tumour region. The protein signal at m/z 12422 was predominantly found in the necrotic region. Additional observations can be made from these data. Protein signals can be observed outside of the tissue section on the resulting images. This may be due to the matrix coverage method, which was performed by manually spraying the matrix solution onto the section. Several papers have reported the minimisation of protein delocalisation from matrix application by using other devices such as robotic printers, which allow an improved matrix deposition [29, 30]. However, the MALDI images were found to be in general agreement with the results from direct profiling analysis in terms of specificity.

The method developed here allows direct protein profiling and imaging to be carried out on the MCF-7 tumour tissue sections. The ability of the technique to differentiate regions within tumour tissue sections was shown using both direct protein profiling and imaging MALDI-MSI analysis. However, statistical analysis is required for disease classification and biomarker validation purposes from such data and the development of methodology for this is described in the next sections [31, 32].

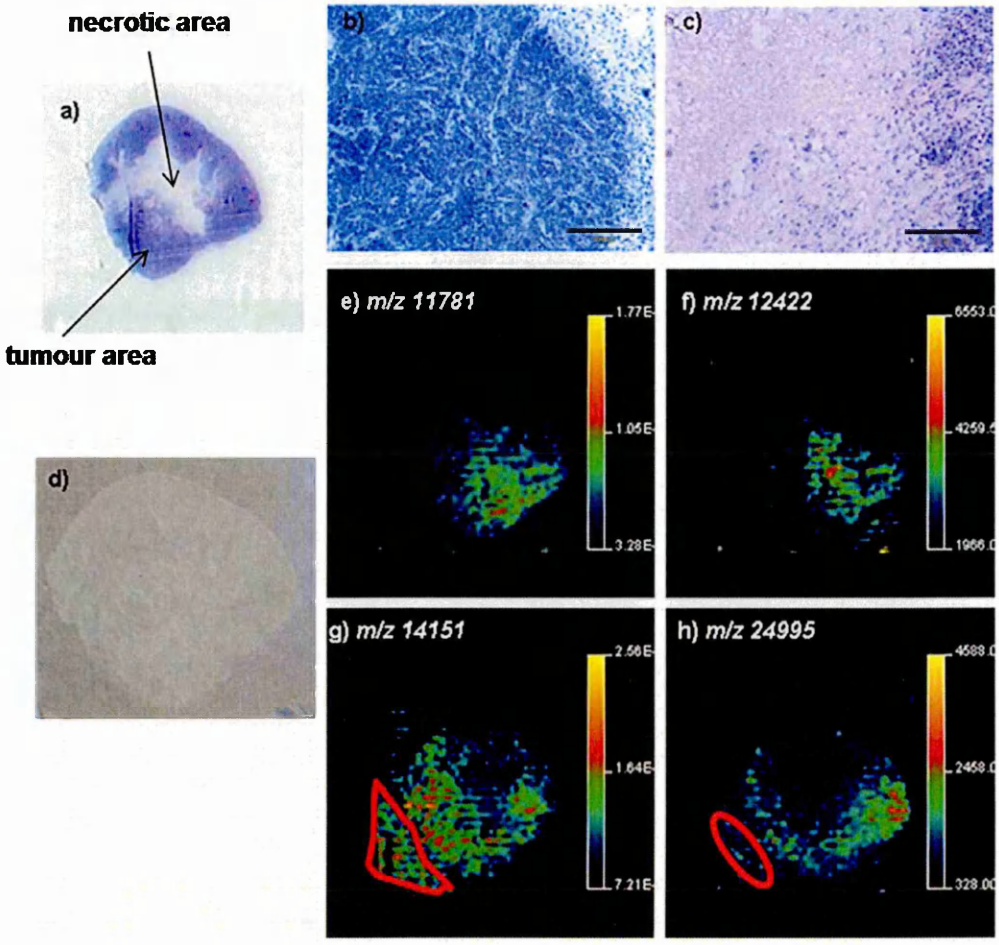

Figure 2.5: **Images of protein distribution within MCF-7 breast tumour xenograft tissue sections.**
Optical and MALDI-MSI images of a MCF-7 breast tumour xenograft section are displayed. Panel a displays a digital scan of a HE staining of a MCF-7 breast tumour xenograft tissue section: the necrotic region (light colour) is surrounded by the tumour area (strong purple). Panels b and c display the microscopic images of the tumour and necrotic area respectively: the image were acquired at x10 magnification. Panel d shows the section after matrix coverage before acquiring MALDI images. Panels e, f, g, and h are MALDI-MS images of protein distributions at m/z 11781, 12422, 14151 and 24995 respectively within the tissue section. However, protein signals can be observed outside the tissue section in the outlined (in red) region on panel g and h, probably due to the matrix deposition method.

2.4.3 Method development for MALDI-MSI data pre-processing

The use of MALDI-MSI for direct profiling and imaging of biological tissues is of interest for clinical purposes and diagnosis. However, before validation in clinical fields, statistical analysis is required. As each MALDI-MSI experiment generates a large amount of data, a workflow has been described by Norris *et al.* showing the need for pre-processing of such data prior to statistical analysis [23]. These pre-processing stages consist of baseline correction, noise removal, normalisation, calibration and spectral alignment.

2.4.3.1 Data alignment using SpecAlign

Using standard instrument software (such as Applied Biosystems Data Explorer^{TM} as used here) one can easily achieve baseline correction, noise suppression and calibration of mass spectra. Indeed proper calibration of the instrument allows reasonable mass accuracy in the linear mode for protein profiling. In some cases the use of an internal calibrant aids alignment of the spectra [23]. Figure 2.6 shows an overlay of protein profiles obtained from tumour and necrotic regions of a xenograft section. Haemoglobin peaks were used as an internal calibrant. Manual calibration was performed using DataExplorer^{TM} software. On these profiles mass shifts between similar compounds were observed. This can be noticed in the zoomed-in spectra where signals at m/z 11312 have been highlighted. Therefore, even if the use of an internal calibrant helps with aligning spectra, the irregularity of the tissue section flatness and/or thickness may induce mass measurement variabilities, meaning an appropriate spectral alignment tool is needed.

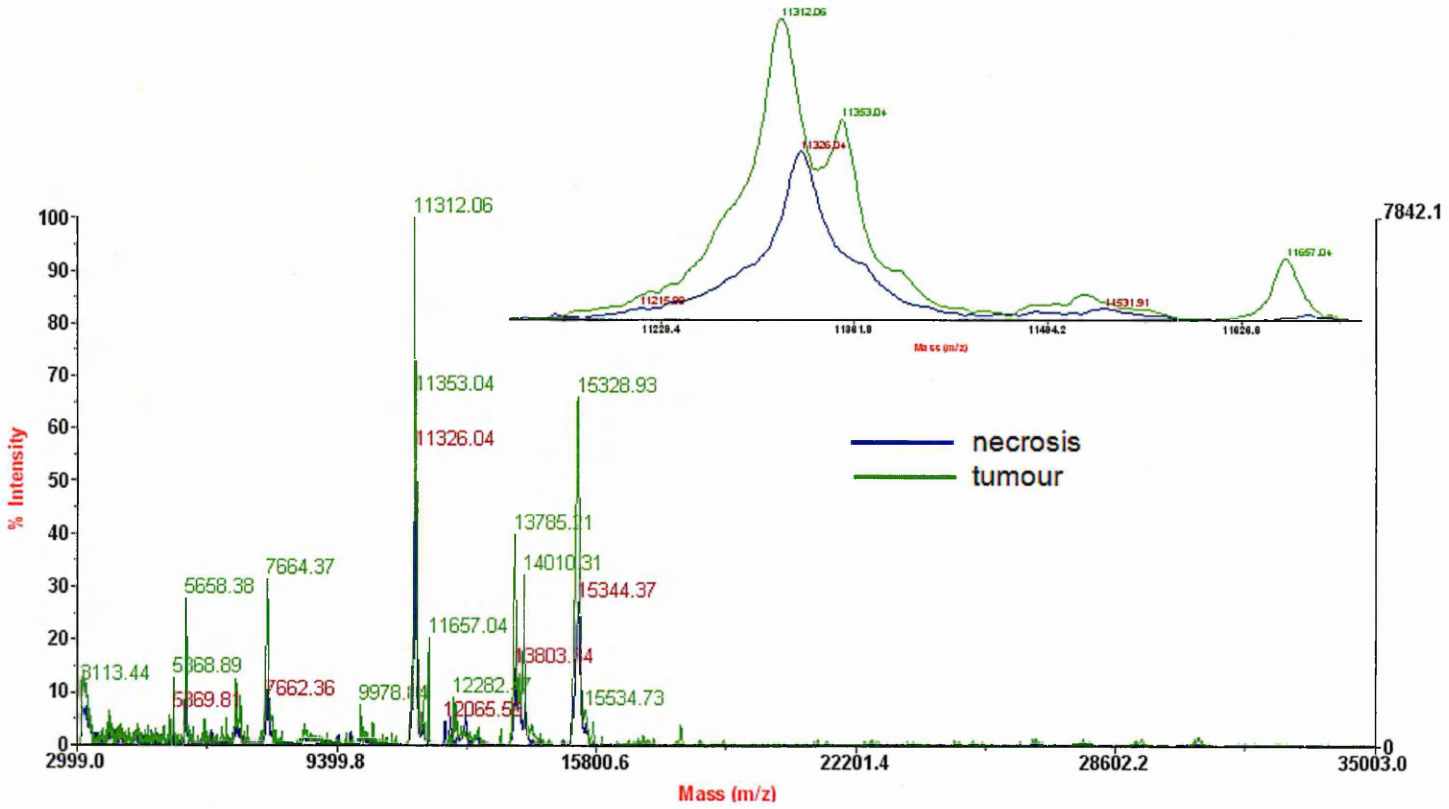

Figure 2.6: **MALDI-MS protein profiles of MCF-7 xenograft tissue sections obtained from necrotic and tumour regions of the section.**
Spectra were processed with DataExplorer^{TM} (Applied Biosystems, Ontario, Canada). These data were baseline corrected, noise removed and calibrated using haemoglobin peaks. Mass shifts were observed when spectra are extended and overlaid: cropped spectra are displayed in the right corner.

In this work, SpecAlign, which is a freely available software tool, was used to aid data pre-processing prior to statistical analysis [24, 33]. The same data were imported into SpecAlign as text files for spectral pre-processing. The pre-processing step consisted of baseline correction, noise removal, normalization by the total ion count (TIC) and finally alignment according to a peak matching method available with the software. Normalising the data allows the projection of all ion intensities onto an average intensity scale to facilitate and improve spectral comparison. In TIC normalisation all spectra are adjusted so they become the same and equal to the average TIC for all spectra [23, 24].

Figure 2.7 shows the aligned spectra produced using SpecAlign. Spectra were aligned using a peak matching method provided by the software. Spectra are presented from m/z 11000 to 12800. The mass shift between spectra is minimised and data are easy to compare.

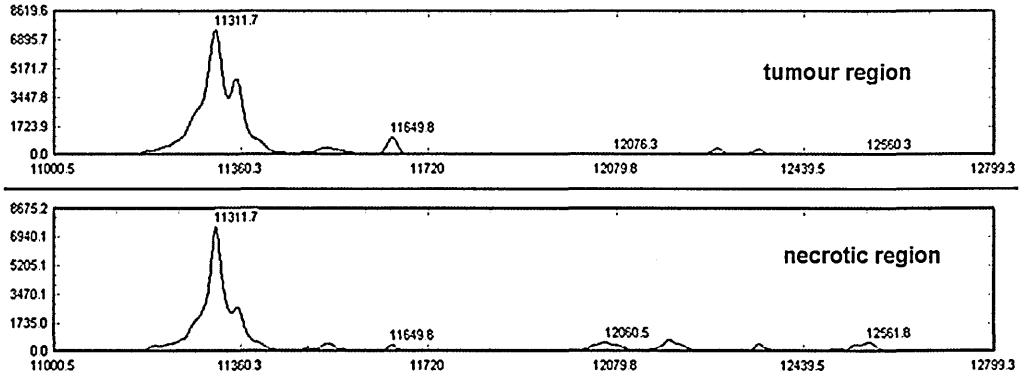

Figure 2.7: **MALDI-MS protein profiles obtained directly from MCF-7 xenograft tissue sections and processed with SpecAlign.**
Spectra were cropped from m/z 11000 to m/z 12800. Data were imported into SpecAlign as text files. Spectra were baseline corrected, noise removed, normalized with the TIC and finally aligned following a peak matching method.

Five serial MCF-7 xenograft tissue sections were used for direct MALDI-MS profiling analysis in order to generate average protein profiles from both tumour and necrotic regions. Figure 2.8 shows examples of the resulting MALDI mass spectra after data pre-processing using SpecAlign software (*i.e.* baseline correction, noise removal, normalisation and spectral alignment). The average mass spectra are displayed in the mass range m/z 3000 to 35000, as signals were not detected above 35000.

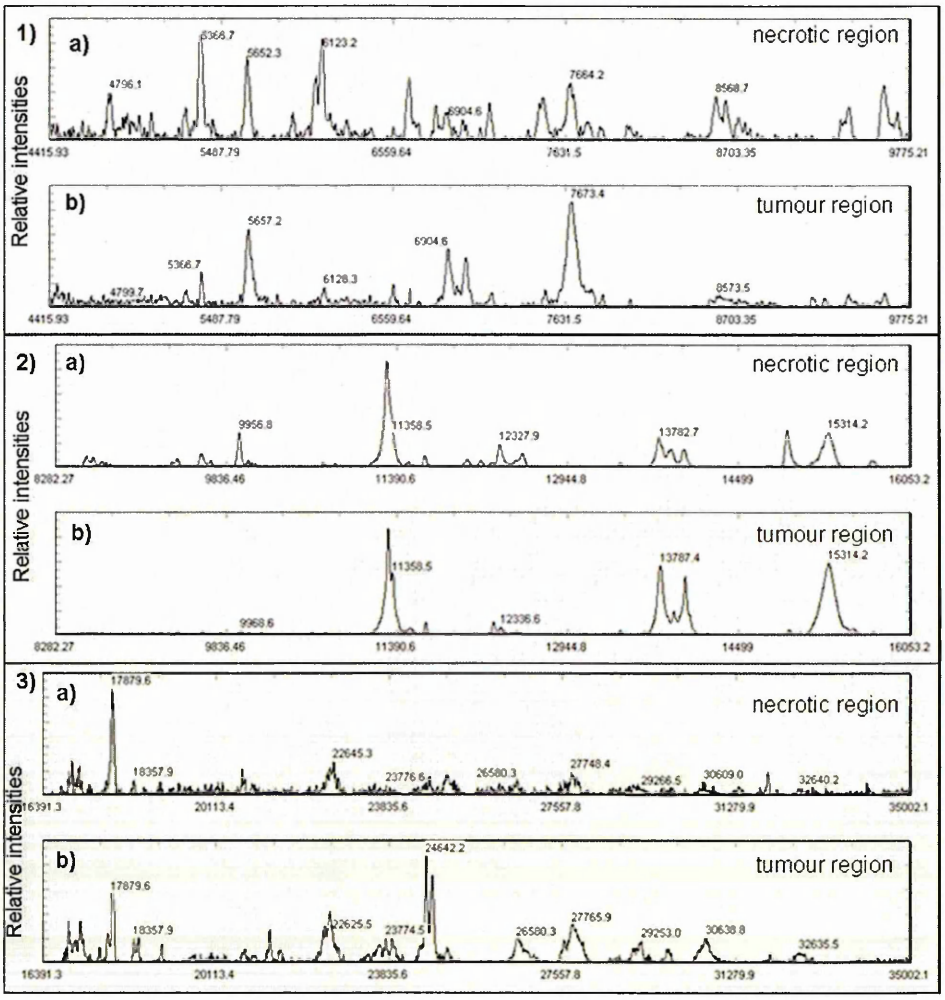

Figure 2.8: **Direct MALDI-MS protein profiles obtained after data acquisition and processing with SpecAlign from a MCF-7 tumour xenograft tissue section.**
Average mass spectra are displayed for both necrotic and tumour regions in the m/z range 4400 to 35000. The mass spectra obtained from both necrotic and tumour regions were cropped from (1) m/z 4400 to 9800, (2) m/z 8280 to 16060 and (3) m/z 16390 to 35000.

Many protein signals were observed and different profiles were obtained from tumour and necrotic regions in terms of signal intensities. The necrotic area was found to be data rich in the m/z range between 4000 and 10000 compared to the tumour region. Necrosis is a non-specific mode of cell death in which lysis of cells takes place. The increased number of observed signals in the necrotic protein profiles could relate to proteolysis occurring during cell death. Some signals were mostly detected in the tumour area including those at m/z 6904.6 and 7673.4. The protein at m/z 7673.4 may correspond to the doubly charged species of haemoglobin alpha. These data are in agreement with those already reported by Reyzer *et.al.* [20], in which this signal was found to be abundant in transgenic breast tumour samples.

It has been reported that histones represent good targets for MALDI-MSI in tumour tissue sections [20, 34]. The obtained profiles from the tumour region were also data rich in the histone mass range (m/z 10000 to m/z 15000). Signals at m/z 11358, 13787 and 15314 are detected in the tumour and necrotic area and may correspond to histone species.

Although the signal-to-noise ratio of protein signals decreased considerably in the mass range above m/z 30000, the obtained protein profiles allow the detection of protein signals in the tumour region. This can clearly be seen in the zoomed in spectra (m/z 17000 to 35000, figures 2.83a and b). Signals at m/z 24642.2, 24772.72, 27765.9 and 30638.8 were only detected in the tumour region.

The use of SpecAlign, which combines calibration and alignment steps, was found to improve data comparison and provides accurate peak assignments. However, whilst it has been reported that spectral alignment carried out before calibration minimises errors in m/z assignment [23], it is not currently possible to import files from SpecAlign back into DataExplorer^{TM}, because the file formats are not compatible.

2.4.3.2 Benefit of data pre-processing for statistical analysis

2.4.3.2.1 *Use of SpecAlign for data pre-processing of MALDI-MS protein profiling*

For statistical analysis, principal component analysis (PCA) was carried out using aligned text spectra obtained from the xenografts. Five spectra were acquired from both tumour and necrotic regions. These spectra were then aligned with SpecAlign software and converted into text files. PCA was performed using a pre-release version of Applied Biosystems/MDS Sciex Markerview^{TM} statistical analysis software (Applied Biosystems/MDS Sciex, Ontario, Canada). A supervised analysis was carried out with a Pareto scaling.

As can be seen in figure 2.9A, the scores plots show clearly 2 different groups corresponding to the tumour and necrotic regions of the tissue section (red and blue plots respectively). Positive and negative principal components 3 (PC3) are observed in the scores plots for the tumour region. This can be explained by the fact that each data set results from a spot analysis, hence showing protein signals highly or less intense within the same region. However, the results are still in agreement with those obtained from direct protein profiling with MALDI-MS. In the loading plots (figure 2.9B) the outlying highlighted ions account for the observed difference between spectra. For example protein species at m/z 11266 and m/z 15308 were found to be abundant in the tumour region.

The same statistical analysis was performed using non aligned data; these were simply calibrated using DataExplorer^{TM} (Figure 2.10). In the scores plots it can be noticed that both the positive and negative principal components 1 and 3 (PC1 and PC3) are observed for the tumour area. The groups are not clearly distinguished, hence making the data difficult to explain. These data demonstrate that spectral alignment with SpecAlign prior to statistical analysis improves the results obtained.

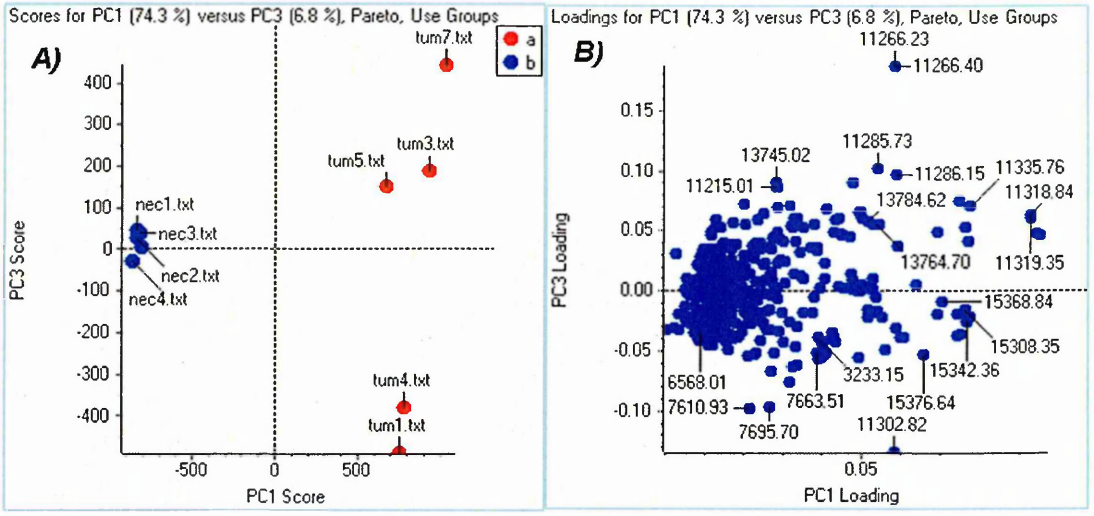

Figure 2.9: **Supervised principal component analysis (PCA) results obtained from aligned protein profiles of MCF-7 xenograft tissue sections.**
Panel (A) displays the score plots which indicate the obtained groups after PCA analysis: red (a) and blue (b) plots correspond to tumour and necrotic regions respectively. Panel (B) shows the corresponding loading plots where characteristic m/z values for the groups defined by the score plots are highlighted.

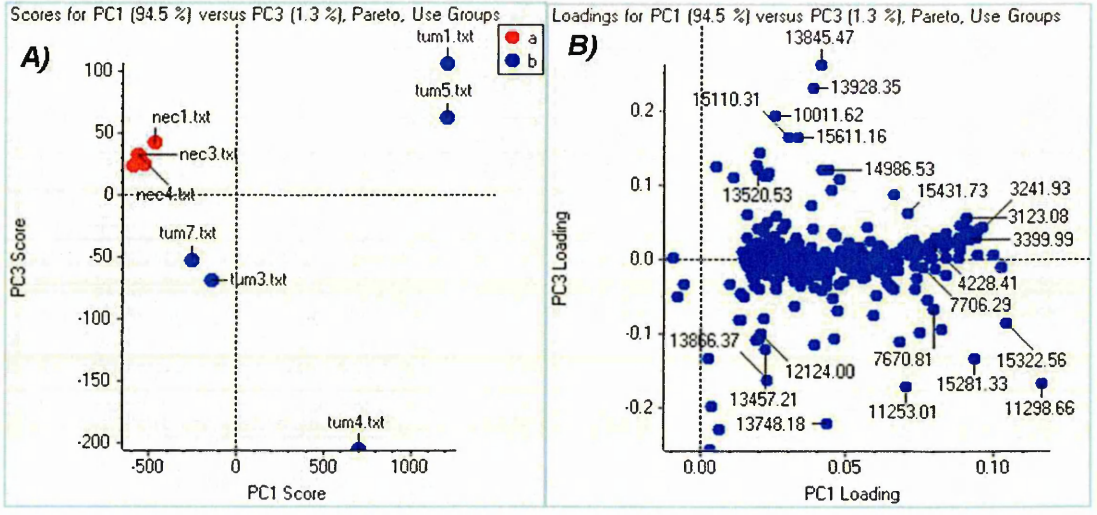

Figure 2.10: **Supervised principal component analysis (PCA) results obtained from non aligned protein profiles of MCF-7 xenograft tissue sections.**
Panel A shows the score plots: red (a) and blue (b) plots are corresponding to necrotic and tumour regions respectively. No distinguished groups are noticed. Panel B displays the corresponding loading plots.

2.4.3.2.2 *Use of SpecAlign for data pre-processing of MALDI-MS protein imaging*

SpecAlign has also proved to be a valuable tool for aiding MALDI-MSI data pre-processing. Images were acquired from xenograft samples. Figure 2.11a represents the histological (H&E) staining of the section. Figure 2.11b shows the matrix coverage onto the section. The resulting images were generated using BioMap software. The regions of interest (ROI) R_1, R_2 and R_3 were then analysed using BioMap and average spectra for each ROI were generated. To represent each ROI, 10 spectra obtained from each were imported into SpecAlign for pre-processing. The method previously described for protein profiling experiments was used (described in section 2.4.3.1). Figure 2.11c shows the resulting spectral alignment of profiles from R_1. Then, supervised PCA was performed (Figure 2.12).

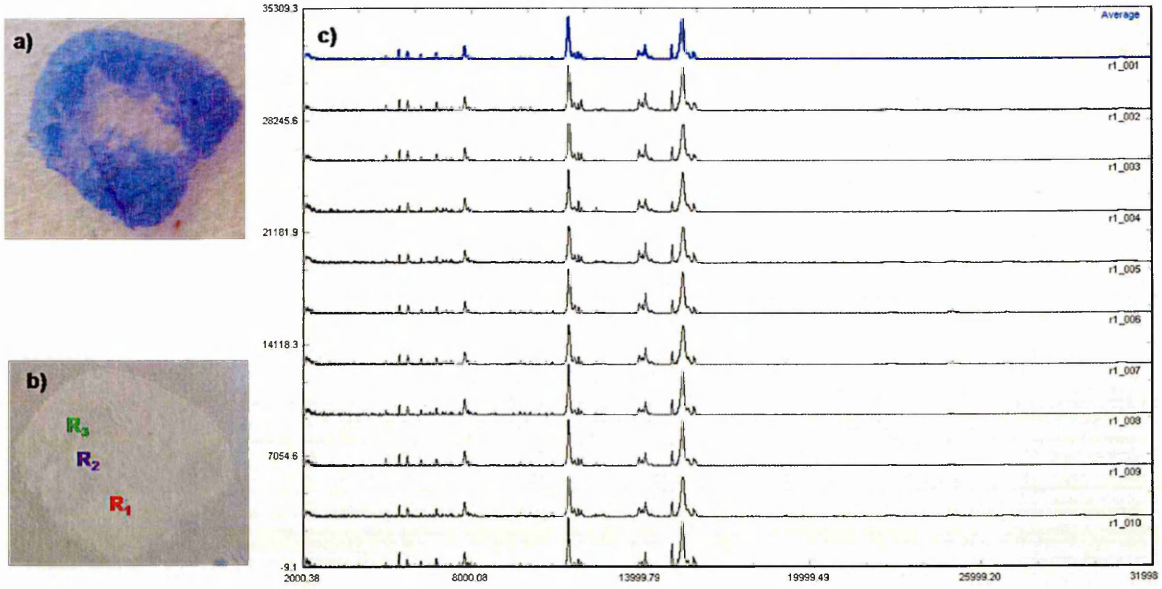

Figure 2.11: **Spectral alignment performed with SpecAlign using MALDI-MS imaging data.**
Panel a shows a HE staining picture of the tissue section. Panel b displays the digital scan of the tissue section after matrix deposition onto the section: R_1, R_2 and R_3 represent the regions of interest analysed with BioMap software. Spectral alignment achieved with SpecAlign using protein profiles from R_1 imported from BioMap into SpecAlign is shown in panel c.

As can be seen in figure 2.12A, groups are easily distinguished in the score plots. The plots from R_2 and R_3 overlap because these ROIs represent regions of necrotic tissue. Histological analysis conducted previously indicated that R_3 contained more lymphocyte cells in comparison to R_2, explaining the differentiation between the two groups. In the corresponding loadings plots (figure 2.12B, proteins at m/z 7749.58 and 15120.58 were found highly expressed in R_1 and m/z 13933 was mainly detected in R_2.

In summary, protein profiles and images were obtained directly from tissue sections using an optimised MALDI-MSI method. By combining a good tissue pre-treatment protocol with an appropriate matrix choice and deposition method, protein distributions within the section were generated. Using MALDI-MSI for direct protein profiling and imaging within the tissue section, it was possible to correlate protein abundance to a specific area of the section. Table 2.1 summarises the results obtained from protein profiling analysis: the relative intensities observed from protein signals are displayed. SpecAlign was found to be a valuable tool for aiding data pre-processing, prior to statistical analysis.

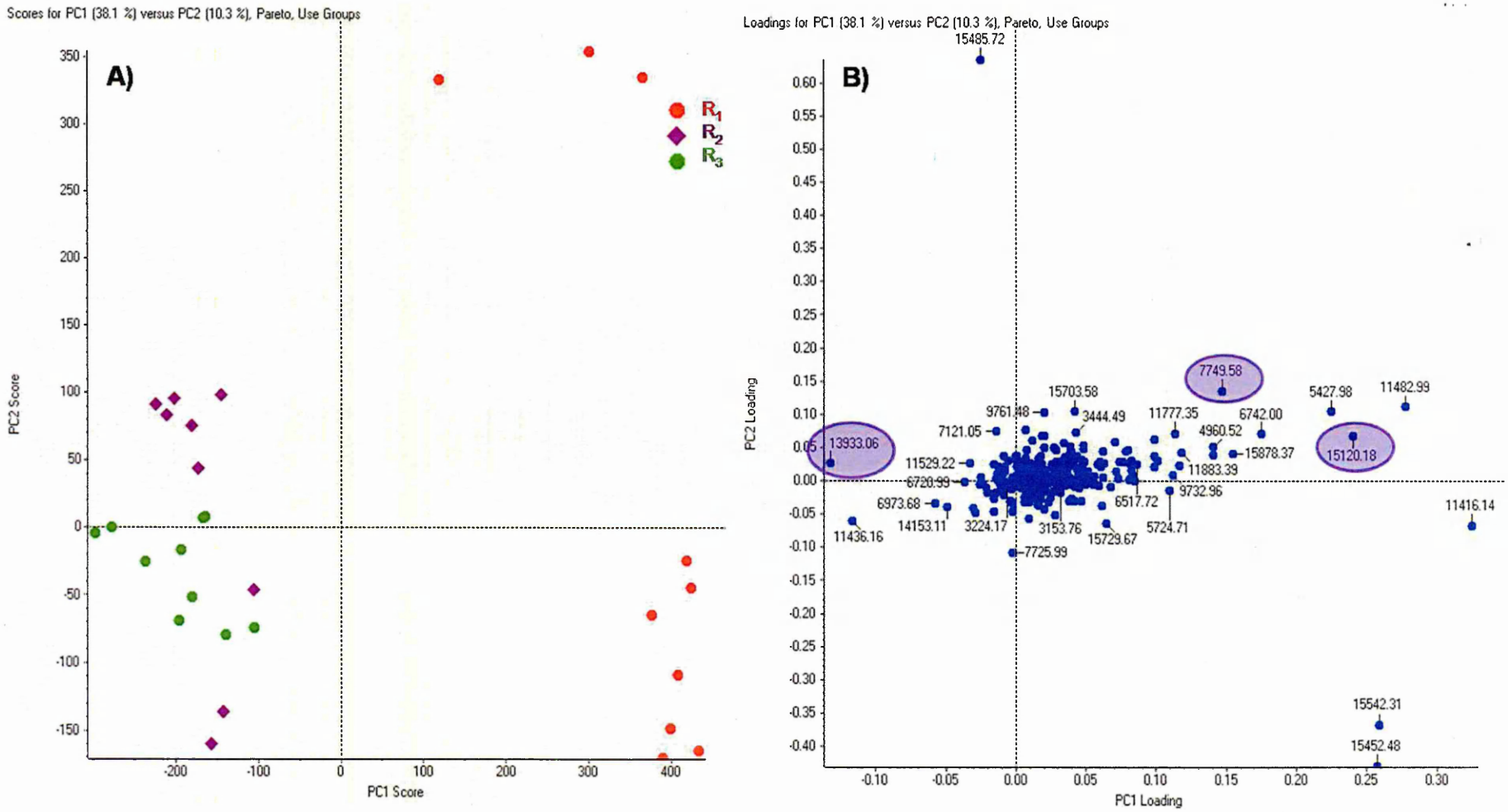

Figure 2.12: **Supervised PCA results obtained from aligned MALDI-MS imaging data obtained from MCF-7 xenograft tissue section.**

Panel A displays the score plots where groups are clearly differentiated. In the scores plots, The spectra exported from the regions of interest R_1, R_2 and R_3 are represented by the red, green and purple plots respectively. (B) The loading plots show the difference between them.

Observed m/z	Tissue region	Relative intensity %	**Observed m/z**	Tissue region	Relative intensity %	**Observed m/z**	Tissue region	Relative intensity %
4236.4	Necrotic	5.64	**7665.2**	Necrotic	5.96	**21267.2**	Tumour	1.22
4623.1	Necrotic	4.86	**7675.7**	Necrotic	5.37	**22411.3**	Tumour	1.73
4781.3	Necrotic	10.93	**7748.3**	Necrotic	4.29	**22456.3**	Tumour	1.15
	Tumour	1.65	**7787.7**	Necrotic	3.24	**22553.9**	Tumour	0.51
4796.1	Necrotic	10.85	**8568.7**	Necrotic	10.01	**22609.4**	Tumour	0.79
	Tumour	2.86		Tumour	3.65	**23505.1**	Tumour	1
4973.586	Necrotic	6.19	**8631.7**	Necrotic	9.47	**23667.9**	Tumour	0.89
	Tumour	1.86	**8708**	Necrotic	6.05	**23772.7**	Tumour	0.59
5054.6	Necrotic	6.11	**8723.3**	Tumour	1.39	**24642.2**	Tumour	3.76
	Tumour	2.14	**8748.4**	Tumour	1.55	**24772.7**	Tumour	3.01
5205.2	Tumour	3.53	**8941.4**	Tumour	2.4	**26580.3**	Tumour	1.36
5214	Tumour	3.95	**9351.9**	Necrotic	5.07	**27765.9**	Tumour	0.79
5267.4	Necrotic	7.11	**9400.7**	Necrotic	8.46	**27807.9**	Tumour	0.55
	Tumour	2.07	**9812**	Necrotic	13.09	**27991.2**	Tumour	0.58
5315.6	Tumour	3.43		Tumour	4.04	**29081.7**	Tumour	0.8
5349.5	Necrotic	23.96	**9775.2**	Necrotic	8.67	**29253**	Tumour	0.83
	Tumour	1.21	**9954.6**	Necrotic	35.39	**29289.3**	Tumour	0.39
5366.7	Necrotic	24.58	**10036.1**	Necrotic	8.44	**29797.3**	Tumour	0.62
	Tumour	7.43	**10067.5**	Necrotic	6.42	**30638.8**	Tumour	0.92
5437.7	Necrotic	6.08	**11189.9**	Necrotic	7.73	**30567.4**	Tumour	
5657.2	Necrotic	20.57	**11293.3**	Necrotic	100	**30634.7**	Tumour	
	Tumour	18.17		Tumour	100	**30697.9**	Tumour	
5664.2	Tumour	3.01	**11358.7**	Necrotic	52.37	**32590.9**	Tumour	
5700.2	Tumour	3.15	**11163.2**	Tumour	62.74			
6075.2	Necrotic	13.81	**12327.9**	Necrotic	22.05			
6123.2	Necrotic	22.68		Tumour	13.38			
	Tumour	4.03	**12336.6**	Tumour	8.62			
6270.2	Necrotic	4.5	**12482.3**	Necrotic	8.14			
6559.6	Tumour	5.74	**12527.8**	Necrotic	13.72			
6657.7	Necrotic	16.36	**13787.4**	Necrotic	28.55			
	Tumour	4.75		Tumour	65.14			
6639.1	Tumour	1.53	**13855.1**	Necrotic	17.08			
6717.4	Necrotic	6.09		Tumour	23.77			
6799.4	Necrotic	4.37	**13984.7**	Necrotic	18.06			
6825.5	Necrotic	9.65		Tumour	58.18			
6904.6	Necrotic	9.78	**14938.2**	Necrotic	35.87			
	Tumour	13.77	**15314.2**	Necrotic	33.38			
6957.1	Necrotic	8.44		Tumour	68.17			
	Tumour	11.3	**16457.7**	Necrotic	8.34			
6974.1	Tumour	4.08		Tumour	9.07			
7011.4	Necrotic	5.61	**16488.2**	Necrotic	3.57			
	Tumour	1.07		Tumour	3.84			
7573.7	Necrotic	9.48	**17879.6**	Necrotic	5.3			
	Tumour	5.26		Tumour	2.78			
7664.2	Necrotic	13.76	**17917.1**	Tumour	1.19			
	Tumour	25.11	**18357.9**	Tumour	1.42			

Table 2.1: **List of detected proteins after direct MALDI-MSI analysis of MCF-7 breast tumour xenograft tissue sections.**
Observed masses are displayed with their corresponding relative intensities in tumour and/or necrotic regions

2.5 Concluding Remarks

Understanding the biological processes that occur in cancer remains challenging and still requires not only the investigation of the molecular compounds involved in these mechanisms, but also their spatial localisation within the tissue section itself. In this chapter, the use of MALDI-MSI for a direct investigation of the proteomic information within tumour tissue sections was described. MALDI-MSI can easily be applied to several types of tissues even if specific tissue treatment and matrices are required. By using this technique direct protein profiling and imaging were performed; additionally regions of interest within the section were differentiated. Some proteins were found to be abundant and mainly located in the tumour regions of MCF-7 xenograft tissue sections. Differences observed in signal intensities allow discrimination between tumour and necrotic regions. This is beneficial because by combining both MALDI data and histological studies, some proteins can be selected regarding their function or involvement in the disease progression. Another interesting aspect of the technique is that unknown proteins or proteins not detected by the histological analysis can be visualised with MALDI MS imaging. The technique was powerful in generating both protein profiles and images across MCF-7 breast tumour tissue sections.

Each MALDI-MSI experiment generates a large amount of data. Variations related to the tissue section itself, the sample preparation as well as the instrument can be observed, and so data pre-processing is required prior to statistical analysis. Here, a pre-processing method was developed using SpecAlign software. Combining SpecAlign with DataExplorer^{TM} has been shown to improve data pre-processing, leading to acceptable statistical analysis and facilitating the interpretation of results. It has been demonstrated that SpecAlign can be used as a complementary tool for MALDI-MS imaging data pre-processing in order to decrease instrument variations considerably. However, the method still needs to be optimised in order to import aligned spectra back into DataExplorer^{TM} for the calibration process.

Direct protein profiling and imaging from tumour tissue sections with MALDI-MS enabled the acquisition of protein distribution. However, to help in understanding the biological process occurring during disease progression, the identification of these proteins is required. Even more desirable is the *in situ* identification and distribution of proteins directly within tumour tissue sections as this will maintain their spatial localisation.

References

[1] Liotta L.A. and Kohn E.C. The microenvironment of the tumourhost interface. *Nature*, 411:375–379, 2001.

[2] Fidler I.J. The pathogenesis of cancer metastasis: the seed and soil hypothesis revisited. *Nature Reviews Cancer*, 3:1–6, 2003.

[3] Pantel K. and Brakenhoff R.H. Dissecting the metastatic cascade. *Nature Reviews Cancer*, 4:448–456, 2004.

[4] Srinivas P.R., Kramer B.S., and Srivastava S. Trends in biomarker research for cancer detection. *Lancet Oncology*, 2:698–704, 2001.

[5] Ramaswamy S. and Perou C.M. DNA microarrays in breast cancer: the promise of personalised medicine. *The Lancet*, 361:1576–1577, 2003.

[6] Fernie A.R., Trethewey R.N., Krotzky A.J., and Willmitzer L. Metabolite profiling: from diagnostics to systems biology. *Nature Reviews Molecular Cell Biology*, 5:763–769, 2004.

[7] Etzioni R., Urban N., Ramsey S., McIntosh M., Schwartz S., Reid B., Radich J., Anderson G., and Hartwell L. The case for early detection. *Nature Reviews Cancer*, 3:243–252, 2003.

[8] Srinivas P. R., Verma M., Zhao Y., and Srivastava S. Proteomics for cancer biomarker discovery. *Clinical Chemistry*, 48:1160–1169, 2002.

[9] Rifai N., Gillette M.A., and Carr S.A. Protein biomarker discovery validation: the long uncertain path to clinical utility. *Nature Biotechnology*, 24:971–983, 2006.

[10] Marko-Varga G., Lindberg H., Lofdahl C.G., Jonsson P., Hansson L., Dahlback M., Lindquist E., Johansson L., Foster M., and Fehniger T.E. Discovery of biomarker candidates within disease by protein profiling: principles and concepts. *Journal of Proteome Research*, 4:1200–1212, 2005.

[11] Caprioli R.M., Farmer T.B., and Gile J. Molecular imaging of biological samples: localization of peptides and proteins using MALDI-TOF MS. *Analytical Chemistry*, 69:4751–4760, 1997.

[12] Stoeckli M., Chaurand P, Hallahan D.E., and Caprioli R.M. Imaging mass spectrometry: A new technology for the analysis of protein expression in mammalian tissues. *Nature Medicine*, 7:493–496, 2001.

[13] Todd P.J., Schaaff T.G., Chaurand P., and Caprioli R.M. Organic ion imaging of biological tissue with secondary ion mass spectrometry and matrix-assisted laser desorption/ionization. *Journal of Mass Spectrometry*, 36:355–369, 2001.

[14] Chaurand P, Schwartz S.A., and Caprioli R.M. Imaging mass spectrometry: a new tool to investigate the spatial organization of peptides and proteins in mammalian tissue sections. *Current Opinion in Chemical Biology*, 6:676–681, 2002.

[15] Chaurand P., Fouchecourt S., DaGue B.B., Xu B.J., Reyzer M.L., Orgebin-Crist M.C., and Caprioli R.M. Profiling and imaging proteins in the mouse epididymis by imaging mass spectrometry. *Proteomics*, 3:2221–2239, 2003.

[16] Chaurand P., Norris J.L., Cornett D.S., Mobley J.A., and Caprioli R.M. New developments in profiling and imaging of proteins from tissue sections by MALDI mass spectrometry. *Journal of Proteome Research*, 5:2889–2900, 2006.

[17] Chaurand P., DaGue B.B., Pearsall R.S., Threadgill D.W., and Caprioli R.M. Profiling proteins from azoxymethane-induced colon tumors at the molecular level by matrixassisted laser desorption/ionization mass spectrometry. *Proteomics*, 1: 1320–1326, 2001.

[18] Lemaire R., Menguellet S.A., Stauber J., Marchaudon V., Lucot J.P., Collinet P., Farine M.O., Vinatier D., Day R., Ducoroy P., Salzet M., and Fournier I. Specific MALDI imaging and profiling for biomarker hunting and validation: fragment of the 11S proteasome activator complex, Reg alpha fragment, is a new potential ovary cancer biomarker. *Journal of Proteome Research*, 6:4127–4134, 2007.

[19] Schwamborn K., Krieg R.C., Reska M., Jakse G., Knuechel R., and Wellmann A. Identifying prostate carcinoma by MALDI-Imaging. *International Journal of Molecular Medicine*, 20:155–159, 2007.

[20] Reyzer M.L., Caldwell R.L., Dugger T.C., Forbes J.T., Ritter C.A., Guix M., Arteaga C.L., and Caprioli R.M. Early changes in protein expression detected by mass spectrometry predict tumor response to molecular therapeutics. *Cancer Research*, 64:9093–9100, 2004.

[21] Rubakhin S.S., Jurchen J.C., Monroe E.B., and Sweedler J.V. Imaging mass spectrometry: fundamentals and applications to drug discovery. *Drug Discovery Today*, 10:823–836, 2005.

[22] Sausville E.A. and Burger A.M. Contributions of human tumor xenografts to anticancer drug development. *Cancer Research*, 66:3351–3354, 2008.

[23] Norris J.L., Cornett D.S., Mobley J.A., Andersson M. Seeley E.H., Chaurand P., and Caprioli R.M. Processing MALDI mass spectra to improve mass spectral direct tissue analysis. *International Journal of Mass Spectrometry*, 260:212–221, 2007.

[24] Wong J.W., Cagney G., and Cartwright H.M. SpecAlign–processing and alignment of mass spectra datasets. *Bioinformatics*, 21:2088–2090, 2005.

[25] Djidja M., Carolan V., Loadman P.M., and Clench M.R. Method development for protein profiling in biological tissues by matrix-assisted laser desorption/ionisation mass spectrometry imaging. *Rapid Communication in Mass Spectrometry*, 22: 1615–1618, 2008.

[26] United Kingdom Co ordinating Committee on Cancer Research (UKCCCR). Guidelines for the Welfare of Animals in Experimental Neoplasia (Second Edition). *British Journal of Cancer*, 77:110, 1998.

[27] Lemaire R., Wisztorski M., Desmons A., Tabet J.C., Day R., Salzet M., and Fournier I. MALDI-MS direct tissue analysis of proteins: improving signal sensitivity using organic treatments. *Analytical Chemistry*, 78:7145–7153, 2006.

[28] Schwartz S.A., Reyzer M.L., and Caprioli R.M. Direct tissue analysis using matrix-assisted laser desorption/ionization mass spectrometry: practical aspects of sample preparation. *Journal of Mass Spectrometry*, 38:699–708, 2003.

[29] Aerni H., Cornett D.S., and Caprioli R.M. Automated acoustic matrix deposition for maldi sample preparation. *Analytical Chemistry*, 78:827–834, 2006.

[30] Shimma S., Furuta M., Ichimura K., Yoshida Y., and Setou M. Direct MS/MS analysis in mammalian tissue sections using MALDI-QIT-TOFMS and chemical inkjet technology. *Surface Interface Analysis*, 38:1712–1714, 2006.

[31] Yanagisawa K., Shyr Y., Xu B.J., Massion P.P., Larsen P.H.and White B.C., Roberts J.R., Edgerton M., Gonzalez A., Nadaf S., Moore J.H., Caprioli R.M., and Carbone D.P. Proteomic patterns of tumour subsets in non-small-cell lung cancer. *The Lancet*, 362:433–439., 2003.

[32] Schwartz S.A., Weil R.J., Thompson R.C., Shyr Y., Moore J.H., Toms S.A., Johnson M.D., and Caprioli R.M. Proteomic-based prognosis of brain tumor patients using direct-tissue matrix-assisted laser desorption ionization mass spectrometry. *Cancer Research*, 65:7674–7681, 2005.

[33] Wong J.W., Durante C., and Cartwright H.M. Application of fast Fourier transform cross-correlation for the alignment of large chromatographic and spectral datasets. *Analytical Chemistry*, 77:5655–5661, 2005.

[34] Chaurand P., Schwartz S.A., and Caprioli R.M. Assessing protein patterns in disease using imaging mass spectrometry. *Journal of Proteome Research*, 3:245–252, 2004.

CHAPTER 3

In situ Protein Identification within Breast Tumour Tissues by MALDI-MSI

3.1 Introduction

The identification of proteins involved in tumour progression or those which might permit improved or novel therapeutic targeting is essential for cancer research. Tissue-based proteomics is becoming an attractive research field as it provides opportunities for biomarker discovery related to disease state, hence improving early detection and diagnosis. Current protein identification techniques are based on the use of LC/MS/MS and 2D gel electrophoresis [1, 2]. Several studies have reported the use of these classical methods for high-throughput proteomic approaches for the identification and quantification of proteins obtained from complex matrices such as cancer cell and tissue lysates [3, 4]. However these techniques require protein extraction, and hence a relatively large amount of tissue sample, prior to protein identification. Furthermore all information regarding the spatial distribution of biomolecules within the tissue sample is lost. Immunohistochemistry (IHC) techniques are commonly used to investigate protein distribution within a tissue section. However IHC requires a target-specific reagent as well as knowledge of individual proteins being analysed.

Direct MALDI-MS analysis of tissue sections is rapidly demonstrating its potential for protein imaging and profiling in the investigation of a range of disease states including cancer [5–9]. Several improvements and advances in the technique have been made including the use of robotic devices to achieve accurate matrix deposition on the tissue section. This has been found to be useful in decreasing protein delocalisation within the tissue section as well as for improving the sensitivity of the technique [10, 11]. One of the most recent and exciting developments in the technique is the use of on-tissue tryptic digestion in order to achieve direct identification of proteins within a tissue section while having at the same time information regarding their spatial distribution. Lemaire *et al.* reported a strategy combining the use of *in situ* micro-digestion and *in situ* extraction of proteins from formalin fixed paraffin embedded (FFPE) tissue sections followed by nano RPLC/MS for the identification of proteins [9]. This approach facilitated and improved the identification and study of the distribution of proteins within archived samples [12]. The use of *in situ* digestion on frozen tissue sections which allowed the identification and distribution of numerous signals within rat brain tissue sections has also been reported [11, 13].

In the work reported here, MALDI-mass spectrometry imaging (MALDI-MSI) has been used to investigate the distribution and for the *in situ* identification of proteins in breast tumour tissue section samples. In the work reported in this thesis, the development and improvement of the *in situ* methodology by incorporating a surfactant in the trypsin digest protocol in a study of frozen and FFPE breast tumour tissue sections is described. This aims to enhance the detection and identification of proteins which are of low abundance or difficult to detect by direct MALDI-MSI. The method was shown to be successful for the identification of numerous protein signals and was able to differentiate between tissue regions within the section. The signal overlap generally encountered after performing on-tissue digestion that makes direct protein identification challenging, is addressed here, by using ion mobility separation (IMS) prior to MALDI-MSI and MALDI-MS/MS. The advantages of using the combination of these technologies following *in situ* digestion are discussed.

3.2 Materials and Methods

3.2.1 Chemical and materials

Modified sequence grade trypsin was purchased from Promega (Southampton, UK). All other materials, including sinapinic acid (SA), alpha-cyano-4-hydroxycinnamic acid (α-CHCA), aniline (ANI), ethanol (EtOH), methanol (MeOH), chloroform ($CHCl_3$), xylene, octyl-α/β-glucoside (OcGlc), trifuoroacetic acid (TFA), haematoxylin, eosin, indium-tin-oxide (ITO) glass slides, hydrogen peroxide (H_2O_2), tri-sodium citrate and ammonium bicarbonate, were purchased from Sigma-Aldrich (Dorset, UK).

3.2.2 Tissue samples

3.2.2.1 MCF-7 breast tumour xenograft samples

MCF-7 breast tumour xenografts were obtained from the Institute of Cancer Therapeutics (Bradford, UK). Investigations and all animal procedures were carried out under a project licence issued by the UK Home Office and guidelines from the United Kingdom Co-ordinating Committee on Cancer Research (UKCCCR) were followed [14]. Female Balb/C immunodeficient nude mice (Harlan UK, Blackthorn, UK) aged 6-8 weeks were used. Mice received CRM diet (SDS, Witham, UK) and water *ad libitum*. Animals were kept in cages in an air-conditioned room with regular alternating cycles of light and darkness. The transplantation of tumour is the same as described in chapter 2 (section 2.2.2.2).

3.2.2.2 Human formalin fixed paraffin embedded (FFPE) breast tumour samples

Ex vivo human breast tumour tissue samples were obtained following fully informed patient consent and local ethical committee approval (Study Number SSREC/04/Q2305 /67 and subsequent amendments). Tissue samples were fixed in 10% buffered formalin for 24 hours, dehydrated in 70% EtOH and paraffin embedded. 5 μm sections were cut using a cryostat (Leica Microsystems, UK) and mounted onto histological Polysine^{TM} glass slides (Menzel-Glaser, Germany). FFPE tissue sections were stored at room temperature until further analysis.

3.2.3 Tissue preparation prior to MALDI-MSI data acquisition

Frozen MCF-7 xenograft tissue samples were cut using a cryostat (Leica Microsystems, UK) operating at -20°C. 10 μm sections were cut and thaw-mounted onto either a TLC foil, from which the stationary phase had been previously removed, or an indium-tin-oxide (ITO) glass slide (Sigma-Aldrich, Dorset, UK). Washing procedures were performed to increase the MS data quality: the rinsing steps consisted of immersing the section for 1 min in cold ethanol solutions (stored at -20°C) at 70 and 90% followed by a 30 sec wash in chloroform ($CHCl_3$) [15]. Sections were then allowed to dry at room temperature before digestion and matrix deposition.

Paraffin wax was removed from FFPE tissue sections according to procedures previously described [3, 9]. Briefly, sections were immersed twice in xylene solution for 10 minutes each time. The sections were then gently hydrated for 3 minutes in 100% EtOH, 95% EtOH and 70% EtOH consecutively. Endogenous peroxidase activity was blocked by incubating the section for 12 minutes in a hydrogen peroxide solution (2% in MeOH). Antigen retrieval (AR) was performed in a microwave oven for 13 minutes at 90°C using a tri-sodium citrate buffer at 0.01M (pH = 6.3) [16, 17]. The 13 minute heating was divided into 2 cycles of 5 minutes and 1 cycle of 3 minutes with a 30 sec interval between cycles in order to check the buffer level in the jar as well as the tissue section. After AR the section was cooled to room temperature and then rinsed with water.

3.2.4 *In situ* enzymatic digestion

In situ enzymatic digestion was performed using trypsin. The trypsin solution was prepared at 50 μg/ml in deionised water (dH_20) containing 0.1% octyl glucoside (OcGlc). The trypsin solution was deposited on the section using either an automatic pipette or robotic devices such as a Chemical Inkjet Printing technology CHIP-1000^{TM} (Shimadzu Biotech, Japan), an ImagePrep^{TM} (Bruker Daltoniks, Bremen, Germany) or a SunCollect^{TM} MALDI-Spotter (SunChrom, Friedrichsdorf, Germany) which can be used as an automatic spotter or sprayer.

3.2.4.1 Manual trypsin deposition using an automatic pipette

Using an automatic pipette, several spots of 2 μl of trypsin solution were deposited onto the tissue section surface at room temperature. Every 5 minutes, the trypsin solution was deposited on the same spots; a total volume of 30 μl of trypsin solution was used.

3.2.4.2 Trypsin deposition using a Chemical Inkjet Printer^{TM} (CHIP-1000^{TM})

The CHIP-1000^{TM} (Shimadzu Biotech, Japan) is a robotic device which uses piezo-electric technology in order to deposit micro-scale reagent onto a target surface [18]. Small droplets of solution can be applied onto specific surfaces including tissue sections [11, 13]. Here using the CHIP-1000^{TM}, 100 pL drops were delivered in 5 drop rounds until 20 nl of trypsin solution/per spot were printed onto the section. The spot-to-spot distance was set at 300 μm.

3.2.4.3 Trypsin deposition using an ImagePrep^{TM}

The ImagePrep^{TM} (Bruker Daltoniks, Bremen, Germany) is an automatic device which allows reagent deposition onto tissue section surfaces by creating vibrational vaporisation under controlled conditions [19]. It is fitted with an optical sensor that monitors reagent (such as trypsin and matrix) depositions as well as sample preparation parameters including the deposition periods, matrix layer thickness, wetness and drying time. Using the ImagePrep^{TM}, a method for trypsin deposition was developed and optimised: 600 μl of trypsin solution were sprayed onto the tissue section over 60 spraying cycles, thus ensuring the tissue is not over wetted. The tissue section was then incubated for 2 hours in a humid chamber at 37°C.

3.2.4.4 Trypsin deposition using a SunCollect^{TM} MALDI-Spotter

Using the SunCollect^{TM} MALDI-Spotter (SunChrom, Friedrichsdorf, Germany) 150 nl of trypsin solution per spot was deposited onto the section. The spot-to-spot distance was set at 400 μm.

The spraying function of the SunCollect^{TM} MALDI-Spotter (SunChrom, Friedrichsdorf, Germany) allows the deposition of fine reagent droplets including trypsin and matrix solution onto the tissue section. Briefly the automatic sprayer is equipped with a

concentric needle connected to a compressed air supply which is fed through the outer section of the concentric needle. The inner section of the concentric needle is a capillary which continuously feeds a stream of reagent solution. This results in a plume of fine solution droplets, the size of which can be changed by adjusting the solution flow rate and/or the compressed air pressure. Using the SunCollect^{TM} MALDI-Spotter the trypsin solution was deposited on the tissue section at increased flow rate over five layers. The first layer was performed at 1 μl/min, the second at 2 μL/min and the last three layers set at 4 μL/min. Humid environmental conditions were maintained while depositing the trypsin on the tissue section. After trypsin deposition the section was incubated for 2 hours in a humid chamber at 37°C with 5% CO_2 to perform enzymatic digestion.

3.2.5 Matrix preparation and deposition

For most applications α-CHCA has been found to be a suitable MALDI matrix for the analysis of low molecular weight compounds [20]. However, alternative matrices have been proposed to improve the co-crystallization process for on-tissue digested peptides, this involved the use of ionic matrices [15, 21, 22]. Here, α-CHCA mixed with aniline (α-CHCA/ANI) was used as an ionic matrix for the analysis of peptides obtained after on-tissue digestion. Matrix solutions were made at 10 mg/ml in ACN:dH_20:TFA (1:1:0.2 in volume) and contained an equivalent amount of aniline (i.e 4.8 μL).

Following enzymatic digestion and incubation, matrix deposition was performed using either an automatic pipette, a CHIP-1000^{TM}, an ImagePrep^{TM} or a SunCollect^{TM} MALDI-Spotter. When using the CHIP-1000^{TM}, the method for matrix deposition was the same as the trypsin deposition. When using the ImagePrep^{TM}, 2 ml of matrix solution were sprayed onto the tissue section over 50 cycles allowing a homogenous matrix coverage to be obtained. When using the SunCollect^{TM} MALDI-Spotter, the matrix was sprayed onto the tissue section was performed at increased flow rate between layers. The first layer was performed at 1 μL/min allowing a matrix seeding process. The second and last three layers were performed at 2 μL/min and 3.5 μL/min respectively.

3.2.6 *In situ* peptide analysis and direct protein identification by MALDI-MS profiling and imaging

3.2.6.1 MALDI-MS profiling and imaging of peptides obtained after *in situ* digestion of breast tumour tissue sections

MALDI-MS profiling and imaging data were acquired in the reflector and positive mode using either an Ultraflex^{TM}II MALDI-TOF/TOF instrument (Bruker Daltoniks, Bremen, Germany) equipped with a Smartbeam^{TM} laser or in the V-mode and positive mode using a MALDI SYNAPT^{TM}HDMS system (Waters Corporation, Milford, MA) operating with a 200 Hz Nd:YAG laser.

When using the Ultraflex^{TM}II MALDI-TOF/TOF instrument, full scan mass spectra and images were recorded from m/z 600 to 5000. FlexImaging^{TM} 2.0 software (Bruker Daltoniks, Bremen, Germany) and BioMap 3.7.5 software (Novartis, Basel, Switzerland) were used for image reconstruction. Standards for spectral calibration consisted of a mixed solution of peptides (Bruker Daltoniks, Bremen, Germany) ranging between m/z 900 and 3500.

When using the MALDI SYNAPT^{TM}HDMS system, full scan mass spectra were recorded from m/z 600 Da to 2500. Images were generated and reconstructed using BioMap 3.7.5 software. Standards consisted of a mixture of poly(ethylene glycol) standards (Sigma-Aldrich, Dorset, UK) ranging between m/z 100 to 3000.

3.2.6.2 MALDI-IMS-MS/MS analysis for direct protein identification from breast tumour tissue sections after *in situ* digestion

MALDI-MS/MS analyses were acquired using a MALDI SYNAPT^{TM}HDMS (Waters Corporation, Manchester, UK) operating in ion mobility separation (IMS) mode directly from the digested tumour tissue sections. A full description of the MALDI SYNAPT^{TM}HDMS instrument has been reported previously [23] and also described in the introduction of this thesis. Briefly the configuration of the instrument allows the separation of ions in the Trap T-Wave^{TM} (pre-IMS) and the Transfer T-Wave^{TM} (post-IMS), operating as two separate collision cells. Collision induced dissociation was performed in the Transfer T-Wave^{TM} after ion mobility separation and optimised based on the precursor ion mass [24]. The obtained spectra were processed using MassLynx^{TM}

(Waters Corporation), mass spectral processing software. Spectral processing consisted of smoothing, baseline correction and the use of a lock mass correction for improving mass accuracy. Spectra were then processed with the MaxEnt 3 algorithm which aims to de-isotope mass spectrometric data and enhance the signal-to-noise ratio [25]. The resulting files were submitted to a MASCOT (Matrix Science, London, UK) query search and searched against the Swissprot database.

Within the MASCOT search engine the parent and fragment ion tolerances were set at 30 ppm and 0.1 Da respectively. The criteria also included up to two missed cleavages and the variable modifications allowed were histidine/tryptophan oxidation and methionine oxidation. *De novo* sequencing was performed manually and using the PepSeq^{TM} (Waters Corporation) *de novo* interactive MS/MS sequencing tool. The parent and fragment ion tolerances were set at 0.1 Da and the threshold was set at 1%. Protein Blast searches against the Swissprot database were also performed to confirm tryptic sequences.

3.3 Results and Discussion

3.3.1 *In situ* protein identification in frozen MCF-7 breast tumour xenografts

3.3.1.1 Matrix optimisation

Direct protein imaging and profiling analysis from xenograft tissue sections with MALDI-MS has enabled the acquisition of protein distribution information. However, to help the understanding of the biological processes occurring during tumour progression, identification of these proteins is required. The possibility of identifying such analytes directly from tissue sections has been assessed. To improve the peptide extraction and direct analysis of digested proteins, micro digestion was performed using a robotic printer. Figures 3.1a and b display digital scans of a MCF-7 breast tumour xenograft tissue section before and after on-tissue digestion and matrix deposition performed using a CHIP-1000^{TM}.

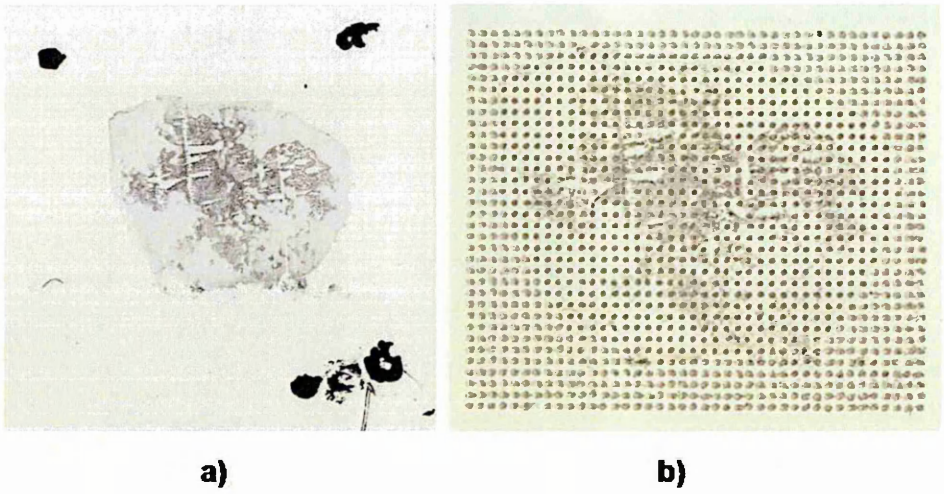

Figure 3.1: **Images of a MCF-7 xenograft tissue section before and after trypsin and matrix deposition using a CHIP-1000^{TM} automatic printer.** (a) Digital scan of a MCF-7 xenograft tissue section prior to on-tissue digestion and matrix deposition. (b) Digital scan of the same tissue section after on-tissue digestion and matrix deposition using a CHIP-1000^{TM} automatic printer: the matrix solution was spotted onto the trypsin spots after on-tissue digestion. The spot-to-spot distance was 300 μm.

Additionally, the matrix solution and the deposition methodology were improved in order to provide the optimum co-crystallisation with the obtained peptides after enzymatic digestion. Figure 3.2 displays peptide profiles obtained after on-tissue digestion of MCF-7 breast tumour xenografts using different matrix concentrations as well as different trypsin and matrix deposition methods. Data acquisition was performed using an Ultraflex^{TM}II MALDI-TOF/TOF instrument. Examination of the obtained mass spectra shows that a higher matrix concentration results in improved quality spectra. Additionally, the use of a robotic device for matrix deposition enhanced peptide extraction and hence increased the number and intensity of detected peptides from the tissue section after *in situ* tryptic digestion.

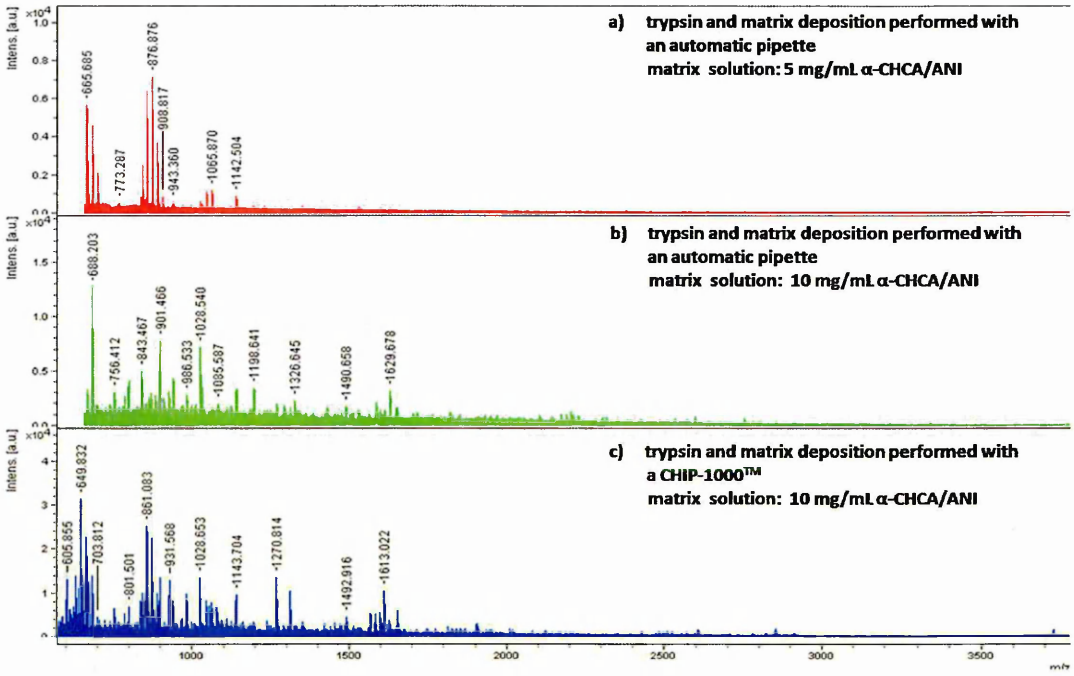

Figure 3.2: **Improvement of trypsin and matrix deposition for *in situ* digestion of MCF-7 xenograft tissue sections.**
Peptide profiles obtained after manual trypsin and matrix deposition using an automatic pipette (a, b) and robotic deposition using a CHIP-1000^{TM} (c). MS analysis performed on each spot clearly shows that a 10 mg/ml matrix solution yields an increased number of detected ion signals with an improved sensitivity compared to a 5 mg/ml solution. Performing on-tissue digestion and matrix deposition using a robotic device improved peptide extraction, hence the sensitivity.

3.3.1.2 Direct peptide analysis within MCF-7 breast tumour xenograft tissue sections using MALDI-MSI after on tissue digestion

Here *in situ* digestion and matrix deposition on xenograft tissue sections were performed using a SunCollect^{TM} MALDI-Spotter. Mass spectra were obtained from each printed spot. Figures 3.3a and b show a digital scan of a xenograft section before digestion and after trypsin/matrix deposition respectively. Mass spectra can be obtained from each printed spot. Figure 3.3c displays a mass spectrum acquired after *in situ* digestion and matrix deposition using an Ultraflex^{TM}II MALDI-TOF/TOF instrument. Numerous peptide signals were detected up to m/z 4000 with a $S/N > 3$. MS/MS analyses were also performed directly onto the tissue section and allowed the identification of a few proteins. Table 3.1shows a list of the identified peptides. Peptide signals resulting from the most abundant proteins such as actin (m/z 1198.7), haemoglobin (m/z 1529.7) and albumin (m/z 1467.8) were readily detected. These signals were used for spectral recalibration purposes. This aimed to improve mass accuracy as well as to enhance database search results.

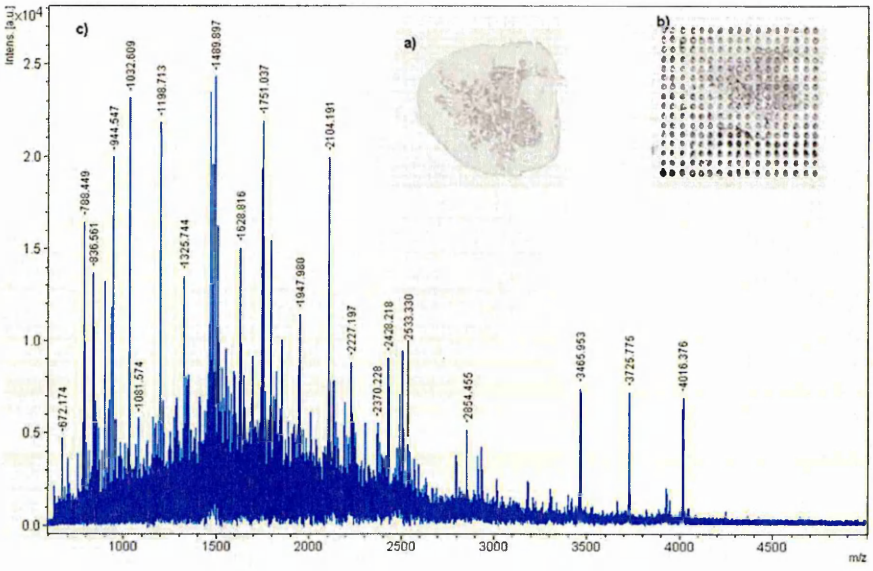

Figure 3.3: **Digital scans of the tissue section and MALDI-MSI direct peptide profiles obtained after *in situ* digestion of a MCF-7 xenograft tissue section.** Digital scans of a xenograft section before (a) and after (b) matrix deposition are displayed. Panel c shows peptide profiling obtained by MALDI-MSI after on-tissue digestion.

Protein Assignment/ Accession number	Protein mass(Da)	Observed m/z with MALDI-MSI	signal-to-noise ratio (S/N)	Sequence	MS/MS ion score	Molecular function
Actin, aortic smooth muscle/ P62736	41982	1198.7	15.6	AVFPSIVGRPR	25	Cell mobility
		1790.9	12.2	SYELPDGQVITIGNER	82	
Albumin/ P02768	69367	1467.8	6.4	RHPDYSVVLLLR	60	
Haemoglobin subunit alpha/ P01942	15085	1529.7	5.4	VGAHAGEYGAEALER	115	
Histone H2A/ P0C0S5	13545	944.5	22.6	AGLQFPVGR	26	gene regulation

Table 3.1: **List of abundant proteins detected after direct MALDI-MSI analysis of MCF-7 breast tumour xenograft tissue sections**

3.3.1.3 An improved method for direct protein identification in frozen MCF-7 breast tumour xenograft tissue sections

In order to improve the detection of low abundance proteins and high mass proteins such as stress proteins and/or membrane-associated proteins, several experimental conditions including different reagents, humidity, digestion time and temperature were evaluated. Figure 3.4 shows a comparison of results obtained after *in situ* digestion performed with trypsin in either water (figure 3.4a) or in a solution containing the detergent octyl glucoside (figures 3.4b and 3.4c).

Examination of the data obtained from *in situ* digestion with trypsin in water only (figure 3.4a) shows that the majority of the signals detected were from the most abundant proteins present in tissue samples *i.e.* actin, haemoglobin and albumin as described above. The use of octyl glucoside (OcGlc) has been found to greatly improve the solubility of the proteins. OcGlc is a non ionic detergent and it has been reported to enhance protein solubilisation, hence improving in gel protein digestion [26–28]. Here octyl glucoside was added to the trypsin buffer, here water, for *in situ* digestion. Adding 0.1% OcGlc to the trypsin solution resulted in the detection of numerous signals in addition to those resulting from the most abundant proteins Therefore, it improved the *in situ* digestion of several proteins. The concentration, *i.e.* 0.1%, used has been found to be compatible with direct MALDI-MSI analysis.

Figure 3.4b shows the resulting peptide profile after *in situ* digestion with a trypsin solution containing OcGlc followed by incubation at room temperature for 18 hours. This increased the number of signals detected and improved protein identification. Hence these data show that incubating the section in a humid environment after trypsin deposition enhances the activity of the trypsin and improves the digestion of low abundance proteins. However optimal trypsin performance was found to be after a digestion time of 2 hours at 37°C with a trypsin solution containing 0.1% OcGlc in a humid chamber (figure 3.4c).

In addition to peptides resulting from the most abundant proteins including actin, haemoglobin and albumin, signals from histone species and stress proteins such as Grp75 (a member of the heat shock protein 70 family, resident within the mitochondria) [29] were identified. Direct protein analysis (profiling and imaging) results were found to be data rich in the histone mass range (see Results and Discussion section in Chapter 2: section 2.4.3.1). Here these results obtained from direct protein identification were in good agreement with those from direct protein analysis as numerous signals were assigned to histone species, including histone H2A, H2B, H3 and H4. Figure 3.5 shows the MS/MS spectrum of m/z 944 which was assigned to peptide T8 arising from histone H2A.

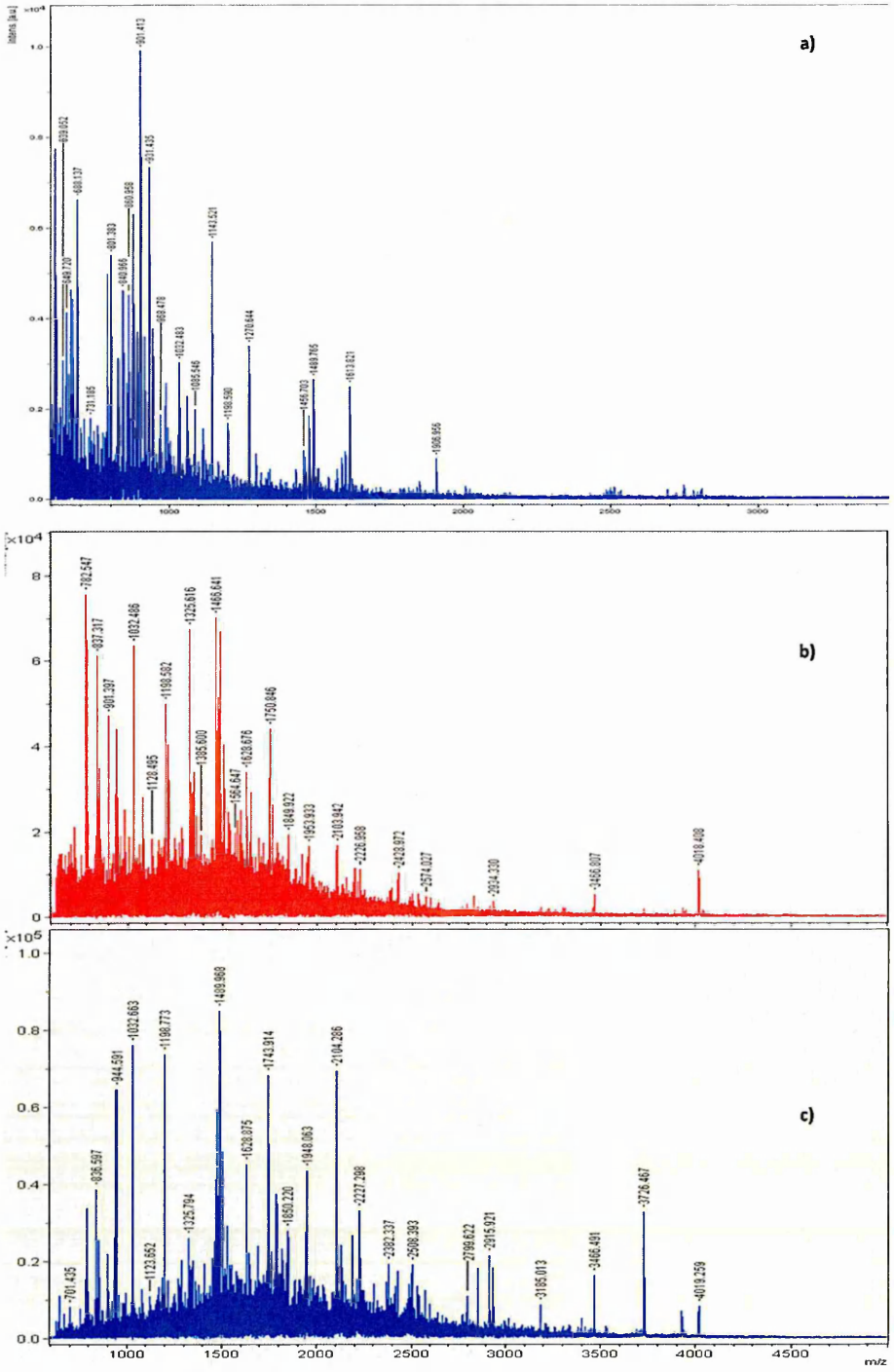

Figure 3.4: **Evaluation of method improvement for *in situ* digestion of frozen MCF-7 xenograft tissue sections.**
Peptide profiles were obtained directly from MCF-7 xenograft tissue sections after *in situ* digestion performed using a SunCollect^{TM} MALDI-Spotter. a) displays the observed peptide profiles after an *in situ* digestion performed with trypsin in water at room temperature in no humid atmosphere. b) shows the observed peptide profiling after *in situ* digestion with a trypsin solution containing 0.1% of OcGlc for 18 hours at room temperature in a humid atmosphere. c) reports the *in situ* digested protein profile when using a trypsin solution containing 0.1% of OcGlc and incubating the section at 37°C for 2 hours in a humid atmosphere.

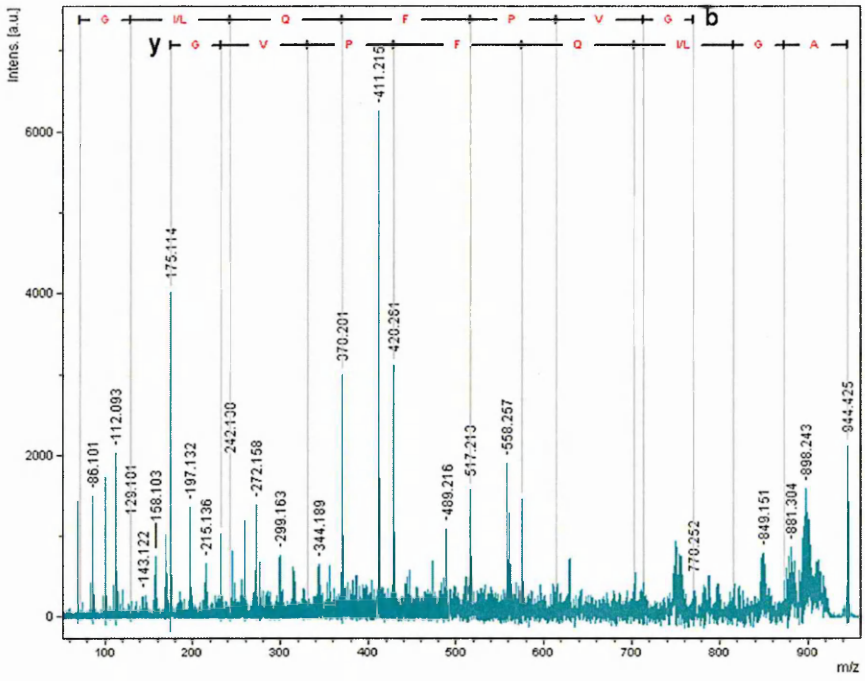

Figure 3.5: **MALDI-MS/MS spectrum of the ion at m/z 944 obtained directly from a MCF-7 xenograft tissue section.**
On-tissue MALDI-MS/MS spectrum of the ion at m/z 944 allowed the identification of the peptide T8 arising from histone H2A. The y and b ion series are displayed [30, 31].

Table 3.2 gives a list of some observed and identified signals in both tumour and necrotic regions: observed m/z values with direct MALDI-MS/MS analysis and protein assignments are reported. The signal at m/z 715 has been assigned to peptide T13 from Grp75, a heat shock protein 70 kDa (Hsp70), using direct MALDI-MS/MS. Hsp70 exists as several isoforms ranging from 66 to 78 kDa and these are known to be molecular chaperones. Hsp70 has been reported previously to be highly expressed in tumour tissues, in a study carried out using immunohistochemistry methods [32]. Here the obtained MALDI-MS data were in good agreement with those results.

Protein Assignment	Accession number	Protein mass (Da)	Observed m/z with MALDI-MSI	Sequence	MS/MS ion score	Molecular function
Actin, aortic smooth muscle	P62736	41982	1198.7	AVFPSIVGRPR	25	Cell mobility
			1790,9	SYELPDGQVITIGNER	82	
Actin, cytoplasmic 1	P60709	41710	1954.1	VAPEEHPVLLTEAPLNPK	48	Cell mobility
Albumin	P02768	69367	1467,8	RHPDYSVVLLLR	60	
Estrogen receptor beta	Q92731	59178	837.4	RSGGHAPR	15, *de novo*	Nuclear hormone
Fibroblast growth factor 13	Q92913	27564	844.5	SGKVTKPK	67, PMF	nervous system development
			958.6	VTKPKEEK		
			1361.7	MSGKVTKPKEEK		
Haemoglobin subunit alpha	P01942	15085	1529.7	VGAHAGEYGAEALER	115	
Grp75, HSP 70 kDa, mitochondrial	P38646	73635	715.4	LVGMPAK	18	Molecular chaperone, control of cell proliferation and call aging
Histone H2A	P0C0S5	13545	944.5	AGLQFPVGR	26	gene regulation
			2104.2	HLQLAIRNDEELNKLLGK	24	
			2915.6	VGAGAPVYLAAVLEYLTAEILEL AGNAAR	44	
Histone H2B	P33778	13819	901.5	LAHYNKR	25	
			1743.8	AMGIMNSFVNDIFER	28	
Histone H3	Q6NXT2	15204	788.5	KLPFQR	28	
			831.5	STELLIR	26	
			1032.6	YRPGTVALR	18	
			1489.9	RSAPATGGVRKPHR	55, Blast	
Histone H4	P62805	11360	1325.7	DNIQGITKPAIR	35	
			1466.8	TVTAMDVVYALKR	29	
High mobility group protein B1	P09429	24878	1944.9	RPPSAFFLFCSEYRPK	35	DNA binding
Metastasis-associated protein 2	O94776	75023	2428.2	DISSSLNSLADSNAREFEEESK	50, PMF	regulation of gene expression as repressor and activator

Table 3.2: **List of identified proteins after *in situ* digestion and direct MALDI-MSI analysis of MCF-7 xenograft tissue sections**

3.3.1.4 Protein localisation within a MCF-7 breast tumour xenograft tissue section by MALDI-MS imaging

MALDI-MS imaging analyses were also performed on serial MCF-7 xenograft tissue sections after *in situ* tryptic digestion. Images were acquired at a spatial resolution of 150 μm using an Ultraflex^{TM}II MALDI-TOF/TOF instrument. Figure 3.6 shows MALDI images of the distribution of some of the identified peptides within a MCF-7 tissue section. Difference in intensities can be observed between the necrotic and tumour areas. The signal at m/z 1489, corresponding to peptide T12-13 from histone H3, was mainly located in the tumour area while the signal at m/z 944, corresponding to peptide T8 from histone H2A, was found in both the necrotic and the tumour regions. The *in situ* digestion method described here enables the identification and localisation of proteins which are hardly detected by direct MALDI-MSI protein analysis due to their high masses or low abundances in tissue samples. These results demonstrated that direct protein analysis and identification through *in situ* digestion of frozen MCF-7 breast tumour xenograft sections has been achieved using MALDI-MSI. However the method still requires further development in order to improve direct MS/MS analysis. Several other biomolecules such as lipids and also matrix adducts can interfere with the ion precursor selection of the analyte of interest.

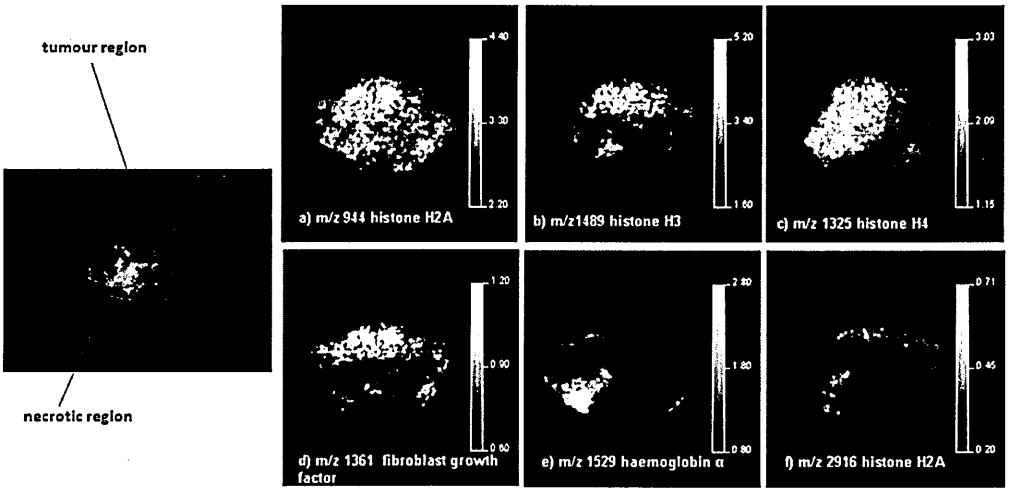

Figure 3.6: **MALDI-MS images of peptide distribution within a MCF-7 xenograft tissue section.**
The localisations of histone peptide species including H2A, H3 and H4, fibroblast growth factor and haemoglobin alpha chain are displayed.

3.3.2 *In situ* protein investigation in human FFPE breast cancer tissue sections

Formalin fixed paraffin embedded (FFPE) tissue samples are the commonest type of preserved tissue in clinical practice. These tissue samples are widely used by histopathologists for assisting the diagnosis and assessing the prognosis of cancers and other diseases. The ability to analyse proteins directly from archival tumour tissue samples that have known outcomes is of important clinical interest since it could provide molecular insights into disease processes and may lead to improved diagnosis and prognosis as well as treatment and prevention. Direct protein analysis by MALDI-MSI analysis of FFPE tissue sections remains challenging because of the presence of protein cross-linking via methylene bridge formation making the analysis difficult to perform. An alternative approach to get as much information as possible from these tissues is to perform *in situ* enzymatic digestion and then to analyse the resulting peptides for protein identification purposes [9].

3.3.2.1 Effect of the use of octyl glucoside (OcGlc) on the *in situ* digestion of FFPE breast tumour tissue sections

The use of a detergent was also assessed for *in situ* digestion of FFPE tumour tissue sections. Adding 0.1% octyl glucoside to the trypsin solution increased the number of peptide signals detected as well as improving signal intensities. Figure 3.7 shows a comparison between direct peptide MALDI-MS profiling obtained after two hours *in situ* digestion from FFPE breast tumour tissue sections either with a trypsin solution containing OcGlc (Figure 3.7a) or with no OcGlc (Figure 3.7b). Spectra were acquired using a MALDI SYNAPT^{TM}HDMS system. It can be clearly seen (Figures 3.7a and b) that more peptide signals are observed after on-tissue digestion with a trypsin solution containing 0.1% OcGlc. The signal at m/z 1790.9, which was identified as peptide T23 from actin, is increased when adding OcGlc to the trypsin buffer for *in situ* digestion.

In addition to the most abundant proteins, several peptide signals assigned to other proteins including membrane-associated proteins have been identified and their distribution within the tissue section studied after *in situ* digestion using detergent addition to the tryptic buffer. This can be seen in the zoomed in spectra. The detection of the

signal at m/z 1095.6, which was assigned to retinoic acid early transcript 1G protein (a single-pass type I membrane protein), was improved.

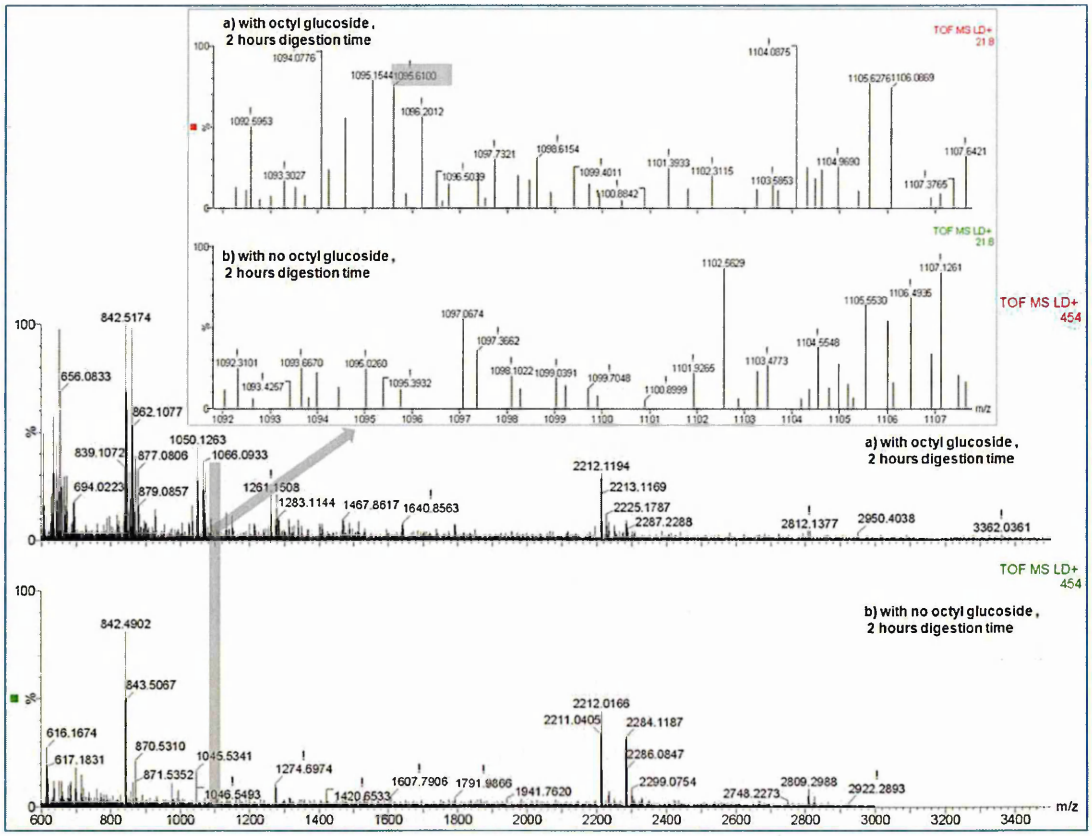

Figure 3.7: **Evaluation of the use of octyl glucoside in the trypsin buffer for *in situ* digestion of FFPE breast tumour tissue sections.**
Panel a shows the direct peptide profile after on-tissue digestion with a trypsin solution containing 0.1% of OcGlc. Panel b displays the direct peptide profile with no OcGlc in the trypsin buffer. Both spectra were acquired after the same digestion time.

Figure 3.8 shows MALDI images of the localisation of tryptic peptides within a FFPE breast tumour section. Images were acquired at a spatial resolution set at 200 μm using the MALDI SYNAPT^{TM}HDMS.

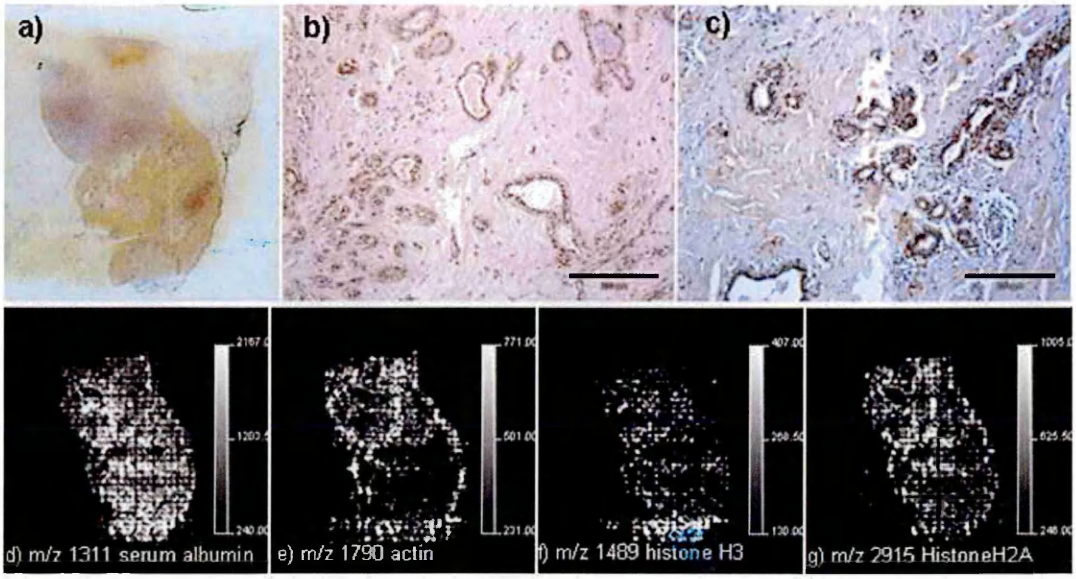

Figure 3.8: **Images of protein localisation within FFPE breast tumour tissue sections.**
Panel a shows a scan of a histological staining of a FFPE breast tumour section. Panels b and c show histological images of tumour cells within the tissue section acquired at a magnification x10. Panels d, e, f and g display the distribution of serum albumin, actin, histone H3 and histone H2A respectively within the tissue section, obtained by MALDI-MSI.

3.3.2.2 Combining ion mobility separation (IMS) with MALDI-MSI yielded improved direct protein identification from FFPE tumour tissue sections

In situ digestion has been found useful for proteomic analysis by MALDI-MSI as it provides direct protein identification and localisation from the tissue section without any need for sample fractionation or extraction of proteins from the tissue section. As numerous peptides are generated this results in a complex mixture of signals from the individual components. As a consequence, signal overlap from peptides and other biomolecules is observed, hence making direct MS/MS analysis difficult to achieve in some cases. Previous methods reported the coupling of nanoLC -nanoESI to MALDI-MSI analysis in order to achieve a better identification of proteins [9]. Here ion mobility separation (IMS) has been found to be a powerful technique for direct analysis of peptides generated after *in situ* digestion.

Coupling IMS to MALDI-MSI aims to improve the selectivity and enhance database searching. Figure 3.9a shows the ion mobility separation of 2 isobaric species of m/z 850 arising from the direct MS/MS analysis. When a MASCOT search was performed on the entire MS/MS spectrum without taking into account the mobility separation, no significant results or potential identification were obtained. However the IMS data can be processed in order to extract individual MS/MS spectra corresponding to each analyte. Figures 3.9b and c display the obtained MS/MS spectra after IMS data processing of the isobaric ions at a driftime^{TM} plot of 3.9 msec and 4.9 msec respectively. These data were imported into MASCOT search, resulting in a better search for protein assignment. The MS/MS spectrum displayed in Figure 3.9b allowed the identification of the ion signal at m/z 850 as a peptide T18 arising from histone H2A.

Using a combination of both IMS and MALDI-MSI has been found to be a valuable tool for the *in situ* identification of proteins in FFPE breast tumour tissue sections. Numerous proteins were identified. Table 3.3 displays a list of identified proteins from FFPE breast tumour tissue sections.

However further method development is still required in order to improve the detection and identification of stress proteins directly from FFPE tissue sections after *in situ* digestion.

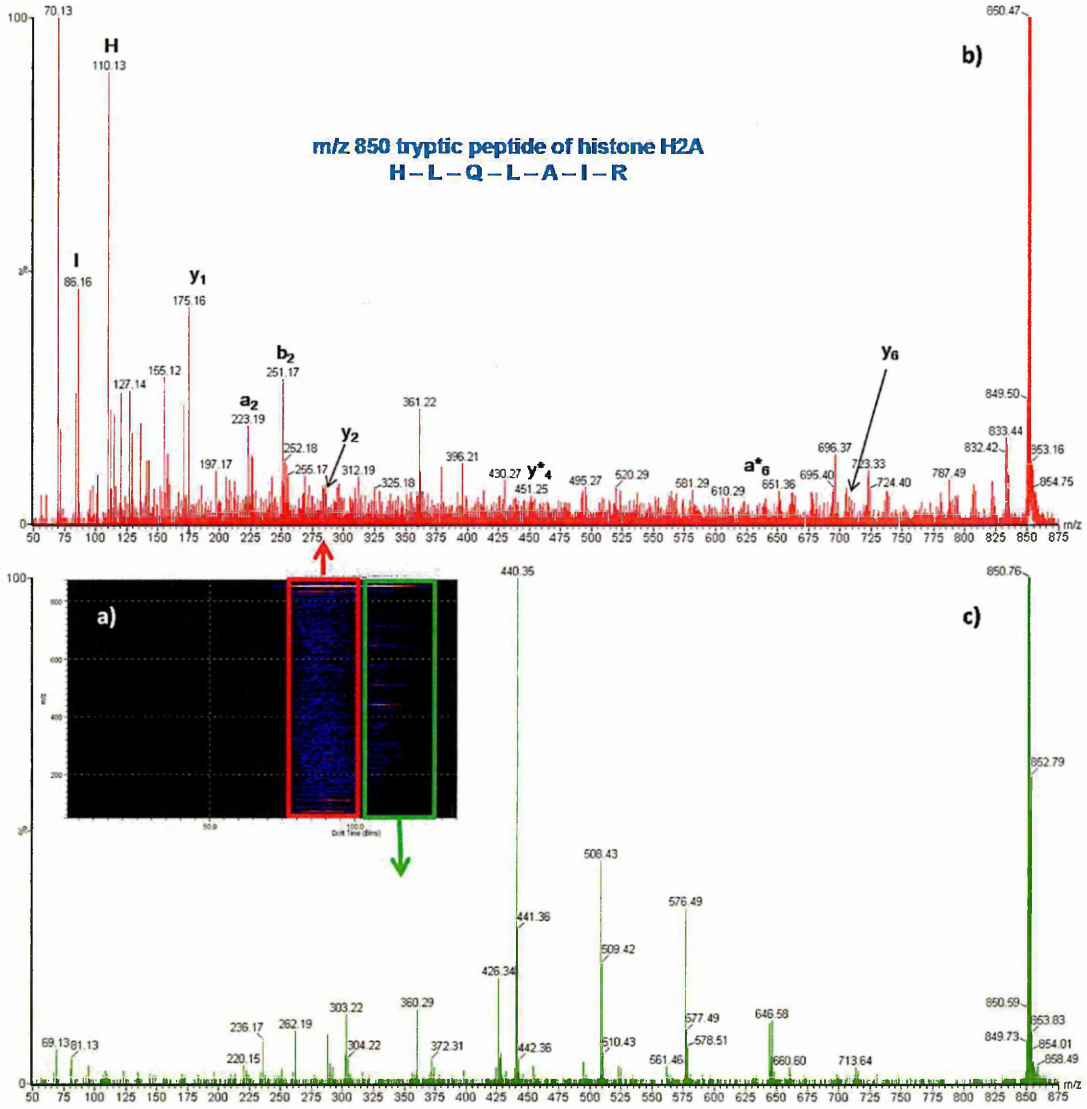

Figure 3.9: **MALDI-IMS-MS/MS spectrum of the ion signal at m/z 850 obtained after *in situ* digestion of human FFPE breast tumour tissue section.** The observed driftime^{TM} plot (a) displays interference between species in IMS-MS/MS analysis mode. These species can be separated using their mobility. Different MS/MS spectra (b and c) can be extracted using the ion mobility separation.

Protein Assignment	Accession number	Protein mass (Da)	Observed m/z with MALDI-MSI	Sequence	MS/MS ion score	Molecular function
Actin, aortic smooth muscle	P62736	41982	1198.7 1790.9	AVFPSIVGRPR SYELPDGQVITIGNER	25 82	Cell mobility
Actin, cytoplasmic 1	P60709	41710	2215.1	DLYANTVLSGGTTMYPGIADR	83	Cell mobility
Albumin	P02768	69367	1311.7 1467.8	HPDYSVVLLLR RHPDYSVVLLLR	75 60	
Haemoglobin alpha	P01942	15085	1087.6 1529.7	MFLSFPTTK + Oxidation (M) VGAHAGEYGAEALER	26 115	
Haemoglobin beta	P68871	15866.8	1274.7	LLVVYPWTQR	27	
Histone H2A	P0C0S5	13545	850.5 944.5 2915.6	HLQLAIR AGLQFPVGR VGAGAPVYLAAVLEYLTAEILEL AGNAAR	18 26 44	gene regulation
Histone H2B	P33778	13819	901.5 1775.8	LAHYNKR AMGIMNSFVNDIFER + 2 Oxidation (M)	28 36	
Histone H3	Q6NXT2	15204	831.5	STELLIR	26	
Histone H4	P62805	11360	1466.8	TVTAMDVVYALKR	35	
Lumican [Precursor]	P51884	38405	1024.6	FNALQYLR	21	Found in the extracellular matrix of human cartilages
Na^+/K^+-ATPase alpha 3 subunit variant [Fragment]	Q53ES0	111779	1002.5	RDLDDLKK	*de novo*	ATP binding, inorganic cation transmenbrane transporter
2-oxoglutarate dehydrogenase E1 component-like, mitochondrial [Precursor]	Q9ULD0	114409	952.5	FMTILRR + Oxidation (M)	21	mitochondrial matrix, oxidation reduction
Retinoic acid early transcript 1G protein [Precursor]	Q6H3X3	37082	1095.6	RPLSGGHVTR + Oxidation (HW)	20	Single-pass type I membrane protein
28S ribosomal protein S18b, mitochondrial [Precursor]	Q9Y676	29377	1105.6	NHKGGVPPQR + Oxidation (HW)	20	structural constituent of ribosome
Uncharacterized protein C2orf34	Q7Z624	36105	1094.6	GPVVSAPLGAAR	23	
Tumour protein 63	Q9H3D4	76736	1127.6	RCPNHELSR + Oxidation (HW)	15+ *de novo*	Acts as a sequence specific DNA binding transcriptional activator or repressor

Table 3.3: **List of protein identified after *in situ* digestion and direct MALDI-IMS-MS/MS analysis on human FFPE breast tumour tissue sections using a MALDI SYNAPT^{TM} instrument.**

3.3.2.3 Effect of antigen retrieval (AR) on the *in situ* digestion of FFPE breast tumour tissue section

Immunohistochemistry (IHC) is currently one of the techniques of choice for the investigation of protein distribution within FFPE tissue sections. IHC protocols for the analysis of FFPE tissue sections include several pre-treatments before the immunostaining of the tissue sections. These pre-treatments are commonly referred to as antigen retrieval (AR). Antigen retrieval is a method based on high temperature heating of FFPE tissue sections immersed in water or buffer solution and aims to reverse the chemical reaction of protein cross-linking resulting from the formalin fixation and return the tissue section to its native form as much as possible [16, 17, 33]. Several improvements of AR methods allowed the standardisation of IHC protocols and demonstrated their values in several studies for retrieving genomic and proteomic information from archived samples [34, 35]. For protein identification from FFPE tissue samples, LC/MS and 2D gel electrophoresis methods have been reported after applying AR to these tissue samples [3].

In the work reported here, the method for *in situ* digestion of FFPE breast tumour tissue sections was improved by applying AR as sample pre-treatment. A classical protocol of AR used for IHC was applied. After AR, on-tissue digestion was performed using a trypsin buffer containing 0.1 % OcGlc. Figure 3.10 shows the plots of the average intensities of the peptide ion signals corresponding to actin (m/z 1198.7) and retinoic acid early transcript 1G protein (m/z 1095.6), with and without AR. Three spectra were used and average peak intensities were calculated. It is clearly observed that the ion signal intensities are increased after applying AR.

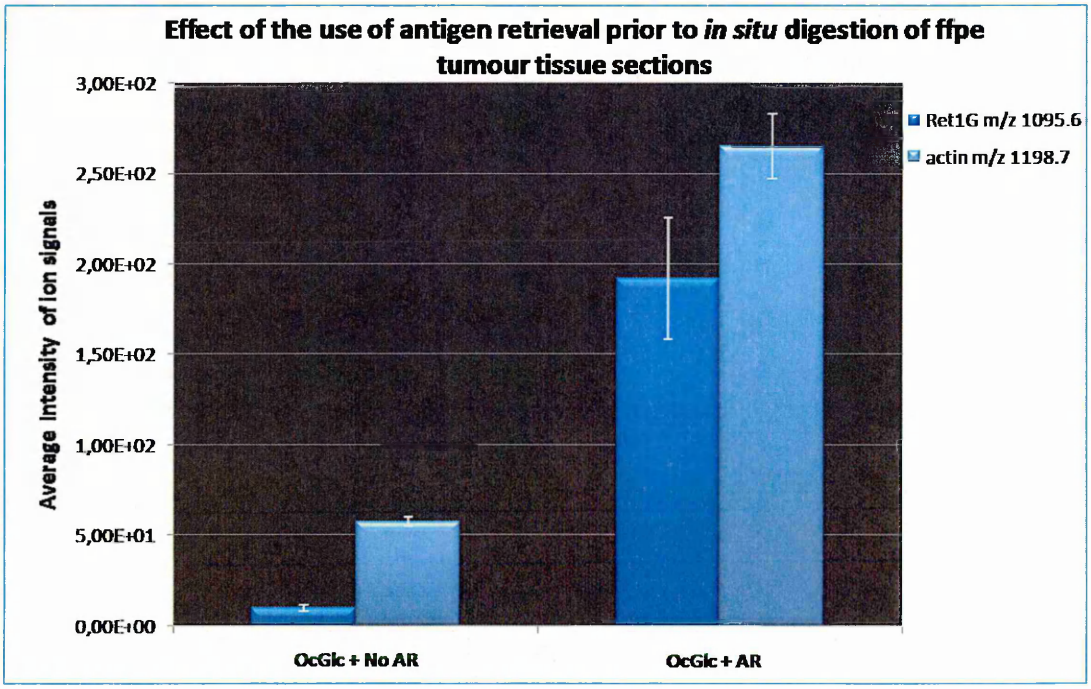

Figure 3.10: **Effect of the use of antigen retrieval prior to *in situ* digestion of FFPE breast tumour tissue sections.**
The average peak intensities of the peptide T3 signal arising from actin (m/z 1198.7) and the peptide T25 from retinoic acid early transcript 1G protein (m/z 1095.6) are shown in the absence and use of AR prior to *in situ* digestion. The use of AR as sample pre-treatment before on-tissue digestion is shown to significantly increase the intensity of the ions detected. Here, n=5.

The method sensitivity is improved when using AR as sample pre-treatment. More signals are detected after using AR prior to *in situ* digestion of FFPE tumour tissue sections with a good signal-to-noise ratio (S/N). This can be noticed in figure 3.11, in which peptide profiles obtained after *in situ* digestion of FFPE breast tumour tissue sections with or without AR as sample pre-treatment are displayed.

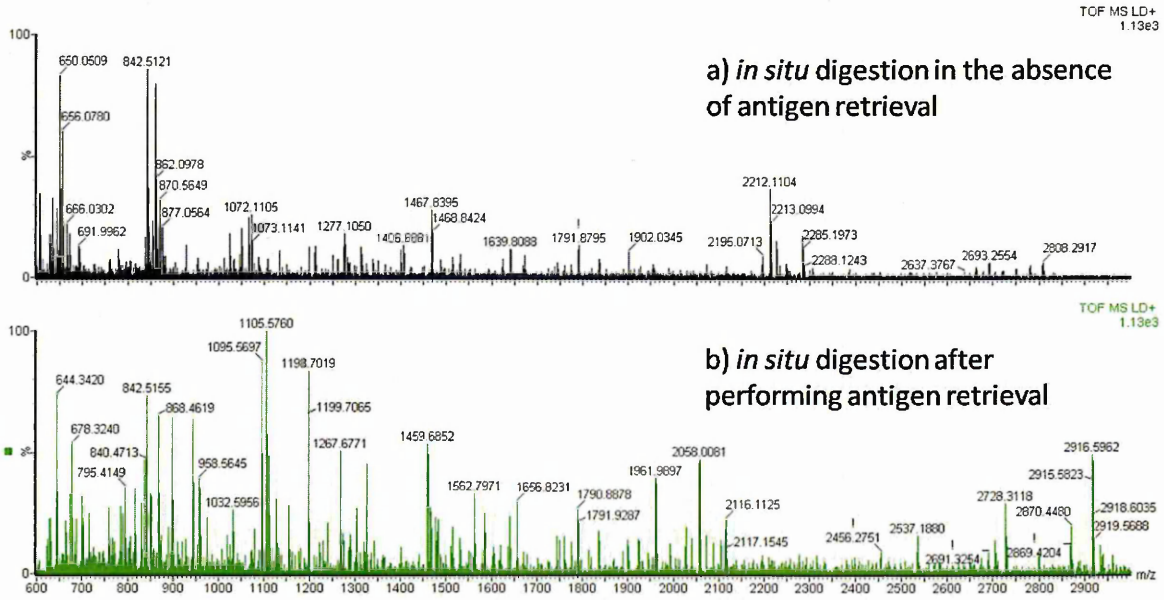

Figure 3.11: **Effect of the use of antigen retrieval prior to *in situ* digestion: Spectral comparison.**
Peptide profiles obtained after antigen retrieval prior to *in situ* digestion. When comparing figures 3.11a and b, numerous signals are detected after incorporating AR as sample pre-treatment prior to *in situ* digestion.

MALDI-MS images were also obtained from FFPE breast tumour tissue sections after AR and on-tissue digestion as sample pre-treatment. Here trypsin and matrix depositions were achieved using an ImagePrep^{TM}. Data acquisition was performed using an Ultraflex^{TM}II MALDI-TOF/TOF instrument. Figure 3.12a displays a digital scan of a tissue section. Several peptides were detected and images of their distributions within the tisue section were obtained with a good S/N ratio. Images were normalised against the matrix adduct peak at m/z 867. No delocalisation of signals was noticed. Figures 3.12b-g display the distribution of tryptic peptides of histone H2A, haemoglobin alpha, Na^+/K^+-ATPase and histone H4 respectively. When examining the data, it can be noticed that tryptic peptides arising from the same protein show the same distribution. This adds confidence to the identification of the given protein. The use of AR in sample pre-treatment does not lead to protein precipitation and/or degradation, but appears to unlock protein information.

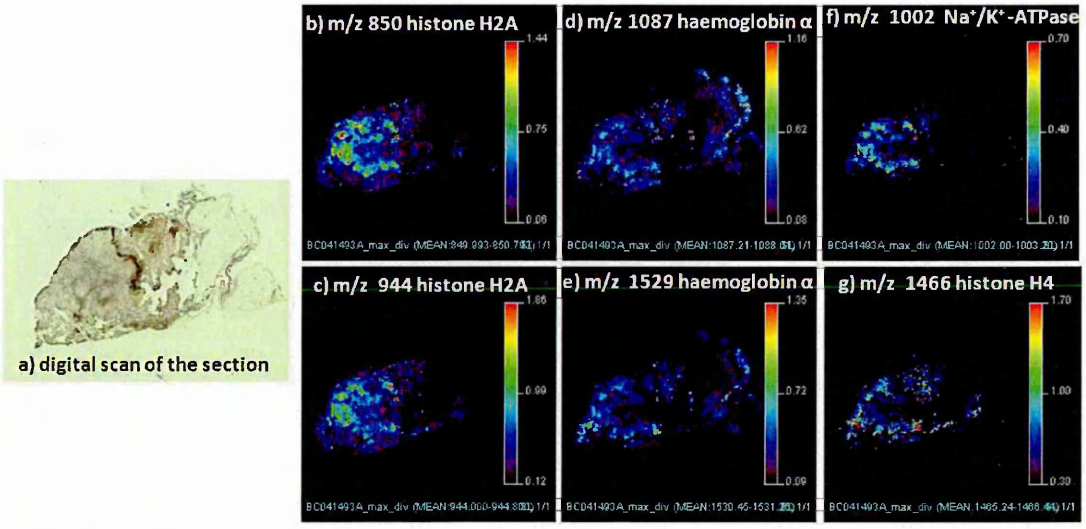

Figure 3.12: **Digital scan of a FFPE breast tumour tissue section and MALDI-MS images of the distribution of peptides within a FFPE breast tumour tissue section after performing antigen retrieval prior to *in situ* digestion.** (a) Digital scan of a FFPE breast tumour tissue section. (b-g) display the obtained distribution of tryptic peptides arising from histone H2A, haemoglobin alpha, Na^+/K^+-ATPase and histone H4, respectively after *in situ* digestion following AR, within a FFPE breast tumour tissue section.

3.4 Concluding Remarks

MALDI-MSI is continuing to show its potential for the investigation of protein distribution directly from tissue sections. It has been shown here that the use of on-tissue digestion enables the direct identification of proteins from both frozen and FFPE tumour tissue sections. The strategy described here highlights an improved methodology for *in situ* protein investigation and identification within frozen and FFPE tumour tissue sections.

The use of automatic micro-scale reagent deposition devices was found to greatly increase the extraction of peptides from tumour tissue sections while performing *in situ* digestion. This improved the sensitivity of the MS method. Another method development involved the use of ionic matrices for the analysis of peptides following on-tissue digestion. α-CHCA/ANI was found to provide an acceptable even crystalisation across both frozen and FFPE breast tumour tissue sections.

One of the key findings of this study has been that the addition of a non-ionic detergent, octyl glucoside, in the trypsin buffer enhanced the detection and localisation of low-abundance proteins and tumour-related proteins within frozen and FFPE tissue sections. Ionisation and detection of membrane-associated proteins were obtained. In the case of FFPE tumour tissue sections, incorporating antigen retrieval as a sample pre-treatment step was also found to unlock several proteins, hence increasing the amount of peptide detected after *in situ* digestion.

Additionally, the use of IMS has been shown to improve the sensitivity as well as the database search results. However, further improvement of the method and protocol refinements may lead to the identification of more proteins. The identification of proteins directly from tissue with MALDI-MSI following *in situ* enzymatic cleavage is a new proteomic approach and has the potential to deliver localisation and identification of tumour protein targets such as stress proteins, angiogenesis factors or drug-resistant biomolecules.

References

[1] Naldi M., Andrisano V., Fiori J., Calonghi N., Pagnotta E., Parolin C., Pieraccini G., and Masotti L. Histone proteins determined in a human colon cancer by high performance liquid chromatography and mass spectrometry. *Journal of Chromatography A*, 1129:73–81, 2006.

[2] Melle C., Osterloh D., Ernst G., Schimmel B., Bleul A., and von Eggeling F. Identification of proteins from colorectal cancer tissue by two-dimensional gel electrophoresis and SELDI mass spectrometry. *International Journal of Molecular Medicine*, 16:11–17, 2005.

[3] Hood B.L., Darfler M.M., Guiel T.G., Furusato B., Lucas D.A., Ringeisen B.R., Sesterhenn I.A., Conrads T.P., Veenstra T.D., and Krizman D.B. Proteomic analysis of formalin-fixed prostate cancer tissue. *Molecular and Cellular Proteomics*, 4: 1741–1753, 2005.

[4] Bodnar W.M., Blackburn R.K., Krise J.M., and Moseley M.A. Exploiting the complementary nature of LC/MALDI/MS/MS and LC/ESI/MS/MS for increased proteome coverage. *Journal of the American Society for Mass Spectrometry*, 14: 971–979, 2003.

[5] Chaurand P., DaGue B.B., Pearsall R.S., Threadgill D.W., and Caprioli R.M. Profiling proteins from azoxymethane induced colon tumors at the molecular level by matrix assisted laser desorption/ionization mass spectrometry. *Proteomics*, 1: 1320–1326, 2001.

[6] Stoeckli M., Chaurand P., Hallahan D.E., and Caprioli R.M. Imaging mass spectrometry: a new technology for the analysis of protein expression in mammalian tissues. *Nature Medecine*, 7:493–496, 2001.

[7] Reyzer M.L., Caldwell R.L., Dugger T.C., Forbes J.T., Ritter C.A., Guix M., Arteaga C.L., and Caprioli R.M. Early changes in protein expression detected by mass spectrometry predict tumor response to molecular therapeutics. *Cancer Research*, 64:9093–9100, 2004.

[8] Schwamborn K., Krieg R.C., Reska M., Jakse G., Knuechel R., and Wellmann A. Identifying prostate carcinoma by MALDI-Imaging. *International Journal of Molecular Medicine*, 20:155–159, 2007.

[9] Lemaire R., Menguellet S.A., Stauber J., Marchaudon V., Lucot J.P., Collinet P., Farine M.O., Vinatier D., Day R., Ducoroy P., Salzet M., and Fournier I. Specific MALDI imaging and profiling for biomarker hunting and validation: fragment of the 11s proteasome activator complex, Reg alpha fragment, is a new potential ovary cancer biomarker. *Journal of Proteome Research*, 6:4127–4134, 2007.

[10] Aerni H., Cornett D.S., and Caprioli R.M. Automated acoustic matrix deposition for MALDI sample preparation. *Analytical Chemistry*, 78:827–834, 2006.

[11] Shimma S., Furuta M., Ichimura K., Yoshida Y., and Setou M. Direct MS/MS analysis in mammalian tissue sections using MALDI-QIT-TOFMS and chemical inkjet technology. *Surface and Interface Analysis*, 38:1712–1714, 2006.

[12] Stauber J., Lemaire R., Franck J., Bonnel D., Croix D., Day R., Wisztorski M., Fournier I., and Salzet M. MALDI imaging of formalin-fixed paraffin-embedded tissues: application to model animals of Parkinson disease for biomarker hunting. *Journal of Proteome Research*, 7:969–978, 2008.

[13] Groseclose M.R., Andersson M., Hardesty W.M., and Caprioli R.M. Identification of proteins directly from tissue: *in situ* tryptic digestions coupled with imaging mass spectrometry. *Journal of Mass Spectrometry*, 42:254–262, 2007.

[14] United Kingdom Co ordinating Committee on Cancer Research (UKCCCR). Guidelines for the Welfare of Animals in Experimental Neoplasia (Second Edition). *British Journal of Cancer*, 77:110, 1998.

[15] Lemaire R., Wisztorski M., Desmons A., Tabet J.C., Salzet M., and Fournier I. MALDI-MS direct tissue analysis of proteins: improving signal sensitivity using organic treatments. *Analytical Chemistry*, 78:7145–7153, 2006.

[16] Yamashita S. Heat-induced antigen retrieval: Mechanisms and application to histochemistry. *Progress in Histochemistry and Cytochemistry*, 41:141–200, 2007.

[17] Xu H., Yang L., Wang W., Shi S.R., Liu C., Liu Y., Fang X., Taylor C.R., Lee C.S., and Balgley B.M. Antigen retrieval for proteomic characterization of formalin-fixed and paraffin-embedded tissues. *Journal of Proteome Research*, 7:1098–1108, 2008.

[18] Franck J., Wisztorski M., Stauber J., Elayed M., Salzet M., and Fournier I. Shimadzu CHIP-1000 for clinical tissue application in MALDI imaging. Technical report, Shimadzu Biotechnology, 2007.

[19] Schuerenberg M., Luebbert C., Deininger S.O., Mueller R., and Suckau D. A new matrix application device for MALDI tissue imaging. Technical report, Bruker Daltonics, 2007.

[20] Schwartz S.A., Reyzer M.L., and Caprioli R.M. Direct tissue analysis using matrix-assisted laser desorption/ionization mass spectrometry: practical aspects of sample preparation. *Journal of Mass Spectrometry*, 38:699–708, 2003.

[21] Armstrong D.W., Zhang L.K., He L., and Gross M.L. Ionic liquids as matrixes for matrix-assisted laser desorption/ionization mass spectrometry. *Analytical Chemistry*, 73:3679–3686, 2001.

[22] Tholey A. and Heinzle E. Ionic (liquid) matrices for matrix assisted laser desorption/ionization mass spectrometry applications and perspectives. *Analytical and Bioanalytical Chemistry*, 386:24–37, 2006.

[23] Pringle S.D., Giles K., Wildgoose J.L., Williams J.P., Slade S.E., Thalassinos K., Bateman R.H., Bowers M.T., and Scrivens J.H. An investigation of the mobility separation of some peptide and protein ions using a new hybrid quadrupole/travelling wave IMS/oa-ToF instrument. *International Journal of Mass Spectrometry*, 261:1–12, 2007.

[24] Riba-Garcia I., Giles K., Bateman R.H., and Gaskell S.J. Evidence for structural variants of a- and b-type peptide fragment ions using combined ion mobility/mass spectrometry. *Journal of the American Society for Mass Spectrometry*, 19:609–613, 2008.

[25] Xia Q., Wang H.X., Wang J., Liu B.Y., Hu M.R., Zhang X.M., and Shen B.F. Nano-ESI MS/MS identification on differentiation-associated proteins in M1 mouse myeloid leukemia cells induced by IL-6. *Acta Academiae Medicinae Sinicae*, 26: 483–487, 2004.

[26] Sutton C.W., Pemberton K.S., Cottrell J.S., Corbett J.M., Wheeler C.H., Dunn M.J., and Pappin D.J. Identification of myocardial proteins from two-dimensional gels by peptide mass fingerprinting. *Electrophoresis*, 16:308–316, 1995.

[27] Cohen S.L. and Chait B.T. Influence of matrix solution conditions on the MALDI-MS analysis of peptides and proteins. *Analytical Chemistry*, 68:31–37, 1996.

[28] Katayama H., Nagasu T., and Oda Y. Improvement of in-gel digestion protocol for peptide mass fingerprinting by matrix-assisted laser desorption/ionization time-of-flight mass spectrometry. *Rapid Communication in Mass Spectrometry*, 15:1416–1421, 2001.

[29] Wadhwa R., Taira K., and Kaul S.C. An Hsp70 family chaperone, mortalin/mthsp70/PBP74/Grp75: what, when, and where? *Cell Stress Chaperones*, 7:309–316, 2002.

[30] Roepstorff P. and Fohlman J. Proposal for a common nomenclature for sequence ions in mass spectra of peptides. *Biomedical Mass Spectrometry*, 11:601, 1984.

[31] Biemann K. Contributions of mass spectrometry to peptide and protein structure. *Biomeical and Environmental Mass Spectrometry*, 16:99–111, 1988.

[32] Aghdassi A., Phillips P., Dudeja V., Dhaulakhandi D., Sharif R., Dawra R., Lerch M.M., and Saluja A. Heat shock protein 70 increases tumorigenicity and inhibits apoptosis in pancreatic adenocarcinoma. *Cancer Research*, 67:616–625, 2007.

[33] Shi S.R., Key M.E., and Kalra K.L. Antigen retrieval in formalin-fixed, paraffin-embedded tissues: enhancements method for immunohistochemical staining based on microwave oven heating tissue sections. *Journal of Histochemistry and Cytochemistry*, 39:741–748, 1991.

[34] Shi S.R., Cote R.J, and Taylor C.R. Antigen retrieval immunohistochemistry: past, present,and future. *Journal of Histochemistry and Cytochemistry*, 45:327–343, 1997.

[35] Shi S.R., Liu C., and Taylor C.R. Standardization of immunohistochemistry for formalin-fixed, paraffin-embedded tissue sections based on the antigen-retrieval technique: from experiments to hypothesis. *Journal of Histochemistry and Cytochemistry*, 55:105–109, 2007.

CHAPTER 4

Targeting of Hypoxia in AQ4N-treated Tumour Xenografts by MALDI-Ion Mobility Separation-Mass Spectrometry Imaging

4.1 Introduction

Hypoxia is a common feature observed in solid tumours [1, 2]. It arises since solid tumours develop abnormal vasculature systems to permit growth and expansion. This results in a poor delivery of oxygen and a lack of nutrients to localised regions within the tumour. Tumour hypoxia is a target of interest in oncology as it has been found to be closely associated with tumour progression, metastasis and aggressiveness and confers resistance to a variety of chemotherapeutic agents as well as radiotherapy [3]. On a cellular level, hypoxia involves a complex molecular response of the hypoxia-inducible factor 1 (HIF-1) pathway which leads to an alteration of the expression of several proteins such as HIF-1, carbonic anhydrase IX (CAIX), glucose transporters (GLUT-1 and GLUT-3), plasminogen activator inhibitor-1 (PAI-1), vascular endothelial growth factor (VEGF) and osteopontin (OPN), which are all potential endogenous hypoxia-related markers [4]. A better understanding of the regulation of these markers in hypoxia may lead to an improvement of current therapeutic options [5].

Several therapeutic strategies designed to target hypoxia are currently under investigation. One of these approaches aims to improve tumour oxygenation, however there is not a method widely accepted in clinical practice [6]. An alternative approach consists of the use of tumour-activated prodrugs (TAP) [7]. Prodrugs are therapeutic compounds that are transformed into pharmacologically active molecules either by metabolism or spontaneous chemical breakdown mechanisms after administration. TAPs are designed to be less toxic anticancer drugs that are selectively activated in tumour tissues [7]. Hypoxia-selective cytotoxins are a new generation of TAP that are selectively activated into cytotoxic agents under hypoxic conditions. Among them is a compound called AQ4N, which is currently undergoing Phase I clinical trials. AQ4N is also known as banoxatrone or 1,4-bis-[2-(dimethylamino-N-oxide)ethyl]amino-5,8-dihydroxyanthracene-9,10-dione and is a very promising bioreductive prodrug. The physical properties and pharmacokinetic studies of AQ4N have been fully reviewed and described [7–10]. Briefly, under hypoxic conditions, AQ4N is reduced by reductase enzymes of the P-450 family including the CYP3A isozyme of NADPH:cytochrome C (P-450) reductase to its active cytotoxic metabolite AQ4 (1,4-bis-[2-(dimethylamino)ethyl] amino-5,8-dihydroxyanthracene-9,10-dione). AQ4 has a high DNA affinity and is the

only bioreductive that inhibits the enzyme topoisomerase II. The inhibition of topoisomerase II by AQ4N synchronises cell growth and therefore AQ4N has been found to sensitise tumours to radio- and chemotherapy treatments [8]. AQ4N has been found to improve and enhance the therapeutic response to radiotherapy and other chemotherapies [11]. Figure 4.1 displays a schematic mechanism of the reductive metabolism of AQ4N in tissue [8].

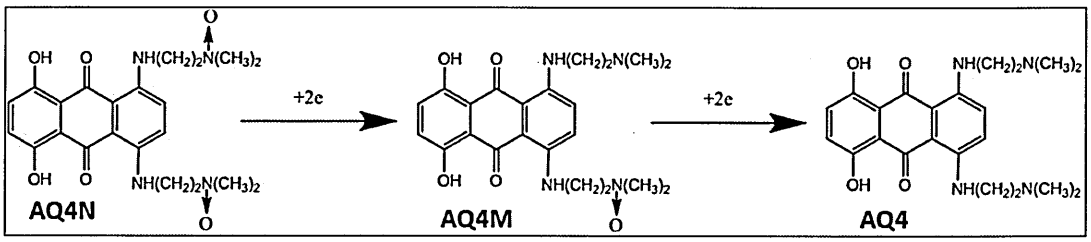

Figure 4.1: **Schematic representation of the reductive metabolism of AQ4N in tissue under hypoxic conditions** [8].
Under hypoxic conditions AQ4N is metabolised by enzymes of the p450 family to the intermediate metabolite AQ4M and then to its active cytotoxic metabolite AQ4.

MALDI-MSI has been previously used to study the distribution of AQ4N and AQ4 in tumour tissue sections. Using this technology, the distribution of AQ4N and AQ4 in AQ4N-treated H460 colon tumour xenograft tissue sections were simultaneously obtained [12]. This was found to be very beneficial as it allowed the localisation of hypoxic regions within the tumour tissue sections. However, to date no studies have reported the investigation of the distribution, expression and *in-situ* identification of hypoxia-related protein markers in correlation with the distribution of AQ4N and its active metabolites in tumour tissue sections using MALDI-MSI. In this chapter, an application and improvement of the methodology explained in chapter 3 is described. It aims to obtain proteomic data from AQ4N dosed tumour xenograft tissue sections and to correlate these data with the drug distribution using MALDI-ion mobility separation-mass spectrometry imaging.

4.2 Materials and Samples

4.2.1 Chemicals and materials

Materials included α-cyano-4-hydroxycinnamic acid (α-CHCA), aniline, ethanol (EtOH), methanol (MeOH), acetonitrile (ACN), chloroform ($CHCl_3$), xylene, octyl-α/β-glucoside (OcGlc), trifluoroacetic acid (TFA), haematoxylin, eosin and carboxymethyl cellulose (CMC) were obtained from Sigma-Aldrich (Dorset, UK). Trypsin was obtained from Promega (Southampton, UK). AQ4N and AQ4 standards were obtained from the Institute of Cancer Therapeutics (Bradford, UK).

4.2.2 Tissue samples

All animal procedures including animal treatment, tumour system and transplantation and drug administration were carried out at the Institute of Cancer Therapeutics (Bradford, UK). The methodologies used are briefly described here in sections 4.2.2.1 and 4.2.2.2. All the animal procedures and handling in this work abide by UK Home Office Regulations and Guidelines [13]. Female Balb/C immunodeficient nude mice (Harlan UK, Blackthorn, UK) aged 6-8 weeks were used. Mice received Teklad 2018 diet(Harlan, UK) and water *ad libitum.* Animals were kept in cages in an air-conditioned room with regular alternating cycles of light and darkness.

4.2.2.1 Transplantation and treatment of tumour samples

SW620 colon tumour xenografts were obtained from the Institute of Cancer Therapeutics, Bradford, UK. The transplantation of tumour is described as follows: SW620 Human colon adenocarcinoma tumours were excised from a donor animal, placed in sterile physiological saline containing antibiotics and cut into small fragments of approximately 2 mm^3. Under brief general inhalation anaesthesia, tumour fragments were implanted in the left and right flank of each mouse using a trocar, and tumour growth was monitored frequently.

4.2.2.2 Drug administration

Once the tumours had reached a volume of 200-400 mm^3, as measured by callipers, mice were administered AQ4N (synthesised in house at the ICT Bradford) at 60 mg/kg

intraperitoneally (ip) and/or pimonidazole hydrochloride (Hypoxyprobe-1), obtained from HPI, Inc. (Burlington, MA) and administered at 60 mg/kg 90 min prior to sampling. Mice were sacrificed and tumours were excised, immediately snap-frozen in liquid nitrogen and stored at -80°C to minimise protein degradation and keep the original sample morphology until further analysis.

4.2.3 Tissue preparation

Frozen tissue samples were embedded in carboxymethyl cellulose (CMC) in order to facilitate the cryosectioning. A CMC gel was made by dissolving 0.1% CMC (by weight) in deionised water. The tissue samples were placed into plastic cryomoulds containing the CMC gel and then frozen using liquid nitrogen. The obtained CMC embedded tissue blocks were cut using a cryostat (Leica Microsystems, UK) operating at -20°C. 10 μm sections were obtained and thaw-mounted onto histological Polysine^{TM} glass slides (Menzel-Glaser, Germany). Tissue sections were rinsed for 1 minute in cold EtOH solutions at 70 and 90% (stored at -20°C) followed by a 15 seconds wash in $CHCl_3$. The sections were then allowed to dry at room temperature prior to *in situ* digestion and matrix deposition. No rinsing steps were performed prior to drug analysis with MALDI-IMS-MSI.

4.3 Methods and Instrumentation

4.3.1 Tissue preparation for the study of the distribution of AQ4N and AQ4 in AQ4N-treated SW620 tumour xenografts

Controls of AQ4N and AQ4 drug standards were diluted to 0.1 and 0.01 mg/mL. 0.5 μL of the obtained solutions were either spiked onto non-treated xenograft tissue sections or spotted alongside AQ4N treated xenograft tissue sections. The spots were allowed to dry at room temperature prior to matrix deposition. α-CHCA was used as the matrix. The matrix solution was prepared at 25 mg/mL in 100% EtOH with 1% TFA as reported previously [12]. Approximately 10 mL of matrix solution were spray coated onto the tissue sections using a gravity fed pneumatic air gun set to 40 psi (Iwata-Medea Inc., Portland, OR, USA).

4.3.2 Tissue preparation for the study of peptide distribution and identification within non-treated and AQ4N-treated xenograft tissue sections

In situ digestion was performed in order to obtain peptide distribution and identification directly from non-treated and AQ4N-treated xenograft tissue sections. The trypsin solution was made at 20 μg/mL in 50 mM ammonium bicarbonate buffer (pH = 8.1) containing 0.1 % octyl glucoside (OcGlc) for *in situ* enzymatic digestion. The trypsin solution was sprayed onto the tissue sections using a SunCollect^{TM} automatic sprayer (SunChrom, Friedrichsdorf, Germany). Using the SunCollect^{TM} automatic sprayer, the trypsin solution was deposited on the tissue section at increased flow rate over five layers. The first layer was performed at 2 μL/min, the second at 3 μL/min and the last three layers set at 4 μL/min. Humid environmental conditions were maintained while depositing the trypsin on the tissue section. After trypsin deposition the tissue section was incubated for 2 hours at 37°C (5% CO_2) in a humid chamber.

An ionic matrix, here α-CHCA mixed with aniline (α-CHCA/ANI), prepared at 5 mg/mL in 50% ACN:0.2%TFA, was used for peptide analysis. The matrix solution was sprayed onto the section using a SunCollect^{TM} automatic sprayer. The matrix deposition onto the tissue section was performed at increased flow rate between layers. The first layer was performed at 1.5 μL/min allowing a matrix seeding process. The second and last three layers were performed at 2.5 μL/min and 3.5 μL/min respectively.

4.3.3 MALDI-IMS-MSI analysis of drug and peptide distributions within non-treated and AQ4N-treated SW620 xenograft tissue sections

4.3.3.1 MALDI-IMS-MS profiling and imaging of drug and *in situ* digested peptide distribution within non-treated and AQ4N-treated SW620 xenograft tissue sections

Prior to MALDI-IMS profiling (MS and MS/MS) and imaging experiments, digital scans of the tissue sections to be analysed were obtained using a CanoScan 4400F flatbed scanner (Canon, Reigate, UK) and then imported into MALDI Imaging Pattern Creator^{TM} software (Waters Corporation, Milford, MA).

For small molecule and peptide analysis, the instrument calibration was performed using standards consisting of a mixture of polyethylene glycol (Sigma-Aldrich, Gillingham, UK) ranging either between m/z 100 to 1000 or between m/z 100 to 3000 respectively prior to MALDI-IMS-MSI analysis. Data were acquired in V-mode and positive mode using a MALDI SYNAPT^{TM}HDMS system (Waters Corporation, Manchester, UK) operating with a 200 Hz Nd:YAG laser. All data were acquired with ion mobility separation in the mass range from m/z 100 to 1000 for small molecule analysis or from m/z 800 to 3000 for peptide analysis. Ion images were acquired at a spatial resolution set at 150 μm with 400 to 600 laser shots per position. Using Driftscope^{TM} software (Waters Corporation, Manchester, UK) ion mobility separation data were extracted and ion images were generated with BioMap 3.7.5.5 software (Novartis, Basel, Switzerland).

4.3.3.2 MALDI-IMS-MS/MS analysis for direct protein identification from non-treated and AQ4N-treated SW620 xenograft tissue sections after *in situ* digestion

MALDI MS/MS analyses were performed using the MALDI SYNAPT^{TM}HDMS (Waters Corporation, Manchester, UK) operating in ion mobility separation (IMS) mode directly from the digested tumour tissue sections. Transfer fragmentation was performed and optimised based on the precursor ion mass [14, 15]. Briefly peptide ions were first separated based on their mobility and then collision-induced dissociation (CID) was performed in the Transfer T-Wave^{TM} (Waters Corporation, Manchester,

UK), thus maintaining the same fragment ion drift time as the corresponding precursor ion. The obtained spectra were processed in MassLynx^{TM} (Waters Corporation, Manchester, UK). MS/MS spectral processing consisted of smoothing, baseline correction and the use of a lock mass based mass correction. Spectra were then processed with the MaxEnt 3 algorithm to de-isotope mass spectrometric data and enhance the signal-to-noise ratio. The resulting files were submitted to a MASCOT (Matrix Science, London, UK) query search and searched against the SwissProt database (release 56.0). Within the MASCOT search engine, the parent and fragment ion tolerances were set at 30 ppm and 0.1 Da respectively. The criteria also included up to two missed cleavages and the variable modifications allowed were protein N terminus acetylation, histidine/tryptophan oxidation and methionine oxidation . *De novo* sequencing was performed manually and using the PepSeq^{TM} *de novo* interactive MS/MS sequencing tool. The parent and fragment ion tolerances were set at 0.1 Da and the threshold was set at 1%. Protein Blast searches against the Swissprot database were also performed to confirm tryptic sequences.

4.3.4 Statistical analysis

4.3.4.1 Principal component analysis-discriminant analysis (PCA-DA)

Principal component analysis (PCA) is one of the methods of choice used in chemometrics to obtain an overview of existing variation within multivariate data sets and identify possible clusters and differences between groups. Here principal component analysis-discriminant analysis (PCA-DA) was carried out using MarkerView^{TM} 1.2 software (Applied Biosystems/MDS Sciex, Concord, Canada). Ten spectra from each tissue section including non-treated, AQ4N and AQ4N Pimonidazole treated SW620 xenograft tissue sections were selected from the obtained MALDI-IMS imaging data using Biomap 3.7.5.5 software and exported as text files where mass/intensity pairs were listed. These text files were loaded into MASCOT Distiller^{TM} (Matrix Science, Boston MA) for spectral de-isotoping purposes. Within MASCOT Distiller^{TM}, the criteria included a minimum signal to noise ratio (S/N) set at 3, a correlation threshold set at 0.6 and a minimum peak half width set at 0.008. The resulting de-isotoped mass spectra were then imported into MarkerView^{TM} 1.2 software for principal component and discriminant analysis (PCA-DA). Prior to PCA-DA, data were normalised to their total area

sum. A supervised PCA-DA was then carried out with a pareto scaling.

4.3.4.2 Orthogonal partial least-squares-discriminant analysis (OPLS-DA)

Orthogonal partial least-squares-discriminant analysis (OPLS-DA) was also performed using MarkerLynx^{TM} (Waters Corporation) software package. The OPLS method consists of an orthogonal correction of the partial least-square technique. It aims to separate predictive variations (such as differences between 2 groups of samples, i.e. treated and non-treated) and also show variations present within a given sample due to experimental errors (instrumentation or data acquisition). In the work reported here, 66 spectra were acquired from each tissue section and processed using MassLynx^{TM} and MarkerLynx^{TM} software packages (Waters Corporation, Manchester, UK). The *automatic peak detection* algorithm (Waters Corporation, Manchester, UK) was applied to the obtained mass spectra in order to remove noise. Using MALDIMerge^{TM} software (Waters Corporation, Manchester, UK), mass sufficient exclusion lists were generated with a peptide tolerance set at 400 mDa, then a mass spectrum/chromatogram for each data file was recreated using DataBridge^{TM} software (Waters Corporation, Manchester, UK) prior to OPLS-DA with MarkerLynx^{TM} software. Within MarkerLynx^{TM} software, the criteria included an intensity threshold set at 100 counts and spectra were normalised against the total intensity count. OPLS-DA was then performed.

4.4 Results and Discussion

4.4.1 Investigation of AQ4N and AQ4 drug distribution within SW620 colon cancer xenogafts

4.4.1.1 Characterisation of AQ4N and AQ4 drug standards with MALDI-IMS-MS

0.5 μl of AQ4N and AQ4 drug standard solutions, made at 10 μg/ml mixed with matrix solution, were spotted onto a MALDI target plate. Figure 4.2 shows the obtained mass spectrum of AQ4N drug standard: the protonated molecule of AQ4N and its sodium adduct ion were observed at m/z 445.2 and 467.2 respectively as well as a fragment ion of AQ4N at m/z 384.2.

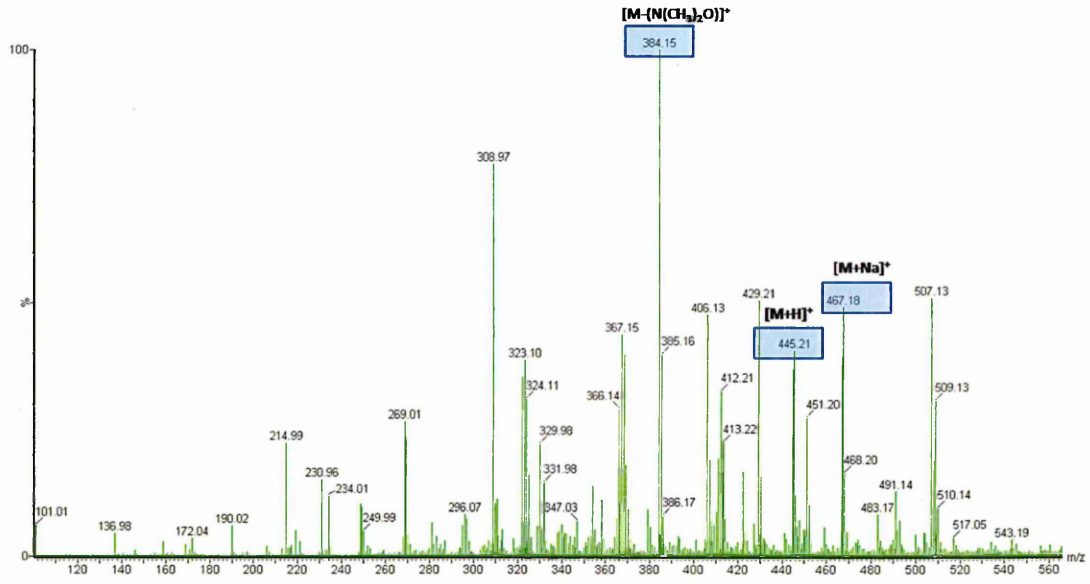

Figure 4.2: **MALDI-MS spectrum of AQ4N drug standard.**
A fragment ion of AQ4N at m/z 384.2, the protonated molecule $[M+H]^+$ and sodium adduct $[M+Na]^+$ of AQ4N at m/z 445.4 and 467.2 respectively were observed.

MALDI-IMS-MS/MS analysis of AQ4N was performed. Figure 4.3a displays the obtained driftscope^{TM} plot of the MS/MS fragmentation of AQ4N. This plot shows the mobility of the ions on the x axis against their m/z values on the y axis. Since the dissociation of the selected ion, here AQ4N, was performed within the transfer region of the instrument, the obtained product ions retained the same drift time as their respective precursor ions.

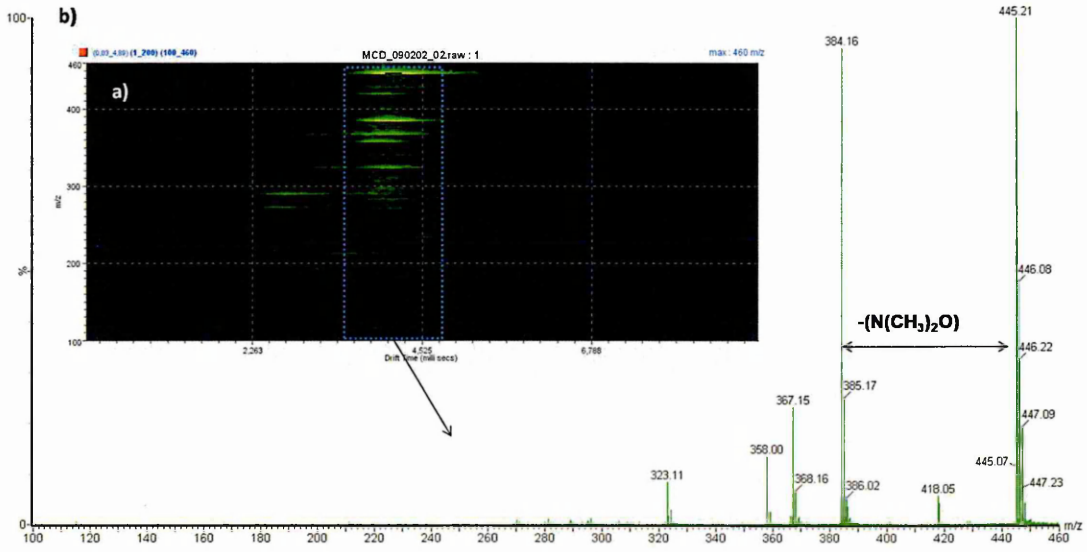

Figure 4.3: **Driftscope^{TM} plot and MALDI-IMS-MS/MS spectrum of AQ4N drug standard.**
(a) Driftscope^{TM} plot of MS/MS fragmentation of AQ4N where peak interference with matrix ions was noticed. (b) MS/MS spectrum of AQ4N drug standard.

Since the MS/MS fragmentation is performed in the transfer cell, the product ions retain the same driftime as their precursor ions. Here one can notice that 2 species are simultaneously detected when examining the driftscope^{TM} plot (figure 4.3a). In fact, the AQ4N product ions display a driftime of 3.85-4.30 msec and the interfering product ions arising from the matrix display a driftime of 2.8-3.4 msec. Using Driftscope^{TM} and MassLynx^{TM} software packages, each individual MS/MS spectrum can be extracted. Figure 4.3b displays the MS/MS spectra of the AQ4N protonated molecule $[M+H]^+$ at m/z 445.2. The y axis of driftscope^{TM} plot (figure 4.3a) indicates that the AQ4N drug has a drift time of 3.85-4.30 msec. The obtained results related to the ion mobility separation of AQ4N were further used to minimise peak interferences and hence specifically

select and reconstruct images of the distribution of the drug within the tissue sections. Examination of the resultant AQ4N MS/MS spectrum shows the presence of the fragment ion at m/z 384.2, thus confirming that AQ4N fragmentation was induced in MS mode. Hence three ions, which are the signals at m/z 384.2, 445.2 and 467.2 corresponding to the AQ4N fragment ion, protonated molecule and sodium adduct respectively, can be used for investigating the distribution of AQ4N within the tissue section in MS and MS/MS mode.

The analysis of AQ4 drug standard was also performed using MALDI-IMS-MS/MS. Figures 4.4a and b show the MS/MS fragmentation of AQ4 with ion mobility separation and the resulting driftscope^{TM} plot. The drift time of AQ4 protonated molecule $[M+H]^+$ at m/z 413.2 was observed between 3.80 and 4.5 msec.

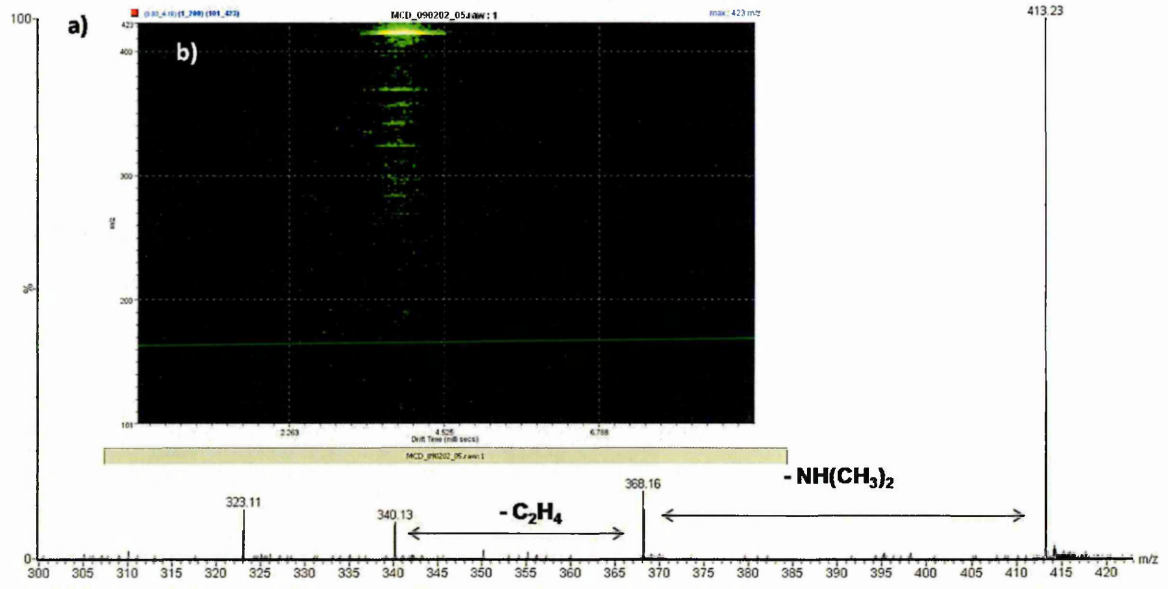

Figure 4.4: **Driftscope^{TM} plot and MALDI-IMS-MS/MS spectrum of AQ4 drug standard.**
(a) Driftscope^{TM} plot of MS/MS fragmentation of AQ4. (b) MS/MS spectrum of AQ4 drug standard.

4.4.1.2 MALDI-IMS-MSI analyis of AQ4N and AQ4 drugs spiked onto SW620 colon cancer xenograft tissue sections

An expanded region from mass spectra acquired from AQ4N and AQ4 spiked on non-treated SW62O colon cancer xenograft tissue sections are displayed in figure 4.5. It can be noticed that both AQ4 ($[M+H]^+$ at m/z 413.2) and AQ4N ($[M+Na]^+$ m/z 467.2) were detected within signal-rich regions of the spectra, where numerous ions arising either from the matrix or other endogenous molecules such as lipids are observed.

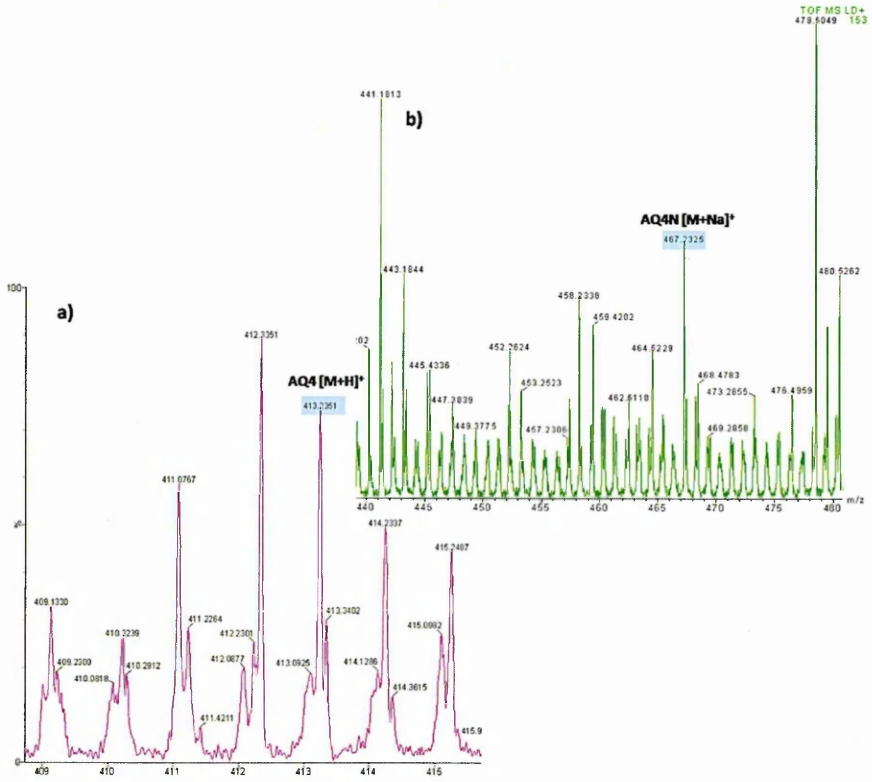

Figure 4.5: **Mass spectra of AQ4 and AQ4N drug standards spiked onto SW620 colon cancer xenograft tissue sections.**
The protonated molecule of AQ4 observed at m/z 413.2 (a) and the sodium adduct of AQ4N observed at m/z 467.2 (b) were detected in signal-rich regions of the spectra along with several potentially interfering peaks.

The use of IMS combined with MALDI-MSI was found to improve the acquired MALDI-MS images of the distribution of AQ4N and AQ4 drug standards spiked onto xenograft tissue sections. Figure 4.6 displays the localisation of AQ4 at m/z 413.2 and AQ4N at m/z 467.2 within the tissue sections with and without IMS. Prior to IMS data extraction, interferences were still noticed. However, when the ions of interest were selectively extracted using their mobility prior to image reconstruction, the exact distribution of both AQ4 and AQ4N spiked onto the tissue sections were obtained.

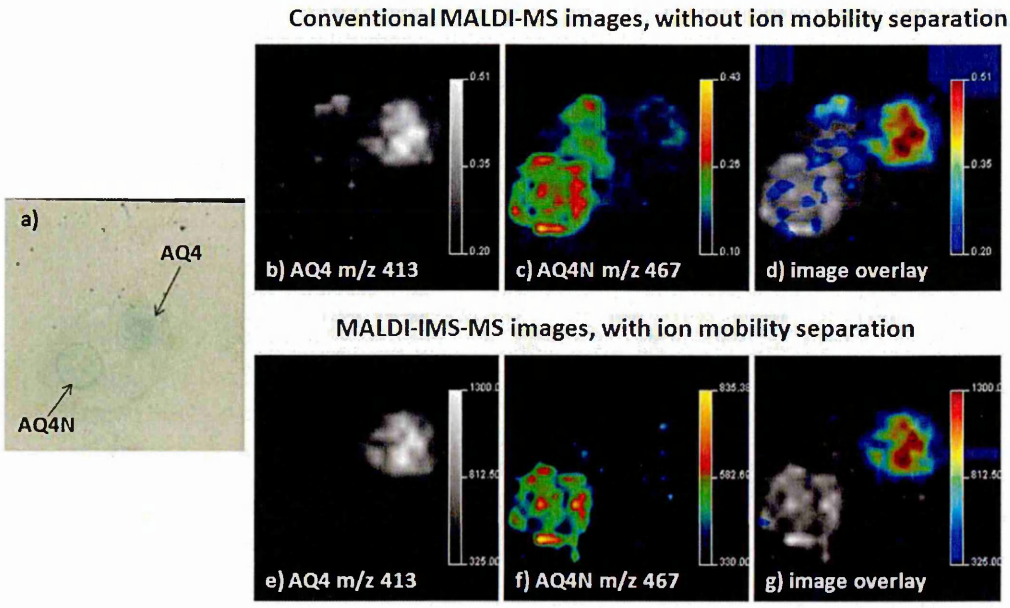

Figure 4.6: **Digital scan of a SW620 colon cancer xenograft tissue section and MALDI-MS images of the distribution of AQ4 and AQ4N drug standards spiked onto SW620 colon cancer xenograft tissue sections.**
(a) Digital scan of the xenograft tissue section spiked with AQ4N and AQ4 drug standards. (b) and (c) Images of the distribution AQ4 (m/z 413.2) and AQ4N (m/z 467.2) without ion mobility separation: peak interferences were noticed in the resulting images. (e) and (f) The use of IMS allowed the true distributions of both AQ4 and AQ4N drug standards spiked onto the tissue section to be obtained. (d) and (g) show overlay images of AQ4N and AQ4 spiked onto the tissue section.

These results demonstrate that a concentration of 10 μg/ml of AQ4N and AQ4 drugs can be detected when spiked onto tumour tissue sections. Additionally the distribution of the spiked drugs within the tissue section can be obtained. Using the IMS, it was possible to minimise peak interferences with AQ4N and AQ4 drugs due to matrix adducts and endogenous compounds such as lipids present in the tissue sample. Hence improved characterisation and localisation of AQ4N and AQ4 within SW620 colon cancer xenograft tissue sections were obtained.

4.4.1.3 MALDI-IMS-MS imaging of the distribution of AQ4N and AQ4 in treated SW620 colon cancer xenografts

MALDI-IMS-MS imaging was then used to study the localisation of AQ4N and its active metabolite AQ4 in AQ4N-treated colon tumour xenograft tissue sections. This work aimed to target tumour regions, and more specifically hypoxic regions, within the tumour tissue sections. Figures 4.7b and c display the distribution of lipid species including the phosphocholine head group at m/z 184 and sphingomyelin(16:0)+Na^+ at m/z 725, which have been reported to be highly abundant in tumour regions [16]. AQ4N distribution within treated tumour was also obtained. It can be noticed that the drug was selectively located in the tumour region of the tissue sections (figure 4.7d). These results were found to be in good agreement with HE histological staining pictures (figure 4.7a) in which the tumour and necrotic area are indicated.

The distribution of AQ4 within the treated tissue sections was not obtained. This can be explained either by the sample preparation or the dose of the drug used for animal treatments. It has been shown that a high concentration of TFA in the matrix solution enhances the crystallisation of AQ4 with the matrix, hence the detection of the drug in tissue sections with MALDI-MS [12]. However a high concentration of TFA may inhibit the AQ4N signal, hence 1% TFA in the matrix solution has been found as an optimum in order to detect both compounds simultaneously [12].

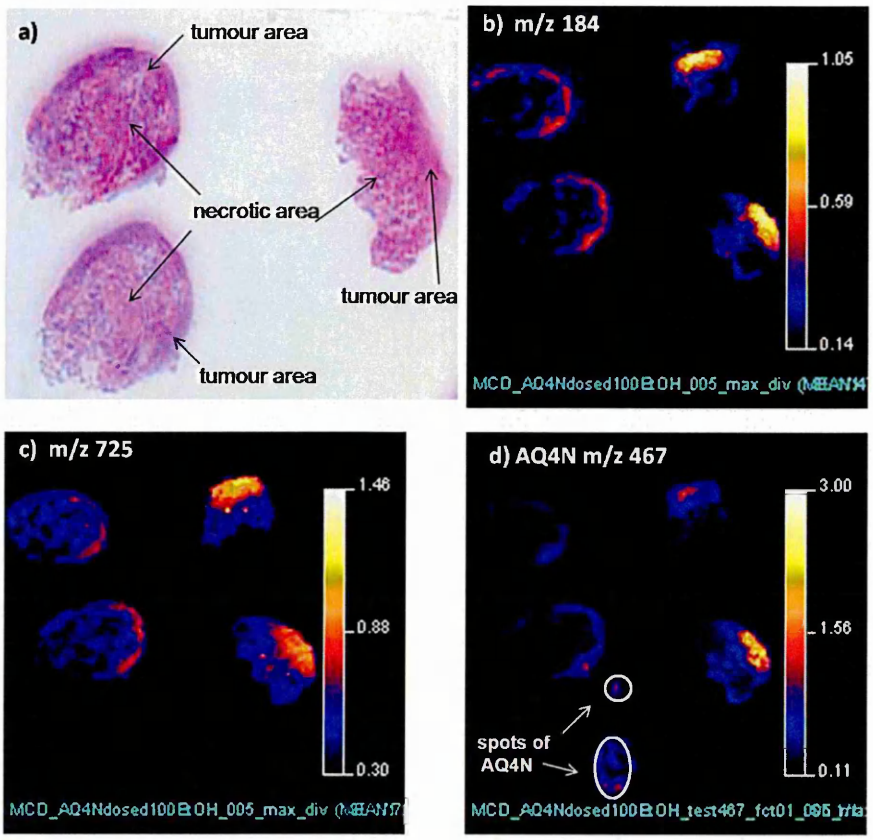

Figure 4.7: **Images of the distribution of lipids and AQ4N drug in treated SW620 colon cancer xenograft tissue sections.**
(a) HE staining digital scans of AQ4N-treated SW620 xenograft tissue sections.(b) and (c) MALDI-MS images showing the distribution of lipid species within AQ4N-treated SW620 xenograft tissue sections which were mainly found in the tumour region. (d) MALDI-MS images of the localisation of AQ4N within the treated tissue section ; spots of AQ4N drug standard were used as positive control.

The poor detection of AQ4 in AQ4N-treated xenografts may also result from the concentration of the drug used for animal treatment. In previously reported studies, simultaneous distributions of AQ4N and AQ4 within xenograft tissue sections were obtained using MALDI-MSI; however these analyses were conducted on xenograft tissue sections obtained from animals treated with AQ4N at a concentration of 100 mg/kg [12]. In the work reported here, the animals used for the study were dosed with AQ4N at a concentration of 60 mg/kg. It has also been reported that a low level of AQ4 in plasma was observed post animal treatment, demonstrating the strong AQ4 dependence on low oxygen level and hence a very low diffusion of the drug out of hypoxic regions of

tumour [9]. An increase in anti-tumour efficacy was observed with AQ4N doses between 50 mg/kg and 200 mg/kg [9]. Improvements of the methodology used here are required for localising AQ4 directly with tumour xenograft tissue sections at such drug dosage level (i.e. 60 mg/kg).

AQ4M is also known as an intermediate metabolite of AQ4N detectable in plasma and whose protonated molecule $[M+H]^+$ is observed at m/z 429.2 with MS. Figure 4.8b displays the distribution of AQ4M within the treated tissue sections. The examination of the MALDI-MS images shows that AQ4M, the intermediate metabolite, is located within the tumour regions but also within the necrotic area which often contain hypoxia regions. By combining information gained from both AQ4N and AQ4M localisation within the treated xenograft tissue sections, tumour regions as well as hypoxic regions within the tumour area were observed. To summarise, the study of the distribution of AQ4N drug and its metabolites within xenograft tissue sections allowed the localisation of hypoxia within tumour regions.

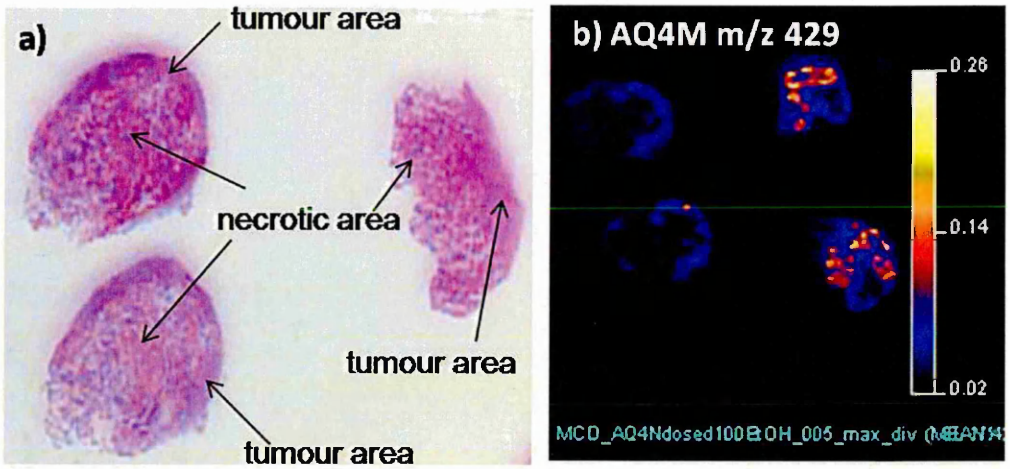

Figure 4.8: **Images of the distribution AQ4M drug in AQ4N-treated SW620 colon cancer xenograft tissue sections.**
(a) HE staining digital scans of AQ4N-treated SW620 xenograft tissue sections.(b) MALDI-MS images showing the distribution of AQ4M within the treated tissue section; the AQ4N spots used as positive control are not highlighted.

4.4.2 MALDI-IMS-MS imaging of peptides after *in situ* digestion of non-treated and AQ4N-treated SW620 colon cancer xenografts

MALDI-MSI technology can be used as a discovery tool as it provides molecular insights such as protein identification and distribution within cancerous tissue sections, and can hence contribute to a better understanding of the morphology and molecular pathology of cancer [17]. Currently there are no hypoxia-related markers that have been identified in correlation to response to AQ4N treatment. In the work reported here, images of peptide distribution were obtained after *in situ* digestion of non-treated and AQ4N-treated SW620 xenograft tissue sections. The animals used for the study were either treated with AQ4N drug only or with AQ4N and pimonidazole, which is a nitroimidazole compound widely used as a qualitative and quantitative marker of tumour hypoxia [18]. Figure 4.9 displays the localisation of some observed peptides within the xenograft tissue sections.

Numerous peptide signals were detected after on-tissue digestion. Examination of the data shows differences in protein intensities when comparing peptide images obtained from non-treated and AQ4N-treated tissue sections. MALDI-MS images of peptide distribution within the tissue section were normalised against the matrix signal at m/z 1066. The peptide signal at m/z 904, which was identified as peptide T210-211 arising from selectin-like osteoblast-derived protein, was found to be highly abundant in non-treated xenograft tissue sections compared to treated samples. This protein is also known as polydom or Sushi, von Willebrand factor type A, EGF and pentraxin domain-containing protein 1 (SVEP1) and plays a biological role in cellular adhesion and may be involved in regulation of cell proliferation, differentiation, and apoptosis [19]. In contrast, the signal at m/z 1032, identified as peptide T12 arising from histone H3, was more intense in AQ4N-treated samples compared to non-treated xenografts.

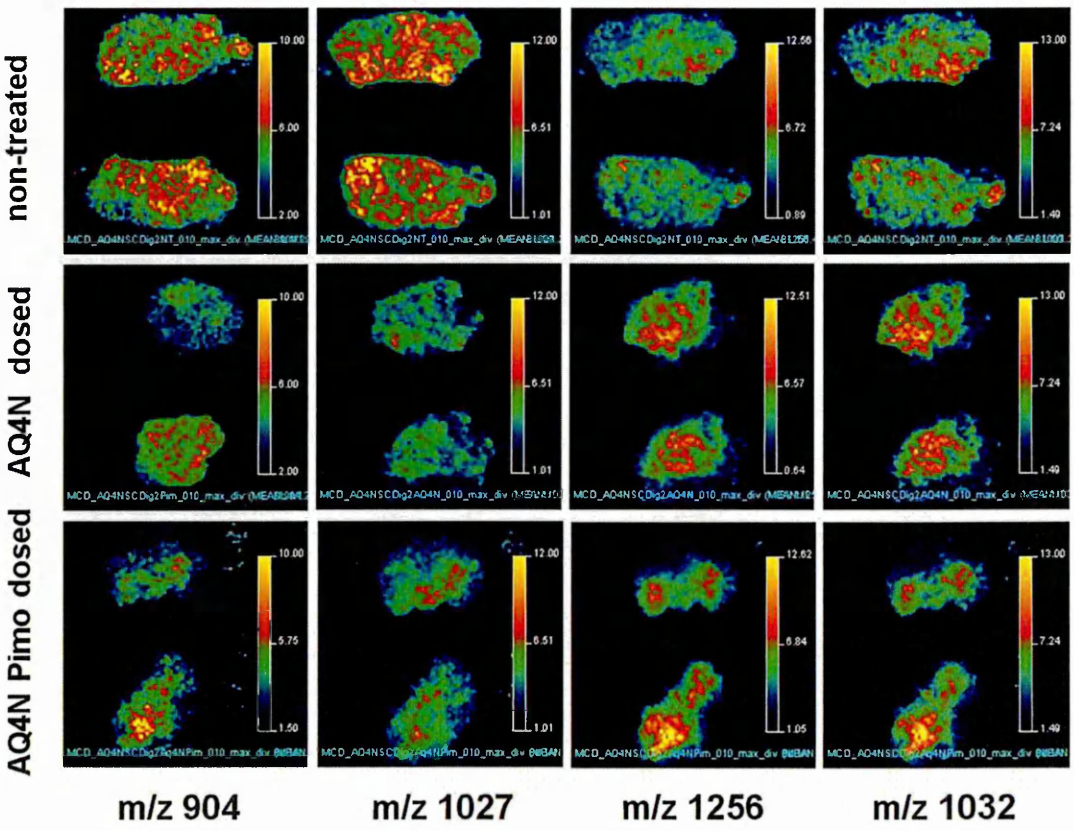

Figure 4.9: **MALDI-IMS-MS images of the peptide distribution within non-treated and AQ4N-treated SW620 colon cancer xenograft tissue sections after *in situ* digestion.**
Several peptide distributions were obtained; here the localisation of ion signals at m/z 904, 1027, 1256 and 1032 is shown. Peptide signals at m/z 904 and 1032 were identified as polydom and histone H3. No identification was obtained for the peptide signals at m/z 1027 and 1256. The peptide signal at m/z 1027 was found to be highly abundant in non-treated tissue sections compared to AQ4N-treated and AQ4N and pimonidazole (AQ4N Pimo)-treated tissue sections.

In order to improve and facilitate data interpretation of the obtained MALDI-MS images, principal component analysis-discriminant analysis (PCA-DA) was performed. PCA is usually used to identify and detect possible clusters from multivariate data sets [20]. Combining PCA with discriminant analysis (DA) involves a further step which consists of identifying classes between samples and is therefore a supervised analysis [21]. In this study, 10 individual mass spectra were exported as text files from each image for a supervised PCA-DA using MarkerView^{TM} software (Applied Biosystems/MDSciex, Canada). Figures 4.10a and b show the resulting scores and loading plots respectively.

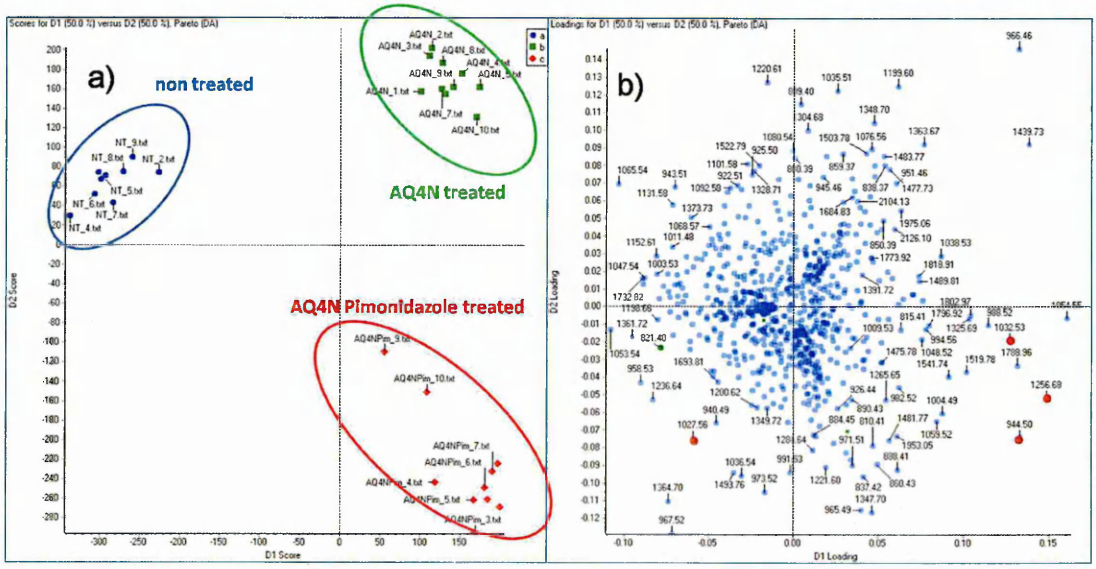

Figure 4.10: **Principal component analysis-discriminant analysis (PCA-DA) of MALDI-IMS-MS images of peptides obtained after *in situ* digestion of non-treated and AQ4N-treated SW620 colon cancer xenograft tissue sections.** (a) and b display the scores and loadings plots respectively. Non-treated tumour samples are separated from AQ4N dosed xenografts. More interstingly, PCA-DA analysis distinguished between treatments administrated to the animals.

In the scores plot (figures 4.10a), discrimination between peptide images obtained from non-treated and AQ4N-treated xenograft tissue samples is observed. There is also a separation between AQ4N-treated and AQ4N and pimonidazole-treated samples. Here PCA-DA allowed the discrimination between peptide profiles according to the type of treatment administer to the animals.

In the loading plots (figures 4.10a), several peptides were found to be characteristic of either the non-treated samples or the AQ4N-treated xenografts. The histone H3 peptide signal at m/z 1032 was found to be predominantly characteristic of AQ4N-treated xenografts. Alternatively the peptide signal at m/z 1027 was found to be highly intense in non-treated tissue sections. These results obtained with PCA-DA analysis were found to be in good agreement with the obtained MALDI-MS images (figure 4.9).

4.4.3 MALDI-IMS-MS profiling of peptides after *in situ* digestion of non-treated and AQ4N-treated SW620 colon cancer xenografts

MALDI-MS imaging and PCA-DA analyses allowed the discrimination between peptide images obtained from non-treated and AQ4N- or AQ4N + Pimonidazole-treated xenograft tissue sections. In order to assess if possible markers can be highlighted, MALDI-IMS-MS profiling was performed followed by orthogonal partial least-squares-discriminant analysis (OPLS-DA). Figure 4.11 displays a digital scan of the tissue sections which were analysed. 66 mass spectra were obtained from each region defined using MALDI Imaging Pattern Creator^{TM} software (Waters Corporation, Milford, MA). An average spectrum was generated for each sample (figure 4.12). Differences in peptide intensities were observed when comparing spectra.

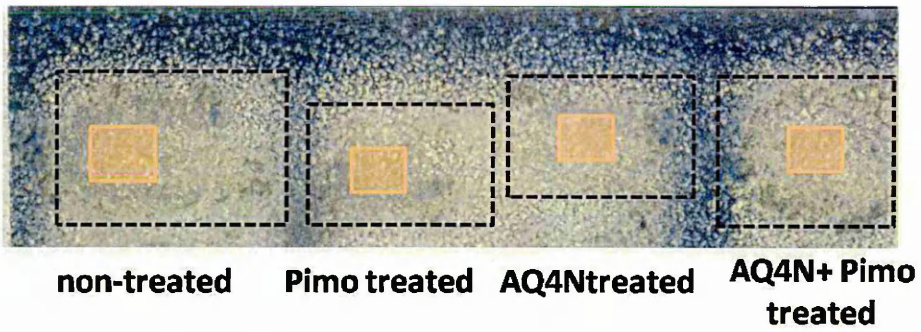

Figure 4.11: **Digital scans of SW620 xenograft tissue sections prior to MALDI-IMS-MS profiling analysis.**
Regions of interest,which were analysed, are highlighted.

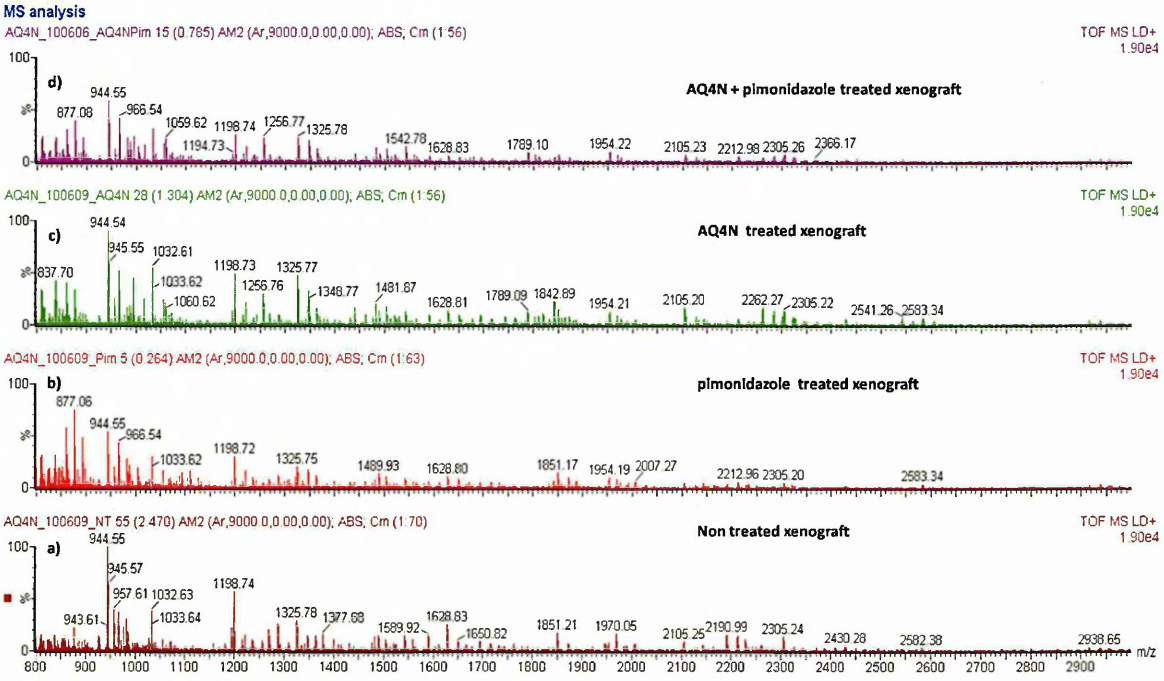

Figure 4.12: **MALDI-IMS-MS average peptide profiles obtained from non-treated, pimonidazole-treated and AQ4N-treated SW620 xenograft tissue sections.**
Several peptide signals were detected. Differences in peptide intensities were noticed when comparing peptide profiles obtained from each tissue section.

OPLS-DA was performed using MarkerLynx^{TM} software. Partial least-squares (PLS) is a multivariate statistical anlytical method often used to obtain a quantitative relationship between two data tables which display spectral data and quantitative values [22]. However, variations due to sample preparation, complexity of the sample matrix and data acquisition are often corrected using OPLS analysis, which aims to filter the data sets, thereby facilitating improved separations and data interpretation of the different types of the innate variations present in the data set [22, 23]. OPLS-DA can also be used to generate a class discrimination between samples. Combining the information obtained from PCA-DA and OPLS-DA may result in an improved method for targeting hypoxia-related markers and also assess the robustness and reproducibility of the method.

Figure 4.13 displays the S-plot of the comparison between non-treated and AQ4N-treated xenograft tissue sections obtained after OPLS-DA. The x axis shows the inter variation between the different samples. Here it can be noticed that groups are clearly separated, as peptide signals at m/z 1032, 1059, , 1060, 1220 and 1347 enable to discriminate AQ4N-treated samples from non-treated samples. Hence peptide signals that significantly represent a group of samples can be highlighted. However direct identification of these peptides is required in order to elaborate further conclusion regarding biologic processes and/or the effect of the drug treatment. The results obtained from OPLS-DA were found to be in good agreement with those obtained from PCA-DA and also with MALDI-IMS-MS profiling and imaging.

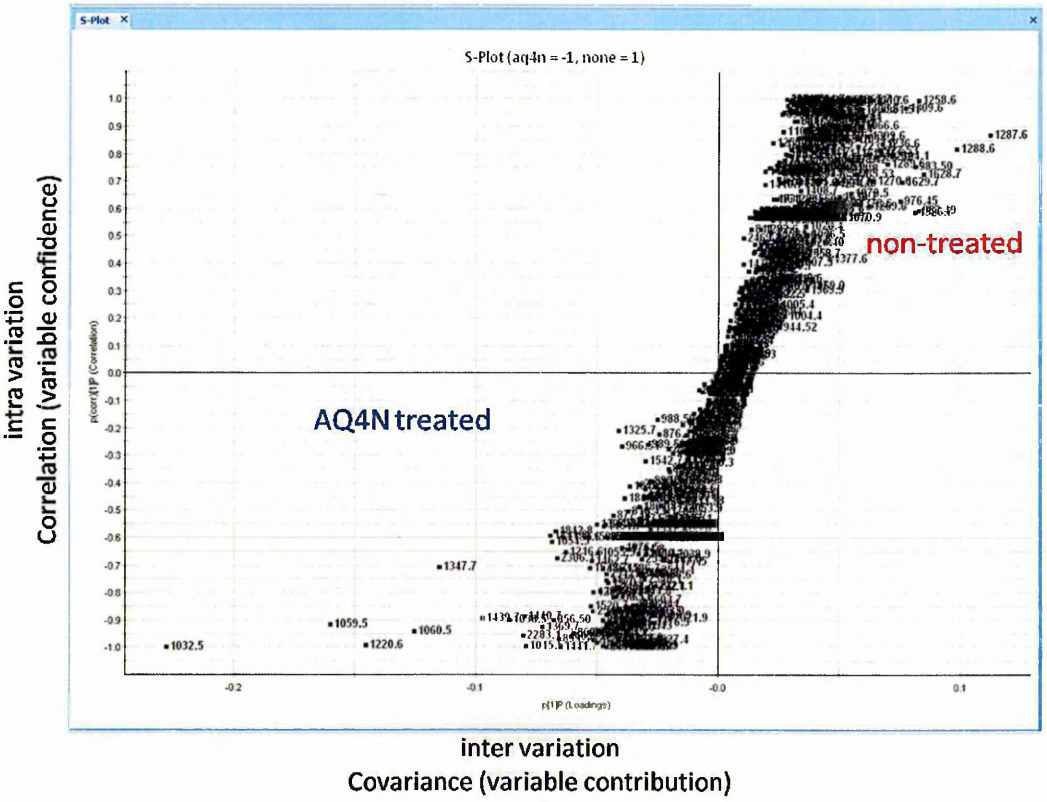

Figure 4.13: **S-plot after OPLS-DA of MALDI-IMS-MS peptide profiles from non-treated and AQ4N-treated SW620 xenograft tissue sections.**
Discrimination between peptide profiles obtained from treated and non-treated samples was noticed. Several peptides were found to be characteristic of a given sample. The ion signal at m/z 1032, arising from histone H3, was found to be more intense in AQ4N-treated samples compared to non-treated.

The peptide profiling comparative study enabled the selection of peptide ion signals for MS/MS fragmentation. However the MS/MS analyses performed directly on-tissue did not allow the identification of several proteins. Table 4.1 displays a list of identified proteins.

Protein Assignment	Accession number	Protein mass (Da)	Observed m/z with MALDI-MSI	Sequence	MS/MS ion score	Molecular function
Actin, aortic smooth muscle	P62736	41982	1198.7	AVFPSIVGRPR	18	Cell mobility
Actin, cytoplasmic 1	P60709	41710	976.4	AGFAGDDAPR	31	
Albumin	P02768	69367	1467,8	RHPDYSVVLLLR	60	
Histone H2A	Q96QV6	14225	944.5	AGLQFPVGR	32	gene regulation
Histone H3	Q6NXT2	15204	1032.6	YRPGTVALR	18	
Histone H4	P62805	11360	1325.7	DNIQGITKPAIR	87	
Polydom	Q4LDE5	390248	1163.6	KWSGASPR, oxidation (HW)	32	Involved in cell adhesion, cell proliferation
Tumor necrosis factor receptor superfamily member 10A	O00220	50029	1105.6	AGRAPGPRPAR	19	mediating apoptosis

Table 4.1: **List of detected proteins after direct MALDI-MS/MS analysis of non-treated and AQ4N-treated SW620 xenograft tissue sections.**

4.5 Concluding Remarks

MALDI-MSI has developed into a new technique that can help in the understanding of the cancer process as well as the responses to treatment. In the work reported here, the methodology used was divided into two parts. First, the distributions of AQ4N and its active metabolites were studied within non-treated and treated SW620 colon cancer xenograft tissue sections. This aimed to localise tumour regions as well as the hypoxic tumour area. However, limitations can be encountered with MALDI-MSI for such studies. In this case isobaric ion interferences with the target compounds, i.e. AQ4N and its active metabolites, were noticed. This limitation was addressed in this study by using ion mobility separation in combination with MALDI-MSI. This resulted in generation of the exact distributions of the compounds of interest with no interfering ions. The *in situ* analysis of AQ4N and its metabolites within the tissue sections allowed the targeting of hypoxia within the tumour section.

The second part of the work aimed to identify hypoxia-related markers. This was achieved using *in situ* digestion followed by MALDI-MSI analysis of non-treated and AQ4N-treated xenograft tissue sections. Indeed, the sensitivity offered by MALDI-MSI analysis of intact proteins directly from tissue sections is in most cases low and results in the detection of mainly the most abundant proteins present in tissue sections such as actin and histone. Therefore the use of *in situ* digestion strategies prior to MALDI-MSI analysis is now a methodology of choice [24, 25], since it leads to direct protein identification. In the work reported here, several peptide signals were observed after *in situ* digestion of non-treated and treated xenograft tissue sections and differences in intensities were observed when comparing profiles and images. Using statistical analysis for data interpretation allowed discrimination between samples as well as the type of treatment administrated to the animals. Several peptides were found to be different in their signal intensities when comparing sample groups.

A problem encountered in this study has been the direct identification of proteins following on-tissue MS/MS fragmentation. Several peptides were found to be abundant and characteristic of a given sample, however the identification of these peptides remains crucial. In this study, several MS/MS analyses allowed good fragmentation of given

peptides, however the database search did not lead to protein identification. This may be explained by existing post-translational modifications, splice variants and the presence of different adducts.

Therefore improvements are required including *de novo* sequencing, the coupling of MALDI-MSI with other molecular imaging techniques and standard analytical protocols used for tissue lysates in order to achieve improved identification and quantification of proteins associated with spatial localisation information. In summary, the methodology described here demonstrates that MALDI-MSI shows huge potential as a powerful biomarker discovery tool.

References

[1] Kunz M. and Ibrahim S.M. Molecular responses to hypoxia in tumor cells. *Molecular Cancer*, 2:23–35, 2003.

[2] Hockel M. and Vaupel P. Tumor hypoxia: definitions and current clinical, biologic, and molecular aspects. *Journal of the National Cancer Institute*, 93:266–276, 2001.

[3] Vaupel P. and Mayer A. Hypoxia in cancer: significance and impact on clinical outcome. *Cancer Metastasis Reviews*, 26:225–239, 2007.

[4] Rademakers S.E., Span P.N., Kaanders J.H.A.M., Sweep F.C.G.J., van der Kogel A.J., and Bussink J. Molecular aspects of tumour hypoxia. *Molecular Oncology*, 2:41–53, 2008.

[5] Cairns R.A., Papandreou I., Sutphin P.D., and Denko N.C. Metabolic targeting of hypoxia and HIF1 in solid tumors can enhance cytotoxic chemotherapy. *Proceedings of the National Academy of Sciences*, 104:9945–9450, 2007.

[6] Rosenberg A. and Knox S. Radiation sensitization with redox modulators: A promising approach. *International Journal of Radiation Oncology, Biology, Physics*, 64:343–354, 2006.

[7] Denny W.A. Tumor-activated prodrugs-a new approach to cancer therapy. *Cancer Investigation*, 22:604–619, 2004.

[8] Patterson L.H. and McKeown S.R. AQ4N: a new approach to hypoxia-activated cancer chemotherapy. *British Journal of Cancer*, 83:1589–1593, 2000.

[9] Loadman P.M., Swaine D.J., Welham K.J., and Patterson L.H. A preclinical pharmacokinetic study of the bioreductive drug AQ4N. *Drug Metabolism and Disposition*, 29:422–426, 2001.

[10] Albertella M.R., Loadman P.M., Jones P.H., Phillips R.M., Rampling R., Burnet N., Alcock C., Anthoney A., Vjaters E., Dunk C.R., Harris P.A., Wong A., Lalani A.S., and Twelves C.J. Hypoxia-selective targeting by the bioreductive prodrug AQ4N in patients with solid tumors: results of a phase I study. *Clinical Cancer Research*, 14:1096–1104, 2008.

[11] Patterson L.H., McKeown S.R., Ruparelia K., Double J.A., Bibby M.C., Cole S., and Stratford I.J. Enhancement of chemotherapy and radiotherapy of murine tumours by AQ4N, a bioreductively activated anti-tumour agent. *British Journal of Cancer*, 82:1984–1990, 2000.

[12] Atkinson S.J., Loadman P.M., Sutton C., Patterson L.H., and Clench M.R. Examination of the distribution of the bioreductive drug AQ4N and its active metabolite AQ4 in solid tumours by imaging matrix-assisted laser desorption/ionisation mass spectrometry. *Rapid Communication in Mass Spectrometry*, 21:1271–1276, 2007.

[13] Workman P., Balmain A., Hickman J.A., Rohas A.M., Mitchison N.A, Pierrepoint C.G., Raymond R., Rowlatt C., Stephens T.C., Wallace J., and Straughan D.W. UKCCCR guidelines for the welfare of animals in experimental neoplasia. *Laboratory Animals*, 22:195–201, 1988.

[14] Pringle S.D., Giles K., Wildgoose J.L., Williams J.P., Slade S.E., Thalassinos K., Bateman R.H., Bowers M.T., and Scrivens J.H. An investigation of the mobility separation of some peptide and protein ions using a new hybrid quadrupole/travelling wave IMS/oa-ToF instrument. *International Journal of Mass Spectrometry*, 261:1–12, 2007.

[15] Riba-Garcia I., Giles K., Bateman R.H., and Gaskell S.J. Evidence for structural variants of a- and b-type peptide fragment ions using combined ion mobility/mass spectrometry. *Journal of the American Society for Mass Spectrometry*, 19:609–613, 2008.

[16] Shimma S., Sugiura Y., Hayasaka T., Hoshikawa Y., Noda T., and Setou M. MALDI-based imaging mass spectrometry revealed abnormal distribution of phospholipids in colon cancer liver metastasis. *Journal of Chromatography B*, 855: 98–103, 2007.

[17] Heeren R.M.A., Smith D.F., Stauber J., Kkrer-Kaletas B., and MacAleese L. Imaging Mass Spectrometry: Hype or Hope? *Journal of the American Society for Mass Spectrometry*, 20:1006–1014, 2009.

[18] Bennewith K.L., Raleigh J.A., and Durand R.E. Orally administered pimonidazole to label hypoxic tumor cells. *Cancer Research*, 62:6827–6830, 2002.

[19] Gilges D., Vinit M.A., Callebaut I., Coulombel L., Cacheux V., Romeo P.H., and Vigon I. Polydom: a secreted protein with pentraxin, complement control protein, epidermal growth factor and von Willebrand factor A domains. *Biochemical Journal*, 352:49–59, 2000.

[20] Jackson J.E. *A User's Guide to Principal Components.* Wiley, 1991.

[21] Defernez M. and Kemsley E.K. The use and misuse of chemometrics for treating classification problems. *Trends in Analytical Chemistry*, 16:216–221, 1997.

[22] Trygg J. and Wold S. Orthogonal projections to latent structures (O-PLS). *Journal of Chemometrics*, 16:119–128, 2002.

[23] Stenlund H., Gorzss A., Persson P., Sundberg B., and Trygg J. Orthogonal projections to latent structures discriminant analysis modeling on *in Situ* FT-IR spectral imaging of liver tissue for identifying sources of variability. *Analytical Chemistry*, 80:6898–6906, 2008.

[24] Lemaire R., Desmons A., Tabet J.C., Day R., Salzet M., and Fournier I. Direct analysis and MALDI imaging of formalin-fixed, paraffin-embedded tissue sections. *Journal of Proteome Research*, 6:1295–1305, 2007.

[25] Wisztorski M., Lemaire R., Stauber J., Menguelet S.A., Croix D., Math O.J., Day R., Salzet M., and Fournier I. New developments in MALDI imaging for pathology proteomic studies. *Current Pharmaceutical Design*, 13:3317–3324, 2007.

CHAPTER 5

IMS-Tag MALDI-MS Imaging of Protein Biomarkers in FFPE Adenocarcinoma Tissue Sections

5.1 Introduction

Advances in genomic and proteomic technologies have been found to provide insights into the complex molecular processes of cancer [1]. Cancer biomarkers are required in order to aid the design and development of tools for early detection, prevention, clinical diagnosis and prognosis as well as treatment [2]. Biomarkers are defined as biological molecules that are measurable indicators of a physiologic state and changes occurring during a disease process [2, 3]. Strategies for cancer biomarker discovery based on the study of mRNA expression have been found to be very informative and beneficial as they have allowed the identification of several potential gene biomarkers. However, mRNA expression very rarely correlates with protein concentration or identify functional proteomic content such as proteolytic cleavage or post-translational modification (PTM) [4]. Proteomic-based strategies for the identification of cancer biomarkers using mass spectrometry (MS) are becoming more and more popular as they provide comprehensive protein characterisation and identification from a wide variety of samples including plasma, cells and tissues [5].

MS analysis of tissue samples has allowed studies of differential protein expression in normal and cancerous tissues leading to the identification of clinical diagnostic and prognostic protein markers [1]. Even more interesting is the use of MALDI-mass spectrometry imaging to obtain the spatial distribution and expression of proteins directly from tissue sections [6]. This approach presents several advantages for improving biomarker discovery as it allows the detection of proteomic information such as protein localisation, relative expression and identification, directly from tumour tissue sections with no requirement for pre-defined targets.

The combination of ion mobility separation (IMS) with MALDI-MSI is a new and promising technology, which has been found to be powerful in improving the method's specificity and selectivity [7]. A new concept called *IMS-Tag MALDI-MSI*, developed in this work, is described for the detection and analysis of biomarkers in human formalin fixed paraffin embedded (FFPE) tumour tissue sections. IMS-Tag MALDI-MSI consists of the use of the efficiency, selectivity and specificity of the IMS to specifically target the ions of interest with no interfering isobaric peaks and then to generate the exact

distribution of this ion within the tissue sections as well as identifying the selected ion using MALDI-MSI.

Using IMS-Tag MALDI-MSI, several known and potential new biomarkers were localised and identified directly from human FFPE adenocarcinoma tissue sections including pancreatic and breast tumours. The methodology used here allowed the targeting and *in situ* identification of glucose regulated protein 78kDa (Grp78), which is known as a tumour biomarker related to the unfolded protein response (UPR), in pancreatic FFPE tumour tissue sections. Additionally using IMS-Tag MALDI-MSI, it was possible to achieve a comparative study between FFPE early stage breast tumour and metastatic lymph node tissue sections, and hence localise and identify tumour biomarkers as well as potential breast tumour metastasis-associated proteins such as heat shock proteins (hsp) and tumour necrosis factor receptor.

It was reported in Chapter 3 (section 3.3.2.3) that the use of antigen retrieval (AR) prior to on-tissue enzymatic digestion was found to be beneficial for *in situ* proteomic investigation as it enabled unlocking of several proteins, hence enhancing the resulting mass spectral signals. However, direct MS/MS analyses for on-tissue protein identification was limited since only a few proteins were identified following a MASCOT database search. In the work reported here, the identification of proline residue oxidation, resulting from the AR protocol, is described. Adding proline oxidation as a variable modification to the MASCOT search criteria greatly increased the number of identified proteins. The limitations and benefits of the methodology used here are described.

5.2 Materials and Methods

5.2.1 Materials

Modified sequence grade trypsin was purchased from Promega (Southampton, UK). A sample of recombinant Grp78 protein was gifted by Dr Valerie Corrigal, Kings College London. All other materials, including alpha-cyano-4-hydroxycinnamic acid (α-CHCA), aniline (ANI), ethanol (EtOH), methanol (MeOH), xylene, octyl-α/β-glucoside (OcGlc), trifluoroacetic acid (TFA), haematoxylin, eosin, hydrogen peroxide (H_2O_2), tri-sodium citrate, ammonium bicarbonate, iodoacetamide and tributylphosphine were purchased from Sigma-Aldrich (Dorset, UK).

5.2.2 Tissue samples

Following fully informed patient consent and full ethical committee approval anonymised 5 μm *ex vivo* human FFPE pancreatic and breast tumour tissue sections were obtained (Study Number SSREC/04/Q2305/67 and subsequent amendments). Tissue samples were fixed in 10% buffered formalin for 24 hours, dehydrated in 70% EtOH and paraffin embedded. 5 μm sections were cut using a cryostat (Leica Microsystems, UK) and mounted onto a histological glass slide. FFPE tissue sections were stored at room temperature until further analysis.

5.2.3 Tissue preparation

Paraffin film was removed from FFPE tissue sections according to methods previously described in chapter 3 (section 3.2.3). Endogenous peroxidase activity was blocked by incubating the section for 12 minutes in a hydrogen peroxide solution made at 3% in MeOH. Antigen retrieval was then performed by heating the section in a microwave oven for 15 minutes at 90°C in a tri-sodium citrate buffer at 0.01M (pH = 6.3) [8]. Three cycles of 5 minutes with a 30 sec interval between cycles in order to check the buffer level in the jar as well as the tissue section were achieved. The section was cooled to room temperature, rinsed with water and then allowed to dry at room temperature before trypsin and matrix deposition.

5.2.3.1 In-solution and *in situ* digestion

The trypsin solution was made at 20 μg/mL in 50 mM ammonium bicarbonate buffer (pH = 8.1) containing 0.1 % octyl glucoside (OcGlc). The recombinant Grp78 standard was digested in solution using the following method: 20 μL of recombinant Grp78 at 0.05 μg/μL was reduced and alkylated using tributylphosphine and iodoacetamide according to the manufacturer's protocol. 20 μL of trypsin solution was then added and the digestion was performed for 2 hours at 37°C (5% CO_2) in a humid environment. The digestion was stopped with ice and the resulting peptide solution was purified using ZipTip C18 pipette tips (Millipore, Hampshire, UK) before MALDI-IMS-MSI analysis.

In situ digestion was performed on FFPE pancreatic and breast tumour tissue sections using a trypsin solution, made at 20 μg/mL in 50 mM ammonium bicarbonate buffer (pH = 8.1) containing 0.1 % octyl glucoside (OcGlc), which was deposited onto the tissue section using either a SunCollect^{TM} MALDI-Spotter (SunChrom, Friedrichsdorf, Germany) or a Portrait®630 automatic spotter (Labcyte Inc., Sunnyvale, USA).

Using the SunCollect^{TM} MALDI-Spotter, the spraying method used for trypsin deposition was the same as described in Chapter 3 (section 3.2.4.4). The trypsin solution was deposited on the tissue section at increased flow rate over five layers. The first layer was performed at 1 μL/min, the second at 2 μL/min and the last three layers set at 4 μL/min. Humid environmental conditions were maintained while depositing the trypsin onto the tissue section. After trypsin deposition the tissue section was incubated for 2 hours at 37°C (5% CO_2) in a humid environment.

The Portrait®630 spotter (Labcyte Inc., Sunnyvale, USA) is an acoustic reagent multispotter and has been described by Aerni *et al* [9]. Briefly the technology consists of using acoustic energy focused under an open reservoir containing the reagent solution toward the sample situated above the reagent reservoir. This results in the ejection and deposition of precise microdroplets onto the targeted sample surface [9]. The volume of a droplet is about 170 pL and a minimum spot-to-spot spatial resolution of 175 μm can be achieved. In the work reported here, 52 cycles were performed for trypsin deposition onto FFPE tissue sections. One drop per position was deposited across the tissue section

during each cycle, hence a total volume of approximately 9 nL of trypsin solution per spot was printed onto the tissue sections. The spot-to-spot spatial resolution was set at 400 μm. After trypsin deposition, the tissue section was incubated for 2 hours at 37°C (5% CO_2) in a humid environment.

5.2.3.2 Matrix deposition

α-CHCA mixed with aniline (α-CHCA/ANI), prepared at 5 and 10 mg/mL in 50% ACN:0.2%TFA, was used as the matrix for peptide analysis.

When using a SunCollect^{TM} automatic sprayer, the matrix solution was made at 5 mg/mL in 50% ACN:0.2%TFA and deposited onto the tissue section at increased flow rate between layers. The first layer was performed at 1 μL/min allowing a matrix seeding process. The second and last three layers were performed at 2 μL/min and 3.5 μL/min respectively.

When using a Portrait®630 spotter, α-CHCA/ANI was made at 10 mg/mL in 50% ACN:0.2%TFA. Since the technology is based on acoustic ejection, there are no limitations in terms of matrix concentrations which can be used as long as the matrix is well dissolved in the solvent. Here, 25 cycles of 5 drops/cycle were deposited onto the tissue section at a spatial resolution of 400 μm, allowing an acceptable crystallisation of the matrix onto the tissue section surface.

5.2.4 Direct MALDI-IMS-MS/MS and MALDI-MS/MS analysis of FFPE adenocarcinoma tissue sections

MALDI-MS/MS analyses were performed using the MALDI SYNAPT^{TM}HDMS (Waters Corporation, Manchester, UK) operating in ion mobility separation (IMS) mode directly from the digested tumour tissue sections. Transfer fragmentation was performed and optimised based on the precursor ion mass [10, 11]. The transfer fragmentation method was described in chapter 3 (section 3.2.6.2). MALDI-MS/MS spectra were also acquired using an automatic run. To do so, mass spectra were first obtained directly from the tissue section. Using MALDIMerge^{TM} software (Waters Corporation), the resulting mass spectra were merged together in order to obtain peptide mass/intensity lists. Excel (Microsoft) was then used to randomly select peptide masses for MS/MS fragmentation. The tissue sections were further defined as a spot target and MS/MS

spectra were automatically acquired based on transfer fragmentation dissociation energy pre-registered in the instrument setting parameters. Figure 5.1 displays an overlay of a standard spot target plate (Waters Corporation) and the tissue section area (highlighted in red).

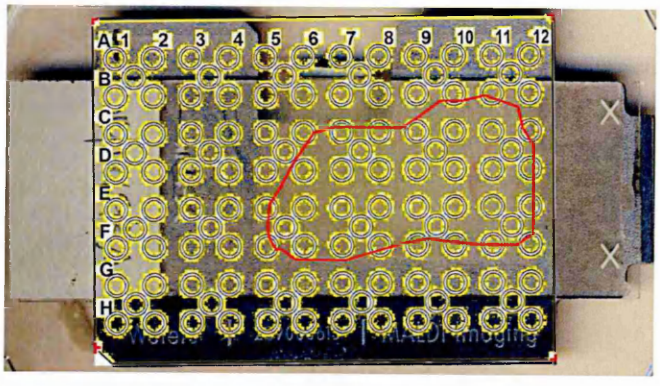

Figure 5.1: **Definition of the tissue section area as a standard spot target plate prior to MALDI-MS/MS automatic acquisition.**
Overlay of a standard spot target plate and the tissue section area which is highlighted in red.

After both manual and automatic MALDI-MS/MS acquisitions, the obtained MS/MS spectra were processed in MassLynx^{TM} (Waters Corporation, Manchester, UK). MS/MS spectral processing methods were the same as described in chapter 3 (section 3.2.6.2). The resulting files were submitted to a MASCOT (Matrix Science, London, UK) query search and searched against the SwissProt database (release 56.0). Within the MASCOT search engine, the parent and fragment ion tolerances were set at 30 ppm and 0.1 Da respectively. The criteria also included up to two missed cleavages and the variable modifications allowed were protein N terminus acetylation, histidine/tryptophan oxidation, methionine oxidation and proline oxidation. *De novo* sequencing was performed manually and using the PepSeq^{TM} (Waters Corporation, Manchester, UK) *de novo* interactive MS/MS sequencing tool. The parent and fragment ion tolerances were set at 0.1 Da and the threshold was set at 1%. Protein Blast searches against the Swissprot database were also performed to confirm tryptic sequences.

5.2.5 MALDI-mass spectrometry imaging

Digital scans of tissue sections were obtained prior to MALDI-IMS-MSI experiments using a CanoScan 4400F flatbed scanner (Canon, Reigate, UK) and then imported into MALDI Imaging Pattern Creator^{TM} (Waters Corporation, Milford, MA) software. This allowed the generation of patterns containing the x and y coordinates of each pixel of the image. The instrument calibration was performed using a standard mixture of polyethylene glycol (Sigma-Aldrich, Gillingham, UK) ranging between m/z 100 to 3000 prior to MALDI-IMS-MSI analysis. Data were acquired in V-mode and positive mode using a MALDI SYNAPT^{TM}HDMS system (Waters Corporation) operating with a 200 Hz Nd:YAG laser. All data were acquired with ion mobility separation in the mass range from m/z 800 to 3000. Peptide images were acquired at a spatial resolution set at 200 μm with 600 laser shots per position. Using Driftscope^{TM}2.1 (Waters Corporation, Manchester, UK) software, mobility data of individual peptide signals were selected and extracted using MALDIExtract^{TM} (Waters Corporation) software. The extracted data were converted into imaging files using MALDI Imaging Convertor^{TM} (Waters Corporation) software and ion images were generated with BioMap 3.7.5.5 software (Novartis, Basel, Switzerland).

5.2.6 Immunohistochemistry

Immunohistochemistry (IHC) was performed on FFPE pancreatic and breast tumour tissue sections using a peroxidase-based staining method. Paraffin was first removed from FFPE tumour tissue sections followed by rehydration through a series of ethanol solutions of increasing water concentrations. Residual endogenous peroxidase activity was blocked by incubating the sections in 2% hydrogen peroxide in methanol for 30 minutes at room temperature followed by AR performed in a microwave oven for 15 minutes until simmering. Sections were incubated for 30 minutes at room temperature in normal goat blocking serum (Vector Laboratories) diluted at 15:1000 to minimise non specific bindings and then incubated for an additional 30 minutes at room temperature with goat anti-human Grp78 antibody (Santa Cruz Biotechnology) at a dilution of 1:100. Tissue sections were washed with phosphate buffered saline (PBS) solution and were incubated with the second antibody biotinylated anti-goat immunoglobulin (Vector Laboratories) at a dilution of 1:20, for 30 minutes at room temperature. An avidin

biotinylated horseradish peroxidase complex solution was then applied to the sections for an additional 30 minutes at room temperature. Grp78 antibody on the sections was visualised using diaminobenzidine and tissue sections were counterstained with haematoxylin for 60 seconds before being dehydrated and coverslipped. Tissue sections were also stained for negative control. Images were obtained using a light microscope (Olympus BX51) operating in brightfield mode using CellD (Olympus) software.

5.2.7 Haematoxylin and eosin (HE) staining protocol

Paraffin was first removed from FFPE tumour tissue sections followed by rehydration through a series of ethanol solutions of increasing water concentrations (100, 95 and 70% ethanol) for three minutes in each solution. The sections were then dipped in tap water for two minutes. The nuclei were stained by immersing the tissue sections in haematoxylin for 30 seconds, followed by a wash under running tap water (a gentle stream of water running into a staining jar was used). The sections were then dehydrated in 70 and 95% EtOH solutions for three minutes and immersed for 20 seconds in eosin solution made at 5% in EtOH. Following eosin staining, the tissue sections were washed in 95% EtOH solutions for five minutes each time, followed by two washes in 100% EtOH for five minutes each time. Tissue sections were then fully dehydrated in xylene for 15 minutes and coverslipped. Images were obtained using a light microscope (Olympus BX51) operating in brightfield mode using CellD software.

5.3 Results and Discussion

5.3.1 Targeting of glucose-regulated protein 78 kDa (Grp78) in human FFPE pancreatic tumour tissue sections

5.3.1.1 Direct MALDI-IMS-MS imaging and validation of Grp78 expression in FFPE pancreatic tumour tissue sections

Recombinant Grp78 protein was digested in-solution in order to assess the peptide mass fingerprint generated and to be expected when performing the same analysis on tissue. Figure 5.2 displays the obtained mass spectrum and some ion signals belonging to Grp78 according to the theoretical Grp78 tryptic digest peptide map are highlighted. The resulting peak list was de-isotoped using the MassLynx^{TM} software and was imported into the MASCOT search engine for a peptide mass fingerprint (PMF) search. Matrix adduct peaks and autolysis tryptic peptides were also removed from the peak list prior to the MASCOT search. Table 5.1a shows the list of tryptic peptide masses which were found to match for the identification of Grp78. The ion signals at m/z 1887, 1934, and 1999 were further analysed using MALDI-MS/MS and sequence assignments were made using MASCOT, thus resulting in the positive identification of Grp78. Table 5.1b displays the obtained peptide sequences.

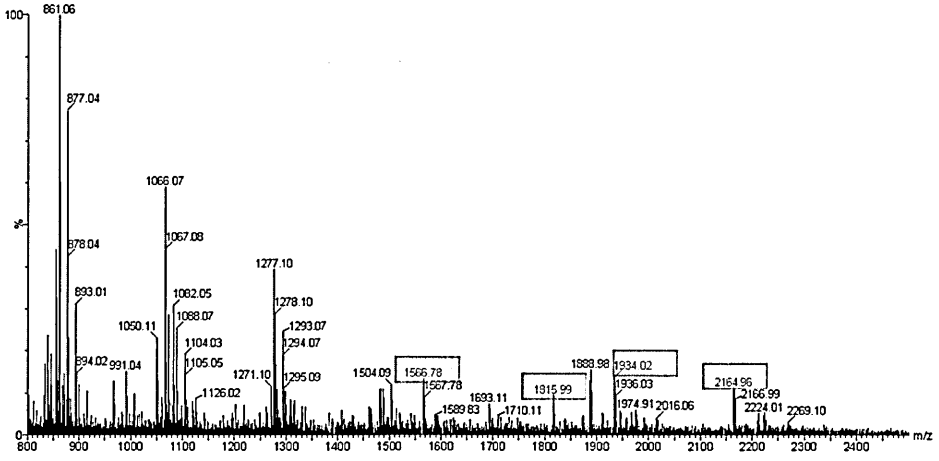

Figure 5.2: **MALDI mass spectrum obtained after in-solution digestion of Grp78 recombinant protein.**
Grp78 tryptic peptides at m/z 1566, 1815, 1934 and 2164 are highlighted. Matrix cluster peaks including signals at m/z 861, 877, 1066 and 1277 can also be observed.

(a) Protein name/ Accession number	Mass (Da)	Observed peptide m/z	Mass error (ppm)	Sequence	MOWSE Score	Sequence coverage (%)
78 kDa glucose-regulated protein (Grp78)/ P11021	72288	1512.75	-4	AKFEELNMDLFR	68	22
		1566.78	1	ITPSYVAFTPEGER		
		1815.99	-5	IINEPTAAAIAYGLDKR		
		1887.97	-1	VTHAVVTVPAYFNDAQR		
		1920.09	33	IQQLVKEFFNGKEPSR		
		1934.01	0	DNHLLGTFDLTGIPPAPR		
		1974.90	-2	IEWLESHQDADIEDFK		
		1999.02	-34	GVPQIEVTFEIDVNGILR		
		2164.97	-8	IEIESFYEGEDFSETLTR		

(b) Protein name/ Accession number	Mass (Da)	Observed peptide m/z	Mass error (ppm)	Sequence obtained after MS/MS fragmentation	MS/MS ion score	Database
78 kDa glucose-regulated protein (Grp78)/ P11021	72288	1887.963	12.9	VTHAVVTVPAYFNDAQR	52	Swissprot
		1934.006	6.23	DNHLLGTFDLTGIPPAPR	79	
		1999.086	13.9	GVPQIEVTFEIDVNGILR	32	

Table 5.1: **List of peptide masses used for the identification of Grp78 after in-solution digestion of Grp78 recombinant protein.**
(a) List of peptide masses matched for the identification of Grp78 with PMF search.
(b) Sequence obtained after MS/MS analysis of selected tryptic peptides.

On-tissue digestion was then performed on FFPE pancreatic tumour tissue sections which were subsequently subjected to MALDI-IMS-MSI analyses. A spot of in-solution digested Grp78 recombinant protein was also imaged along with the tissue section as a positive control (circled in figure 5.3c-e). To reconstruct the MALDI-MS images, only data resulting from the ion mobility separation were used. Figures 5.3a and b show digital scans of the tissue section before and after trypsin and matrix deposition using a Portrait®630 spotter respectively.

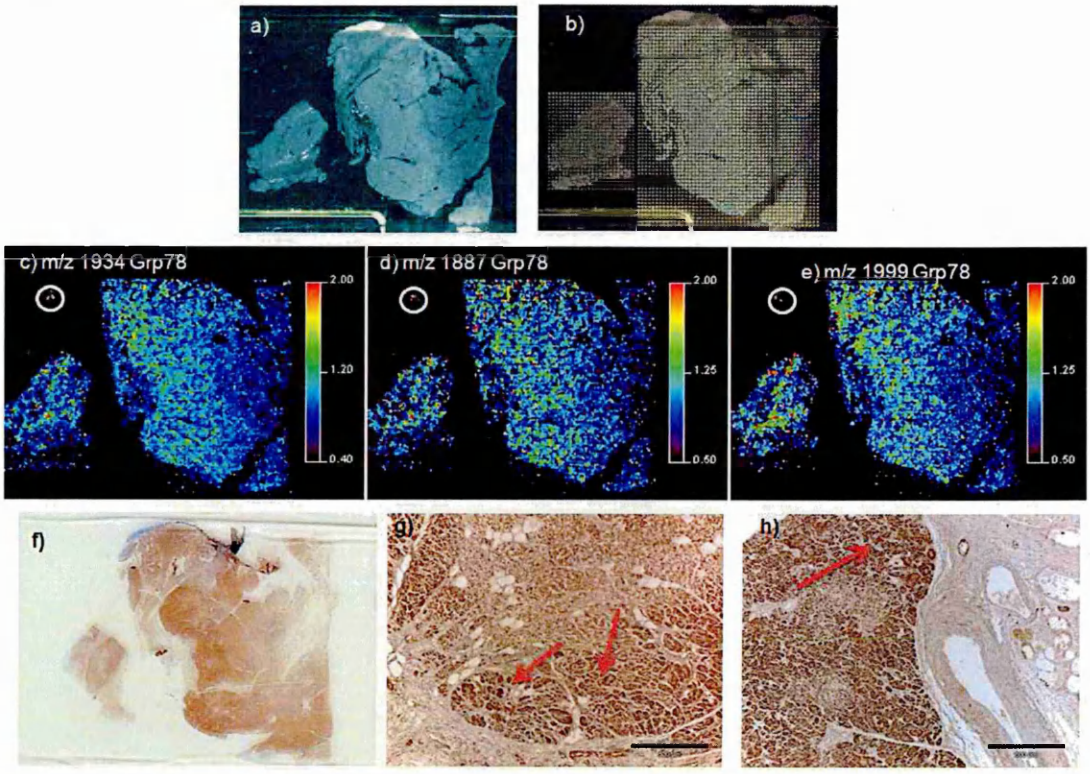

Figure 5.3: **Images of the distribution of Grp78 within FFPE pancreatic tumour sections.**
(a, b) Digital scans of the tissue section before and after trypsin and matrix deposition using a Portrait®630 spotter respectively. (c-e) MALDI-IMS-MS images of the distribution of Grp78 tryptic peptides within FFPE pancreatic tumour sections. (f) Digital scan of the tissue section after immunohistochemical staining of Grp78. (g,h) Microscopic images of immunohistochemical staining of Grp78 within the tissue section showing a high expression of Grp78 in tumour cells (red arrows indicate tumour cells): the images were obtained at magnification x10.

Figures 5.3c, d and e display the localisation of tryptic peptides including signals at m/z 1934, 1887 and 1999 respectively within the tissue section. These signals were previously identified as arising from Grp78. These findings were confirmed using the positive control spot of Grp78 recombinant protein imaged simultaneously with the tissue section. In order to validate these results, immunohistochemical analysis was performed. Figures 5.3f, g and h show the IHC staining of Grp78 within the tissue section. Grp78 was found to be highly expressed in tumour cells. When comparing the IHC staining images and the MALDI-IMS-MS images obtained from the tumour tissue sections, Grp78 was found to be mainly located in the tumour region. The MALDI images were found to be in good agreement with those obtained by the IHC study.

5.3.1.2 Direct MALDI-IMS-MS/MS analysis and *in situ* identification of Grp78 within FFPE pancreatic tumour tissue sections

Direct MALDI-IMS-MS and MS/MS analyses were performed on the FFPE pancreatic tumour tissue sections in order to confirm the identification of Grp78. Figures 5.4a and b display a mass spectrum and the corresponding Driftscope^{TM} plot obtained from the tumour region of the tissue section. This plot gives a graphical representation of the ion-mobility drift-time versus mass-to-charge ratio for detected ions. Using ion mobility, separation between doubly charged ions and singly charged peptides can be achieved. Examination of the data shows the detection of tryptic peptides arising from Grp78 including ions at m/z 1887, 1934 and 2164. The ion at m/z 2164 can be seen in the zoomed in spectrum insert.

MS/MS analysis of the peptide signals at m/z 1887, 1934 and 1999 directly from the tissue surface allows confirmation of the assignment of these signals to Grp78. Figure 5.5 displays the MS/MS spectrum obtained for the peptide at m/z 1934.

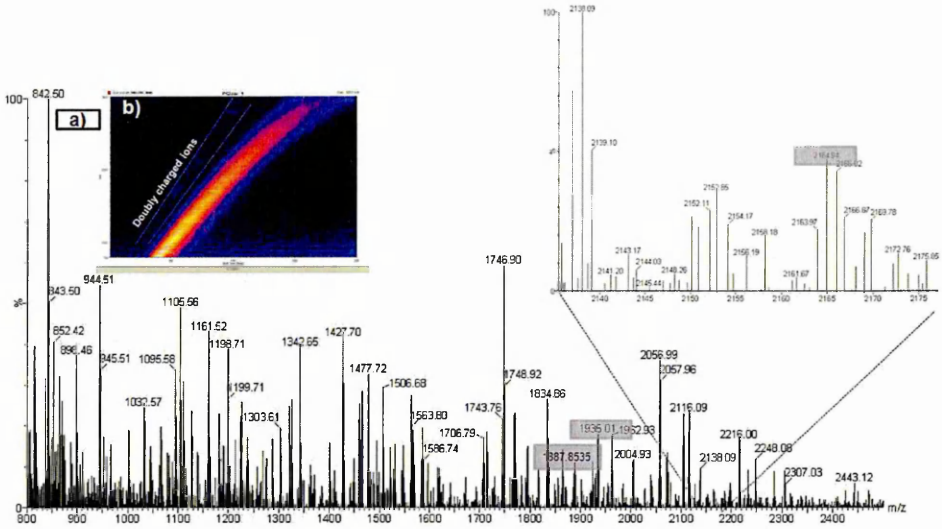

Figure 5.4: **Investigation of the detection of Grp78 tryptic peptides within FFPE pancreatic tumour sections by MALDI-IMS-MS profiling.**
(a) MALDI-MS peptide profile obtained directly from the pancreatic tumour tissue section showing the detection of Grp78 tryptic peptides. (b) Driftscope^{TM} plot obtained from direct MALDI-MS profiling of FFPE pancreatic tumour tissue sections where the peptide ions are separated based on their ion mobility.

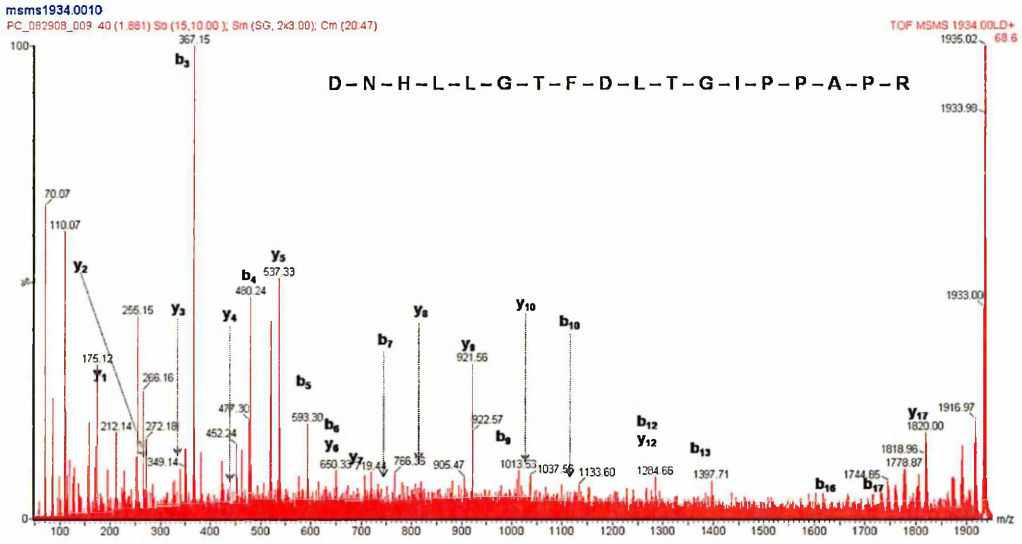

Figure 5.5: **MALDI-IMS-MS/MS spectrum of the peptide ion at m/z 1934 acquired directly from a FFPE pancreatic tumour tissue section.**
The spectrum was normalised to the fragment ion signal at m/z 367. The peptide ion at m/z 1934 was identified as a Grp78 tryptic peptide.

Several other peptide signals were also analysed by MS/MS directly from FFPE pancreatic tumour tissue sections. Here the use of IMS was found to be beneficial as it allowed separation of isobaric species including peptides, hence improving the database search for protein identification. Figure 5.6a displays the Driftscope^{TM} plot obtained for the ion signal at m/z 1400 where two species were simultaneously detected. When performing a MASCOT search on the entire spectrum, a MASCOT MS/MS ion score of 50 was obtained for periostin. However these peptides can be separated from each other based on their mobility (Figures 5.6b and c) which results in an increase in the level of confidence in assigning the protein identification, as shown by the resulting MASCOT MS/MS ion score of 75 for the same protein (see table 5.2).

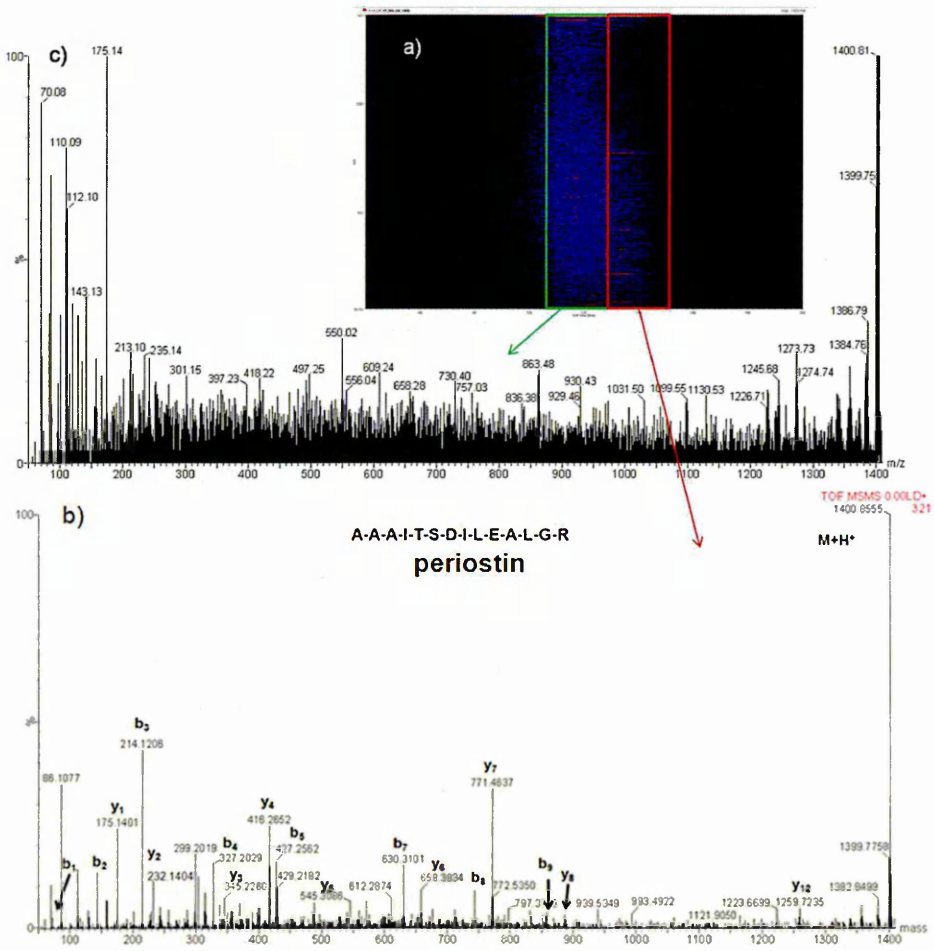

Figure 5.6: **MALDI-IMS-MS/MS spectrum of the ion signal at m/z 1400 acquired directly from a FFPE pancreatic tumour tissue section.**
(a) Driftscope^{TM} plot of the MS/MS spectrum of the ion signal at m/z 1400, which shows the simultaneous detection of 2 isobaric peptides. These MS/MS spectra were separated using the ion mobility separation, thus allowing an improved database search result for the protein identification. (b) MS/MS spectrum of the peptide T27 arising from periostin. (c) MS/MS spectrum of another peptide signal at m/z 1400 which was not identified.

Table 5.2 displays a list of peptides identified directly from FFPE pancreatic tumour tissue sections.

Protein name/ Accession number	Mass (Da)	Observed peptide m/z	Mass error (ppm)	Sequence	MS/MS ion score	Sequence coverage (%)
Actin, aortic smooth muscle/ P62736	41982	1198.72	12.9	AVFPSIVGRPR	46	7.2
		1790.90	2.96	SYELPDGQVITIGNER	75	
Actin, cytoplasmic 1/ P60709	41710	1954.06	0.78	VAPEEHPVLLTEAPLNPK	108	10.4
		2215.08	4.22	DLYANTVLSGGTTMYPGIADR	61	
Albumin/ P02768	69321	1149.63	15.4	LVNEVTEFAK	37	3.6
		1311.73	7.05	HPDYSVVLLLR	57	
Collagen alpha-1(I)/ P02452	138827	886.44	0.87	GSEGPQGVR	30	6
		1297.62	8.77	GESGPSGPAGPTGAR	39	
		1546.77	13.88	GETGPAGPAGPVGPVGAR	74	
		1690.78	0.74	DGEAGAQGPPGPAGPAGER	45	
Collagen alpha-2(I)/ P08123	129209	1235.63	11.37	TGHPGTVGPAGIR, oxidation (HW)	30	4.7
		1477.73	14.66	GLHGEFGLPGPAGPR, oxidation (HW)	20	
		1562.77	9.65	GETGPSGPVGPAGAVGPR	36	
78 kDa glucose-regulated protein (Grp78) / P11021	72288	1887.95	12.9	VTHAVVTVPAYFNDAQR	10	5.5
		1934.00	6.23	DNHLLGTFDLTGIPPAPR	76	
Haemoglobin alpha / P69905	15258	1087.57	17.3	MFLSFPTTK, oxidation (M)	26	17
		1529.74	2.57	VGAHAGEYGAEALER	115	
Haemoglobin beta / P68871	15988	1274.73	2.22	LLVVYPWTQR	27	
Histone H2A.Z/ P0C0S5	13545	944.53		AGLQFPVGR	26	
Histone H2B / P33778	13942	1775.84	20.6	AMGIMNSFVNDIFER, 2 oxidation (M)	36	
Histone H3-like/Q6NXT2	15204	1032.59	4.15	YRPGTVALR	19	
Histone H4/ P62805	11360	1325.74	7.59	DNIQGITKPAIR	39	24.5
		1466.80		TVTAMDVVYALKR	29	
Pancreatic alpha-amylase/ P04746	57670	1427.70	2.60	ALVFVDNHDNQR	59	
Pancreatic triacylglycerol lipase precursor / P16233	51124	1746.90	19.58	FIWYNNVINPTLPR	58	
Periostin/ Q15063	93255	1400.78	6.62	AAAITSDILEALGR	75	
Serine/threonine-protein kinase/ Q9Y3S1	242525	1327.72	6.13	GLTLPCLPWRR, oxidation	23	

Table 5.2: **List of some tryptic peptides identified after *in situ* digestion of FFPE pancreatic tumour tissue sections using direct MALDI-IMS-MS/MS.** All database searches for protein identification were performed using the Swissprot human database.

IMS has been also found powerful to minimise peak interferences observed in MALDI-MS images. Images acquired by conventional MALDI-MS can be a composite of the distribution of multiple ions. Figure 5.7a shows a Driftscope^{TM} plot of detected peptides where an isobaric peak interference was observed with an actin tryptic peptide at m/z 1198. Figure 5.7b displays the distribution of the ion signal at m/z 1198. The concept IMS-Tag MALDI-MSI, developed in this work, which combines high-efficiency ion mobility separations and MALDI-MS has been used to determine the distribution of an actin tryptic peptide at m/z 1198 without interference from simultaneously ionised isobaric ions (figures 5.7c and d).

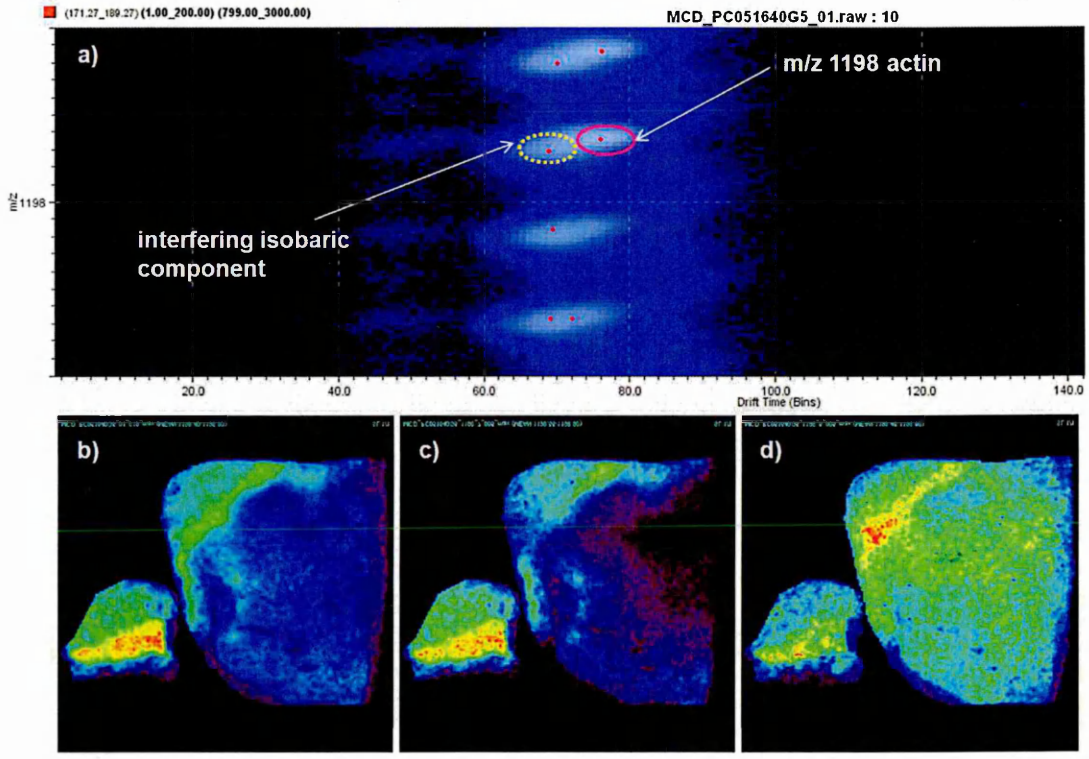

Figure 5.7: **Driftscope^{TM} plot, conventional MALDI-MS and IMS-Tag MALDI-MS images of actin tryptic peptide and isobaric peak interference obtained from a FFPE pancreatic tumour tissue section.**
(a) Driftscope^{TM} plot of observed peptides in the mass range m/z 1196 to 1200: the red dots indicate the detected peptide peaks. (b) Distribution of the ion signal at m/z 1198 using conventional MALDI-MSI, without ion mobility separation. Imaging with ion mobility separation allows the determination of the exact distribution of actin tryptic peptide at m/z 1198 (c) free of interfering isobaric component (d).

Using the IMS-Tag MALDI-MSI, the distributions of some identified peptides within the FFPE pancreatic tumour tissue section are shown in figure 5.8. It can be noticed that peptide signals arising from the same protein display an identical distribution across the tissue section (figures 5.8b and c). This is very beneficial as it allows the confirmation of the identification of protein obtained by direct MS/MS analysis and protein database search. More interestingly, the information resulting from the imaging experiment can be used to target and identify other tryptic peptides arising from the same protein with only PMF searches with no requirement for MS/MS analysis since the same distribution across the tissue section should be observed.

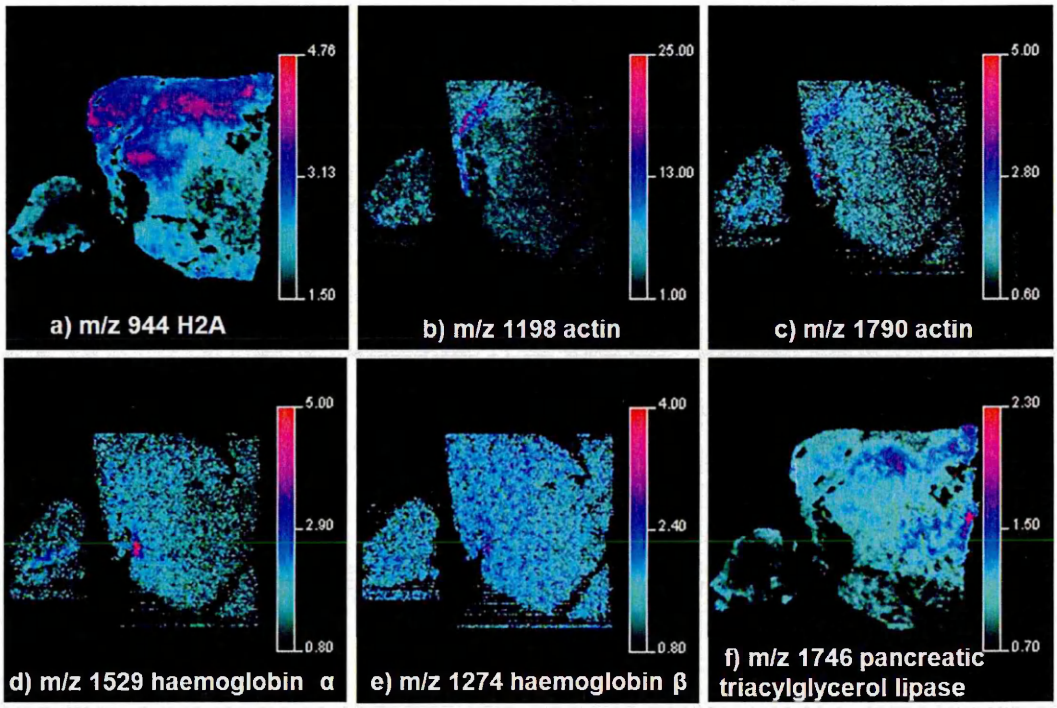

Figure 5.8: **IMS-Tag MALDI-MS images of peptide distribution within a FFPE pancreatic tumour tissue section.**
The localisations of histone H2A, actin, haemoglobin and pancreatic triacyglycerol lipase are displayed.

5.3.1.3 Discussion

Pancreatic cancer is one of the most common malignant causes of death in the UK and is still associated with poor prognosis despite therapeutic options which include surgical resection and chemotherapy [12]. Direct proteomic analysis of tumour samples by MALDI-MSI is of great interest as it provides insights into protein distribution, abundance and identification within a given tissue section in a single experiment. Even more desirable is the possibility of investigating the proteome information directly from archived samples with known clinical outcome as it may assist biomarker discovery, hence resulting in the improvement of clinical diagnosis and prognosis.

In this section, the key outcomes are the localisation and identification of the glucose-regulated protein 78 kDa (Grp78), which is known as a tumour biomarker, directly within FFPE pancreatic tumour tissue sections. Grp78 is a key molecular chaperone within the endoplasmic reticulum (ER) and member of the Hsp70 family [13–15]. It provides the trigger for the activation of the signal cascade known as the unfolded protein response (UPR), a cellular stress response [16, 17]. The UPR is activated when malfolded proteins are accumulated in the ER lumen [17, 18]. Briefly UPR activation aims to enhance cellular survival by preventing irreversibly malfolded proteins from being exported for use and stabilising the remaining protein production. This requires an up-regulation of molecular chaperones including Grp78. If adverse micro environmental conditions are severe or prolonged in normal cells, the UPR can initiate apoptosis. The tumour environment has been shown to be a region of physiologic endoplasmic reticulum stress [16]. The UPR is poorly characterised in cancer, however it could be a key mechanism in permitting tumour cell survival in an acidotic, hypoxic and glucose deprived environment and it has been shown to alter chemosensitivity to a variety of established anticancer agents [19, 20]. Grp78 has been found to be highly expressed in several cancer cell lines as well as tumour tissues and has been correlated with tumour growth and aggressiveness as well as resistance to chemotherapies [21, 22]. This is the first time that the distribution and *in situ* identification of Grp78 has been described using MALDI-MSI combined with ion mobility separation. In the work reported here, Grp78 was found to be mainly located in tumour regions using MALDI-IMS-MSI. The specificity and selectivity of the method applied allowed the targeting of a relatively low abundance protein biomarker directly in archived pancreatic tumour tissue sections.

The validation of Grp78 was achieved using immunohistochemistry staining which was found to be in good agreement with the obtained MALDI-IMS images.

Although MALDI-MSI is a technique that allows direct protein profiling and *in situ* identification within tissue sections, direct protein identification after *in situ* digestion of tissue sections can be challenging, as the biomolecules are contained in a complex mixture. The use of ion mobility separation, combined with MALDI-MS profiling and imaging, was found to be a valuable tool for direct protein identification after *in situ* digestion of FFPE tissue sections. IMS has been found to allow the separation of a range of ions based on their collision cross-sections, i.e. based on their structure and conformation. Here, IMS has been found to be a powerful tool as it allowed the separation of isobaric tryptic peptides with an acceptable limit of detection and mass accuracy. Coupling IMS and MALDI-MSI has also been found to improve the specificity and selectivity as well as facilitate database searches for protein identification.

The experimental strategy described here allowed the rapid screening of the distribution of peptides and their identification after *in situ* digestion of FFPE pancreatic tumour tissue sections using MALDI-IMS-MS profiling and imaging. The localisation of peptides arising from the same protein can be used to confirm protein identification but also to target other tryptic peptides of the same protein and hence increase the level of confidence in the identification and localisation of the given protein. However optimisation of the protocol is still required in order to achieve the identification of more protein tumour markers, including those which are involved in the UPR cascade, directly from tissue sections using direct MALDI-IMS-MS/MS profiling and imaging. Further work was directed to the improvement of the *in situ* identification and *in situ* quantification of protein markers involved in tumour growth, including the identification of existing post-translational modifications and/or other chemical modifications (section 5.3.2).

5.3.2 Antigen retrieval prior to *in situ* digestion of FFPE tissue sections yields proline modification

The use of antigen retrieval as sample pre-treatment prior to *in situ* digestion of FFPE tissue sections has been found to be beneficial for MALDI-MSI analysis of proteins directly within FFPE tissue sections as it allowed unlocking and enhancement of tryptic peptide signals (described in Chapter 3, section 3.3.2.3). However direct protein identification by MALDI-MS/MS from tissue sections remains challenging due to either overlapping signals, existing unidentified protein post-translational modifications and/or chemical protein modifications resulting from sample preparation. The use of IMS combined with direct MALDI-MS/MS analysis of FFPE tissue sections has been found to improve the selectivity of the method and hence improved the database searches for protein identification [7]. However several peptide signals remain unidentified, thus requiring the elucidation of existing protein modifications in order to improve protein identification. Several papers described the mechanism involved in AR, however there is a lack of information on the chemical protein modification induced by the AR protocol [23].

MALDI-MS/MS spectra were acquired directly from human FFPE breast tumour tissue sections. Figure 5.9 displays the MS/MS spectrum of the peptide signal at m/z 1286. Using *de novo* sequencing, a modification of the proline residue was noticed at a mass shift of M+16. This corresponded to addition of a hydroxyl group (OH) to proline amino acid, hence an oxidation (or hydroxylation) of proline residues.

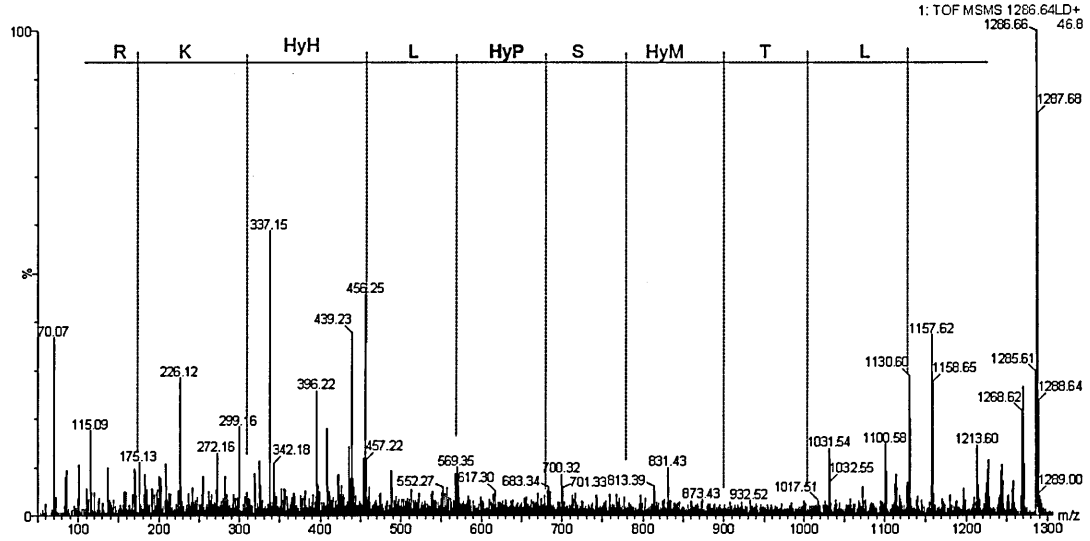

Figure 5.9: **MALDI-MS/MS spectrum of the peptide signal at m/z 1286 acquired directly from FFPE breast tumour tissue section.**
Oxidation of histidine, methionine as well as proline residues as is observed. The peptide was identified as arising from histone-lysine N-methyltransferase protein.

Proline hydroxylation is a common protein modification which occurs in mammalian cells as well as plants [24, 25]. Among the amino acids, proline and lysine are the most likely to be hydroxylated [24]. Hydroxyproline is derived either from the oxidation of proline by hydroxyl radical compounds [24–26] or following hydroxylation of proline by prolyl hydroxylases during collagen synthesis [27].

In the work reported here, the identification of proline hydroxylation shown in figure 5.9 may be explained by a chemical derivatisation occurring during the sample preparation. The method employed here described the use of AR prior to on-tissue enzymatic digestion with the aim of unlocking several protein signals. However, one of the steps of the AR protocol involves an incubation of the tissue section for 12 minutes at room temperature in a solution containing 3% hydrogen peroxide (H_2O_2). It has been reported that hydroxyl radicals can be formed in several ways including by reduction of H_2O_2 by metals ions contained in biological systems in aqueous solution. Hydroxyl radicals are very active compounds and several studies reported the ability of proline to quench hydroxyl radicals and form different compounds including hydroxyproline [24, 25]. Figure 5.10 displays the mechanisms of hydroxylation of proline [24]. Hence the oxidation

of proline amino acid residues observed in figure 5.9 may result from hydroxylation of proline during the incubation of the tissue section in hydrogen peroxide solution.

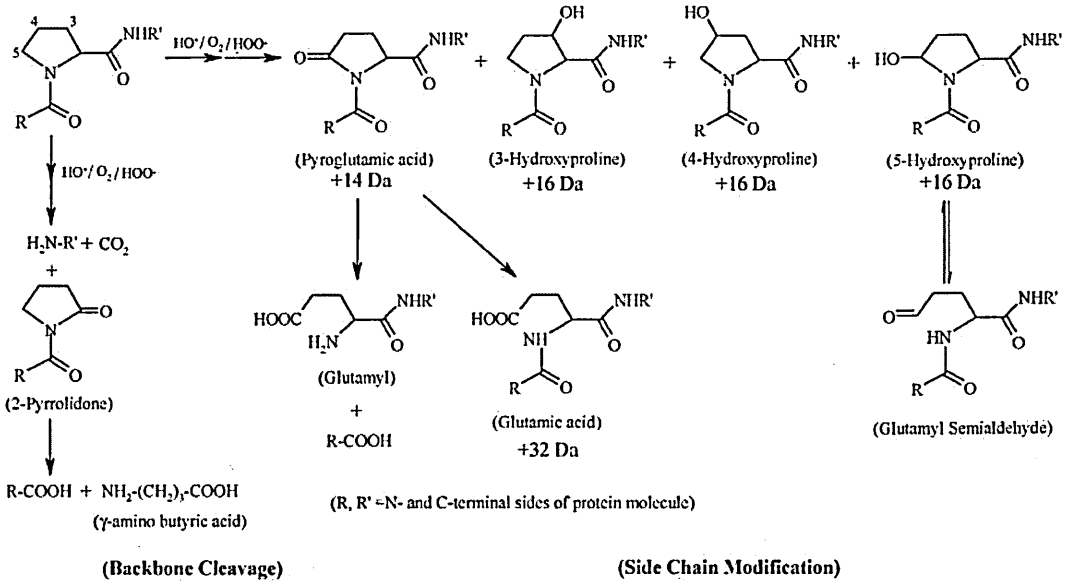

Figure 5.10: **Mechanism of proline oxidation with hydroxyl radicals** [24] (reproduced with permission from American Chemical Society publisher).
Following chemical or biochemical reactions of proline with hydroxyl radicals, hydroxyproline species can be obtained. This corresponds to an addition of +16 Da to the mass of proline residues. This modification does not lead to a cleavage of the amino acid chain backbone and hence can be observed after tryptic digestion followed by tandem mass spectrometric analysis.

Adding proline oxidation as a variable modification to the MASCOT search criteria allowed the identification of numerous proteins. 61 MALDI-MS/MS spectra were acquired directly from FFPE breast tumour tissue sections using an automatic data acquisition. When performing a MASCOT search without taking into account proline oxidation as a variable modification, only 11 peptides were identified. In contrast, 33 peptide signals were identified when adding proline oxidation as a variable modification to the MASCOT search criteria. Table 5.3 displays a list of the peptide signals identified directly from FFPE breast tumour tissue sections. It can be noticed that several peptides were identified as arising from collagen species. Hydroxyproline is the principal amino acid found in collagen proteins resulting from the hydroxylation of proline by prolyl hydroxylase enzyme during collagen synthesis. Figure 5.11 displays a MS/MS spectrum of the peptide signal at m/z 1303 which has been identified as a collagen species. It can be noticed that 3 proline residues were hydroxylated.

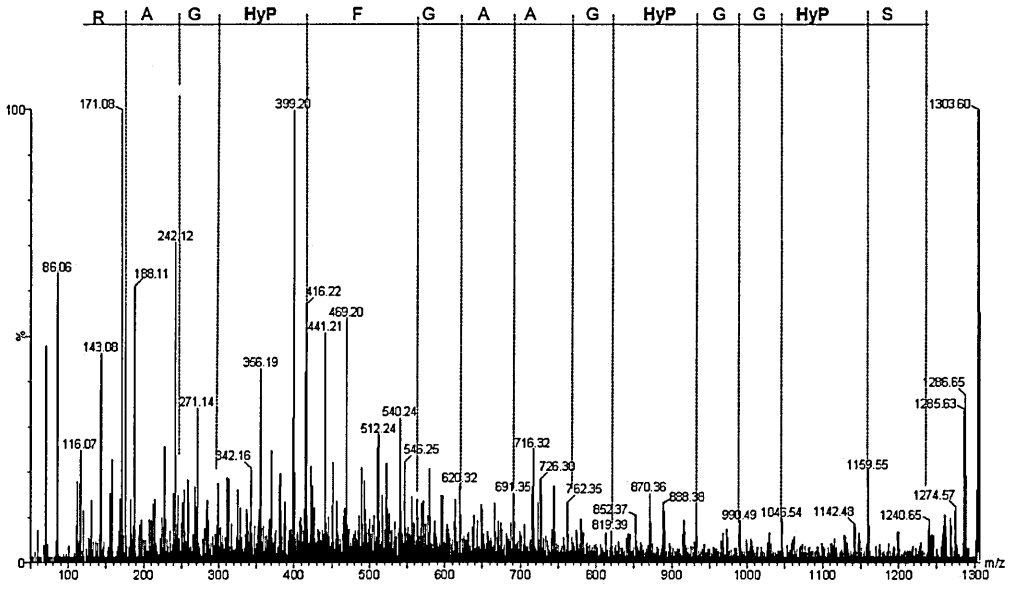

Figure 5.11: **MALDI-MS/MS spectrum of the peptide signal at m/z 1303 acquired directly from FFPE breast tumour tissue section.**
The peptide was identified as arising from Collagen alpha-1(III) chain.

Several peptide signals arising from collagen species can be noticed in table 5.3. Collagen is one of the most abundant proteins present in connective and muscle tissues. Using proline oxidation as a variable modification for MASCOT protein database searches may result in the selection of numerous collagen tryptic peptides which can be removed from the peptide mass list in order to perform the identification of other proteins present in lower abundance than collagen proteins.

In the work reported here, proline oxidations observed in tryptic peptide fragments other than those arising from collagen proteins, may derive from the hydroxylation of proline when incubating the tissue section in hydrogen peroxide solution. The Uniprot database showed that only the phosporylation of serine and threonine residues are listed as possible post-translational modifications which may occur to histone-lysine N-methyltransferase. Hence, the presence of hydroxyproline observed in the amino acid sequence (see table 5.3) derives from a chemical modification occurring during incubation in hydrogen peroxidase solution prior to the AR sample preparation.

Table 5.3: **List of tryptic peptides identified after *in situ* digestion of FFPE breast tumour tissue sections using direct MALDI-IMS-MS/MS.**

Protein name/ Accession number	Mass (Da)	Observed peptide m/z	Mass error (ppm)	Sequence	MS/MS ion score	location and function
Actin, cytoplasmic 1/ P60709	41710	976.43	-13.5	AGFAGDDAPR	21	Cytoplasm, cell mobility
		1198.69	-9.60	AVFPSIVGRPR	12	
Collagen alpha-1(I)/ P02452	138827	836.43	-3.75	GPAGPQGPR	55	
		852.43	-0.76	GPPGPQGAR, Oxidation (P)	31	
		1105.57	-8.06	GVQGPPGPAGPR, Oxidation (P)	24	
		1546.79	-0.49	GETGPAGPAGPVGPVGAR	75	
		1585.76	-4.98	GANGAPGIAGAPGFPGAR, 3 Oxidation (P)	34	
		1775.87	2.81	GARGEPGPTGLPGPPGER, Acetyl (N-term); 2 Oxidation (P)	11	Extra cellular matrix, secreted Fibril organisation, blood vessel development
Collagen alpha-2(I)/ P08123	129209	868.45	-18.3	VGAPGPAGAR, Oxidation (P)	14	
		960.45	-11.7	AGVMGPPGSR, Oxidation (M); Oxidation (P)	16	
		1562.79	-1.9	GETGPSGPVGPAGAVGPR	26	
		1580.73	-19.9	GPPGESGAAGPTGPIGSR, Oxidation (P)	79	
		1751.80	-16.2	GPPGAVGSPGVNGAPGEAGR, 3 Oxidation (P)	50	
		1775.87	-3.52	RGPNGEAGSAGPPGPPGLR, 2 Oxidation (P)	39	
		1833.89	3.97	RGPNGEAGSAGPPGPPGLR, Acetyl (N-term); 3 Oxidation (P)	28	

Continued on Next Page...

Table 5.3 – Continued

Protein name/ Accession number	Mass (Da)	Observed peptide m/z	Mass error (ppm)	Sequence	MS/MS ion score	location and function
Collagen alpha-1(III)/ P02461	138479	836.43	-3.75	GAPGPQGPR	43	
		852.43	-0.76	GPPGPQGAR, Oxidation (P)	25	
		1094.58	-9.87	GPPGLAGAPGLR, 2 Oxidation (P)	37	
		1111.59	-4.6	GRPGLPGAAGAR, 2 Oxidation (P)	41	
		1154.56	-1.11	GLAGPPGMPGPR, Oxidation (M); 2 Oxidation (P)	33	
		1303.61	4.85	GSPGGPGAAGFPGAR, 3 Oxidation (P)	48	
		1320.66	-7.12	GPPGPAGANGAPGLR, 2 Oxidation (P)	18	
		1508.72	9.67	GESGPAGPAGAPGPAGSR, Oxidation (P)	20	
		1702.79	2.81	GEMGPAGIPGAPGLMGAR, 2 Oxidation (M); 2 Oxidation (P)	13	
		1833.89	-9.76	GPPGPQGLPGLAGTAGEPGR, 3 Oxidation (P)	12	
		2104.07	-3.70	GSPGAQGPPGAPGPLGIAGITGAR, 3 Oxidation (P)	25	
Collagen alpha-1(X)/ Q03692	66117	1466.67	-9.59	GLNGPTGPPGPPGPR, 6 Oxidation (P)	21	
Heat-shock protein beta-1/ P04792	22768	987.61	-1.22	RVPFSLLR	26	Cytoplasm, nucleus, Involved in stress resistance
		1163.61	-7.54	LFDQAFGLPR	31	
Histone H2A.Z/ P0C0S5	13545	944.53	-5.55	AGLQFPVGR	41	Nucleus, Gene regulation

Continued on Next Page...

Table 5.3 – Continued

Protein name/ Accession number	Mass (Da)	Observed peptide m/z	Mass error (ppm)	Sequence	MS/MS ion score	location and function
Histone-lysine N-methyltransferase/ O14686	563831	1095.55	0.21	GGAHGGRGRGR, Acetyl (N-term); Oxidation (HW)	14	Nucleus, Acts as a coactivator for estrogen receptor, activates transcription
		1286.64	-6.24	NLTMSPLHKR, Acetyl (N-term); Oxidation (HW); Oxidation (M); Oxidation (P)	23	
Keratin, type II cytoskeletal 7/ P08729	51386	1406.68	-18.8	SIHFSSPVFTSR, Acetyl (N-term)	40	Cytoplasm, structural molecule
Obscurin-like protein 1/ O75147	152786	1111.59	5.44	NGAVVTPGPQR, Oxidation (P)	33	muscle development

5.3.3 IMS-Tag MALDI-MS imaging of biomarkers and metastasis-associated protein markers in human FFPE breast adenocarcinoma tissue sections

Metastasis is a complex molecular process which occurs often in cancers. It involves a multistep molecular mechanism in which tumour cells escape from the primary tumour site to other distant organs, hence creating new neoplasm environments [28]. Metastatic lymph nodes result also from sequenced steps which involve breaching of the basement membrane by tumour cells, infiltration into the extracellular matrix, invasion into the lymphatic vessels, transport to local lymph node, adherence and proliferation of tumour cells [28, 29]. Tumour growth and progression results also from defects in apoptotic pathways during cell cycles. Protein markers of tumour progression and metastasis formation are required in order to improve therapies and hence target appropriate genes and/or proteins. In this section, FFPE early stage (ES) and metastatic lymph node (MLN) breast tumour tissue sections were analysed using IMS-Tag MALDI-MS imaging in order to perform a comparison study and highlight possible protein markers that can be used as indicators of tumour progression and metastasis-associated proteins.

5.3.3.1 *In situ* identification of protein tumour markers within human FFPE early stage breast cancer tissue sections using IMS-Tag MALDI-MS imaging

Figures 5.12 displays a mass spectrum acquired directly from FFPE early stage breast tumour tissue sections after antigen retrieval and on-tissue digestion using MALDI-IMS-MS. Numerous peptide signals were detected. Ion signals corresponding to tryptic autolysis peptides as well as collagen protein tryptic peptide signals were removed from the mass list prior to a PMF search. However no significant results for protein identification were obtained when performing a PMF MASCOT search.

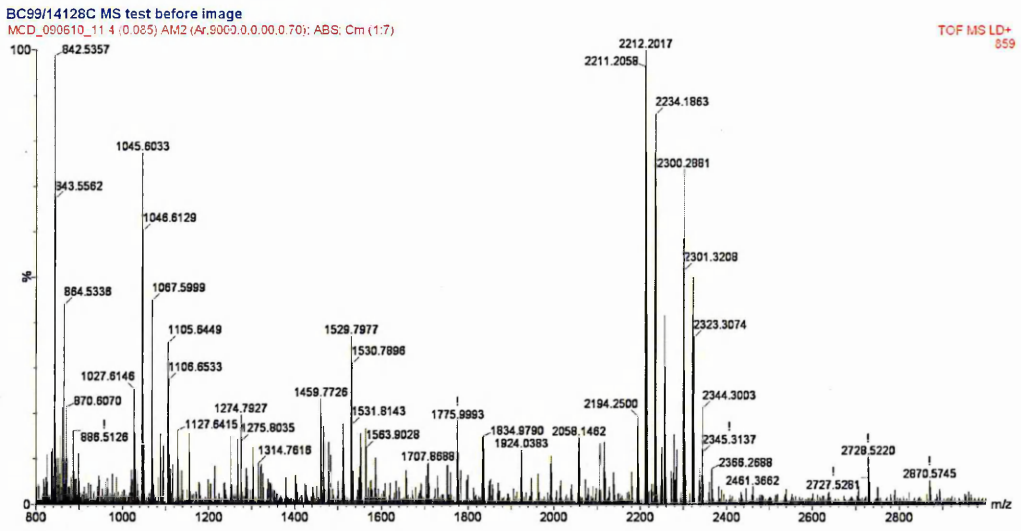

Figure 5.12: **MALDI-IMS-MS peptide profile acquired directly from a FFPE early stage breast tumour tissue section.**
Numerous signals are detected. Among them, several peptides arising from trypsin autolysis and collagen species were observed.

Table 5.4 shows a complete list of identified proteins from MALDI-MS/MS analyses followed by a protein database search, which were grouped into biological processes using the PANTHER (Protein ANalysis THrough Evolutionary Relationships) classification system. PANTHER is a freely available software which aims to correlate protein sequence evolution to molecular functions and biological processes [30, 31]. The use of PANTHER software has been reported to achieve more robust classification of proteins into molecular functions, biological processes and pathways [32]. Table 5.4 displays a classification of identified proteins in FFPE early stage breast cancer tissue sections into biological process using PANTHER.

Table 5.4: **List of proteins identified after *in situ* digestion of FFPE breast tumour tissue sections using direct MALDI-IMS-MS/MS.** Proteins were grouped into biological processes using the PANTHER classification system.

Biological Process	Protein name/ Accession number	Mass (Da)	Observed peptide m/z	Sequence	MS/MS ion score	Molecular function/ Pathways
Apoptosis	**RelA-associated inhibitor/ Q8WUF5**	89036	1067.52	RSDAGSYRR	16	Select regulatory molecule
Blood circulation and gas exchange	**Haemoglobin alpha/ P69905**	15085	1087.6	MFLSFPTTK, Oxidation (M)	26	
			1529.7	VGAHAGEYGAEALER	115	Other transfer/carrier protein
	Haemoglobin beta/ P68871	15866.8	1274.7	LLVVYPWTQR	27	
Cation transport	**Na^+/K^+-ATPase alpha 3 subunit variant/ Q53ES0**	111779	1002.5	RDLDDLKK	*de novo*	Ion channel, Cation transporter
Cytoskeletal protein	**Actin, cytoplasmic 1/ P60709**	41710	976.43	AGFAGDDAPR	21	cell mobility, Actin and actin related protein
			1198.69	AVFPSIVGRPR	12	
			2215.1	DLYANTVLSGGTTMYPGIADR	83	
Cell adhesion	**Collagen alpha-1(I)/ P02452**	138827	836.43	GPAGPQGPR	55	
			852.43	GPPGPQGAR, Oxidation (P)	31	
			1105.57	GVQGPPGPAGPR, Oxidation (P)	24	
			1546.79	GETGPAGPAGPVGPVGAR	75	
			1585.76	GANGAPGIAGAPGFPGAR, 3 Oxidation (P)	34	
			1775.87	GARGEPGPTGLPGPPGER, Acetyl (N-term); 2 Oxidation (P)	11	
	Collagen alpha-2(I)/ P08123	129209	868.45	VGAPGPAGAR, Oxidation (P)	14	

Continued on Next Page...

Table 5.4 – Continued

Biological Process	Protein name/ Accession number	Mass (Da)	Observed peptide m/z	Sequence	MS/MS ion score	Molecular function/ Pathways
			960.45	AGVMGPPGSR, Oxidation (M); Oxidation (P)	16	
			1562.79	GETGPSGPVGPAGAVGPR	26	
			1580.73	GPPGESGAAGPTGPIGSR, Oxidation (P)	79	
			1751.80	GPPGAVGSPGVNGAPGEAGR, 3 Oxidation (P)	50	
			1775.87	RGPNGEAGSAGPPGPPGLR, 2 Oxidation (P)	39	
			1833.89	RGPNGEAGSAGPPGPPGLR, Acetyl (N-term); 3 Oxidation (P)	28	
	Collagen alpha-1(III)/ P02461	138479	836.43	GAPGPQGPR	43	
			852.43	GPPGPQGAR, Oxidation (P)	25	
			1094.58	GPPGLAGAPGLR, 2 Oxidation (P)	37	
			1111.59	GRPGLPGAAGAR, 2 Oxidation (P)	41	
			1154.56	GLAGPPGMPGPR, Oxidation (M); 2 Oxidation (P)	33	
			1303.61	GSPGGPGAAGFPGAR, 3 Oxidation (P)	48	
			1320.66	GPPGPAGANGAPGLR, 2 Oxidation (P)	18	
			1508.72	GESGPAGPAGAPGPAGSR, Oxidation (P)	20	
			1702.79	GEMGPAGIPGAPGLMGAR, 2 Oxidation (M); 2 Oxidation (P)	13	
			1833.89	GPPGPQGLPGLAGTAGEPGR, 3 Oxidation (P)	12	
			2104.07	GSPGAQGPPGAPGPLGIAGITGAR, 3 Oxidation (P)	25	
	Collagen alpha-1(X)/ Q03692	66117	1466.67	GLNGPTGPPGPPGPR, 6 Oxidation (P)	21	Extracellular matrix structural protein
	Lumican [Precursor])/ P51884	38405	1024.6	FNALQYLR	21	Receptor Extracellular matrix

Continued on Next Page...

Table 5.4 – Continued

Biological Process	Protein name/ Accession number	Mass (Da)	Observed peptide m/z	Sequence	MS/MS ion score	Molecular function/ Pathways
Cell cycle control	**Tumour protein 63/ Q9H3D4**	76736	1127.6	RCPNHELSR, Oxidation (HW)	15, *de novo*	Other transcription factor
	RelA-associated inhibitor/ Q8WUF5	89036	1067.52			Select regulatory molecule
Cell proliferation and differentiation	**Tumour protein 63/ Q9H3D4**	76736	1127.6			
	RelA-associated inhibitor/ Q8WUF5	89036	1067.52			
Chaperone Protein folding	**Heat-shock protein beta-1/ P04792**	22768	987.61	RVPFSLLR	26	
			1163.61	LFDQAFGLPR	31	Chaperones, p38 MAPK pathway, VEGF signaling pathway, Angiogenesis
Chromatin packaging and remodeling	**Histone H2A.Z/ P0C0S5**	13545	944.53	AGLQFPVGR	41	
	Histone H3-like/ Q6NXT2	15204	1032.6	YRPGTVALR	20	
	Histone H4/ P62805	11360	1325.74	DNIQGITKPAIR	39	Gene regulation, histone

Continued on Next Page...

Table 5.4 – Continued

Biological Process	Protein name/ Accession number	Mass (Da)	Observed peptide m/z	Sequence	MS/MS ion score	Molecular function/ Pathways
	Histone-lysine N-methyltransferase/ O14686	563831	1095.55	GGAHGGRGRGR, Acetyl (N-term); Oxidation (HW)	14	Acts as a coactivator for estrogen receptor, methyltransferase
			1286.64	NLTMSPLHKR, Acetyl (N-term); Oxidation (HW); Oxidation (M); Oxidation (P)	23	
Dehydrogenase	**2-oxoglutarate dehydrogenase E1 component-like/Q9ULD0**	114409	952.5	FMTILRR, Oxidation (M)	21	Dehydrogenase, Tricarboxylic acid pathway
Hydrolase	**Na^+/K^+-ATPase alpha 3 subunit variant/ Q53ES0**	111779	1002.5	RDLDDLKK		
Muscle development	**Obscurin-like protein 1/ O75147**	152786	1111.59	NGAVVTPGPQR, Oxidation (P)	33	Guanyl-nucleotide exchange factor
Protein biosynthesis, other metabolism	**28S ribosomal protein S18b/ Q9Y676**	29377	1105.6	NHKGGVPPQR, Oxidation (HW)	20	Ribosomal protein
Transport	**Albumin/ P02768**	69321	1311.73	HPDYSVVLLLR	57	Other transfer/carrier protein
	Haemoglobin alpha/ P69905	15085	1087.6			
	Haemoglobin beta/ P68871	15866.8	1274.7			
	Na^+/K^+-ATPase alpha 3 subunit variant/ Q53ES0	111779	1002.5			

In this study, the number of identified proteins remains low when compared to classical MS proteomic approaches such as 2D gel electrophoresis, LC-MS/MS and quantitative ESI-LC/MS/MS [32, 33]. However, based on the fact that a direct proteomic methodology is employed here, numerous peptides were attributed to proteins with no pre-extraction and purification.

Examination of the data reported in table 5.4 revealed that several protein classes were identified directly from FFPE ES breast cancer tissue sections, including proteins involved in metabolism, cell proliferation and stress response. Peptide signals arising from heat-shock protein beta1 (HSPB1 or Hsp27) were also observed. Hsp27 has been reported to be up-regulated in early stage breast cancer [34, 35].

5.3.3.2 Study of the distribution of tumour markers within human FFPE early stage breast cancer tissue sections using IMS-Tag MALDI-MS imaging

MALDI-IMS-MS images of the distribution of peptides within FFPE early stage breast cancer tissue sections were also generated in order to study the localisation of identified proteins within the tissue sections after *in situ* digestion. Figure 5.13 displays the localisation of actin, histone H2A, haemoglobin alpha and beta chain and Hsp27 within FFPE ES breast cancer tissue sections. Examination of these images shows that the distribution of actin, histone H2A and Hsp27 within the tissue sections allows discrimination between regions. Hsp27 has been reported to be over-expressed in early stage breast cancers as well as correlated with cell proliferation, actin polymerisation and chaperone processes. Hence the distribution of Hsp27 within ES breast cancer tissue sections obtained using MALDI-IMS-MSI may indicate the localisation of tumour regions.

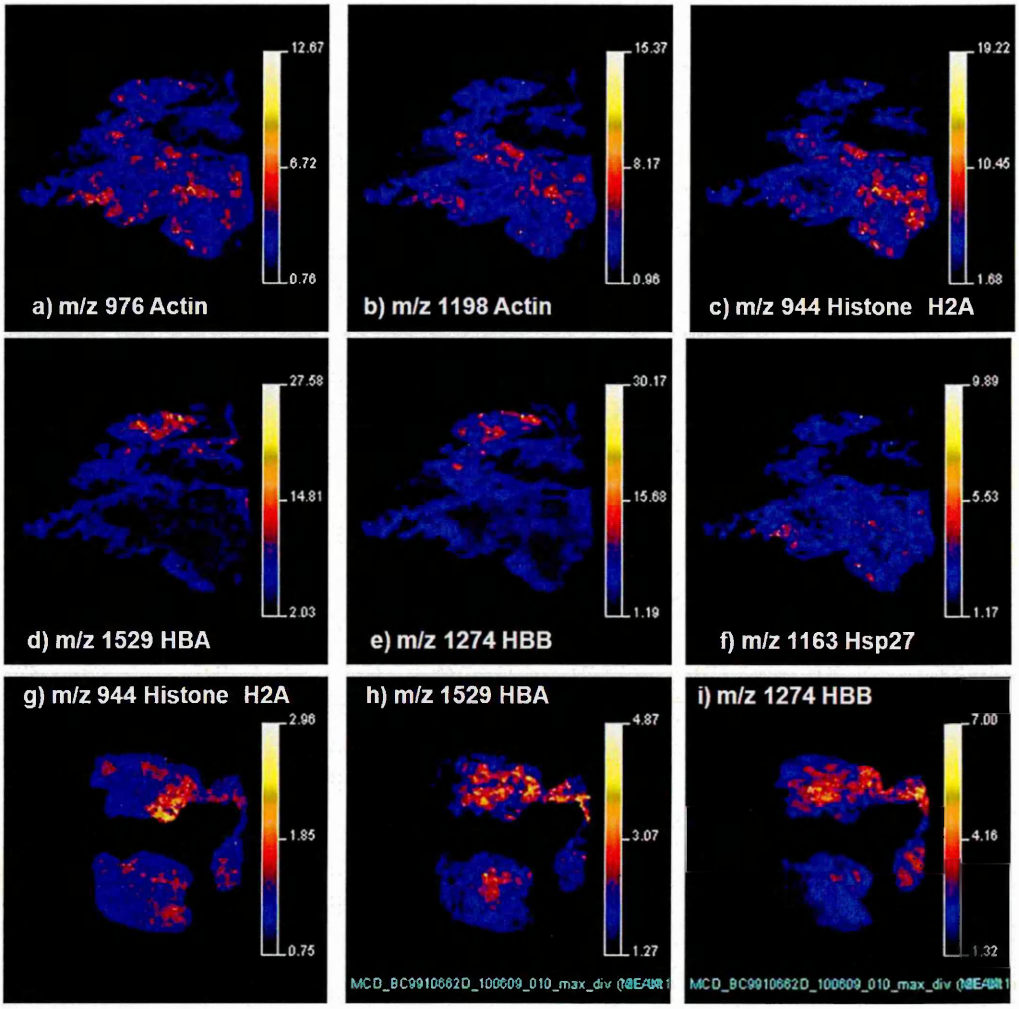

Figure 5.13: **MALDI-IMS-MS images of the distribution of proteins within FFPE early stage breast tumour tissue sections after *in situ* digestion.** The first two rows show images of the localisation of actin, histone H2A, haemoglobin alpha and beta chain and Hsp27 tryptic peptides within a FFPE early stage breast tumour tissue section. The third row displays the localisation of histone H2A, haemoglobin alpha and beta chain tryptic peptides within another FFPE early stage breast tumour tissue section. The distribution of Hsp27 may show the localisation of tumour regions within the tissue sections.

To verify this hypothesis, HE and immunohistochemistry staining were performed on consecutive breast tumour tissue sections. Figure 5.14 displays the obtained images. In both HE (figures 5.14a,b and c) and IHC (figures 5.14d, e and f) staining images, tumour regions were localised within the tissue sections. In figure 5.14a, b and c, tumour regions were found to be colocalised with the obtained spatial distribution of Hsp27 tryptic peptide at m/z 1163 by MALDI-MSI (figure 5.13f). The results obtained using MALDI-IMS-MSI analyses were found to be in good agreement with those obtained with histological staining. Here, the use of MALDI-IMS-MSI allowed the targeting of proteins present in tumour cells, and hence the localisation of tumour regions within tissue sections. In the work reported here, classifying proteins into molecular functions or biological processes contributed to the generation of images of the distribution of proteins which were found to play a key role in tumour cell progression, and hence to the localisation of tumour regions using IMS-Tag MALDI-MSI.

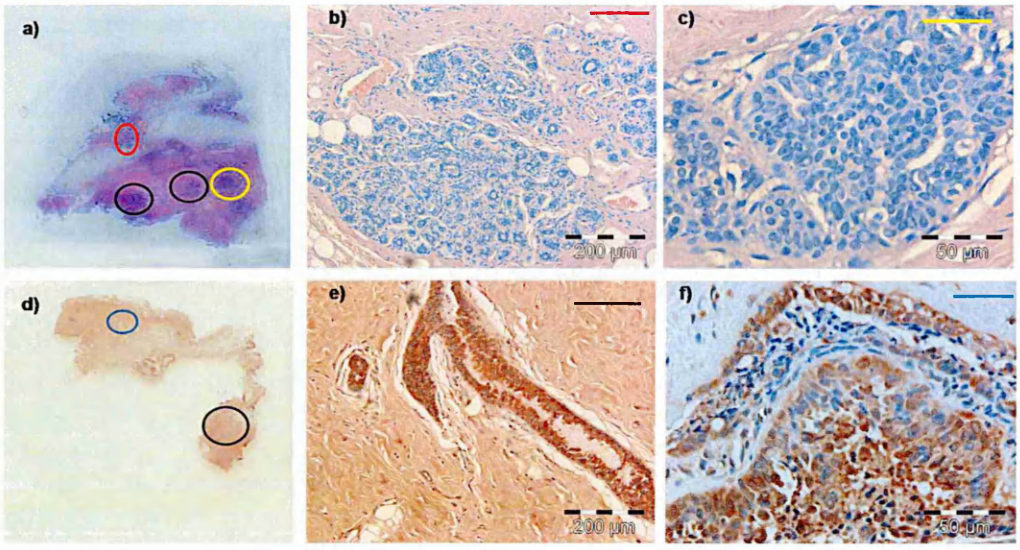

Figure 5.14: **HE and immunohistochemistry (IHC) staining pictures of FFPE early stage breast cancer tissue sections.**
(a) and (d) display digital scans of the tissue sections after HE and IHC Grp78 staining respectively. (b) and (c) show images of tumour cells within the tissue section after HE staining at magnifications of x10 and x40 respectively and were acquired from the region of the tissue section defined by the red and yellow circles in (a) respectively. (e) and (f) show images of tumour cells within the tissue section after IHC Grp78 staining at magnifications of x10 and x40 respectively and were acquired from the region of the tissue section defined by the black and blue circles in (d) respectively.

Several studies have reported a significant correlation of Grp78 expression with tumour stage and behaviour [13, 36]. Grp78 has been found to be associated with local tumour growth in early stage adenocarcinoma [36] and can be used as a prediction factor of responsiveness to chemotherapy in breast cancers [19]. In the work reported here, a spot of in-solution digested Grp78 recombinant protein was imaged alongside the tumour tissue sections. Figure 5.15 displays the distribution of peptide signals at m/z 1887 and 1934, which were identified as Grp78 tryptic peptides (section 5.3.1.2), within FFPE ES breast tumour tissue sections. These peptides were found to be localised within the tumour areas of the tissue sections identified by HE staining (figure 5.14a). Additionally, the positive control of in-solution digested Grp78 recombinant protein spot was also highlighted in the MALDI-MS images. Hence the distribution of the peptide ions at m/z 1887 and 1934 may correspond to the localisation of Grp78 within the tumour tissue section. However, MALDI-MS/MS analysis and/or Grp78 immunohistochemical staining are required to validate the results.

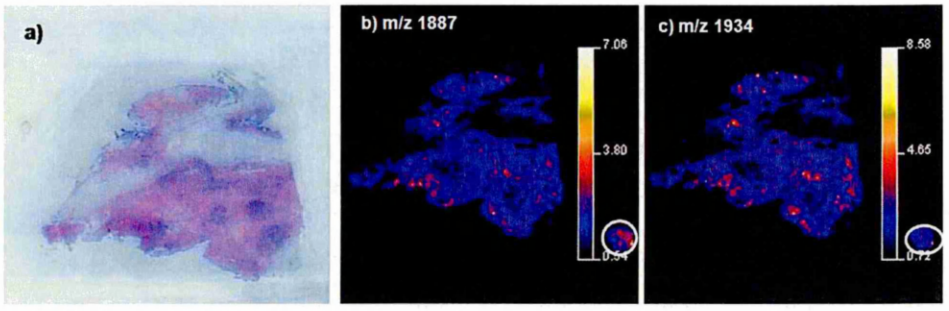

Figure 5.15: **MALDI-IMS-MS images of the distribution of the peptide signals at m/z 1887 and 1934 within FFPE early stage breast cancer tissue sections, along with a scan of the tissue section after HE staining.**
(a) displays a digital scan of the tissue section after HE staining. (b) and (c) display the distribution of the peptide signals at m/z 1887 and 1934 respectively within a FFPE early stage breast cancer tissue section. A spot of in-solution digested Grp78 recombinant protein was imaged alongside the tissue section. The distribution of these peptides may correspond to the localisation of Grp78 within the tissue section.

5.3.3.3 *In situ* identification of breast tumour metastasis-associated proteins within FFPE metastatic lymph node breast cancer tissue sections

MALDI-mass spectra were acquired directly from FFPE breast cancer metastatic lymph node tissue sections. The obtained mass spectra were subjected to a PMF search using MASCOT. The peptide mass tolerance was set at 80 ppm. Prior to the PMF search, ion signals corresponding to matrix adducts, tryptic autolysis peptides and collagen-derived peptides were removed from the mass list. Only proteins with a significant MASCOT score, i.e. with a score greater than 56, were selected. Thus, interleukin-1 receptor type I and zinc finger protein 616 were identified with PMF MASCOT scores of 66 and 56 respectively. Figure 5.16 displays the obtained results. However the identification of zinc finger protein 616 by PMF was not confirmed since the obtained MASCOT score was not higher than 56. Direct MALDI-IMS-MS/MS analysis was also performed on FFPE breast cancer metastatic lymph node tissue sections. Numerous peptide signals were identified as arising from collagen species but also other proteins were identified, including Hsp27 as well as tumour necrosis factor receptor. Table 5.5 displays a list of proteins identified in addition to those shown in table 5.4.

Protein name/ Accession number	Mass (Da)	Observed peptide m/z	Mass error (ppm)	Sequence	MOWSE Score	Sub-location and Function
Tumor necrosis factor receptor superfamily member 10A/ O00220	50029	1105.63	23	AGRAPGPRPAR	22	Membrane, receptor, apoptosis
Interleukin-1 receptor type I/ P14778	65361	32 peptides matched using a PMF search			66	Membrane, receptor, immunity response

Table 5.5: **List of additional tryptic peptides identified after *in situ* digestion of FFPE breast cancer metastatic lymph node tissue sections using direct MALDI-IMS-MS/MS.**
All database searches for protein identification were performed using Swissprot human database.

Mascot Search Results

User : marie
Email : marie-claude.djidja@student.shu.ac.uk
Search title :
Database : SwissProt 56.6 (405506 sequences; 146166984 residues)
Taxonomy : Homo sapiens (human) (20413 sequences)
Timestamp : 9 Jan 2009 at 08:44:12 GMT
Top Score : 66 for IL1R1_HUMAN, Interleukin-1 receptor type I OS=Homo sapiens GN=IL1R1 PE=1 SV=1

Probability Based Mowse Score

Protein score is -10*Log(P), where P is the probability that the observed match is a random event.
Protein scores greater than 56 are significant (p<0.05).

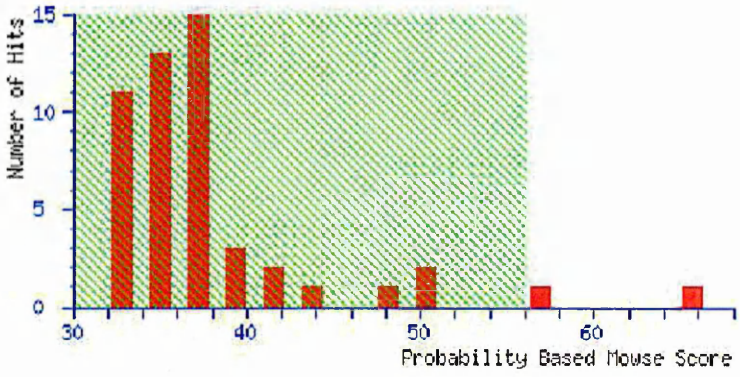

1.	IL1R1_HUMAN Mass: 65361 Score: 66 Expect: 0.0056 Queries matched: 32
	Interleukin-1 receptor type I OS=Homo sapiens GN=IL1R1 PE=1 SV=1

2.	ZN616_HUMAN Mass: 90205 Score: 56 Expect: 0.049 Queries matched: 55
	Zinc finger protein 616 OS=Homo sapiens GN=ZNF616 PE=2 SV=1

Figure 5.16: **Peptide mass fingerprint MASCOT search results obtained from MALDI mass spectra of FFPE breast cancer metastatic lymph node tissue section.**
Interleukin-1 receptor type I and zinc finger protein 616 were identified with the PMF MASCOT search. The identification of zinc finger protein 616 was not confirmed as the obtained MASCOT score was not higher than 56.

5.3.3.4 Principal component analysis-discriminant analysis of FFPE breast cancer metastatic lymph node tissue sections

Using BioMap 3.7.5.5 software, a rapid screening of the results obtained from imaging analysis allowed the visualisation of 3 distinct regions within the FFPE breast tumour MLN tissue section. In order to confirm these observations, principal component analysis-discriminant analysis (PCA-DA) was performed. Figure 5.17a displays the distribution of the peptide ion signal at m/z 1325 as a MALDI-MS image which allows the visualisation of the 3 regions defined as 1, 2 and 3. Peptide profiles were then exported from MALDI-MSI data for PCA-DA.

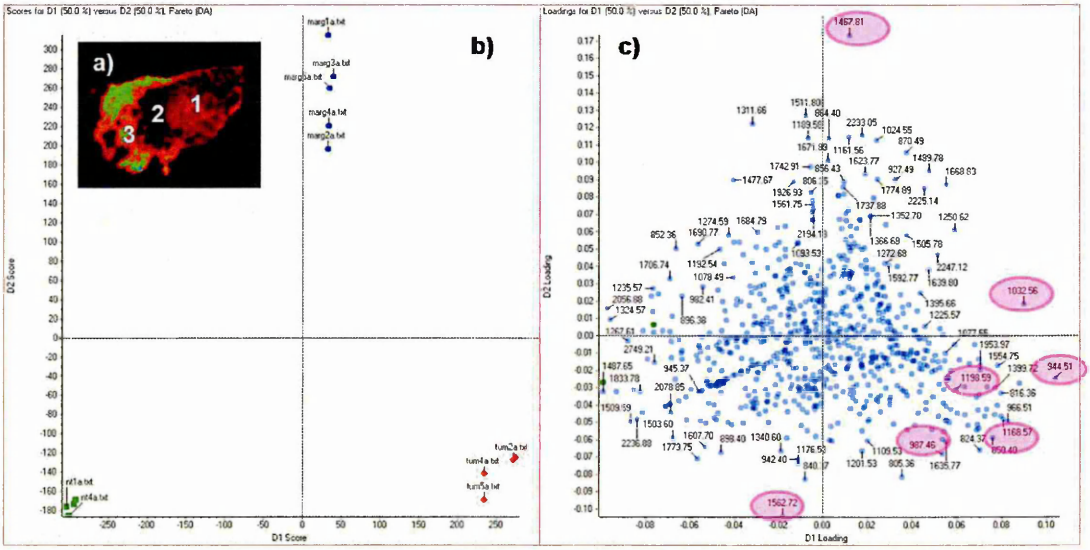

Figure 5.17: **PCA-DA of peptide profiles exported from MALDI-IMS-MS images of FFPE metastatic lymph node breast cancer tissue section.**
(a) MALDI-IMS-MS image of the peptide ion signal at m/z 1325 showing 3 distinct regions defined as 1, 2 and 3. (b) The scores plots show discrimination between regions within the tissue section. (c) The loadings plots highlighted characteristic masses including peptide signals at 944, 987 and 1198 corresponding to histone H2A, Hsp27 and actin respectively, which were found to be predominantly present in the tumour region.

The method employed for PCA-DA was the same as described in chapter 4 (section 4.3.4.1). Figure 5.17b displays the scores plots obtained, where 3 groups within the tissue section were distinguished: the groups were defined by the red, blue and green spots. The red spots corresponded to spectra obtained from the right central region of the tissue section (region 1), the green spots resulted from profiles from the outer area of the tissue section (region 3) and the blue spots represented spectra obtained from the margin (region 2).

In the loadings plots (figure 5.17c), several peptide signals were found to be characteristic masses of each distinct region. Peptide ions at m/z 944, 987 and 1198, corresponding to histone H2A, Hsp27 and actin respectively, were found to be associated with the central area of the tissue section (defined by the red spots in figure 5.17a). The results obtained from MALDI-MS images of FFPE early stage breast cancer tissue sections demonstrated that histone H2A and Hsp27 were mainly found in tumour regions (section 5.3.3.2). Here, the results obtained with PCA-DA allowed the localisation of tumour regions within MLN breast cancer tissue sections.

Regions corresponding to a margin (blue spots in figure 5.17a) and surrounding area (green spots in figure 5.17a) within the tissue section were also distinguished by PCA-DA. It can also be noticed that peptide profiles resulting from the surrounding area were found to be data rich with collagen tryptic peptides. The peptide signals at m/z 1562 and 1833 were identified as collagen alpha-2(I) and collagen alpha-1(III) tryptic peptides respectively. The signal at m/z 1467, which was not identified, however was mainly found to be localised in the margin. PCA-DA allowed discrimination between regions within the tissue section, and also the identification of characteristic masses for each distinct regions.

5.3.3.5 Study of the distribution of tumour markers within FFPE breast cancer metastatic lymph node tissue sections

To confirm the results obtained with PCA-DA, MALDI-IMS-MS images of the distribution of peptide localisation within FFPE MLN breast tumour tissue sections were also generated. Figure 5.18 displays the localisation of peptides from several proteins within the tissue section. Examination of the obtained images allowed the identification of 3 regions present in the tissue section. The right central area of the tissue section was found to be data rich in several peptides arising from proteins which were found to be associated with tumour regions, such as histone H2A, actin, Hsp27 and Grp78 (figures 5.18b, c and f-i). These results were found to be in good agreement with those obtained with PCA-DA. This indicated the presence of tumour cells within this area of the MLN tissue section. In contrast, some peptides were found to be mainly localised in the margin and surrounding area, including signals at m/z 1467 and 1481 (figures 5.18k and l).

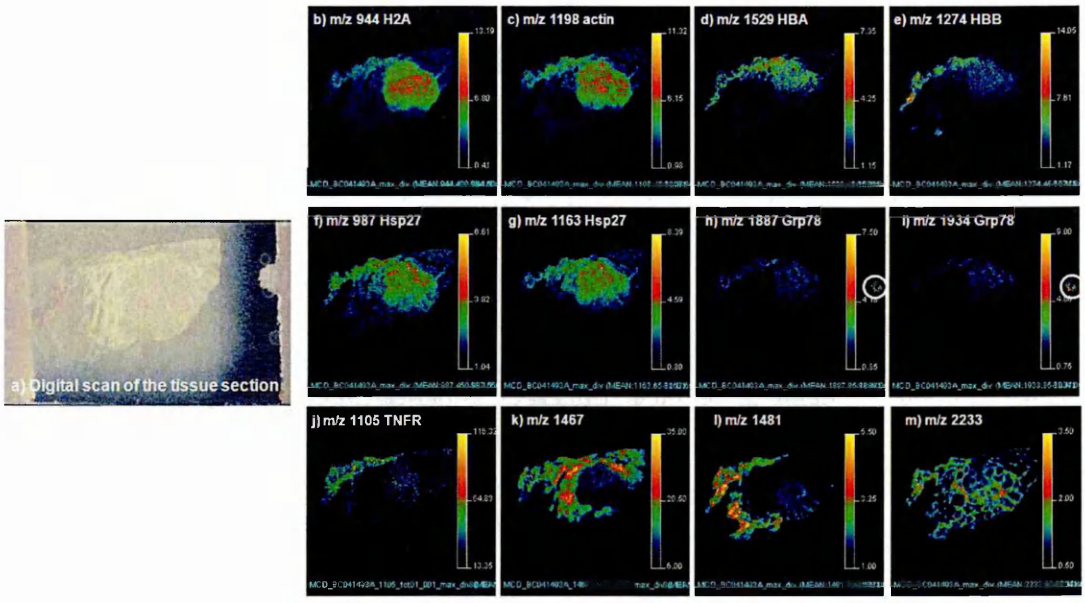

Figure 5.18: **MALDI-IMS-MS and digital images of the distribution of peptides after *in situ* digestion of FFPE breast cancer metastatic lymph node tissue sections.**
(a) Digital scan of the tissue section obtained prior to MALDI-IMS-MSI analysis.
(b-m) Distribution of peptides within the tissue section. Peptides were identified as arising from (b) histone H2A, (c) actin, (d-e) haemoglobin alpha and beta chain respectively, (f-g) Hsp27, (h-i) Grp78, (j) tumour necrosis factor receptor. (k-m) Distribution of peptide signals at m/z 1467, 1481 and 2233 respectively, which were not identified.

5.3.3.6 Discussion

Breast cancer is the second most common cancer in the world and one of the major causes of female mortality [33]. Advances in breast cancer research have led to the detection and identification of proliferation factors, oncogenes and tumour suppressor genes which are involved in tumour progression [33]. Currently, patients suffering from breast cancer are usually tested for the expression of oestrogen and progesterone receptors, as well as human epidermal growth factor receptor 2 (Her2) protein. This has been found to help in decision making regarding diagnostics and prognostics as well as treatment. However breast cancer often presents resistance to chemotherapy [35, 37], which can be explained by defects or changes in regulation of proteins and/or genes involved in apotosis or that affect the level of intracellular drug targets [37, 38]. Hence, improving biomarker discovery for tumour progression and metastasis may enhance drug development.

In this section, the use of MALDI-IMS-MSI was described for targeting tumour protein markers as well as metastasis-associated proteins in FFPE ES and MLN breast cancer tissue sections. Using the specificity and selectivity of the methodology described here, several proteins were identified directly from tumour tissue sections after *in situ* digestion and further classified using the PANTHER classification system, into molecular functions and biological processes. The distribution of peptides within FFPE ES breast cancer tissue sections allowed the localisation of tumour regions and hence the targeting of proteins which may be associated with tumour growth, metabolism and cell proliferation. Among them Hsp27 was found to be mainly located in tumour regions of the tissue sections. This was found to be in good agreement with previous studies which reported an over-expression of Hsp27 in breast cancer cells and to be associated with tumour growth as well as resistance to chemotherapy [35, 37].

The identified proteins found to be localised in tumour regions of ES breast cancer tissue sections were also present in tumour cells in breast cancer MLN tissue sections. Proteins related to apoptosis and inflammatory response, including tumour necrosis factor receptor and interleukin 1 receptor were also identified. Some peptide signals were also found to be only detected in FFPE breast cancer MLN tissue sections. This demonstrated the presence of metastasis-associated proteins. However limitations were encountered when performing direct protein identification. Extensive *de novo* sequencing approaches are therefore required in order to identify existing protein modifications and hence achieve more protein identification directly from the tissue sections. In the work reported here, tumour protein markers were localised within FFPE early stage and metastatic lymph node breast cancer tissue sections using IMS-Tag MALDI-MSI.

5.4 Concluding Remarks

In this chapter, the use of MALDI-MSI technology as a biomarker discovery tool is described via both bottom-up and top-down proteomic approaches. Here, adenocarcinoma tissue sections were investigated using MALDI-MS imaging methodology in order to identify and localise tumour biomarkers directly within the tissue sections. Successful identification of heat shock proteins, including Grp78 and Hsp27, directly within adenocarcinoma tissue sections was achieved. Even more interestingly, the study of their distribution across the tissue sections revealed that these proteins were mainly located and highly intense in tumour regions. These results were found to be in agreement with studies reported previously, where hsps were found to be highly expressed in tumour cells or tumour tissue sections [35, 37]. Furthermore Grp78 and Hsp27 are known as tumour biomarkers since they are correlated with tumour growth, progression and resistance to chemotherapy. In the work reported here, some proteins found to be located in tumour regions within early stage breast cancer tissue sections were also found to be present in tumour cells in metastatic lymph nodes using MALDI-MSI. This demonstrated the ability of the technique to identify tumour markers as well as potential metastasis-associated proteins with no requirement for pre-defined targets.

The use of *in situ* digestion and ion mobility separation with MALDI-MSI has been found to be beneficial for protein identification directly from tissue sections. However direct identification of proteins within tissue section by MALDI-IMS-MS/MS remains challenging. This may be due to existing post-translational modifications. In the work reported here, the identification of proline oxidation as a protein modification which occurs during the sample preparation facilitated the MASCOT search as well as *de novo* sequencing for protein identification. However, method improvement is still required in order to overcome remaining limitations associated with direct protein identification. Alternative methodologies have been reported. Methods including *in situ* chemical derivatisation [39] and/or the use of other enzymes such as Lys-N may enhance identification of proteins directly from tissue sections [40]. Additionally, high resolution mass spectrometry imaging technologies such as FT-ICR MS imaging can improve mass measurement accuracy for on-tissue MS/MS analysis for protein identification [6, 41].

In the work reported here, IMS-Tag MALDI-MSI analyses of FFPE adenocarcinoma tissue sections allowed the localisation of tumour regions within tissue sections. Even more interestingly, the distribution and identification of tumour biomarkers that are indicators of tumour growth, proliferation and metastasis-associated were obtained. This was found to be beneficial as it could help in biomarker discovery and also in tumour classification models. However to design tumour classification systems, a large number of samples are required as well as the combination of high-throughput analysis with statistical tools.

References

[1] Srinivas P. R., Verma M., Zhao Y., and Srivastava S. Proteomics for cancer biomarker discovery. *Clinical Chemistry*, 48:1160–1169, 2002.

[2] Rifai N., Gillette M.A., and Carr S.A. Protein biomarker discovery validation: the long uncertain path to clinical utility. *Nature Biotechnology*, 24:971–983, 2006.

[3] Srinivas P. R., Kramer B. S., and Srivastava S. Trends in biomarker research for cancer detection. *Lancet Oncology*, 2:698–704, 2001.

[4] Abd El-Rehim D.M., Ball G., Pinder S.E., Rakha E., Paish C., Robertson J.F., Macmillan D., Blamey R.W., and Ellis I.O. High-throughput protein expression analysis using tissue microarray technology of a large well-characterised series identifies biologically distinct classes of breast cancer confirming recent cDNA expression analyses. *International Journal of Cancer*, 116:340–350, 2005.

[5] Wisztorski M., Lemaire R., Stauber J., Menguelet S.A., Croix D., Math O.J., Day R., Salzet M., and Fournier I. New developments in MALDI imaging for pathology proteomic studies. *Current Pharmaceutical Design*, 13:3317–3324, 2007.

[6] Heeren R.M.A., Smith D.F., Stauber J., Kkrer-Kaletas B., and MacAleese L. Imaging Mass Spectrometry: Hype or Hope? *Journal of the American Society for Mass Spectrometry*, 20:1006–1014, 2009.

[7] Djidja M.C., Francese S., Loadman P.M., Sutton C.W., Scriven P., Claude E., Snel M.F., Franck J., Salzet M., and Clench M.R. Detergent addition to tryptic digests and ion mobility separation prior to MS/MS improves peptide yield and protein identification for *in situ* proteomic investigation of frozen and formalin-fixed paraffin-embedded adenocarcinoma tissue sections. *Proteomics*, 9:2750–2763, 2009.

[8] Xu H., Yang L., Wang W., Shi S., Liu C., Liu Y., Fang X., Taylor C.R., Lee C.S., and Balgley B.M. Antigen retrieval for proteomic characterization of formalin-fixed and paraffin-embedded tissues. *Journal of Proteome Research*, 7:1098–1108, 2008.

[9] Aerni H., Cornett D.S., and Caprioli R.M. Automated acoustic matrix deposition for MALDI sample preparation. *Analytical Chemistry*, 78:827–834, 2006.

[10] Pringle S.D., Giles K., Wildgoose J.L., Williams J.P., Slade S.E., Thalassinos K., Bateman R.H., Bowers M.T., and Scrivens J.H. An investigation of the mobility separation of some peptide and protein ions using a new hybrid quadrupole/travelling wave IMS/oa-ToF instrument. *International Journal of Mass Spectrometry*, 261:1–12, 2007.

[11] Riba-Garcia I., Giles K., Bateman R.H., and Gaskell S.J. Evidence for structural variants of a- and b-type peptide fragment ions using combined ion mobility/mass spectrometry. *Journal of the American Society for Mass Spectrometry*, 19:609–613, 2008.

[12] Neoptolemos J.P., Dunn J.A., Stocken D.D., Almond J., Link K., Beger H., Bassi C., Falconi M., Pederzoli P., Dervenis C., Fernandez-Cruz L., Lacaine F., Pap A., Spooner D., Kerr D.J., Friess H., and Buchler M.W. Adjuvant chemoradiotherapy and chemotherapy in resectable pancreatic cancer: a randomised controlled trial. *Lancet*, 358:1576–1585, 2001.

[13] Lee A.S. GRP78 induction in cancer: therapeutic and prognostic implications. *Cancer Research*, 6:3496–3499, 2007.

[14] Shnyder S.D., Mangum J.E., and Hubbard M.J. Triplex profiling of functionally distinct chaperones (ERp29/PDI/BiP) reveals marked heterogeneity of the endoplasmic reticulum proteome in cancer. *Journal of Proteome Research*, 7:3364–3372, 2008.

[15] Arap M.A., Lahdenranta J., Mintz P.J., Hajitou A., Sarkis A.S., Arap, W., and Pasqualini R. Cell surface expression of the stress response chaperone GRP78 enables tumor targeting by circulating ligands. *Cancer Cell*, 6:275–284, 2004.

[16] Scriven P., Brown N.J., Pockley A.G., and Wyld L. The unfolded protein response and cancer: a brighter future unfolding? *Journal of Molecular Medicine*, 85:331–341, 2007.

[17] Lee A.S. Mammalian stress response: induction of the glucose-regulated protein family. *Current Opinion in Cell Biology*, 4:267–273, 1992.

[18] Watowich S.S. and Morimoto R.I. Complex regulation of heat shock- and glucose-responsive genes in human cells. *Molecular and Cellular Biology*, 8:393–405, 1988.

[19] Lee E., Nichols P., Spicer D., Groshen S., Yu M.C., and Lee A.S. GRP78 as a novel predictor of responsiveness to chemotherapy in breast cancer. *Cancer Research*, 66: 7849–7853, 2006.

[20] Dong D., Ko B., Baumeister P., Swenson S., Costa F., Markland F., Stiles C., Patterson J.B., Bates S.E., and Lee A.S. Vascular targeting and antiangiogenesis agents induce drug resistance effector GRP78 within the tumor microenvironment. *Cancer Research*, 65:5785–5791, 2005.

[21] Langer R., Feith M., Siewert J.R., Wester H.J., and Hoefler H. Expression and clinical significance of glucose regulated proteins GRP78 (BiP) and GRP94 (GP96) in human adenocarcinomas of the esophagus. *BioMed Central*, 8:70–78, 2008.

[22] Shu C.W., Sun F.C., Cho J.H., Lin C.C., Liu P.F., Chen P.Y., Chang M.D., Fu H.W., and Lai Y.K. GRP78 and Raf-1 cooperatively confer resistance to endoplasmic reticulum stress-induced apoptosis. *Journal of Cellular Physiology*, 215: 627–635, 2008.

[23] Yamashita S. Heat-induced antigen retrieval:mechanisms and application to histochemistry. *Progress in Histochemistry and Cytochemistry*, 41:141–200, 2007.

[24] Xu G. and Chance M.R. Hydroxyl radical-mediated modification of proteins as probes for structural proteomics. *Chemical Reviews*, 107:3514–3543, 2007.

[25] Matysik J., Alia, Bhalu B., and Mohanty P. Molecular mechanisms of quenching of reactive oxygen species by proline under stress in plants. *Current Science*, 82: 525–532, 2002.

[26] Kurahashi T., Miyazaki A., Suwan S., and Isobe M. Extensive investigations on oxidized amino acid residues in H_2O_2-treated Cu,Zn-SOD protein with LC-ESI-Q-TOF-MS, MS/MS for the determination of the copper-binding site. *Journal of the American Chemical Society*, 123:9268–9278, 2001.

[27] Manning J.M. and Meister A. Conversion of proline to collagen hydroxyproline. *Biochemistry*, 5:1154–1165, 1966.

[28] Fidler I.J. The pathogenesis of cancer metastasis: the *seed and soil* hypothesis revisited. *Nature Reviews Cancer*, 3:453–458, 2003.

[29] Kanazawa N., Oda T., Gunji N., Nozue M., Kawamoto T., Todoroki T., and Fukao K. E-cadherin expression in the primary tumors and metastatic lymph nodes of poorly differentiated types of rectal cancer. *Surgery Today*, 32:123–128, 2002.

[30] Thomas P.D., Campbell M.J., Kejariwal A., Mi H., Karlak B., Daverman R., Diemer K., Muruganujan A., and Narechania A. PANTHER: a library of protein families and subfamilies indexed by function. *Genome Research*, 13:2129–2141, 2003.

[31] Mi H., Guo N., Kejariwal A., and Thomas P.D. PANTHER version 6: protein sequence and function evolution data with expanded representation of biological pathways. *Nucleic Acids Research*, 35:D247–D252, 2007.

[32] Ho J., Kong J.W., Choong L.Y., Loh M.C., Toy W., Chong P.K., Wong C.H., Wong C.Y., Shah N., and Lim Y.P. Novel breast cancer metastasis-associated proteins. *Journal of Proteome Research*, 8:583–594, 2009.

[33] Ou K., Yu K., Kesuma D., Hooi M., Huang N., Chen W., Lee S.Y., Goh X.P., Tan L.K., Liu J., Soon S.Y., Bin Abdul Rashid S., Putti T.C., Jikuya H., Ichikawa T., Nishimura O., Salto-Tellez M., and Tan P. Novel breast cancer biomarkers identified by integrative proteomic and gene expression mapping. *Journal of Proteome Research*, 7:1518–1528, 2008.

[34] Laguens G.E., Coronato S., Spinelli O., Laguens R.P., and Di Girolamo W. Can breast cancer Hsp 27 (Heat Shock Protein 27000) expression influence axillary lymph node status? *The Breast*, 10:179–181, 2000.

[35] Kang S.H., Kang K.W., Kim K.H., Kwon B., Kim S.K., Lee H.Y., Kong S.Y., Lee E.S., Jang S.G., and Yoo B.C. Upregulated HSP27 in human breast cancer cells reduces Herceptin susceptibility by increasing Her2 protein stability. *BioMed Central Cancer*, 8:286–295, 2008.

[36] Wang Q., He Z., Zhang J., Wang Y., Wang T., Tong S., Wang L., Wang S., and Chen Y. Overexpression of endoplasmic reticulum molecular chaperone GRp94 and GRp78 in human lung cancer tissues and its significance. *Cancer Prevention and Detection*, 29:544–551, 2005.

[37] Hansen R.K., Parra I., Lemieux P., Oesterreich S., Hilsenbeck S.G., and Fuqua S.A. Hsp27 overexpression inhibits doxorubicin-induced apoptosis in human breast cancer cells. *Breast Cancer Research and Treatment*, 56:187–196, 1999.

[38] Arrigo A.P., Simon S., Gibert B., Kretz-Remy C., Nivon M., Czekalla A., Guillet D., Moulin M., Diaz-Latoud C., and Vicart P. Hsp27 (HspB1) and alphaB-crystallin (HspB5) as therapeutic targets. *FEBS Letters*, 581:3665–3674, 2007.

[39] Edirisinghe P.D., Moore J.F., Skinner-Nemec K.A., Lindberg C., Giometti C.S., Veryovkin I.V., Hunt J.E., Pellin M.J., and Hanley L. Detection of *in situ* derivatized peptides in microbial biofilms by laser desorption 7.87 ev postionizaton mass spectrometry. *Analytical Chemistry*, 79:508–514, 2007.

[40] Taouatas N., Drugan M.M., Heck A.J., and Mohammed S. Straightforward ladder sequencing of peptides using a lys-N metalloendopeptidase. *Nature Methods*, 5: 405–407, 2008.

[41] Taban I.M., Altelaar A.F., van der Burgt Y.E., McDonnell L.A., Heeren R.M., Fuchser J., and Baykut G. Imaging of peptides in the rat brain using MALDI-FTICR mass spectrometry. *Journal of the American Society for Mass Spectrometry*, 18:145–151, 2007.

CHAPTER 6

Novel Molecular Tumour Classification using MALDI-Mass Spectrometry Imaging of Tissue Micro Arrays

6.1 Introduction

Cancer classification is usually based on the morphological and histopathological appearances of the tumour. Commonly, cancers are graded on the tumour node metastasis (TNM) approach with the variables being tumour size, presence or absence of tumour cells in dependent lymph nodes and the presence or absence of distant metastatic tumour deposits [1, 2]. However, tumours with the same histopathological and morphological features can pursue very different clinical courses: the response to chemotherapy may be attenuated or a theoretically curative resection can be complicated by early recurrence [3]. In order to improve the ability of clinicians to make more accurate patient-tailored prognoses novel tumour classification models are required. Such classifications will most likely be based on molecular information, i.e. genomic and proteomic data that provide insights into tumour progression, aggressiveness and resistance to therapy. In order to assess biological and clinical differences between tumour samples, a high-throughput analysis of heterogeneity within tumour tissue samples is required.

The introduction of tissue micro array (TMA) technologies has facilitated high-throughput analysis of a large number of archived samples for clinical applications as well as biomarker validation. It allows simultaneous analysis of a large number of specimens in a single experiment [4, 5]. TMAs consist of paraffin blocks of up to a thousand individual biopsy cores arranged in arrays and allowing multiple analyses. Several studies have described the use of TMA sections for high-throughput clinical and molecular analysis of tumour samples, leading to biomarker validation [6, 7]. The ability to identify and study the distribution of biomarkers directly from a large number of formalin fixed paraffin embedded (FFPE) tumour samples with known outcome is of important clinical interest as it could lead to a novel tumour classification system [4–7].

Matrix assisted laser desorption/ionisation- mass spectrometry imaging (MALDI-MSI) is rapidly becoming a powerful technology for studying the distribution and *in situ* identification of several classes of compounds including proteins, lipids, drugs and other small molecules directly within biological tissue sections. It hence provides and creates new fundamental and translational research opportunities in various fields including cancer biomarker discovery [8–10]. Recently the use of MALDI-MSI has been

described for the direct analysis of *in situ* digested proteins within a formalin fixed paraffin embedded lung cancer TMA showing the reproducibility of the method as well as the discrimination between cancer tissue types [11]. Of further interest is the use of statistical analysis, including principal component analysis (PCA) and hierarchical clustering analysis, in correlation with MALDI-MSI which has been reported in several studies [12–14]. The selection and highlighting of characteristic ion masses whose relative abundance in the tissue closely define and represent a region of interest of the tissue section or a sample type was clearly demonstrated.

The aim of this work is to establish a novel approach to molecular tumour classification based on MALDI-MSI of pancreatic TMA. Using the specificity and selectivity of the technique in combination with principal component analysis-discriminant analysis (PCA-DA) class differentiation between tumour samples was obtained. Several identified peptides were found to be characteristic proteins of tumour classes and the results were found to be statistically significant. The methodology used here describes a novel proof-of-concept and also explains the benefits of such an approach.

6.2 Materials and Methods

6.2.1 Materials

Modified sequence grade trypsin was purchased from Promega (Southampton, UK). All other materials, including alpha-cyano-4-hydroxycinnamic acid (α-CHCA), aniline (ANI), ethanol (EtOH), methanol (MeOH), xylene, octyl-α/β-glucoside (OcGlc), trifluoroacetic acid (TFA), haematoxylin, eosin, hydrogen peroxide (H_2O_2), tri-sodium citrate and ammonium bicarbonate, were purchased from Sigma-Aldrich (Dorset, UK).

6.2.2 Tissue samples

Following fully informed patient consent and full ethical committee approval anonymised 5 μm *ex vivo* human FFPE pancreatic tumour tissue sections were obtained (Study Number SSREC/04/Q2305/67 and subsequent amendments). AccuMax^{TM} FFPE pancreatic cancer TMA were purchased from Stretton Scientific (Stretton, UK). TMA samples contain either 60 adenocarcinoma needle cores from 30 patients and 8 non-neoplastic needle cores or 60 adenocarcinoma needle cores from 30 patients (2 spots from each cancer case) and 30 non-neoplastic needle cores (corresponding normal tissues). Figure 6.1 displays the layout of the TMA samples.

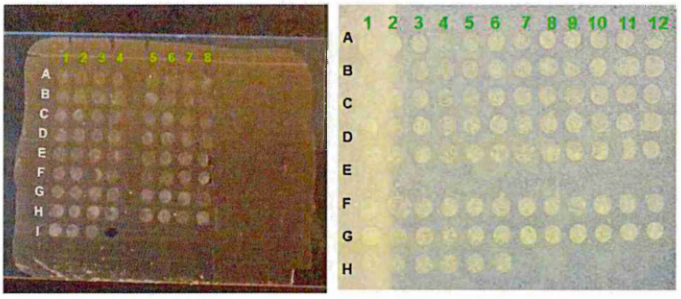

Figure 6.1: **FFPE pancreatic cancer tissue micro array layouts.**
(a) Schematic layout of pancreatic cancer TMA containing 68 needle cores. (b) Schematic layout of pancreatic cancer TMA containing 90 needle cores after matrix deposition.

6.2.3 Tissue preparation

The methodology used for tissue preparation was the same as that described in chapter 5 (section 5.2.3). Briefly, the paraffin film was removed from FFPE tissue sections using xylene. Following peroxidase blocking in hydrogen peroxide solution made at 3% in MeOH, antigen retrieval (AR) was performed in tri-sodium citrate buffer for 13 minutes in a microwave oven over 2 cycles of 5 minutes and one cycle of 3 minutes. Here, the duration of AR was reduced to 13 minutes in order to minimise loss of the needle cores during the microwave heating. The tissue sections were cooled to room temperature, rinsed with water and then allowed to dry at room temperature before trypsin and matrix deposition.

6.2.4 *In situ* digestion and matrix deposition

The methodology employed for *in situ* digestion was the same as that described in chapter 5 (section 5.2.3.1). Briefly, the trypsin solution was made at 20 μg/mL in 50 mM ammonium bicarbonate buffer (pH = 8.1) containing 0.1 % octyl glucoside (OcGlc) and deposited onto the tissue sections using a SunCollect^{TM} automatic sprayer (SunChrom, Friedrichsdorf, Germany). After trypsin deposition, the tissue section was incubated for 2 hours at 37°C (5% CO_2) in a humid environment.

α-CHCA mixed with aniline (α-CHCA/ANI) was used as the matrix. The matrix solution was prepared at 5 mg/mL in 50% ACN and 0.2% TFA and was sprayed onto the tissue sections using a SunCollect^{TM} automatic sprayer.

6.2.5 Direct MALDI-MS profiling and imaging

MALDI-MS profiles were acquired in the reflector and positive ion mode using an Ultraflex^{TM}II MALDI-TOF/TOF instrument (Bruker Daltoniks, Bremen, Germany) equipped with a Smartbeam^{TM} (Bruker Daltoniks, Bremen, Germany) laser. Prior to data acquisition, the instrument was calibrated using a standard mixture of peptides (Bruker Daltoniks, Bremen, Germany) ranging between m/z 900 and 3500. Full scan mass spectra were recorded from m/z 600 to 5000. FlexAnalysis^{TM} 2.0 and FlexImaging^{TM} 2.0 software (Bruker Daltoniks, Bremen, Germany) were used for data processing.

MALDI-IMS-MS profiling and imaging data were acquired in V-mode and positive ion mode using a MALDI SYNAPT^{TM}HDMS system (Waters Corporation, Manchester, UK) operating with a 200 Hz Nd:YAG laser. The instrument calibration was performed using a standard mixture of polyethylene glycol (Sigma-Aldrich, Gillingham, UK) ranging between m/z 100 to 3000 prior to MALDI-IMS-MSI analysis. Prior to MALDI-IMS-MSI experiments, digital scans of tissue sections were obtained using a CanoScan 4400F flatbed scanner (Canon, Reigate, UK) and then imported into MALDI Imaging Pattern Creator^{TM} (Waters Corporation, Milford, MA) software. All data were acquired with ion mobility separation in the mass range from 800 Da to 3000 Da. Peptide images were acquired at a spatial resolution of 200 μm with 600 laser shots per position. Using Driftscope^{TM} (Waters Corporation, Milford, MA) software, mobility data of individual peptide signals were selected and extracted using MALDIExtract^{TM} (Waters Corporation, Milford, MA) software. The extracted data were converted into imaging files using MALDI Imaging Convertor^{TM} (Waters Corporation, Milford, MA) software and ion images were generated with BioMap 3.7.5.5 software (Novartis, Basel, Switzerland).

6.2.6 Direct MALDI-IMS-MS/MS and MALDI-MS/MS data acquisition

On-tissue MALDI-IMS-MS/MS and MALDI-MS/MS analyses were performed using a MALDI SYNAPT^{TM}HDMS (Waters Corporation, Manchester, UK) using the same methodology as that described in chapter 5 (section 5.2.4).

MASCOT (Matrix Science, London, UK) query searches were performed against the UniProt database (release 56.0). Within the MASCOT search engine, the parent and fragment ion tolerances were set at 30 ppm and 0.1 Da respectively. The criteria also included up to two missed cleavages and the variable modifications allowed were protein N terminus acetylation, histidine/tryptophan oxidation, methionine oxidation and proline oxidation. *De novo* sequencing was performed manually and also using the PepSeq^{TM} (Waters Corporation, Milford, MA) *de novo* interactive MS/MS sequencing tool. The parent and fragment ion tolerances were set at 0.1 Da and the threshold was set at 1%. Protein Blast searches against the Swissprot database were also performed to confirm tryptic sequences.

6.2.7 MALDI- IMS-MS/MS imaging

Digital scans of the tissue sections were also obtained using a CanoScan 4400F flatbed scanner (Canon, Reigate, UK) prior to MALDI-IMS-MS/MS imaging. Imaging patterns were created using MALDI Imaging Pattern Creator^{TM} (Waters Corporation, Milford, MA) software depending on the desired number of peptide ion signals to be monitored. Image acquisition was performed using the MALDI SYNAPT^{TM}HDMS system (Waters Corporation, Manchester, UK) with ion mobility separation at a spatial resolution of 300 μm, as two MALDI-IMS-MS/MS images were acquired from one tissue section. Ion images were generated with BioMap 3.7.5.5 software.

6.3 Results and Discussion

6.3.1 Evaluation of the method specificity

TMA technology allows several samples to be analysed simultaneously, thus minimising time, costs and the amount of samples required for the analysis. The specificity of the MALDI-MSI technique was demonstrated here by profiling adenocarcinoma and non-neoplastic tissue cores. Figure 6.2 displays the peptide profiles obtained after *in situ* digestion of a pancreatic cancer TMA, where different peptide profile patterns were observed when comparing adenocarcinoma and non-neoplastic cores. Peptide profiles were obtained using an Ultraflex^{TM}II MALDI-TOF/TOF instrument (Bruker Daltoniks, Bremen, Germany).

The method employed here was found to be very sensitive as peptide signals were detected above m/z 4000. Here, tissue needle cores defined as *adenocarcinoma 1* , *adenocarcinoma 2* and *non-neoplastic* corresponded to the tissue core spots A1, A5 and I1 respectively as described in the TMA layout (figure 6.2a). These samples were diagnosed as stage IIA, moderately and poorly differentiated. When comparing MALDI-MS peptide profiles, differences in the peptide signals detected as well as peptide signal intensities were noticed. This demonstrated the potential of the technique to differentiate tumour samples. Different peptide profiles were also observed when comparing tumour samples and non-neoplastic tissue cores. This shows the specificity of the methodology employed.

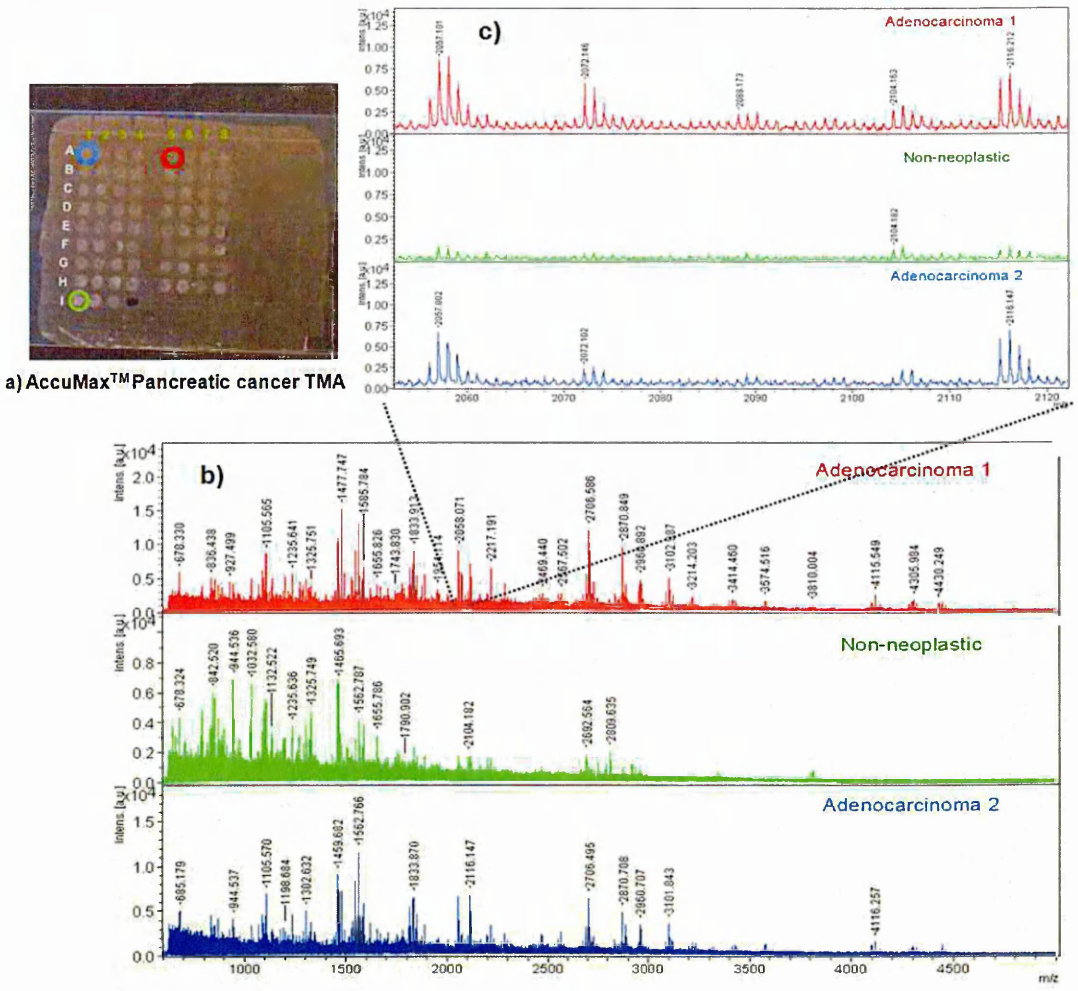

Figure 6.2: **TMA layout and MALDI-MS peptide profiles obtained after on-tissue digestion of FFPE pancreatic cancer TMA samples.**
(a) FFPE pancreatic cancer TMA layout. Peptide profiles were acquired using an Ultraflex^{TM}II MALDI-TOF/TOF instrument (Bruker Daltoniks). (b) MALDI-MS spectra of peptides observed after *in situ* digestion of TMA samples: peptide profiles resulting from adenocarcinoma and non-neoplastic cores are shown. (c) Expanded regions of the spectra. Differences in peptide signal intensities can be observed: the peptide signal at m/z 2072 was only detected in adenocarcinoma peptide profiles.

6.3.2 Direct MALDI-IMS-MS and MS/MS analysis of tissue micro array sections

The layout of the pancreatic cancer TMA sections used here is displayed in figure 6.3a. It comprised 90 needle core biopsies of 1 mm diameter each from tumour tissues spotted in duplicate and diagnosed as adenocarcinoma moderately, poorly or well differentiated with their corresponding normal tissues. Figure 6.3b shows the TMA sections after matrix coverage prior to MALDI mass spectrometry imaging analysis. MALDI mass spectra were generated from each tissue section. Figure 6.3c displays an example of a mass spectrum, obtained from a tissue core after antigen retrieval treatment and *in situ* digestion, in the mass range m/z 800 to 3000.

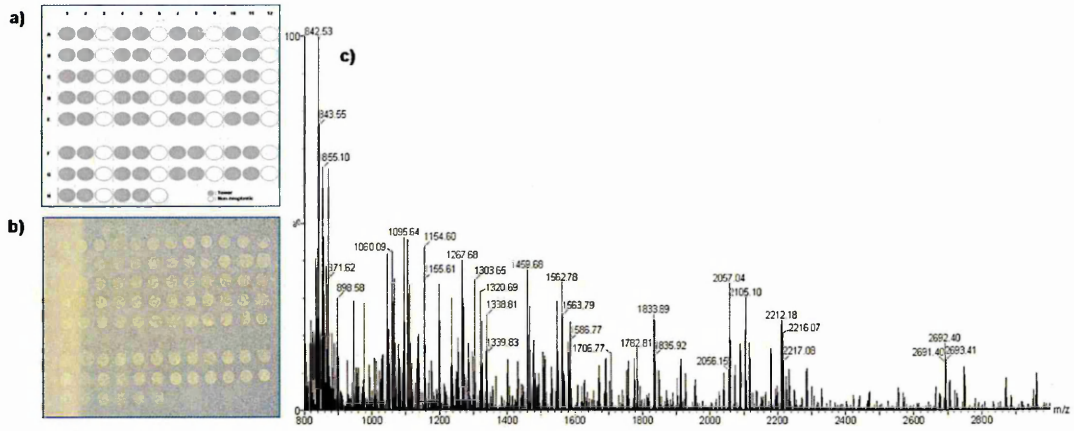

Figure 6.3: **TMA layout and MALDI mass spectrum obtained from one tissue core after *in situ* digestion of FFPE pancreatic tissue micro array sections.** (a) Schematic TMA layout and (b) digital scan of the TMA after *in-situ* tryptic digestion and matrix coverage. (c) MALDI mass spectrum obtained from one tissue core after *in situ* digestion.

More than 500 individual peptide signals per spectrum were detected. From this mass list, peptide ions were selected for MS/MS analysis directly within the tissue sections. 320 peptide m/z values were randomly selected from the obtained mass spectra using Excel (Microsoft 2003). This aimed to obtain a mass list of high and low intensity peptide signals for MALDI-MS/MS analyses. MALDI-MS/MS analyses were then acquired from these 320 peptide ions. To do so, the tissue micro-array glass slide was redefined as a MALDI spot target plate for an automatic MS/MS run as described in chapter 5 (section 5.2.4). Using automatic MALDI-MS/MS data acquisition directly

from the TMA, it is not possible currently to use the IMS. However, the MASCOT database searches allowed the identification of numerous proteins. Manual acquisitions of MALDI-IMS-MS/MS spectra were also performed in order to achieve more protein identification. Figure 6.4a displays the Driftscope^{TM} plot of the MS/MS fragmentation of the peptide ion at m/z 1477. This diagram shows the separation of ions based on their mobility where their corresponding driftime is plotted against their m/z values. Here, it can be noticed in figure 6.4b that two species were simultaneously detected at m/z 1477. Using their mobility, it was possible to separate the MS/MS spectrum of the fragmentation of the peptide from the unknown compound. The peptide was identified as a tryptic peptide arising from type I collagen alpha-2 chain (figure 6.4b). The other compound was not identified. Table 6.1 displays a list of tryptic peptide signals with their corresponding MASCOT identifications.

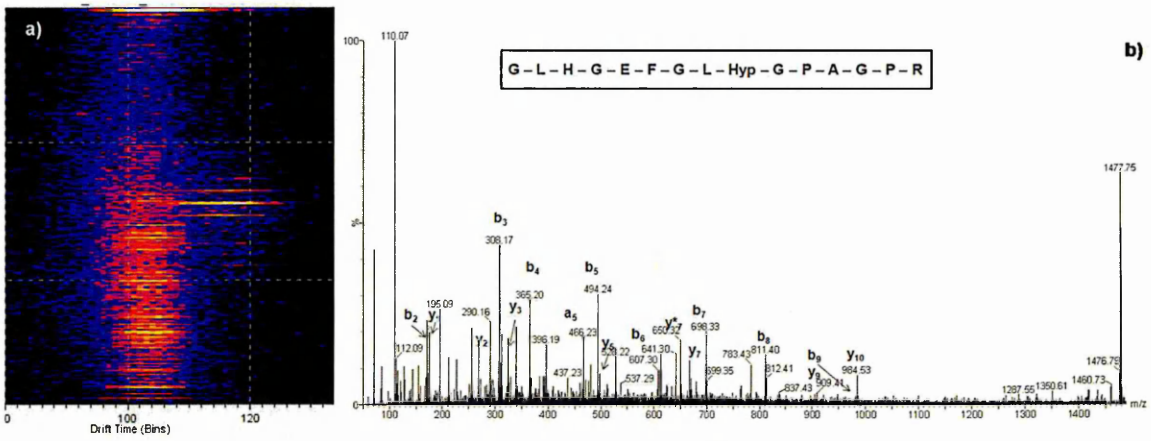

Figure 6.4: **Driftscope^{TM} plot and MALDI-IMS-MS/MS spectrum of the ion signal at m/z 1477 acquired directly from FFPE pancreatic TMA tissue sections.**
(a) Driftscope^{TM} plot of the MS/MS fragmentation of the ion signal at m/z 1477 where two isobaric compounds were simultaneously detected. (b) The MS/MS spectrum of the peptide ion at m/z 1477 was separated from the interfering unknown compound using the ion mobility separation: the peptide was identified as type I collagen.

Table 6.1: **List of tryptic peptides identified after *in situ* digestion of pancreatic cancer TMA sections using direct MALDI-IMS-MS/MS.** All database searches for protein identification were performed using the UniProt human database.

Protein name/ Accession number	Mass (Da)	Observed peptide m/z	Mass error (ppm)	Sequence	MS/MS ion Score
Actin, aortic smooth muscle/ P62736	41982	1198.72	12.9	AVFPSIVGRPR	40
		1790.90	2.96	SYELPDGQVITIGNER	75
Actin, cytoplasmic 1/ P60709	41710	1954.06	0.78	VAPEEHPVLLTEAPLNPK	108
		2215.08	4.22	DLYANTVLSGGTTMYPGIADR	61
Albumin/ P02768	69321	1149.63	15.4	LVNEVTEFAK	37
		1311.73	7.05	HPDYSVVLLLR	57
Breast cancer type 1 susceptibility protein/ P38398	207592	852.4	-19.81	NHQGPKR, oxidation (HW)	33
Collagen alpha-1(I)/ P02452	138799	886.44	0.87	GSEGPQGVR	30
		898.51	-4.91	GVVGLPGQR, oxidation (P)	18
		1088.56	17.2	GFPGADGVAGPK, oxidation (P)	18
		1105.56	-14.13	GVQGPPGPAGPR, oxidation (P)	35
		1297.62	8.77	GESGPSGPAGPTGAR	39
		1302.63	-13.69	GPSGPQGPGGPPGPK, oxidation (P)	42
		1459.68	-6.41	GSAGPPGATGFPGAAGR, 2 oxidation (P)	50
		1465.69	-2.99	GEPGPTGLPGPPGER, 3 oxidation (P)	60
		1546.78	-13.88	GETGPAGPAGPVGPVGAR	74
		1561.78	-12.57	DGLNGLPGPIGPPGPR, 3 oxidation (P)	42
		1655.78	-8.25	GSPGEAGRPGEAGLPGAK, 3 Oxidation (P)	19
		1690.78	0.74	DGEAGAQGPPGPAGPAGER	45
		1706.75	-11.59	DGEAGAQGPPGPAGPAGER, oxidation (P)	100
		1742.77	18.2	GEPGSPGENGAPGQMGPR, oxidation (M); 2 oxidation (P)	31
		1812.88	-2.40	VGPPGPSGNAGPPGPPGPAGK, 3 oxidation (P)	22
		1816.85	-9.90	GPPGPMGPPGLAGPPGESGR, 2 oxidation (P)	51
		1832.85	-2.95	PPGPMGPPGLAGPPGESGR, Oxidation (M); 2 Oxidation (P)	68

Continued on Next Page...

Table 6.1 – Continued

Protein name/ Accession number	Mass (Da)	Observed peptide m/z	Mass error (ppm)	Sequence	MS/MS ion Score
		1848.85	-2.88	GPPGPMGPPGLAGPPGESGR, Oxidation (M); 3 Oxidation (P)	34
		2003.95	-11.65	GEPGPVGVQGPPGPAGEEGKR, 2 oxidation (P)	55
		2198.99	12.10	GDAGAPGAPGSQGAPGLQGMPGER, 4 oxidation (P)	67
		2454.23	-1.06	GPPGSAGAPGKDGLNGLPGPIGPPGPR, 4 oxidation (P)	20
		2703.23	-4.11	GAPGDRGEPGPPGPAGFAGPPGADGQ PGAK, 4 oxidation (P)	16
		2705.29	-9.56	GFSGLQGPPGPPGSPGEQGPSGASGPA GPR, 3 oxidation (P)	58
		2869.39	-4.86	GLTGPIGPPGPAGAPGDKGESGPSGPAG PTGAR, 2 oxidation (P)	72
Collagen alpha-2(I)/ P08123	129333	1184.49	-0.33	DGNPGNDGPPGR, 2 Oxidation (P)	44
		1217.62	-0.45	NPARTCRDLR, oxidation (P)	19
		1235.63	-11.37	TGHPGTVGPAGIR, oxidation (P)	36
		1267.67	-0.27	GIPGPVGAAGATGAR, oxidation (P)	9
		1477.73	-14.66	GLHGEFGLPGPAGPR, oxidation (P)	65
		1562.78	-9.65	GETGPSGPVGPAGAVGPR	36
		1619.77	-7.25	GPNGEAGSAGPPGPPGLR, 2 oxidation (P)	58
		1664.72	-29.36	AGEDGHPGKPGRPGER, 3 oxidation (P)	11
		1766.78	-24.95	GPNGDAGRPGEPGLMGPR, 2 oxidation (P)	13
		1775.86	-10.73	RGPNGEAGSAGPPGPPGLR, 2 oxidation (P)	53
		1829.90	-0.52	TGPPGPSGISGPPGPPGPAGK, 3 oxidation (P)	11
		1845.91	5.05	TGPPGPSGISGPPGPPGPAGK, 4 oxidation (P)	16
		2567.22	-16.74	GENGVVGPTGPVGAAGPAGPNGPPGP AGSR, oxidation (P)	28
		2832.33	-6.84	GEQGPAGPPGFQGLPGPSGPAGEVGK PGER, 3 oxidation (P)	13
		2865.36	-20.55	GPKGENGVVGPTGPVGAAGPAGPNGPP GPAGSR., 2 oxidation (P)	20
Collagen alpha-1(III)/ P02461	138470	1138.57	-0.23	GLAGPPGMPGPR, oxidation (M); oxidation (P)	16
		1508.68	-15.99	GESGPAGPAGAPGPAGSR, oxidation (P)	41

Continued on Next Page...

Table 6.1 – Continued

Protein name/ Accession number	Mass (Da)	Observed peptide m/z	Mass error (ppm)	Sequence	MS/MS ion Score
		1530.72	-8.94	DGTSGHPGPIGPPGPR, 2 Oxidation (P)	52
		2539.13	-4.58	GETGPPGPAGFPGAPGQNGEPGGKGER, 4 Oxidation (P)	25
		2641.26	0.05	GEGGPPGVAGPPGGSGPAGPPGPQGVKGER, 4 Oxidation (P)	19
		2950.44	-7.73	GPTGPIGPPGPAGQPGDKGEGGAPGLPGIAGPR, 4 Oxidation (P)	54
Basic fibroblast growth factor receptor 1/ P11362	91809	1832.95	-12.19	TVKFKCPSSGTPNPTLR	15
78 kDa glucose-regulated protein (Grp78)/ P11021	72288	1887.95	12.9	VTHAVVTVPAYFNDAQR	10
		1934.00	6.23	DNHLLGTFDLTGIPPAPR	76
Haemoglobin alpha/ P69905	15258	1087.57	17.3	MFLSFPTTK, oxidation (M)	26
		1529.74	2.57	VGAHAGEYGAEALER	115
Haemoglobin beta/ P68871	15988	1274.73	2.22	LLVVYPWTQR	27
Histone H2A.Z/ P0C0S5	13545	944.53	-5.55	AGLQFPVGR	26
Histone H2B/ P33778	13942	1775.84	20.6	AMGIMNSFVNDIFER, 2 oxidation (M)	36
Histone H3-like/ Q6NXT2	15204	1032.59	4.15	YRPGTVALR	19
Histone H4/ P62805	11360	1325.74	7.59	DNIQGITKPAIR	39
		1466.80	-3.72	TVTAMDVVYALKR	29
Pancreatic alpha-amylase/ P04746	57670	1427.70	2.60	ALVFVDNHDNQR	59
Pancreatic triacylglycerol lipase precursor/ P16233	51124	1746.90	19.58	FIWYNNVINPTLPR	58
Periostin/ Q15063	93255	1400.78	6.62	AAAITSDILEALGR	75
Protocadherin-1/ Q08174	114676	1141.71	-22.74	QPQLIVMGNLDR, acetyl (N-term); xidation (M)	20
Serine/threonine-protein kinase/ Q9Y3S1	242525	1327.72	6.13	GLTLPCLPWRR, oxidation	23

Continued on Next Page...

Table 6.1 – Continued

Protein name/ Accession number	Mass (Da)	Observed peptide m/z	Mass error (ppm)	Sequence	MS/MS ion Score
Tumor necrosis factor receptor superfamily member 10A/ O00220	50029	1105.63	2.98	AGRAPGPRPAR	19
Zinc finger protein 219/ Q9P2Y4	76830	1303.65	6.08	AGPGGEAGPGGALHR	23

6.3.3 Principal component analysis-discriminant analysis (PCA-DA) of tissue micro-array sections

Principal component analysis (PCA) is a statistical method commonly used for reducing the dimensionality of a multivariate data set whilst retaining most of the original information. Discriminant analysis (DA) is often used to define a classification from an observation of pre-defined groups. PCA-DA is a two stage supervised statistical technique, the number of variables in the data set is first reduced by the use of PCA before a second discriminant analysis is performed. PCA-DA takes into account user supplied information about external variables (group information) when reducing the dimensionality of the datasets in the first stage. Therefore, it is better suited than PCA for clustering analysis [15]. Here, PCA-DA was used as a statistical analytical method with the aim of generating a classification model based on sample clusters defined by PCA. Peptide profiles obtained from MALDI-IMS-MS imaging of TMA sections were evaluated by principal component analysis-discriminant analysis (PCA-DA). For this analysis, the selected peptide profiles were de-isotoped with MASCOT Distiller^{TM} software and the resulting peak lists were used for PCA-DA. Each peak list consisted of 300 individual peptide signals. An exclusion peak list containing matrix adducts as well as trypsin peptide peaks was used. PCA-DA consisted of assessing if a model of classification could be generated and then validating these results using another set of data.

6.3.3.1 PCA-DA of a *training* set of data for the generation of tumour classification models

Peptide profiles obtained from adenocarcinoma cores were separated into two data sets: the first data set was used as a *training* data set in order to generate a model of classification and the second was used as a *test* data set for validating the classification model [24]. Then PCA-DA was conducted on peptide profiles from the training data set in order to assess possible differences between adenocarcinoma cores. For this purpose, 40 spectra obtained from the adenocarcinoma cores were loaded into MarkerView^{TM} 1.2 software for PCA-DA. The results of PCA-DA is visualised as a projection of scores and loadings plots. The scores plots represent the variance of the original variables, i.e. the obtained sample groups. The loadings plots describe the variable behaviour and differences between the observed groups. Figures 6.5a and b display the obtained scores and loading plots respectively. The scores plots show that spectra were grouped in 3 classes. For result interpretation purposes, the group defined by the blue spots was named group 1; group 2 and group 3 were defined by the red and green spots respectively.

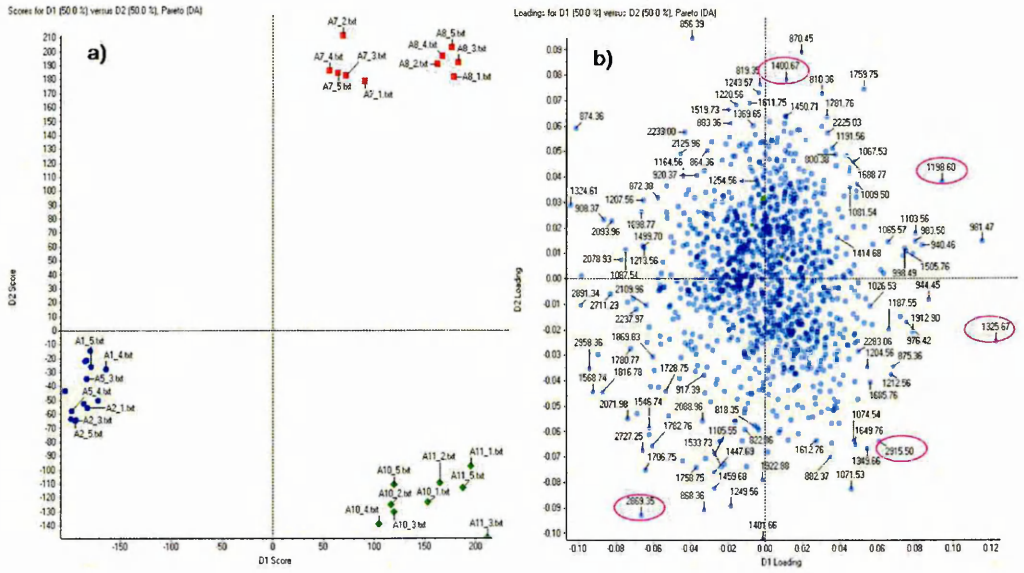

Figure 6.5: **PCA-DA of peptide profiles exported from MALDI-IMS-MS images of FFPE pancreatic tumour TMA sections.**
(a) Tumour samples were separated into three groups by PCA-DA, which are indicated by the blue, red and green spots. (b) The loading scores indicate characteristic ion masses which are specific to a given group.

Examination of the data showed that spectra obtained from duplicate biopsies of the same tumour were contained in the same group. This demonstrates that the method is potentially reproducible. In the scores plot (figure 6.5a), it can be noticed that D1 scores separates group 1 from group 2 and group 3. Group 2 and group 3 are also separated as they display negative and positive values of D2 respectively. According to the pathological classification provided with the TMA samples, group 2 and group 3 present the same tumour grade and lymph node stage. Here using MALDI-MSI followed by PCA-DA, separations between the tumour samples, which were not highlighted using the conventional tumour metastasis node (TMN) classification, were obtained based on direct proteomic analysis. Examination of the loading plots (figure 6.5b) revealed that several peptide signals were found to be characteristic of a given group.

In order to assess if the peptide signals highlighted in the loading scores were statistically significant so as to enable the classification of tumour samples, a *t-test* was performed using MarkerView^{TM} 1.2 software. Each tumour group was compared to the other two in terms of obtained peptide profiles. The *t-test* was found to be in good agreement with the results obtained with PCA-DA as it highlighted the same peptide m/z values which were found to be characteristic of a tumour group when performing PCA-DA. Figure 6.6 displays the mean of the peptide signal intensities and standard deviation of the peptide signal intensities in each group. Several peptide signals were found to be characteristic of each given group.

Group 1 (n = 15) was compared to group 2 (n = 10) and group 3 (n = 10). The peptide signal at m/z 1105, identified as a peptide T8-9 arising from tumour necrosis factor receptor, was found to be highly intense in group 1 when compared to group 2 and group 3. Peptide signals at m/z 1325 and 1327, arising from histone H4 and serine/threonine protein kinase respectively, were also found to be significantly characteristic of group 1. When comparing group 2 (n = 10) to groups 1 and 3, and group 3 (n = 10) to group 1 and group 2, it can be noticed that several peptide signals were found to be of high intensity in a given group, hence allowing the discrimination between classes. The results obtained from the *t-test* were found to be in good agreement with those obtained from PCA-DA (figure 6.5). Here the PCA-DA based on high-throughput peptide profiles obtained with MALDI-IMS-MSI allowed significant discrimination between tumour samples.

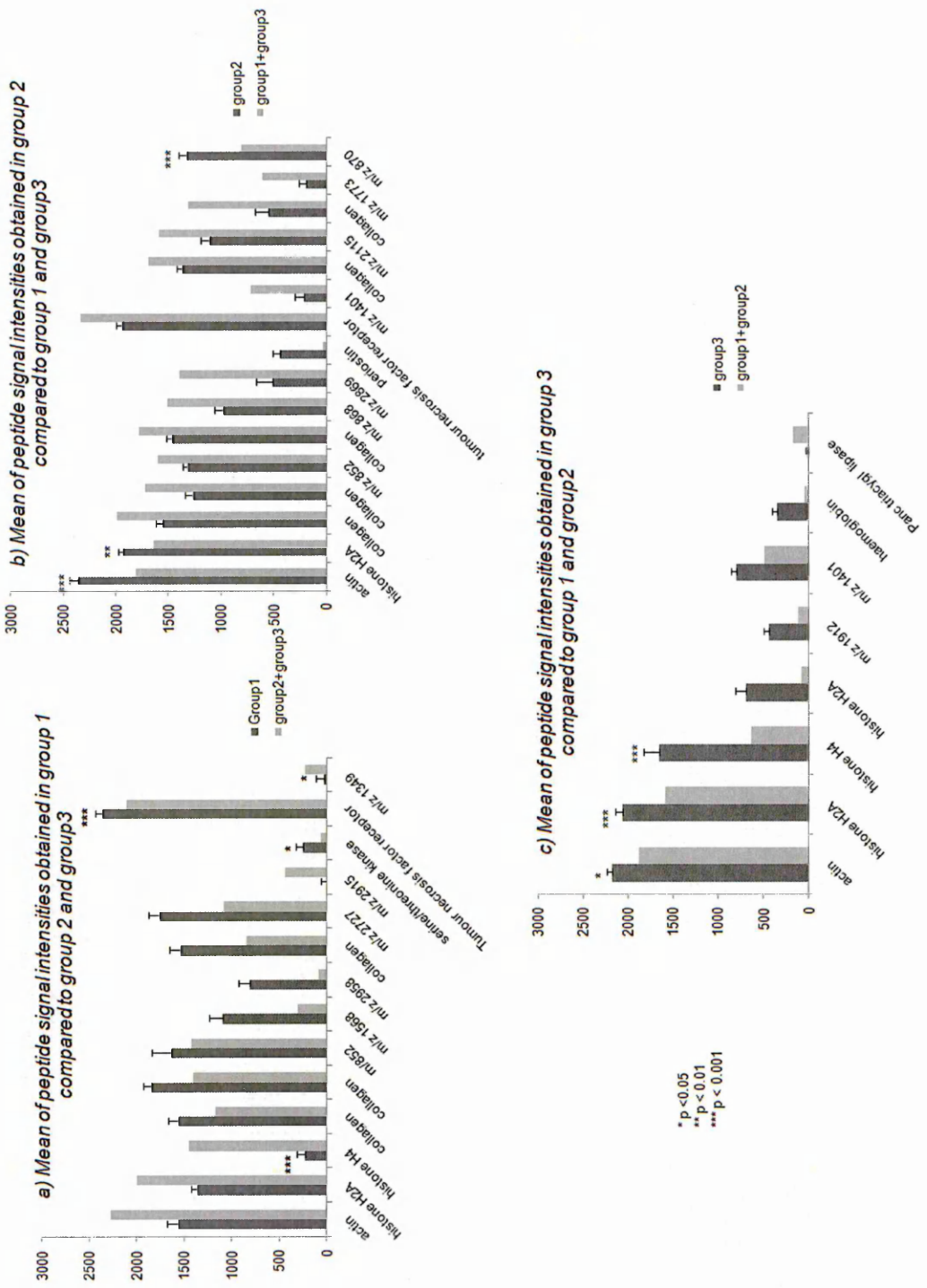

Figure 6.6: **Comparison of the mean of peptide signal intensities between tumour classes using a *t-test*.**

6.3.3.2 Validation of the tumour classification model using a *test* data set

PCA-DA of the first set of data allowed the generation of a classification model in which peptide profiles obtained from tumour tissue cores were distinguished. The second step of the statistical analysis was assessing if the model generated correctly described and classified tumour tissue sections using another data set obtained from the TMA. For this purpose, PCA-DA was performed on 35 other spectra. Figure 6.7a displays the obtained scores where tumour groups were noticed.

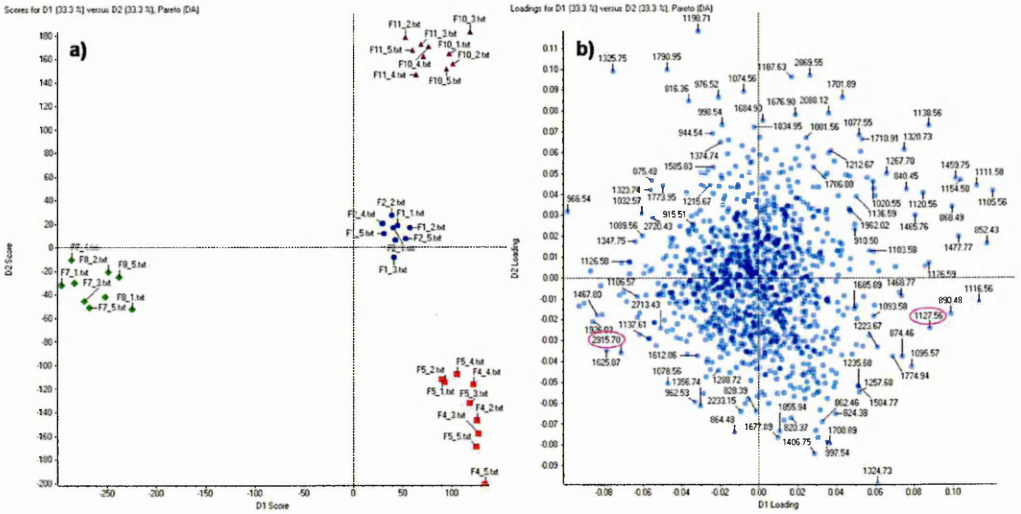

Figure 6.7: **Validation of the PCA-DA results using another set of data.** Discrimination between tumour samples was obtained when examining (a) the resulting scores plots and (b) loading plots.

In the loading plots (figure 6.7b), several peptides were found to be class identifiers. More interesting is the highlight of the same peptide signals, which were found to be class identifiers from the training set, as characteristic masses for distinguishing tumour groups in the test set. It can be noticed for instance that the peptide signal at m/z 2915, which corresponds to a tryptic peptide of histone H2A, was found to be highly intense in a tumour group obtained with the test data set. This demonstrates that the methodology used here is potentially robust. These results were found to be in agreement with those obtained from the PCA-DA of the training data set. The methodology described here allowed the validation of proof-of-principle as it shows that tumour classes were generated based on molecular information i.e. protein distribution and *in situ* identification within pancreatic cancer TMA using MALDI-IMS-MSI

combined with PCA-DA.

Additionally a discrimination between non-neoplastic and tumour cores were obtained. This highlights the specificity of the methodology. A total of 54 spectra were used for PCA-DA. Figure 6.8a displays the scores plots where group separation can be noticed. Peptide profiles obtained from normal tissue sections are separated from those obtained from tumour tissue cores. Examination of the data obtained from the loading plots (Figure 6.8b) highlights several peptide signals, including peptides at m/z 944, 1198, 1400 and 1477, which were identified as tryptic peptides arasinf from histone H2A, actin, periostin and type I collagen alpha-2 chain respectively, which were found to be highly intense in tumour samples.

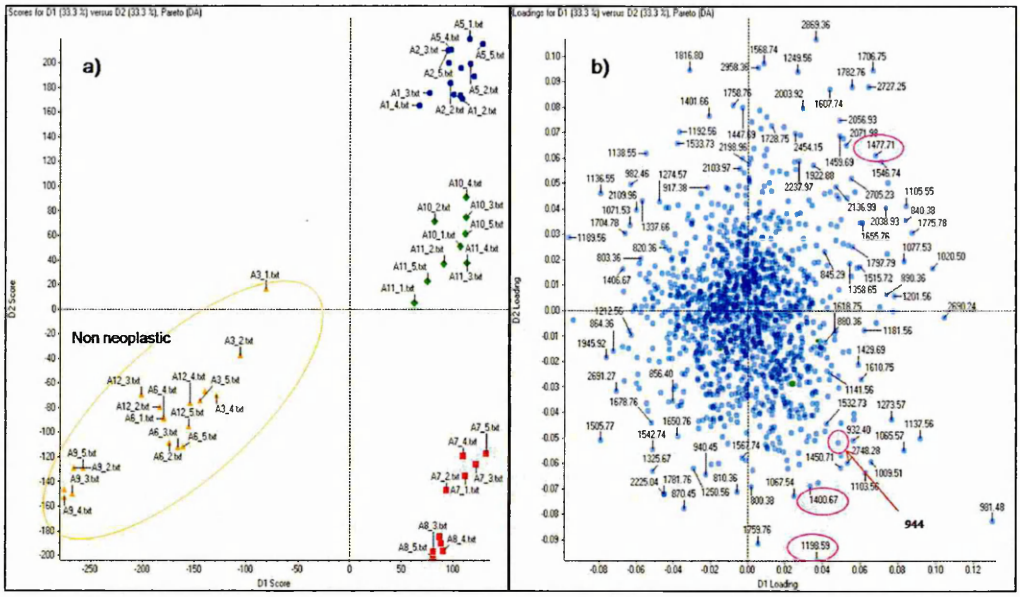

Figure 6.8: **PCA-DA of peptide profiles exported from MALDI-IMS-MS images of tumour and non-neoplastic tissue cores of FFPE pancreatic TMA sections.**
(a) The obtained scores plots display that non-neoplastic tumour samples are distinguished from tumour samples as well as discrimination between tumour samples. (b) The loadings plot highlights peptide ions that are specific to the obtained groups.

6.3.4 MALDI-IMS-MS imaging of tissue micro-array sections and FFPE pancreatic tumour tissue sections

Using MALDI-IMS-MSI, peptide distributions within the tissue microarray sections were also generated. Figure 6.9 shows the distribution of some observed peptide signals within the TMA sections. Images were normalised against the matrix ion signal at m/z 867. These peptides were identified as actin, periostin, haemoglobin alpha-chain and histone H2A respectively. The results obtained from imaging analysis were in good agreement with those obtained from PCA-DA.

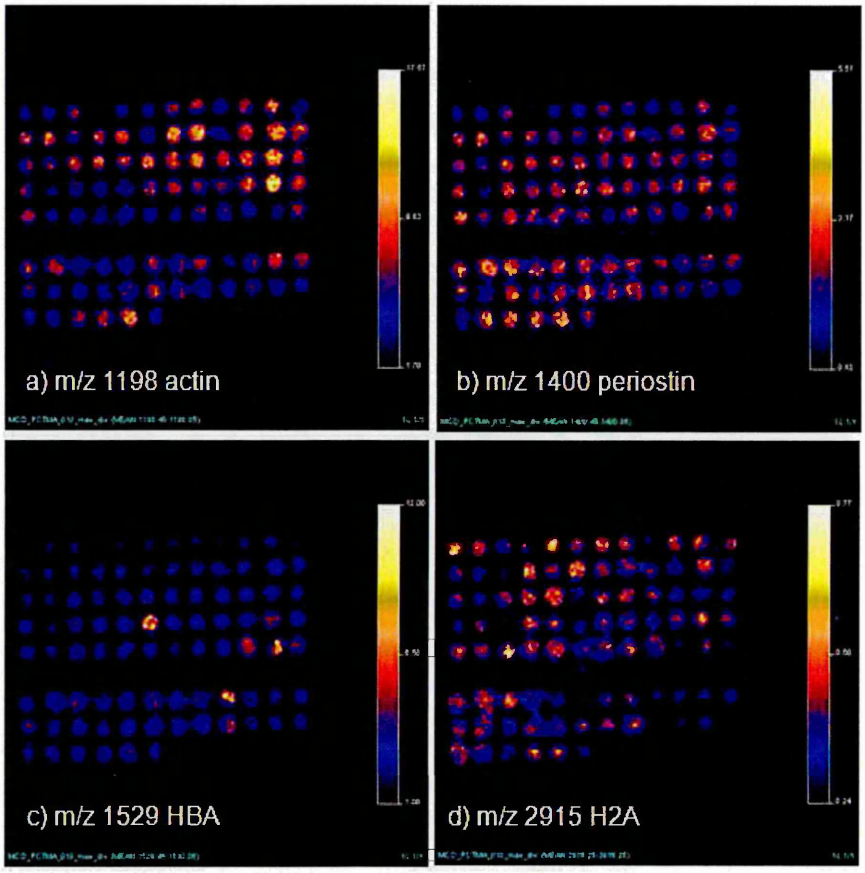

Figure 6.9: **MALDI-IMS-MS images of the localisation of peptides within FFPE pancreatic TMA sections after *in situ* digestion.**
The distributions of (a) actin, (b) periostin, (c) haemoglobin alpha chain and (d) histone H2A are displayed.

FFPE pancreatic tumour tissue sections were subsequently analysed using MALDI-IMS-MSI. The data generated from statistical analysis of the pancreatic tumour tissue microarray allowed the selection of characteristic ion signals that were used for highlighting tumour regions. Figures 6.10a, b and c display the distribution of ion signals at m/z 944, 1032 and 1477, identified as histone H2A, histone H3 and type I collagen respectively. These were found to be located in the tumour regions. Figures 6.10d, e and f show the HE staining images of the tissue section were tumour regions are highlighted. The HE staining pictures were found to be in good agreement with the obtained MALDI-IMS-MS images.

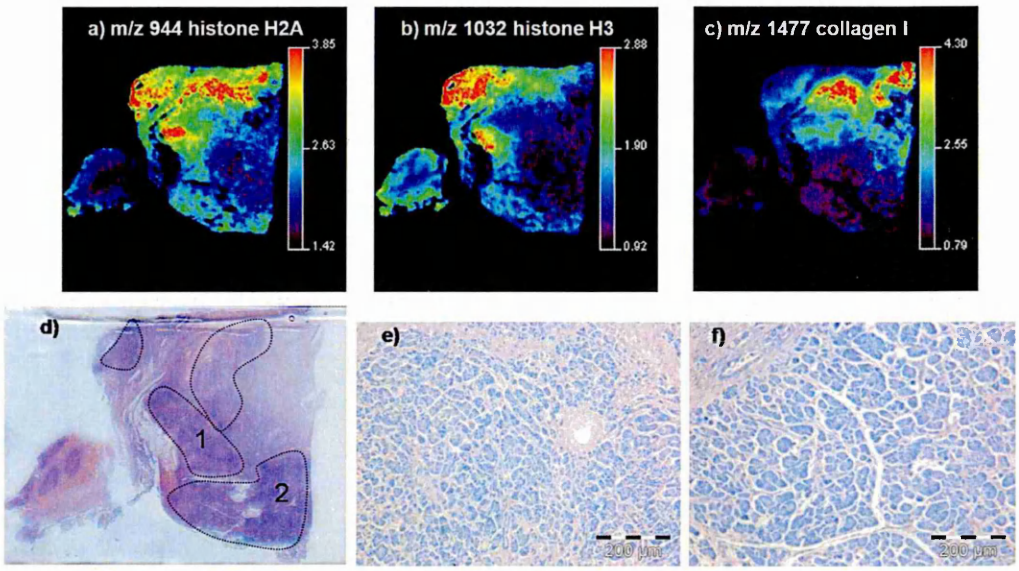

Figure 6.10: **Images of the distribution of peptides within a FFPE pancreatic tumour tissue section.**
(a-c) MALDI-IMS-MS images of the distribution of histone H2A, histone H3 and type I collagen tryptic peptides respectively. Images were normalised against the matrix adduct at m/z 877. (d) HE staining of a FFPE human pancreatic cancer with the localisation of tumour regions. (e) and (f) are microscopic images acquired from tumour regions 1 and 2 of figure 6.10d at magnification x10 showing tumour cells.

Tumour necrosis factor receptor was also detected and identified from FFPE pancreatic cancer tissue sections. The upper panel of figure 6.11 (figure 6.11a) displays the resulting MALDI-IMS-MS/MS spectrum of the ion signal at m/z 1105 identified directly from FFPE pancreatic tissue sections as a tryptic peptide arising from tumour necrosis factor receptor. The lower panels of figure 6.11 (figure 6.11b, c, d and e) display MALDI-IMS-MS/MS images of the distribution of tumour necrosis factor receptor tryptic peptide at m/z 1105 as well as some y and b product ions including y_8 (m/z 821), b_7 (m/z 607) and b_5 (m/z 453).

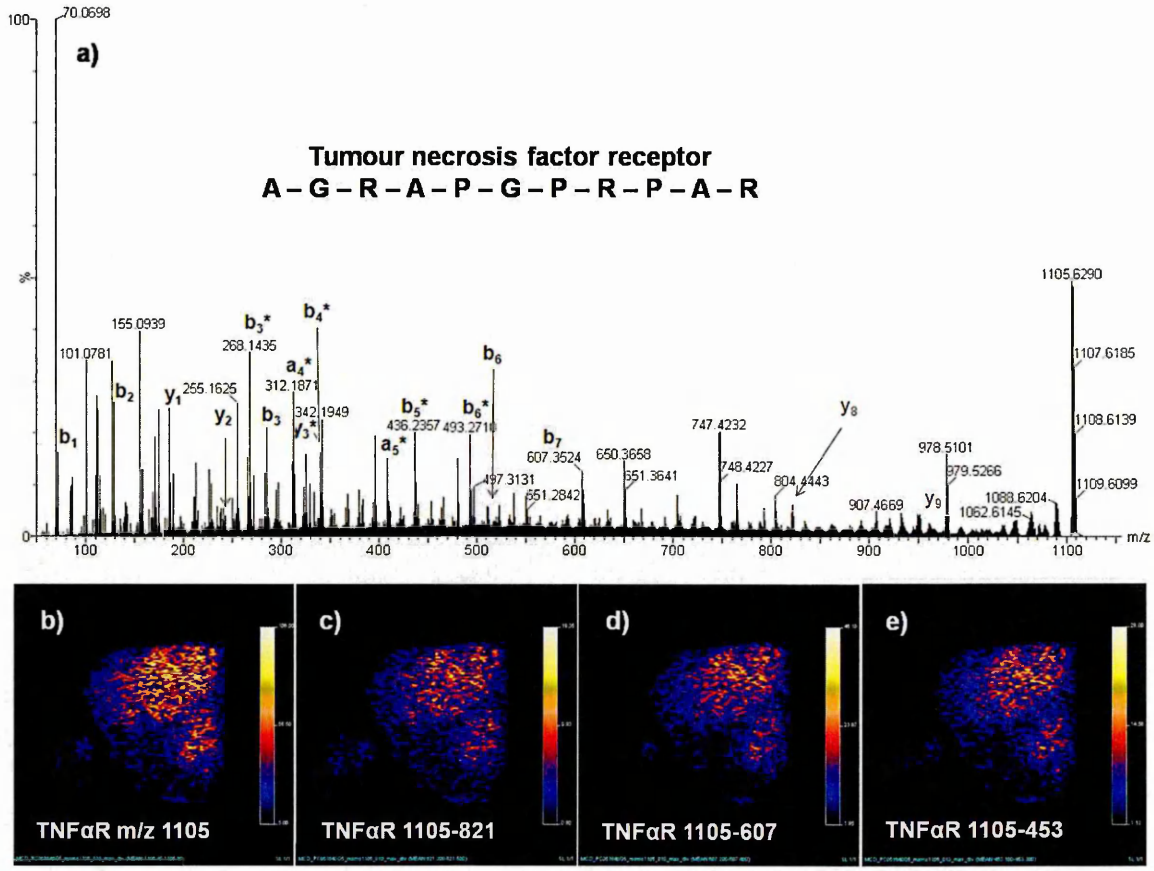

Figure 6.11: **MALDI-IMS-MS/MS spectrum and images of the distribution of tumour necrosis factor receptor within a FFPE pancreatic tumour tissue section.**
(a) MALDI-IMS-MS/MS spectrum of the peptide signal at m/z 1105 which was identified as arising from tumour necrosis factor receptor. (b-e) MALDI-IMS-MS/MS images of the distribution of product ions of the tumour necrosis factor receptor tryptic peptide signal at m/z 1005.

6.4 Concluding Remarks

Pancreatic cancer is the 10th most common cancer in the UK but the 6th most common cause of cancer death. Many patients present late with inoperable disease. Current limited therapeutic options include surgical resection and chemotherapy; however this cancer is still associated with a very poor prognosis [16]. The most recent national figures for the United Kingdom show a 1 year survival of 13% and a 5 year survival of 2-3% overall. Where possible, surgical resection offers the best chance of extended survival with a median survival of 11-20 months (5 year survival 7-25%) compared to 6-11 months for patients with Stage III (non resectable locally advanced) disease and 2-6 months for patients with metastatic disease.

There are no globally recognised classification systems for pancreatic tumours. The most clinically relevant current classification technique relies on radiological staging into potentially resectable, locally advanced or non-resectable and metastatic disease. Novel tumour classification systems are required in order to improve clinical diagnosis and treatment.

In the work reported here, a novel methodology for pancreatic tumour classification models is described using MALDI-IMS-MSI and PCA-DA analysis of tissue micro-array sections. Using this strategy, high-throughput analysis of TMA sections by MALDI-IMS-MSI allowed the visualisation of numerous peptides within the tissue sections after *in situ* enzymatic digestion. The differences obtained in peptide profiles reflect the complexity and heterogeneity of the molecular nature of the disease. In the work reported here, distinct peptide profile patterns obtained by MALDI-IMS-MSI have contributed to generating classes of pancreatic tumour using PCA-DA. Discriminations between peptide profiles and images obtained from adenocarcinoma cores were observed. In some cases, tumour samples presenting the same pathologic classification (tumour grade, lymph node stage) were found to be significantly different after performing PCA-DA. Using other sets of data, the methodology was validated as tumour classes which exhibited the same peptide tumour class identifiers as the training data set were generated. This demonstrates the robustness of the method. A proof-of-concept was hence established, since MALDI-MSI combined with PCA-DA of TMA sections allowed the design of a novel molecular tumour classification model based on *in situ* proteomic information.

Several peptides were found to be characteristic of an obtained tumour class. Data such as those could be used to build a proteomic platform or database of peptides and/or proteins that can help to distinguish between samples with known or unknown clinical outcomes. Indeed the methodology reported here allowed tumour classification, and also spatial localisation and *in situ* identification of several peptide candidates from TMA sections in a single experiment and therefore fewer samples were required compared to other classical proteomic approaches. The *in situ* identification of several proteins directly from the tissue sections was also achieved.

The use of ion mobility separation combined with MALDI-MSI has been found to be beneficial for the study of proteome patterns and their identification directly within TMA cores as it allowed the generation of the exact distribution of peptides within tissue sections by minimising peak interferences and hence facilitated the database search for protein identification. Several peptide signals were identified as type I collagen which was found with a high signal intensity within tumour tissue cores. These results confirm previous studies which described an up-regulation of type I collagen in pancreatic cancer cells which promotes the proliferation of cancer cells [17]. Tumour necrosis factor receptor (TNFR) was also identified in the pancreatic TMA. It has been reported that tumour necrosis factor was found to be over-expressed in patients with pancreatic cancer and that it is involved in metabolic changes associated with cancer [18]. However, further analyses are required in order to explain these findings and to correlate them with clinical information.

It can be noticed that although about 300 MS/MS spectra were acquired for protein identification, only about 100 signals have been identified to date; numerous peptides remained unidentified following MS/MS analyses and protein database searches. This can be explained by existing post-translational modifications as well as protein variants. Method improvements including *de novo* sequencing are required in order to identify these modifications and identify further proteins.

FFPE pancreatic cancer tissue sections were also investigated with MALDI-IMS-MSI. Using the characteristic peptides of the tumour region highlighted by the statistical analysis, the results were in good agreement with those obtained with histological staining in terms of located tumour regions.

The outline strategy described here allowed the rapid screening of the distribution of peptides and their identification after *in situ* digestion of FFPE pancreatic tumour tissue micro-array sections using MALDI-ion mobility separation- mass spectrometry profiling and imaging. The results obtained from the statistical analysis of the direct peptide imaging of TMA sections demonstrated that a novel tumour classification model based on direct proteome information is feasible. However a large number of samples with more detailed clinical information including survival, time to recurrence and chemoresponsiveness are required. Here one of the limitations of the study has been that only limited clinical information is obtained with a commercial TMA. Even so, this enabled the establishment of a methodology for molecular tumour classification using MALDI-MSI and PCA-DA.

References

[1] Wang J., Bo T.H., Jonassen I., Myklebost O., and Hovig E. Tumor classification and marker gene prediction by feature selection and fuzzy c-means clustering using microarray data. *BioMed Central Bioinformatics*, 4:60–71, 2003.

[2] Demichelis F., Magni P., Piergiorgi P., Rubin M.A., and Bellazzi R. A hierarchical Naive Bayes Model for handling sample heterogeneity in classification problems: an application to tissue microarrays. *BioMed Central Bioinformatics*, 7:514–525, 2006.

[3] Abd El-Rehim D.M., Ball G., Pinder S.E., Rakha E., Paish C., Robertson J.F., Macmillan D., Blamey R.W., and Ellis I.O. High-throughput protein expression analysis using tissue microarray technology of a large well-characterised series identifies biologically distinct classes of breast cancer confirming recent cDNA expression analyses. *International Journal of Cancer*, 116:340–350, 2005.

[4] Battifora H. and Mehta P. The checkerboard tissue block. An improved multitissue control block. *Laboratory Investigation*, 63:722–724, 1990.

[5] Kononen J., Bubendorf L., Kallioniemi A., Barlund M., Schraml P., Leighton S., Torhorst J., Mihatsch M.J., Sauter G., and Kallioniemi O.P. Tissue microarrays for high-throughput molecular profiling of tumor specimens. *Nature Medicine*, 4: 844–847, 1998.

[6] Rosen D.G., Huang X., Deavers M.T., Malpica A., Silva E.G., and Liu J. Validation of tissue microarray technology in ovarian carcinoma. *Modern Pathology*, 17:790–797, 2004.

[7] Kleiner H.E., Krishnan P., Tubbs J., Smith M., Meschonat C., Shi R., Lowery-Nordberg M., Adegboyega P., Unger M., Cardelli J., Chu Q., Mathis J.M., Clifford J., De Benedetti A., and Li B.D. Tissue microarray analysis of eIF4E and its downstream effector proteins in human breast cancer. *Journal of Experimental and Clinical Cancer Research*, 28:5–15, 2009.

[8] Chaurand P., Schwartz S.A., and Caprioli R.M. Assessing protein patterns in disease using imaging mass spectrometry. *Journal of Proteome Research*, 3:245–252, 2004.

[9] Stoeckli M., Staab D., Schweitzer A., Gardiner J., and Seebach D. Imaging of a beta-peptide distribution in whole-body mice sections by MALDI mass spectrometry. *Journal of The American Society for Mass Spectrometry*, 18:1921–1924, 2007.

[10] Reyzer M.L., Caldwell R.L., Dugger T.C., Forbes J.T., Ritter C.A., Guix M., Arteaga C.L., and Caprioli R.M. Early changes in protein expression detected

by mass spectrometry predict tumor response to molecular therapeutics. *Cancer Research*, 64:9093–9100, 2004.

[11] Groseclose M.R., Massion P.P., Chaurand P., and Caprioli R.M. High-throughput proteomic analysis of formalin-fixed paraffin-embedded tissue microarrays using MALDI imaging mass spectrometry. *Proteomics*, 8:3715–3724, 2008.

[12] Djidja M., Carolan V., Loadman P.M., and Clench M.R. Method development for protein profiling in biological tissues by matrix-assisted laser desorption/ionisation mass spectrometry imaging. *Rapid Communication in Mass Spectrometry*, 22:1615–1618, 2008.

[13] Trim P.J., Atkinson S.J., Princivalle A.P., Marshall P.S., West A., and Clench M.R. Matrix-assisted laser desorption/ionisation mass spectrometry imaging of lipids in rat brain tissue with integrated unsupervised and supervised multivariant statistical analysis. *Rapid Communication in Mass Spectrometry*, 22:1503–1509, 2008.

[14] Deininger S.O., Ebert M.P., Futterer A., Gerhard M., and Rocken C. MALDI imaging combined with hierarchical clustering as a new tool for the interpretation of complex human cancers. *Journal of Proteome Research*, 7:5230–5236, 2008.

[15] Hoogerbrugge R., Willig S.J., and Kistemaker P.G. Discriminant analysis by double stage principal component analysis. *Analytical Chemistry*, 55:1710–1712, 1983.

[16] Neoptolemos J.P., Dunn J.A., Stocken D.D., Almond J., Link K., Beger H., Bassi C., Falconi M., Pederzoli P., Dervenis C., Fernandez-Cruz L., Lacaine F., Pap A., Spooner D., Kerr D.J., Friess H., and Buchler M.W. Adjuvant chemoradiotherapy and chemotherapy in resectable pancreatic cancer: a randomised controlled trial. *Lancet*, 358:1576–1585, 2001.

[17] Armstrong T., Packham G., Murphy L.B., Bateman A.C., Conti J.A., Fine D.R., Johnson C.D., Benyon R.C., and Iredale J.P. Type I collagen promotes the malignant phenotype of pancreatic ductal adenocarcinoma. *Cancer Research*, 10:7427–7437, 2004.

[18] Ariapart P., Bergstedt-Lindqvist S., van Harmelen V., Permert J., Wang F., and Lundkvist I. Resection of pancreatic cancer normalizes the preoperative increase of tumor necrosis factor alpha gene expression. *Pancreatology*, 2:491–494, 2002.

CHAPTER 7

Continuous Rastering Imaging and Multiple Reaction Monitoring MALDI-MS Imaging using a 20 kHz Repetition Rate Laser

7.1 Introduction

Molecular imaging is one of the techniques of choice to investigate the complexity of the spatial localisation of proteins contained in biological tissue sections. MALDI-mass spectrometry is becoming a translational research tool with the potential to be used in clinical studies as it allows the study of the distribution of several compounds including peptides and proteins directly within tissue sections and hence provides molecular insights into the complexities of biological processes. However, in order for the technique to be fully established as a routine tool and to be used at the optimum of its performance, several limitations associated with the currently available instrumentation need to be overcome and resolved [1, 2]. Among these limitations are those which are associated with the spatial resolution of the image, the sensitivity and the data acquisition time.

Improvements in mass spectrometry instrumentation have resulted in enhanced mass accuracy and resolution as well as sensitivity and data acquisition time. Hence MS technologies are often used for high throughput analysis in several fields, including proteomics [3]. In the case of MALDI-MS, these improvements include the design of new laser technologies as well as electronics and optics devices [4–7]. The laser type is a key feature to take into account for MALDI-MSI experiments as it influences the amount of ions generated in the source, the image resolution and also the data acquisition time [2, 6]. Common standard nitrogen (N_2) lasers are being replaced by solid-state lasers for MALDI-MS profiling and imaging experiments. Traditional N_2 lasers provide a high energy power, however they operate at a shot-to-shot repetition rate comprised of 1-30 Hz [4]. Since several laser shots, typically between 100 and 1000, are required to generate spectra per position during a MALDI-MS image acquisition, this can result in data acquisition times of several hours, up to 60 hours in some cases, depending on the tissue section area to be analysed [2] and the spatial resolution required. Orthogonal MALDI-TOFMS (o-MALDI-TOFMS) instrument geometries have the ability to operate at 10 kHz which allows the detection of a continuous ion beam from the source, hence considerably enhancing the sensitivity. However this capacity is limited when using standard N_2 lasers which have a repetition rate of 1-30 Hz.

The introduction of solid-state lasers, which have a higher repetition rate (between 1 and 10 kHz) than standard N_2 lasers, has been shown to improve high throughput MS and MALDI-MS imaging data acquisition by enhancing the ion yield and hence the signal intensity, while maintaining data quality in terms of mass accuracy and sensitivity [4]. The use of Nd:YAG (neodymium-doped yttrium aluminium garnet; Nd:$Y_3Al_5O_{12}$) lasers has been reported as an improvement in MALDI-MSI instrumentation [8–10]. Nd:YAG lasers have a long lifetime, good reproducibility and high repetition rate compared to N_2 lasers. Smartbeam^{TM} (Bruker Daltoniks, Bremen, Germany) laser technology has been reported and allows modulation of the Nd:YAG laser beam over the tissue surface [8]. This results in a more focused laser beam with a laser pulse which has been found to be compatible with a wide range of matrices and increases ionisation of several compounds. 1 kHz repetition rate Nd:YAG lasers have also been described to be used in a dynamic pixel mode which involves a figure of eight movement of the focused laser beam within each spot, thus allowing the desorption of several analytes [11]. Using high repetition rate solid state lasers can result in improved image sensitivity and resolution as well as allowing fast data acquisition. Recently, the use of continuous laser ablation rastering across the tissue section has been shown to reduce considerably MALDI-MS imaging data acquisition time, while preserving an acceptable image resolution and sensitivity [12].

The aims of this chapter are to evaluate a 20 kHz repetition rate solid-state laser for performing continuous laser raster MALDI-MS imaging and multiple reaction monitoring MALDI-MS imaging (MRM-MALDI-MSI) of peptides after *in situ* digestion of tumour tissue sections. The MRM-MALDI-MSI analysis of peptides directly within *in situ* digested tissue sections, described in this work, has demonstrated a novel proof-of-principle which combines the dynamic pixel scanning mode capability offered by the instrument with MRM analysis and may allow specific images of monitored peptide fragments. This may improve the sensitivity of the MALDI-MSI methodology and as well as provide an approach to relative quantification of peptide signals within directly within tissue sections. The current limitations and advantages of the methodologies employed are discussed.

7.2 Materials and Methods

7.2.1 Materials

Modified sequence grade trypsin was purchased from Promega (Southampton, UK). All other materials, including alpha-cyano-4-hydroxycinnamic acid (α-CHCA), aniline (ANI), ethanol (EtOH), methanol (MeOH), chloroform ($CHCl_3$), xylene, octyl-α/β-glucoside (OcGlc), trifluoroacetic acid (TFA), haematoxylin, eosin, hydrogen peroxide (H_2O_2), tri-sodium citrate and ammonium bicarbonate were purchased from Sigma-Aldrich (Dorset, UK).

7.2.2 Tissue samples

7.2.2.1 Rat brain tissue samples

Rat brain samples were obtained from the Sheffield Hallam University laboratory (Biomedical Research Centre, Sheffield Hallam University, Sheffield, UK) directly after animal sacrifice. Samples were immediately snap-frozen in liquid nitrogen and stored at -80°C to minimize protein degradation through enzymatic proteolysis and to preserve the sample morphology.

7.2.2.2 Human formalin fixed paraffin embedded (FFPE) pancreatic tumour samples

Following fully informed patient consent and full ethical committee approval anonymised 5 μm *ex vivo* human FFPE pancreatic tumour tissue sections were obtained (Study Number SSREC/04/Q2305/67 and subsequent amendments). Tissue samples were fixed in 10% buffered formalin for 24 hours, dehydrated in 70% EtOH and paraffin embedded. 5 μm sections were cut using a cryostat (Leica Microsystems, UK) and mounted onto histological Polysine^{TM} glass slides (Menzel-Glaser, Germany). FFPE tissue sections were stored at room temperature until further analysis.

7.2.3 Tissue preparation

Frozen rat brain tissue samples were cut using a cryostat (Leica Microsystems, UK) operating at -20°C. 10 μm sections were cut and thaw-mounted onto histological Polysine^{TM} glass slides (Menzel-Glaser, Germany). Washing procedures were per-

formed to increase the MS data quality: the rinsing steps consisted of immersing the section for 1 min in cold ethanol solutions (stored at -20°C) at 70 and 90% followed by a 30 second wash in chloroform ($CHCl_3$). Sections were then allowed to dry at room temperature before digestion and matrix deposition.

Prior to on-tissue digestion and matrix deposition, FFPE pancreatic tumour tissue sections were prepared as described in chapters 5 and 6 (sections 5.2.3 and 6.2.3).

7.2.4 Trypsin and matrix deposition

Trypsin solution was made at 20 μg/ml in 50 mM ammonium bicarbonate buffer (pH = 8.1) containing 0.1 % octyl glucoside (OcGlc). The methods used for *in situ* digestion of both frozen rat brain and FFPE pancreatic tumour tissue sections were the same as described in chapter 5 (section 5.2.3.1) using a SunCollect^{TM} automatic sprayer (SunChrom, Friedrichsdorf, Germany).

α-CHCA mixed with aniline (α-CHCA/ANI), prepared at 5 mg/ml in 50% ACN:0.2% TFA, was used as the matrix for peptide analysis. The matrix deposition onto the tissue sections was performed using a SunCollect^{TM} automatic sprayer (SunChrom, Friedrichsdorf, Germany).

7.2.5 Direct MALDI-MSI analysis

MALDI-MSI experiments were performed using a modified Q-Star® Pulsar *i* quadrupole time-of-flight mass spectrometer (Applied Biosystems/MDS Sciex, Concord, Ontario, Canada) fitted with an oMALDI^{TM} 2 (Applied Biosystems/MDS Sciex, Concord, Ontario, Canada) orthogonal MALDI source. The original laser was replaced with a 20 kHz repetition rate solid state yttrium vanadate (Nd:YVO_4) laser (Elforlight Ltd, Daventry, UK). The Nd:YVO_4 laser was used at a power of 2.9 μJ and a repetition rate of 5 kHz. Areas of the tissue sections to be imaged were defined using oMALDI^{TM} Server 5.1 software (Applied Biosystems/MDS Sciex, Concord, Ontario, Canada). Prior to data acquisition, instrument calibration was performed using a standard mixture of peptides (Applied Biosystems/MDS Sciex, Concord, Ontario, Canada) ranging from m/z 900 to 1800. Data acquisition was performed in the mass range m/z 800 to 2000. Images were obtained with a spatial resolution of 150μm X 150μm using Raster image^{TM} acquisition with a slow speed setting. Ion images were processed using oMALDI^{TM} Server 5.1

software (Applied Biosystems/MDS Sciex, Concord, Ontario, Canada).

7.2.6 MRM-MALDI-MS imaging data acquisition

In order to perform MRM experiments, the m/z value of the compound of interest, here the peptide, must be known as well as its fragment ions and hence their MS/MS fragmentation patterns [13]. MS/MS analyses were performed on some peptides in order to define the collision-induced dissociation (CID) parameters which should be used for the MRM analysis. In the MS/MS method used here, the collision energy and the collision gas were set at 90 and 20 respectively. MS/MS peptide sequencing was performed with a quadrupole operating at a low resolution. MRM-MALDI-MSI data acquisition was achieved using the same CID parameters as for the MS/MS analyses, enhancing the signal response in the desired mass range for MRM scanning. MRM-MALDI-MS images were acquired at 400 μm spatial resolution in a spot-to-spot acquisition mode with dynamic pixel. In the work reported here, based on direct MALDI-MS/MS analyses performed on human FFPE pancreatic tumour tissue sections (described in chapters 5 and 6), 8 peptide mass signals, identified as arising from several proteins including actin, glucose-regulated protein 78 kDa (Grp78), haemoglobin alpha and beta, histone H2A, pancreatic alpha-amylase, periostin and tumour necrosis factor receptor, were selected for MRM screening.

7.3 Results and Discussion

7.3.1 MALDI-MS raster imaging with a 20 kHz repetition rate laser

Conventional MALDI-MSI experiments performed in microprobe mode involve a spot-to-spot laser ablation across the tissue section, so that mass spectra are recorded from an individual position during a certain accumulation time followed by a switch off of the laser while the plate stage is moved to the adjacent position. This results in a spot-to-spot data acquisition, where the distance between laser spot centres defines the image resolution. High resolution MALDI-MS images have been produced using this method, however the observed data acquisition time was very long, up to 55 hours in some cases [2]. Here, MALDI-MS images of peptide localisation were obtained within a frozen rat brain tissue section after *in situ* digestion using a continuous laser raster imaging mode. Figure 7.1 shows the distribution of peptide signals within the tissue section. Images were normalised against the matrix peak at m/z 1066.

For the acquisition of the images shown in figure 7.1, the continuous laser rastering imaging mode was performed at a fast speed setting. This was found to considerably decrease the sensitivity and also produced dead pixels in the resulting images. However, the advantage of using a high repetition rate laser is demonstrated here as the images produced of peptide localisation within the tissue section allowed the discrimination of regions associated with the rat brain morphology. Even if a poor resolution was observed, it can be noticed that the peptide signal at m/z 1274 (figure 7.1f), which has been identified as arising from haemoglobin beta, was found to be localised at the edge of the tissue section where blood was observed after animal sacrifice.

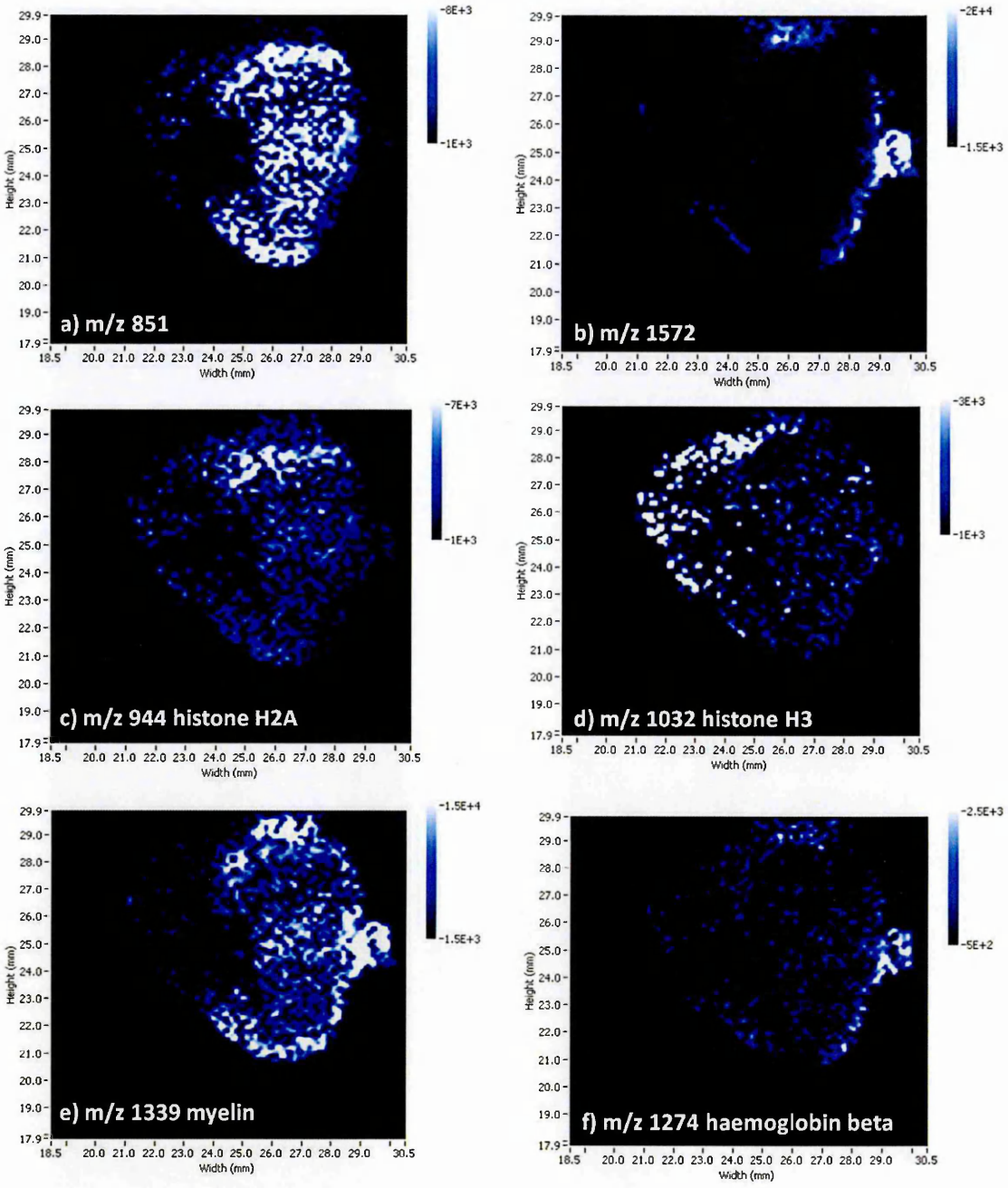

Figure 7.1: **Images of peptide distribution within a frozen rat brain tissue section obtained with MALDI-MS raster imaging after *in situ* digestion.** A 20 kHz repetition rate laser was used for continuous laser raster imaging. The distribution of several peptide signals, including (a) m/z 851, (b) m/z 1572, (c) histone H2A, (d) histone H3, (e) myelin and (f) haemoglobin beta, within the tissue section was obtained.

FFPE pancreatic tumour tissue sections were also imaged using a continuous laser raster imaging mode. Figure 7.2 displays the obtained MALDI-MS raster images of peptide distribution within an *in situ* digested FFPE pancreatic tumour tissue section. The localisations of the actin, histone H2A, tumour necrosis factor receptor and haemoglobin beta and alpha within the tissue section were shown.

Here, continuous laser raster imaging was performed at a slow speed setting, so that dead pixels were not observed in the obtained images. Using a slow speed laser raster was also found to improve the signal sensitivity when compared to the images obtained at a fast speed laser setting. It can also be noticed that the resulting peptide images were comparable to those obtained using a MALDI SYNAPT^{TM}HDMS system (Waters Corporation, Manchester, UK) in terms of observed signal distribution (chapters 5 and 6). However, the data acquisition time for the MALDI-MS raster images was approximately 1h30 compared to 8 hours when performing spot-to-spot imaging, acquired at spatial resolution of 200 μm using a MALDI SYNAPT^{TM}HDMS system (Waters Corporation, Manchester, UK) fitted with a 200 Hz ND:YAG laser. Imaging and profiling data resulting from MALDI-MSI analysis of *in situ* digested FFPE tissue sections often present poor S/N ratio as well as poor signal sensitivity. Here, the obtained S/N ratio and signal sensitivity allowed the generation of acceptable images of the localisation of peptide within *in situ* digested FFPE tissue sections using continuous laser raster imaging data acquisition.

Using a 20 kHz repetition rate laser for continuous laser raster MALDI-MSI allowed fast screening of the tissue sections for peptide analysis after *in situ* digestion and the generation of their distributions within the tissue section, while maintaining an acceptable data quality in terms of S/N ratio and sensitivity. Such an approach can be used prior to acquisition of high resolution images using conventional (i.e. spot-to-spot) MALDI-MSI data acquisition. It can also be used in order to highlight regions of interest within the tissue sections and perform further more specific, sensitive and quantitative MALDI-MS imaging such as multiple reaction monitoring analyses.

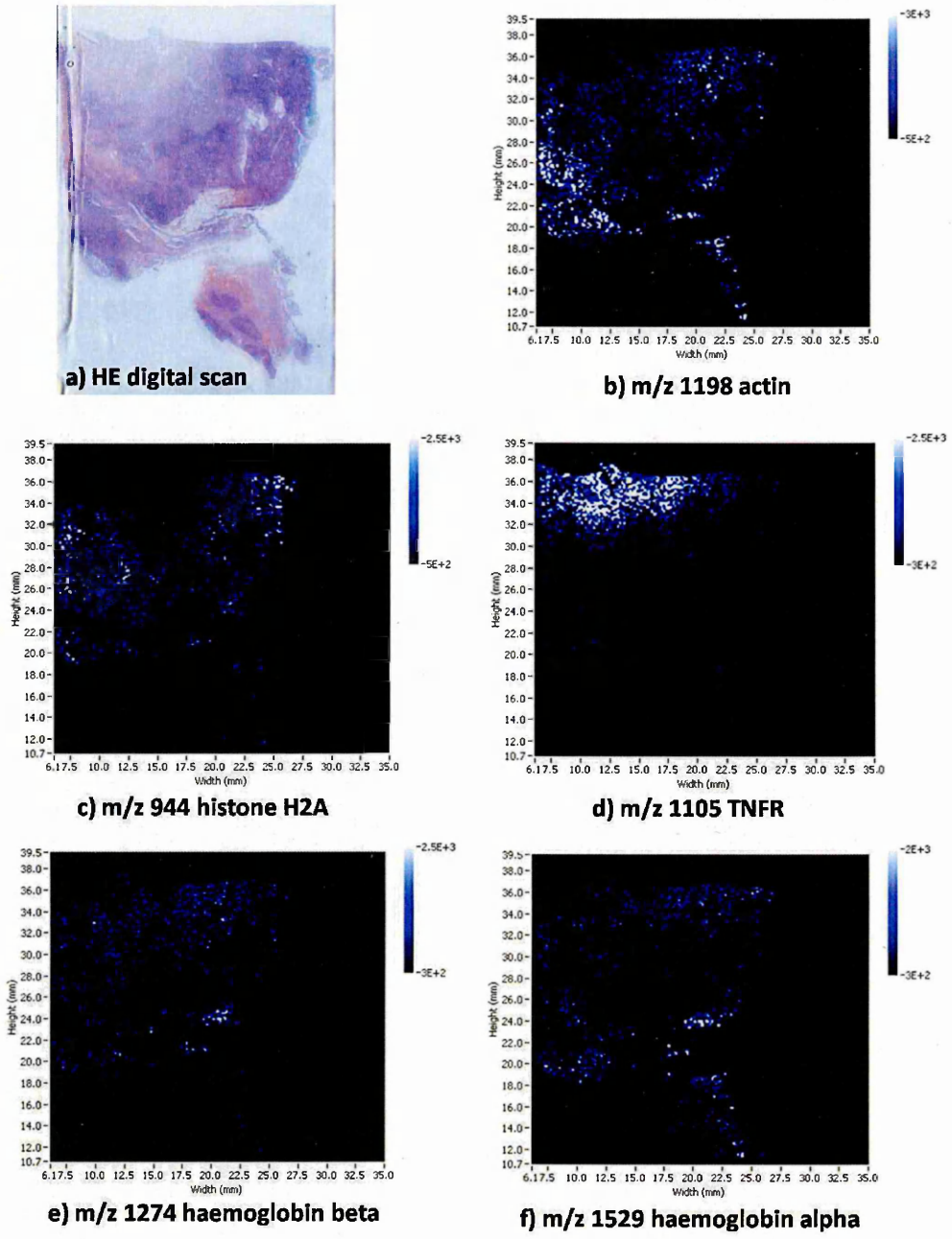

Figure 7.2: **Digital scan of a FFPE pancreatic tumour tissue section after HE staining and images of peptide distribution within this tissue section obtained with MALDI-MS raster imaging after *in situ* digestion.**
(a) Digital scan of a FFPE pancreatic tumour tissue section after HE staining . A 20 kHz repetition rate laser was used for continuous laser raster imaging. The distribution of several peptide signals, including (b) actin, (c) histone H2A, (d) tumour necrosis factor receptor, (e) haemoglobin beta and (f) haemoglobin alpha, within the tissue section was obtained.

7.3.2 MRM MALDI-MS imaging screening of peptides directly within *in situ* digested FFPE pancreatic tumour tissue sections

7.3.2.1 Evaluation of MALDI-MS/MS analysis directly within *in situ* digested FFPE pancreatic tumour tissue sections using a 20 kHz repetition rate laser

One of the requirements for MRM analysis is that the m/z values of the compounds of interest and significant product ions are known. The high repetition rate laser was evaluated for on-tissue MS/MS analysis. The peptide signal at m/z 944, which was identified as arising from histone H2A using a MALDI SYNAPT^{TM}HDMS system (Waters Corporation, Manchester, UK), was sequenced using tandem MS with a 10kHz repetition rate solid-state laser. Figures 7.3 and 7.4 display the obtained MS/MS spectra using each instrument respectively.

Good sequence coverage was observed. When comparing the spectrum in figure 7.3 to the MS/MS spectrum of the peptide at m/z 944 (figure 7.4) obtained using a MALDI SYNAPT^{TM} HDMS system (Waters Corporation, Manchester, UK), identical fragmentation patterns were observed.

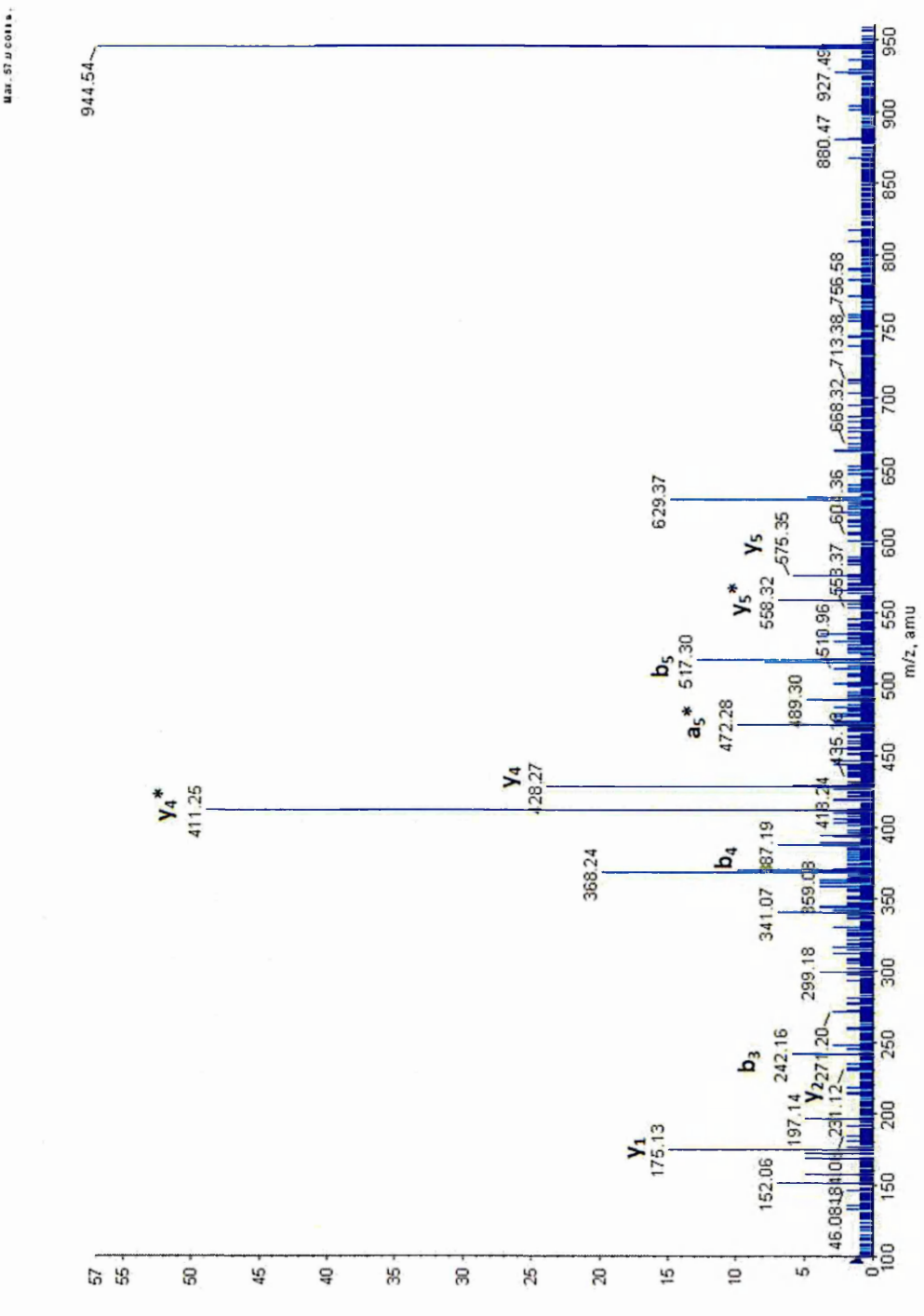

Figure 7.3: **MALDI-MS/MS spectrum of the peptide signal at m/z 944 obtained directly after *in situ* digestion of a FFPE pancreatic tissue section using a Q-Star® Pulsar *i* QTOF MS instrument fitted with a 20 kHz repetition rate laser.** A good fragmentation pattern was observed: a, b and y ions are displayed.

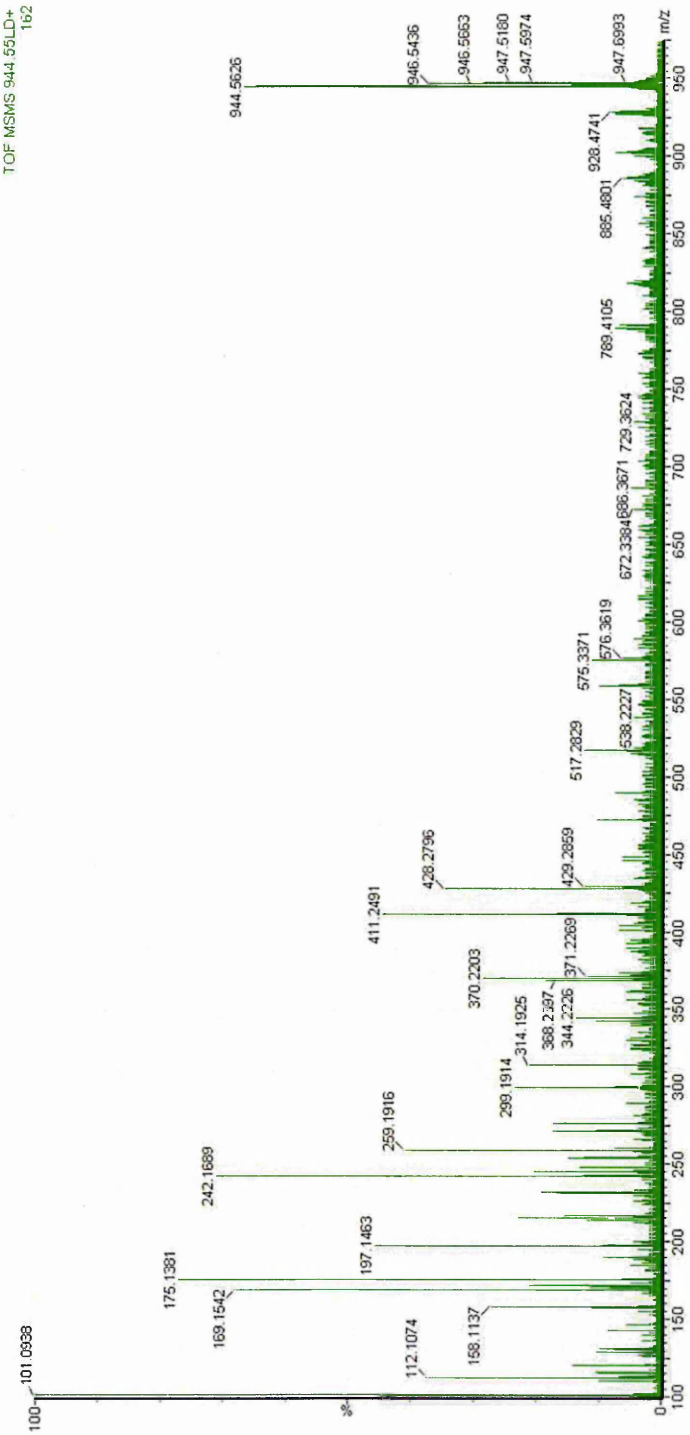

Figure 7.4: **MALDI-MS/MS spectrum of the peptide signal at m/z 944 obtained directly after *in situ* digestion of a FFPE pancreatic tissue section using a MALDI SYNAPT^{TM} HDMS system.**

Using MS/MS data obtained with a MALDI SYNAPT^{TM}HDMS system (Waters Corporation, Manchester, UK), as described in previous chapters including chapters 5 and 6, eight peptide precursor ions, with their corresponding most intense product ions present in the MS/MS spectrum, were selected for MRM-MALDI-MSI analysis. Table 7.1 displays a list of the selected peptide signals and their corresponding product ions: a total of 26 transitions were plotted.

Protein name/ Accession number	Peptide m/z	Fragment ions
Histone H2A.Z/ P0C0S5	944.53	370. 21 b_4 411. 25 y_4* 428.28 y_4 575.33 y_5
Tumor necrosis factor receptor/ O00220	1105.64	436.23 b_5* 493.25 b_6* 650.37 d_8
Actin, aortic smooth muscle/ P62736	1198.72	272.17 y_2 468.27 y_4 615.35 b_6
Haemoglobin beta/ P68871	1274.73	227.18 b_2 326.85 b_3 670.34 y_5*
Periostin/ Q15063	1400.78	327.21 b_4 416.26 y_4 771.50 y_7
78 kDa glucose-regulated protein (Grp78)/ P11021	1934.01	367.14 b_3 520.29 b_4 537.32 y_5 921.57 y_9
Haemoglobin alpha/ P69905	1529.74	365.2 b_4 436.23 b_5 622.30 b_7
Pancreatic alpha-amylase/ P04746	1427.70	783.35 y_6 417.23 y_3 284.20 b_3

Table 7.1: **List of peptide masses used for MRM-MALDI-MSI analysis of FFPE pancreatic tumour tissue sections.**
Peptide signals are listed in the order of monitored reactions. Note: y* or b* represent y or b ions with a loss of H_2O

7.3.2.2 MRM-MALDI-MS Imaging of peptides within *in situ* digested FFPE pancreatic tumour tissue sections using a 20 kHz repetition rate laser

MRM is a sensitive and specific MS scanning approach. To perform MRM, precursor ions and their corresponding product ions, collectively called transitions, are selected and each MS scan monitors a specific transition [13]. Such an approach can be very beneficial for the investigation of peptide distribution within the tissue section using MALDI-MSI as it may lead to specific and sensitive data acquisition, since it reflects an amino acid sequence of a given peptide. In the work reported here, the use of a 20 kHz repetition rate laser may improve data quality and acquisition time for such analysis.

In a first approach, MRM-MALDI-MSI analyses of selected peptides were acquired at 250 μm spatial resolution using a 20 kHz repetition rate Nd:YVO_4 laser. Figure 7.5 displays the localisation of histone H2A and haemoglobin beta within a FFPE pancreatic tissue section.

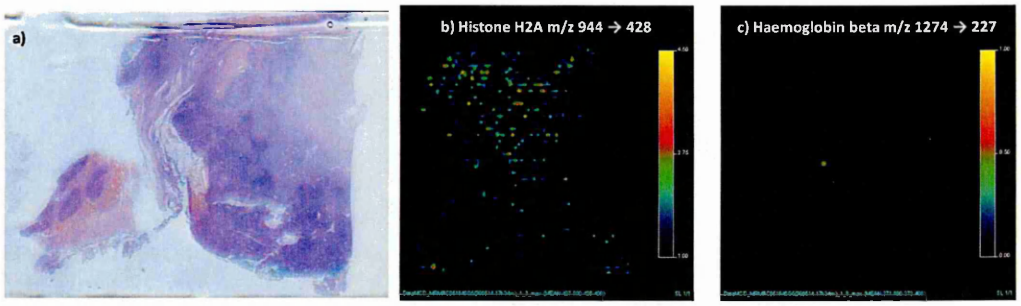

Figure 7.5: **Images of peptide distribution within a FFPE pancreatic tissue section obtained with MRM-MALDI-MS imaging without using dynamic pixel option after *in situ* digestion.**
A 20 kHz repetition rate laser was used for MRM-MALDI-MS imaging data acquisition. (a) Digital scan of a FFPE pancreatic tissue section obtained after HE staining. The distribution of peptide transitions, including (b) histone H2A (m/z 944 → 428) and (c) haemoglobin beta (m/z 1274 → 227) was obtained. Images were acquired at 250 μm spatial resolution. A poor signal sensitivity was noticed as the dynamic pixel operating mode was not used.

The transitions of histone H2A peptide signal at m/z 944 to 428 and haemoglobin beta peptide ion at m/z 1274 to 227 are shown. A considerable loss of sensitivity was noticed for the transition of haemoglobin beta tryptic peptide ion at m/z 1274 to 22. Here, when acquiring images at 250 μm spatial resolution, it was not possible to have the high repetition rate laser operating in the dynamic pixel mode. This resulted in a complete ablation of each pixel across the tissue section for only the first transition monitored.

Using a 20 kHz repetition rate laser in the dynamic pixel mode may improve the detection and sensitivity of each selected transition. However, it is currently impossible to use the dynamic pixel mode with the modified Q-Star® Pulsar *i* QTOF instrument (Applied Biosystems/MDS Sciex, Concord, Ontario, Canada) fitted with a 20 kHz repetition rate Nd:YVO_8 laser when acquiring an image at a spatial resolution higher than 400 μm. This current limitation is related to the software settings. However, in order to assess if such an analytical method can be used for fast, specific and sensitive *in situ* identification and localisation of peptide within on-tissue digested tissue sections, MRM-MALDI-MSI was performed at 400 μm. Figure 7.6 displays the obtained images.

The images were obtained at a low spatial resolution, however an improved sensitivity was observed since the localisation of several peptide transitions are displayed in figure 7.6. This showed that the use of a high repetition rate laser in dynamic pixel mode allowed an improved detection and sensitivity of targeted peptides within *in situ* digested tumour tissue sections. This demonstrates a novel proof-of-principle and that such a methodology is feasible. However, further software and method improvement are required for the method to be used at its optimum.

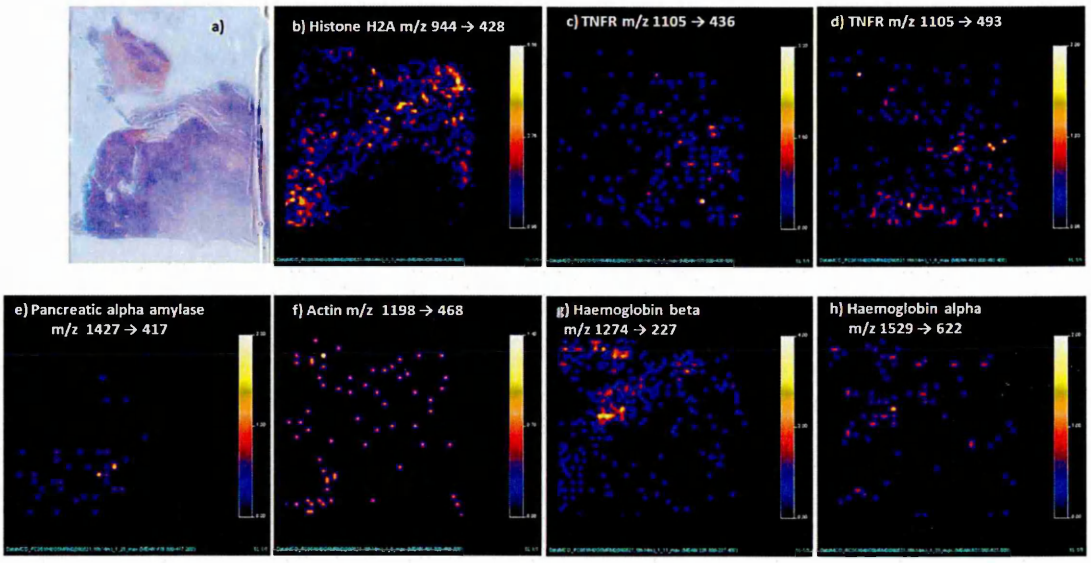

Figure 7.6: **Images of peptide distribution within a FFPE pancreatic tissue section obtained with MRM-MALDI-MS imaging using the dynamic pixel option after *in situ* digestion.**
A 20 kHz repetition rate laser was used for MRM-MALDI-MS imaging data acquisition. (a) Digital scan of a FFPE pancreatic tissue section obtained after HE staining. The distribution of peptide transitions, including (b) histone H2A (m/z 944 → 428), (c, d) tumour necrosis factor receptor (m/z 1105 → 436, 493), (e) pancreatic alpha amylase (m/z 1427 → 417), (f) actin (m/z 1198 → 468), (g) haemoglobin beta (m/z 1274 → 227) and (h) haemoglobin alpha (m/z 1529 → 622) was obtained. Images were acquired at 400 μm spatial resolution. An improved signal sensitivity was noticed as the dynamic pixel operating mode was used here.

7.4 Concluding Remarks

MALDI-MS imaging is now demonstrating its potential for studying peptide distribution within tissue sections and allowing *in situ* protein identification while providing spatial distribution information within the tissue sections. Developments in instrumentation and methodology are currently being made in order to improve MALDI-MS image spatial resolution, thereby achieving cellular resolution while maintaining high sensitivity and specificity. MALDI-MS image resolution is currently limited by several factors, including the laser irradiation spot size and the matrix coverage method. Studies have reported the achievement of high resolution images using various methodologies including oversampling [14], reduction of the laser irradiation spot [6] as well as improvements in matrix coverage methods [15, 16]. However, in some cases, high resolution MALDI-MS images were obtained at the expense of loss in signal sensitivity and/or long data acquisition time. Therefore, the laser repetition rate is a key factor to take into account as it may improve signal sensitivity and/or reduce data acquisition time.

In the work reported here, using a 20 kHz repetition rate laser for continuous laser raster imaging enabled fast data acquisition but also acceptable signal detection and sensitivity. By defining an optimum speed for the laser raster across the tissue sections, images of the distribution of peptides within *in situ* digested tissue sections were generated and enabled tumour regions within a FFPE pancreatic tissue section to be highlighted. Improved MALDI-MS image spatial resolution has been reported using continuous laser raster MALDI-MS imaging data acquisition [12]. However, in the work reported here, improvement of image resolution was not observed, but the obtained signal sensitivity allowed detection and discrimination between tissue regions. This methodology can be used to perform rapid tissue section screening prior to the acquisition of high resolution images using a spot-to-spot laser ablation.

Additionally, a proof-of-concept was described by means of MRM-MALDI-MSI analysis of peptides after *in situ* digestion of FFPE tumour tissue sections. Such an approach has not been reported before. MRM is one of the most sensitive MS analysis methodologies as it allows fast, sensitive and specific detection as well as quantification of compounds present in a given sample [13]. Here, MRM has been used in combination with MALDI-MSI using a 20 kHz repetition rate Nd:YVO_4 laser. This demonstrated that a more specific approach to targeting and studying the distribution of a given protein or tumour marker within the tissue section can be achieved, since pre-selected transitions from a peptide, hence from a specific amino acid sequence, are monitored and imaged directly from the tissue section after *in situ* digestion. The use of a high repetition rate laser has been found to improve signal sensitivity.

In summary, in this chapter, specific and targeted methodologies were described using MALDI-MSI technologies, showing other potentials of the technique as a biomarker discovery tool.

References

[1] Heeren R.M.A., Smith D.F., Stauber J., Kkrer-Kaletas B., and MacAleese L. Imaging Mass Spectrometry: Hype or Hope? *Journal of the American Society for Mass Spectrometry*, 20:1006–1014, 2009.

[2] Goodwin R.J., Pennington S.R., and Pitt A.R. Protein and peptides in pictures: Imaging with MALDI mass spectrometry. *Proteomics*, 8:3785–3800, 2008.

[3] Mann M. and Kelleher N.L. Precision proteomics: the case for high resolution and high mass accuracy. *Proceedings of the National Academy of Sciences*, 105: 18132–18138, 2008.

[4] McLean J.A., Russell W.K., and Russell D.H. A high repetition rate (1 kHz) microcrystal laser for high throughput atmospheric pressure MALDI-quadrupole-time-of-flight mass spectrometry. *Analytical Chemistry*, 75:648–654, 2003.

[5] Moskovets E., Preisler J., Chen H.S., Rejtar T., Andreev V., and Karger B.L. High-throughput axial MALDI-TOF MS using a 2-kHz repetition rate laser. *Analytical Chemistry*, 78:912–919, 2006.

[6] Chaurand P., Schriver K.E., and Caprioli R.M. Instrument design and characterization for high resolution MALDI-MS imaging of tissue sections. *Journal of Mass Spectrometry*, 42:476–489, 2007.

[7] Wisztorski M., Lemaire R., Stauber J., Menguelet S.A., Croix D., Math O.J., Day R., Salzet M., and Fournier I. New developments in MALDI imaging for pathology proteomic studies. *Current Pharmaceutical Design*, 13:3317–3324, 2007.

[8] Holle A., Haase A., Kayser M., and Hohndorf J. Optimizing UV laser focus profiles for improved MALDI performance. *Journal of Mass Spectrometry*, 41:705–716, 2006.

[9] Claude E., Snel M., McKenna T., and Langridge J. Direct tissue imaging and characterization of phospholipids using MALDI SYNAPT HDMS system. Technical report, Waters, 2008.

[10] Djidja M.C., Francese S., Loadman P.M., Sutton C.W., Scriven P., Claude E., Snel M.F., Franck J., Salzet M., and Clench M.R. Detergent addition to tryptic digests and ion mobility separation prior to MS/MS improves peptide yield and protein identification for *in situ* proteomic investigation of frozen and formalin-fixed paraffin-embedded adenocarcinoma tissue sections. *Proteomics*, 9:2750–2763, 2009.

[11] Applied Biosystems. Multiplexing MALDI Mass Spectrometry Imaging using Dynamic Pixel Imaging. Technical report, Applied Biosystems/MDS Siex, 2007.

[12] Simmons D.A. Improved MALDI-MS imaging performance using continuous laser rastering. Technical report, MDS Analytical Technologies, 2008.

[13] Yang X. and Lazar I.M. MRM screening/biomarker discovery with linear ion trap MS: a library of human cancer-specific peptides. *BioMed Central Cancer*, 9:96–106, 2009.

[14] Jurchen J.C., Rubakhin S.S., and Sweedler J.V. MALDI-MS imaging of features smaller than the size of the laser beam. *Journal of the American Society for Mass Spectrometry*, 16:1654–1659, 2005.

[15] Aerni H., Cornett D.S., and Caprioli R.M. Automated acoustic matrix deposition for MALDI sample preparation. *Analytical Chemistry*, 78:827–834, 2006.

[16] Schuerenberg M., Luebbert C., Deininger S.O., Mueller R., and Suckau D. A new matrix application device for MALDI tissue imaging. Technical report, Bruker Daltonics, 2007.

CHAPTER 8

Conclusion and Further Work

Changes in protein expression and profile patterns are observed in several diseases including cancers and are used to discriminate between healthy and cancerous tissues as well as between classes of cancers. Improvements in mass spectrometry instrumentation have led to it being widely used for high-throughput analysis in order to characterise potential biomarkers that can help in cancer research.

MALDI-MSI techniques represent an enormous development and improvement in MS imaging technologies. In fact, MALDI-MSI is becoming a novel translational approach for cancer biomarker discovery since it allows the study of the distribution and the identification of proteins directly within tumour tissue sections with no requirement for pre-defined targets. The aim of this thesis was to develop efficient methodologies, which addressed sample preparation, instrumentation and data acquisition issues, in order to apply MALDI-MSI to protein biomarker targeting and discovery directly within tumour tissue sections.

The use of MALDI-MSI for direct analysis of proteins within tumour tissue sections was achieved by optimising tissue section washing protocols, the composition of matrix solutions and matrix deposition. However, other solvents should be investigated for tissue section washing prior to direct MALDI-MSI analysis in order to improve the detection of low abundance proteins. The developments reported here resulted in improvement in sensitivity for the detection of several protein signals, and hence allowed discrimination between regions within the tissue sections. Data pre-processing methods were also developed using freely available software, with the aim of reducing instrumental and experimental errors prior to statistical analysis.

Using MALDI-MSI for direct protein analysis within tumour tissue sections resulted in the localisation and detection of protein signals which were found to be characteristic in differentiating between tissue regions. In chapter 3, on-tissue digestion was reported for protein identification directly from both frozen and FFPE tissue sections and protein identifications were correlated with their observed distribution within the tissue sections. The addition of a non-ionic detergent, here octyl glucoside, to the trypsin solution was shown to greatly improve the solubilisation of low abundance and

membrane-associated proteins for tryptic digestion. The use of ion mobility separation combined with MALDI-MSI was found to be beneficial in minimising peak interferences, hence improving the specificity for direct protein identification through peptide sequencing by tandem MS/MS.

MALDI-IMS-MSI was found to be a rapid and efficient approach to study the distribution and identification of tumour hypoxia-associated proteins within AQ4N-treated tumour xenografts in correlation with the *in situ* localisation of the drug and its metabolites. The use of such an approach allowed the discrimination between non-treated and AQ4N-treated tumour xenografts and also between the type of drug treatment. Further work is recommended in order to improve the detection and *in situ* validation of protein markers such as angiogenic factors and glucose transporters. A quantitative study of the expression of such proteins in correlation with AQ4N treatment is highly desirable since it may help in assessing the efficiency of the drug.

The concept of IMS-Tag MALDI-MSI, developed in this thesis, allowed the localisation and *in situ* identification of tumour biomarkers using both bottom-up and top-down proteomic approaches directly within FFPE adenocarcinoma tissue sections. The identification of protein modifications, including proline oxidation, resulting from the sample preparation process has been found to be beneficial for protein identification. Further work will be required, including the use of other proteases and extensive *de novo* sequencing, in order to identify more proteins.

In chapter 6, the use of MALDI-MSI has been demonstrated for high-throughput analysis using tissue micro array technologies. This allowed the design of a novel tumour classification model based on molecular information obtained with MALDI-IMS-MSI and statistical analysis. This shows the huge potential of the technique as it may offer the possibility of building a protein database for tumour classifications and also the possibility that those could be used to select the appropriate required treatments. This can also generate biomarker candidates that can be further validated using other methods such as IHC, western blot, etc. Further desirable work could be to study a large data set of TMA that includes several patients with detailed clinical information.

Additionally method improvements may be performed in order to achieve the identification and semi-quantification of more peptides and biomarkers from TMA sections. This may lead to a better understanding of cancer progression and aggressiveness when correlating the MALDI-MSI data with clinical information from the patients. The coupling of PCA-DA statistical analysis with artificial network analysis in order to link peptides and/or proteins with tumour class and even appropriate treatment may also be explored.

One of the challenges of the MALDI-MSI technique is its efficient use for *in situ* quantification. Chapter 7 of this thesis describes and discusses the use of MRM-MALDI-MSI as a methodology for a more specific *in situ* localisation and identification of proteins within tumour tissue sections after on-tissue digestion. However, further developments in the current instrumentation, including laser technologies and software, are still required.

Several methods, as well as new concepts, have been developed and improved in this thesis in order to use MALDI-MSI at its optimum capacity as a biomarker discovery tool. Further work will require the use of other types of reagent, the combination of various mass analysers and the development of statistical analysis software in order to standardise MALDI-MSI protocols as well as achieve improved biomarker discovery directly within tissue sections.

Appendices

Appendix 1: Publications

Djidja M.C., Claude E., Snel M.F., Scriven P., Carolan V. and Clench M.R., **Novel molecular tumour classification using MALDI-mass spectrometry imaging of tissue micro array**, *Analytical and Bioanalytical Chemistry* 2009, *submitted.*

Djidja M.C., Claude E., Snel M.F., Scriven P., Francese S., Carolan V. and Clench M.R., **MALDI-ion mobility separation-mass spectrometry imaging of glucose-regulated protein 78 kDa (Grp78) in human formalin fixed paraffin embedded pancreatic adenocarcinoma tissue sections**, *Journal of Proteome Research* 2009, DOI: 10.1021/pr900522m.

Djidja M.C., Francese S., Loadman P.M., Sutton C.W., Scriven P., Claude E., Snel M.F., Franck J., Salzet M. and Clench M.R., **Detergent addition to trypsin digest and ion mobility separation prior to MS/MS to improve peptide yield and protein Identification for *in situ* proteomic investigation of frozen and FFPE adenocarcinoma tissue sections**, *Proteomics* 2009; 9:2750-2763.

Scriven P., Djidja M.C., Francese S., and Clench M., **Proteomic Profiling of human pancreatic adenocarcinoma by MALDI-mass spectrometry imaging**, *European Journal of Surgical Oncology* 2008; 34:1083.

Djidja M.C., Carolan V., Loadman P. M., and Clench M. R., **Method development for protein profiling in biological tissues by matrix assisted laser desorption/ionization mass spectrometry imaging**, *Rapid Communication in Mass Spectrometry* 2008; 22: 1615-1618

Appendix 2: Oral presentation

Direct Proteomic Investigation of Human Pancreatic Adenocarcinoma by MALDI-Mass Spectrometry Imaging. Faculty Research Day, Health and Wellbeing, Sheffield Hallam University, December 2008.

Appendix 3: Poster presentations

MALDI-Ion Mobility Separation-Mass Spectrometry Imaging for direct Biomarker Targeting in Human Breast Adenocarcinoma. International Mass Spectrometry Conference (IMSC) September 2009, Bremen, Germany.

Targeting of Hypoxia-related Proteins in AQ4N treated solid Tumour Xenografts by MALDI-Ion Mobility Separation- Mass Spectrometry Imaging. American Society for Mass Spectometry (ASMS) Conference June 2009, Philadelphia, USA.

Proteomic Profiling of human Pancreatic Adenocarcinoma by MALDI-Mass Spectrometry Imaging. European Society of Surgical Oncology Congress September 2008, The Hague, The Netherlands.

Direct Proteomic Investigation in human Pancreatic Adenocarcinoma by MALDI-Mass Spectrometry Imaging. British Society for Mass Spectrometry (BMSS) Meeting September 2008, York, UK.

Best Poster Award: ***In situ*** **Investigation of Protein expression in Adenocarcinoma tissue sections by MALDI-Mass Spectrometry Imaging.** British Society of Proteomic Research (BSPR) Meeting July 2008, Cambridge, UK.

Visualisation and *in situ* characterisation of proteins in adenocarcinoma tissue sections by direct MALDI-Mass Spectrometry Imaging. American Society for Mass Spectometry (ASMS) Conference June 2008, Denver, USA.

Updated version of **Method development for protein profiling in biological tissues by MALDI- Mass Spectrometry Imaging (MALDI- MSI).** British Society for Mass Spectrometry (BMSS) Meeting September 2007, Edinburgh, UK.

Method development for protein profiling in biological tissues by MALDI-Mass Spectrometry Imaging (MALDI- MSI). American Society for Mass Spectometry (ASMS) Conference June 2007, Indianapolis , USA and The Royal Society Of Chemistry Analytical Research Forum (RSC ARF) July 2007, Glasgow, UK.